ATOMIC WEAPONS ESTABLISHMENT

AWE REPORT NO. O 18/89

Source Mechanisms of Some Large Earthquakes Determined using the Relative Amplitude Method

R M Rogers
*R G Pearce

* Department of Geology and Geophysics, University of Edinburgh

CONTENTS

SUMMARY

This report describes the application of the Relative Amplitude Moment Tensor Program (RAMP) to a group of 51 large earthquakes originally drawn up for study at the General Assembly of the International Association for Seismology and Physics of the Earth's Interior (IASPEI) in 1985. RAMP is designed to determine the range of moment tensors compatible with the observed relative amplitudes of *P*, *pP* and *sP*, and three components of direct *S*. The moment tensor encompasses any seismic source, which may include an explosive (isotropic) component as well as a non-double couple deviatoric component.

All the earthquakes are found to be compatible with the conventional double couple model, though not to the complete exclusion of other source types. Constraint on the isotropic component is almost invariably tighter than on the deviatoric component, and is dependent on the nature of the data available. Constraint on the orientation of the source is generally much tighter than on source type.

The solutions obtained using RAMP and those obtained by other methods are compared. Solutions obtained using the first motion method and the Multi-channel Signal Enhancement (MSE) method, which depend most heavily upon the form of the *P* wave agree most closely with the *P* wave data used in RAMP. Solutions obtained using the Centroid-Moment Tensor (CMT) method, which is biased towards the *S* waveform, agree more closely with the *S* wave observations used in RAMP. However, most of the solutions from all three of these methods lie outside the range of moment tensors found to be compatible using RAMP.

1. INTRODUCTION

Several methods are now available for determining the moment tensor of an earthquake; the moment tensor is a convenient way of describing the force system acting at an earthquake source. Usually the source is assumed to be a point in space and time. Pearce and his co-workers (1,2,3,4,5) have developed a method that makes use of the relative amplitudes of observed seismic phases such as *P*, *pP* and *sP*. Much of the early stimulus for this work came from interest in developing methods for distinguishing between earthquakes and explosions on the basis of their radiated seismic signals - methods that might be used for the verification of compliance with test ban treaties.

Initially the relative amplitude method used only data from *P* seismograms and assumed that the source mechanism was a double couple. The solutions are then all those double couple orientations that are compatible with the observations. The method has now been developed to the stage where the range of solutions covers all those that can be represented by a symmetric moment tensor (ie, sources in which angular momentum is conserved - a reasonable restriction) and includes amongst other source types the explosion and implosion, compensated linear vector dipoles (CLVDs) and tensile cracks, as well as the conventional double couple.

Examples of the application of the relative amplitude method for distinguishing between earthquakes and explosions are given elsewhere (eg, Pooley et al (6), McLaughlin et al (7)). The purpose of this report is to compare moment tensors obtained using the "Relative Amplitude Moment Tensor Program" (RAMP) with those obtained by other methods to determine the strengths and weaknesses of the various methods. The incentive to do this arose from discussions at the General Assembly of IASPEI (International Association for Seismology and Physics of the Earth's Interior) held in Tokyo in 1985. Fifty-one earthquakes (the "IASPEI list") were selected for study at that Assembly and participants were invited to produce focal mechanism solutions for them.

The IASPEI list earthquakes are taken from a wide range of locations and depths worldwide (although 42 were less than 100 km deep). All the earthquakes are large, only eight having $m_b < 6.0$; the source hypocentres and magnitudes are listed in table 1. Comparisons are made between the RAMP results and the results derived using first motion (Needham (8)), centroid-moment tensor (CMT) (Ekström et al (9)) and multi-channel signal enhancement (MSE) (Sipkin (10)) methods.

In order to ensure that all participants had a sound base from which to work, waveform data were made available through the United States Geological Survey (USGS). The data consisted of digital three component seismograms from a number of stations worldwide, though the densest coverage was in the United States. Long and short period seismograms were both available for all of the stations, and for some there were also intermediate period records. These digital seismograms were distributed to participants on standard half-inch digital magnetic tapes, together with the requisite software for recovering the desired data. A waveform catalogue showing the printed seismograms was also made available (Zirbes and Moon (11)).

The CMT and MSE methods, like RAMP, used the digital data made generally available to all IASPEI participants, while the first motion data employed by Needham (8) includes additional stations.

2. THE RELATIVE AMPLITUDE MOMENT TENSOR PROGRAM (RAMP)

The Relative Amplitude Moment Tensor Program (RAMP) was first introduced by Rogers and Pearce (12), and more fully described by Pearce and Rogers (4) and Rogers (5); the following provides a brief summary.

2.1 Synopsis of the method

The method is designed to reveal all possible moment tensors for a seismic event, using as its input observations of the relative amplitudes of the phases *P*, *pP* and *sP*, and of the three components of direct *S* at a series of teleseismic stations. The method is able to test all source types resolvable into three orthogonal dipoles; this includes the pure explosion and source types having an explosive or implosive component.

Each relative amplitude observation takes the form of maximum and minimum permissible amplitudes for a phase, and its polarity. Since only relative amplitudes are considered, the amplitude limits may be specified in any units, so long as all phases to be considered together are measured in the same units. The polarity may be specified as positive, negative, or unknown, or it may be specified as the same as or opposite to the polarity of another observed phase. In practice, S waves are tested separately from P, pP and sP, because of uncertainty over the relative attenuation of P and S waves over the transmission path. Normally, S wave data is limited in effect to observations of the polarity (or relative polarity) of the horizontal components (Pearce and Rogers (4)).

For each mechanism under test, the theoretical ratio between the amplitudes of each possible pair of the specified phases is calculated, and if it falls within the limits inferred from the measured bounds, then the mechanism is deemed to be "compatible" with the observations; otherwise it is "incompatible". This operation is repeated for each station at which phases are specified. Those mechanisms compatible with all the specified phase pairs are said to be "fully compatible" with the dataset.

2.2 Source representation

The source is described in terms of the source type and its orientation, which are expressed by separate parameters. The orientation is described by three angles; σ, δ and ψ. In the case of a double couple these correspond to the strike, dip and slip angles of the source, respectively. For other source types, the physical meaning of the angles is less clear, but they retain the same relationship with the principal axes of stress.

The source type is described by two parameters, T and k. T expresses the deviatoric component of the source type (ie, variation between double couple, CLVD, and negative CLVD), and k the proportion of volume change in the source (implosive or explosive component). The total moment tensor is given by:

$$M = (1-|k|)\begin{bmatrix} \min(2,2-T) & 0 & 0 \\ 0 & \max(-2,-(2+T)) & 0 \\ 0 & 0 & T \end{bmatrix} + k\begin{bmatrix} 2 & 0 & 0 \\ 0 & 2 & 0 \\ 0 & 0 & 2 \end{bmatrix}$$

It is seen that the separate expression of the orientation allows the source type to be expressed as a diagonalised moment tensor, independent of the orientation. Since no information on absolute amplitudes is used, no parameter is required to describe the magnitude of the source, and hence only five parameters are used.

2.3 Graphical representation of results

Compatible mechanisms are represented using two types of graphical display; the vectorplot (Pearce (1)) and the source type plot (Pearce and Rogers (4), Hudson et al (13)).

The vectorplot (figure 1) is used to display those orientations of a given source type found to be compatible. A vector is drawn for each compatible orientation, in the position corresponding to its δ (dip) and ψ (slip) angles, and at an angle from the vertical equal to σ (strike).

The source type plot (figure 2) represents a projection of the five-dimensional parameter space onto the two dimensions used for the source type. Circles are drawn on the plot, centred on those source types found to have at least one compatible orientation. Their size is proportional to the number of orientations found to be compatible for the particular source type.

3. PROCESSING METHOD

Because the earthquakes are large, long period seismograms are used; the dominant frequencies of the radiation from large earthquakes are outside the passband of short period seismometers. The surface-reflected phases cannot be reliably observed on long-period seismograms for shallow earthquakes because the *P*, *pP* and *sP* arrivals interfere. For this reason, in the absence of broadband seismograms, the solutions presented here for the shallow earthquakes are derived using only *P* wave polarity and *S* wave polarisation data. However, as will be shown, even these data provide a significant constraint on the source parameters, particularly the source orientation; in some cases the source type is also well defined.

The search grid is normally set at 10° intervals in the three orientation parameters, 0.25 in T and 0.2 in k; in a few cases where very little constraint is imposed by the data on orientations, the angular increment is increased to 15° in order to reduce processing time and storage space requirements. Similarly, in a few cases where constraint is very strong, increments of 5° or even 2° are used. These values are chosen to permit solutions to be computed within a reasonable time span without restricting the search space.

Because the response of the long period seismometers at stations in the SRO network was subject to problems of non-linearity, the relative amplitude bounds made from such stations are substantially widened. However, seismograms from these stations may still be capable of providing usable relative amplitude information, albeit with wider bounds. These are assessed by individual examination.

4. RESULTS

The earthquakes are divided into three groups according to their depths: "shallow" (depth < 100 km), "intermediate" (100 to 300 km) and "deep" (> 300 km). This classification reflects the differences in the way that the data can be used, and hence the quality of results expected; for the shallow earthquakes, *pP* and *sP* are hidden in the *P* wave coda and are generally unidentifiable; at intermediate depth the separation is great enough to permit approximate amplitudes to be assigned to many of the *pP* and *sP* arrivals; for the deep earthquakes these phases are well separated and the presence of coda brings few problems.

In order to simplify assessment of the results, the earthquakes are further classified according to the degree of constraint imposed by the data on the source mechanism. For source type and orientation separately, each of the 51 earthquakes is placed into one of three categories, with an approximately equal number of earthquakes in each, representing "strong", "average" and "weak" constraint. For source type, compatibility of less than 10% of source types is defined as "strong" constraint, while compatibility of more than 50% of source types is defined as "weak" constraint. To classify the constraint on orientation, the proportion of orientation space found to be compatible is calculated for each source type, and the mean of the non-zero values is found. This procedure is adopted because it eliminates the effects of constraint on source type, and mitigates the effects of rotational symmetry as T or k approaches 1. A mean value of less than 0.1% is defined as "strong" constraint, while a mean of over 0.6% is defined as "weak" constraint. It is recognised that such a system of classification is inevitably arbitrary; however, it is intended only to provide an approximate guide to the quality of each result in the context of the group.

Appendix A contains the relative amplitude bounds specified for each observed phase, for all 51 earthquakes. A graphical summary of the results for each earthquake appears in appendix B, which also includes graphical representations of the mechanisms derived by Ekström et al (9), Sipkin (10) and Needham (8).

4.1 The shallow earthquakes

4.1.1. Introduction

It is normally impossible to extract relative amplitude information from P waves because of the masking of the surface reflected phases pP and sP by the coda of the initial P wave arrival; therefore only the P wave polarity is specified, with arbitrary wide amplitude bounds (typically 1 to 100 units). In addition to these first motion data, the polarities of the S wave in the horizontal components may also be used; polarity information may be read for direct S waves from sources at any depth with little or no variation in quality.

For the following discussion, it is convenient to divide the shallow earthquakes into two groups. Of the 42 earthquakes, 21 have all identifiable P wave wave first motions of the same polarity. These are referred to as "group A", while the remaining 21 earthquakes have mixed first motion polarities, and fall into "group B". This division corresponds with the difference in constraint upon source type and orientation to be expected from the two types of P wave first motion dataset, though additional constraint is provided by the S wave polarity observations. The members of each group are identified in table 2.

4.1.2 Group A earthquakes

The fact that the P wave polarity is the same at all stations at which it is observed unambiguously indicates that the likely orientation is an approximately 45^{o} dip slip type (for a double couple - other orientations may be applicable for other source models), but rotations about a vertical axis are completely or almost completely undefined by P wave data. Depending on the distribution of stations on the focal sphere, other orientations may also be compatible with the observations.

Given the lack of constraint imposed by P wave polarities alone, it is not surprising to find that the source type and orientation constraints for the great majority of these earthquakes fall into the "weak" or "average" categories (see table 2); two typical examples are shown in figure 3. In fact, there is only one exception, namely earthquake 26 (figure 4), for which the constraints on both source type and orientation are found to be "strong". Such a result can only be achieved when the S wave observations provide the major constraint. This is borne out by the distribution of compatible source types - only source types with $T =$ 0.0 are fully compatible, whereas the source type is much less strongly defined in k, reflecting the fact that S waves convey no information about k, and P wave first motions can generally impose little constraint on T.

4.1.3 Group B earthquakes

The contrast in the quality of the results between group A and group B earthquakes is immediately apparent from table 2. Whereas in group A, only one earthquake achieves a "strong" rating for constraint on either source type or orientation, and most of the classifications are "weak", the position is almost exactly reversed in group B. Only three of the 21 earthquakes in this group have the constraint on either source type or orientation classified as "weak" (earthquakes 9, 31 and 51, discussed individually below), and more than half of the individual classifications are "strong".

In the case of earthquake 9, only six stations are used in the analysis, which fall into two groups of three on the focal sphere (figure 5). The first group lies in the north-western quadrant, and shows positive first motion at all three stations, while the second group lies in the southern part of the focal sphere. The most westerly of these stations also shows a positive first motion, while the remaining two show a negative P wave polarity. Thus there is a constraint on the position of one of the nodal surfaces of the P wave radiation, but very little constraint is placed upon its alignment or its shape.

For earthquake 31, thirteen stations are used, of which four show a negative and eight a positive P wave first motion (the remaining station is only used for observations of S wave polarity). The stations are distributed in three well separated groups on the focal sphere; one in the north-west, one in the north-east and one in the south (figure 6). The southern group of stations show a negative first motion; the remaining groups show a positive first motion. Thus one P wave nodal surface is constrained to run roughly east-west and to have a steep dip; however, the position of the intermediate axis of stress, and the form of the nodal surfaces near it are not well defined. No value of T is prohibited, and the source type constraint is classified as "weak", the orientation constraint being in the "average" category.

For earthquake 51, only P wave first motions are used. This is because the earthquake appears to be a double earthquake, the second part being much larger than the first, for which the solution is presented. This means that the S waves for the first earthquake are unclear, being obscured by the coda of the preceding phases and of low amplitude compared with the immediately following S waves from the second sub-event. Of the P wave observations, all but one are positive, with one station (AFI) in the south-east of the focal sphere showing a negative first motion (figure 7). This constrains the source to have at least one steeply dipping nodal surface. Steep dip-slip double couples can satisfy the observations, as can a very small range of strike-slip orientations.

4.2 The intermediate depth earthquakes

At depths greater than about 100 km, the separation in time between the P wave and the pP arrival, and between pP and sP, begins to allow some measurements to be made of the surface reflected phases in addition to the direct P and S used for the shallower earthquakes. However, particularly if pP has a relatively high amplitude, it may still not be possible to make proper measurements of *sP*. Similarly, a small *pP* phase will still be difficult to measure in the coda of a relatively large *P* wave.

Three of these earthquakes (Nos. 18, 27 and 36) are discussed in more detail by Rogers and Pearce (12). The remaining two, earthquakes 43 and 46, were omitted from that study because of apparent waveform complexity. Choy and Engdahl (14) confirm from broadband records that earthquake 46 is indeed complex. They further suggest that earthquake 27 is also complex, and that earthquakes 18 and 36 show evidence of multiple arrivals. However, this is not directly evident in the long period data used by Rogers and Pearce (12) and in this study.

Earthquake 18 is the only earthquake out of the 51 to be relocated in depth for the purposes of this analysis. This is done on the basis of *P*-*pP* delay times observed on long period records from several stations, which are in clear disagreement with the NEIC depth of 180 km. The revised depth is set to 120 km. Choy and Engdahl (14), using broadband data, also found the earthquake to be shallower than the published figure, but redetermined the depth as 138 km. They also suggest that the earthquake was complex, having a strong second sub-event, differently oriented from the first, giving rise to systematic variations in the relative amplitudes of the two *P* arrivals across the focal sphere. This is not apparent from the long period seismograms used by Rogers and Pearce (12) and in this study. Despite the widening of the bounds on all relative amplitudes observed at SRO stations (see section 3), the constraint on orientation space is found to be "strong", while that on source type is "average". These categorisations reflect the fact that two stations, close together, show a positive first motion, while the remaining nine are negative. Thus the course of one nodal surface is constrained over a small part of its length, but the region close to the intermediate axis of stress is not well defined.

Earthquake 27 is located in the Tonga Islands region. All but one of the stations show a negative first motion, while the polarity of the first motion at the remaining station is unclear, apparently being near-nodal. The depth of the source allows measurements to be made of the amplitudes of the surface reflected phases, but the bounds must still be widened because of interference from the coda of *P*, and of *pP* in the case of *sP*, so that the constraints on the source type and orientation are only "average".

Earthquake 36 is in the USSR - Afghanistan border region. All of the *P* wave first motions are of positive polarity, indicating a dip slip type orientation; furthermore, the amplitude bounds of the surface reflected phases reflect once again the presence of coda from preceding phases. There is thus limited information contained in the *P*, *pP* and *sP* measurements. Nevertheless, a solution is obtained with "strong" constraint on both source type and orientation, largely on the strength of the constraint imposed by the *S* wave data (Rogers and Pearce (12)).

Earthquake 43 is located in the Banda Sea, which means that the station coverage available at teleseismic distances is limited; eight stations are used, all of which are contained in a 215° arc of azimuth, leaving the western side of the focal sphere almost completely unsampled. In addition, despite the source being at 178 km depth, the relative amplitudes of *P*, *pP* and *sP* are not clear, possibly due to source complexity. Thus, apart from *S* wave data, the observations from several stations are restricted to *P* wave first motions, and where relative amplitude bounds are specified, they allow a wide range of amplitude ratios. All the observed *P* wave first motions are of positive polarity. These difficulties restrict the constraints on both source type and orientation to the "weak" category, orientations being grouped around the 45° dip slip type.

Source complexity also adversely affects the data for earthquake 46, which occurred in the Hindu Kush region. However, the station coverage is slightly better than for earthquake 43, having 10 stations used. Once again, all *P* wave observations are of positive polarity, indicating an approximately 45° dip slip orientation. Only very wide *P*, *pP* and *sP* relative amplitude bounds can be specified for six stations, the remaining four yielding only *P* wave first motion data. Constraints on source type and orientation are both classified as "average".

4.3 The deep earthquakes

These four earthquakes (listed in table 2) have been studied by Stimpson (15), but using only the *P*, *pP* and *sP* data. The results presented here represent the constraint imposed by Stimpson's *P*-group data with the further inclusion of the *S* wave horizontal component polarity data described previously. This section summarises the results; a more complete discussion of the *P*, *pP*, *sP* data and results is provided by Stimpson (15).

It is found that the solutions are constrained very strongly by clearly observable *P*, *pP* and *sP* phase amplitudes. Even so, the *S* wave observations provide a significant additional constraint in all four cases, generally reducing the size of the compatible region of solution space determined using only *P*, *pP* and *sP* by 40 to 60%.

Earthquake 14 occurred in the east USSR - north east China border region. Because of low signal to noise ratios, *P*, *pP* and *sP* relative amplitudes are measured at only five stations (Stimpson (15)). At three of these stations, the first motion is positive, and at two negative. However, *S* wave polarity observations can be made for ten stations. Despite the small data set, the constraints on both source type and orientation are both classified as "strong", the source type being close to the double couple and the orientation near pure dip slip.

Earthquake 28 is located in the Peru-Brazil border region. The first motions at all 16 stations are negative, indicating an approximately 45° dip slip orientation. Although the constraint on orientation falls into the "strong" category, the source type constraint is "average". The value of k is between -0.4 and 0.0; the value of T is between ± 0.5. This clearly represents better constraint on source type than is found for the majority of similarly orientated (group A) shallow earthquakes.

Earthquake 47 occurred near the South coast of Honshu, Japan. Eleven stations are used for *S* wave data, while eight provide *P*, *pP* and *sP* measurements; most of the stations used are grouped in the north and east of the focal sphere. All observed *P* wave first motions are positive. The constraints on both source type and orientation are in the "strong" category. The addition of *S* waves provides much tighter constraint on the source type than was achieved by Stimpson (15) using only *P* group data.

Earthquake 49 is located in the Mindanao, Philippine Islands region. Six stations are used to provide *P*, *pP* and *sP* observations, of which four have a negative first motion and two positive. *S* wave polarisation data are taken from three stations. The constraints on both the source type and orientation are classified as "strong".

5. COMPARISON WITH OTHER SOLUTIONS

5.1 Introduction

In this section we compare the results obtained from RAMP with those obtained by Ekström et al (9), using the CMT method, by Sipkin (10), using the MSE method, and by Needham (8), using the *P* wave first motion ("FM") technique. The procedure used is to run RAMP, using the same data as before, but testing explicity the compatibility of the "best" solutions obtained by these authors (shown in table 3 using RAMP-type parameters). The agreement between the RAMP solutions and the "best" solutions of the other authors is then expressed by the number of observations with which the latter are incompatible; these can be divided into *P*-wave and *S*-wave observations for further analysis. Solutions falling within the range of solutions derived using RAMP will have no incompatible observations.

It should be noted that these methods do not provide as much flexibility as RAMP in specifying the source type. For the first-motion method, a double couple source is assumed, while the CMT and MSE methods allow a generalised source type but without volume change (in RAMP terms, k is assumed to be zero).

5.2 General

The number of "*P*" (ie, *P*, *pP*, *sP*) and *S* observations with which each of the CMT, MSE and FM solutions is found to be incompatible is given in table 4.

Eight CMT and a different eight MSE solutions fall within the range of compatible solutions found using RAMP. Taking all 51 earthquakes as a whole, the CMT results are incompatible with 100 *P* observations and 62 *S* observations, while the MSE solutions are incompatible with 68 *P* observations and 92 *S* observations. It is therefore clear that there is a significant difference of emphasis between the two inversion procedures. This may be attributed to the different data used by each algorithm. The CMT method uses the entire seismogram up to the onset of the fundamental mode surface wave, and in consequence its results are biased towards matching the *S* waveform preferentially because of its large amplitude, and thus usually large residuals. The MSE algorithm does not depend upon the direct *S* waveform at all; it matches only the *P* waveform from each seismogram.

The value of $|T|$ is in general larger in the CMT solutions than in the MSE solutions - in only 14 cases out of the 51 is $|T|$ larger in the MSE solution. This is in agreement with results reached using other earthquakes by Sipkin (16), who suggests that the discrepancy may be due - at least in part - to the fact that the CMT data includes a large proportion of signal from between the arrivals of specific phases. These sections would have a reduced signal to noise ratio, while the MSE data are formed only of the isolated *P* wave group, where the signal to noise ratio is relatively high.

The solutions obtained by Needham (8) differ from those of Ekström et al and Sipkin in three important respects. Firstly, they are derived using a traditional *P* wave first motion technique, rather than waveform inversion methods. Secondly, they assume *a priori* a double couple source type throughout, and thirdly, data from additional stations have been used to augment those supplied in digital form by the USGS.

As might be expected, the results from this method show much greater agreement with the *P* observations than with those of *S*. The 48 solutions presented are found to be incompatible with a total of 107 *S* observations and only 36 *P* observations. No solution is offered for three of the earthquakes where, because data are sparse, neither nodal plane can be properly constrained. There are only four earthquakes for which the FM solutions are completely compatible with all the observations used in the RAMP analysis; however, 26 solutions are fully compatible with the *P* wave observations used in RAMP. The total number of incompatible observations is thus slightly fewer than those for the CMT and MSE methods, but the bias towards observed *P* wave compatibility is stronger even than for the MSE method. This is probably due to the fact that both the FM and RAMP methods rely solely on direct observation of specific seismogram features - indeed, the RAMP data may be seen as a superset of the FM data. Discrepancies between the FM solution and RAMP *P* wave observations may be at least partly explained by the fact that there are sometimes internal inconsistencies in the FM dataset. An example of this is provided by earthquake number 1 (see Rogers and Pearce (12)). For a number of the FM solutions, the slip angle is given as 90° (ie, the slip vector is directly up- or down-dip), when the position of one nodal plane cannot be constrained accurately by the data available. This may be responsible for many of the *S* wave incompatibilities (see for instance earthquakes 20, 21 and 30).

5.3 The shallow earthquakes

Table 5 shows a summary of the number of incompatible *P* and *S* wave observations found for the CMT, MSE and FM solutions for the shallow group A and group B earthquakes. For the FM solutions, the main feature of interest is that there are substantially more incompatible *S* wave observations in group A than in group B. Group A consists mostly of approximately 45° dip slip earthquakes, which are generally not well constrained by first motion observations; in particular, the slip angle is often set to 90° because it cannot be defined by the data. If this is different from the true slip angle, then the *S* wave polarisation directions at any point on the focal sphere may be in error. In group B, which consists almost entirely of strike-slip earthquakes, the orientation is usually well defined by first motion data, so the errors arising in the *S* wave radiation pattern are generally small.

The MSE results show a similar behaviour with regard to *S* wave compatibility; however, there are many more *P* wave observations found to be incompatible with the MSE solutions for group B than for group A. As strike-slip orientations are generally well defined by *P* wave polarities, this seems likely to be caused by the use of a whole-waveform matching technique, which is liable to yield solutions that do not necessarily match observable seismogram features. This is perhaps shown up particulary for strike-slip orientations because there are more stations close to *P* wave nodes, where a mismatch of polarity does not necessarily entail a large error in absolute amplitude.

A different pattern is shown by the CMT results, for which the number of incompatible *S* waves is almost the same for both groups of earthquakes, being rather fewer than for the FM and MSE methods. However, the number of *P* wave incompatibilities is much larger for group B. Indeed, in group A, the CMT results suffer fewer than half the number of *P* wave incompatibilities of the other methods; in group B the figure is more than double that for either of the other methods. Such a pattern must be due to the *S* wave domination of the CMT solution. *P* waves provide much less information about the position and shape of the nodal surfaces for group A earthquakes than for group B; thus the use of *S* waves greatly increases the amount of information available. However, in the case of group B, there is much information to be gained from *P* waves, upon which the CMT method places less weight, matching preferentially the form of the generally higher-amplitude *S* waves. Once again, the frequent proximity of stations to *P* wave nodes in group B earthquakes means that the polarity of low-amplitude *P* waves may be incorrectly modelled.

5.4 The intermediate-depth and deep earthquakes

There are five intermediate-depth earthquakes in the IASPEI list. The results from the FM method show incompatiability with a total of seven *P* and five *S* phase pairs for all five earthquakes. The only one of these for which the FM solution is incompatible with more than two phase pairs is number 18, a steep dip-slip earthquake, for which three *P* and two *S* phase pairs are incompatible.

The MSE results show less close agreement overall, being incompatible with a total of sixteen *P* and four *S* phase pairs for the five earthquakes. However, this includes one earthquake, number 27, again a steep dip-slip earthquake, for which there is complete compatibility with the RAMP data. As with the FM results, earthquake 18 shows most incompatibility, being incompatible with nine *P* and one *S* wave phase pairs.

The overall agreement of the CMT results is similar to that for the MSE results. A total of nineteen *P* and two *S* wave phase pairs are found to be incompatible for the five earthquakes. Closest to full compatibility is the solution for earthquake 36, an approximately 45° dip-slip earthquake, for which one *P* phase pair is incompatible. As with the MSE and FM methods, earthquake 18 is least well matched with the RAMP solution, having nine *P* wave and one *S* wave phase pairs incompatible. These are not the same phase pairs as for the MSE solution even though they are equal in number.

Comparisons of the RAMP solutions with those for the CMT and FM methods for the deep earthquakes were made by Stimpson (15), who included only *P*, *pP* and *sP* in his data.

The FM solutions for earthquakes 14, 28 and 49 are in close agreement with the observations used for RAMP. A total of seven phase pairs (four *P* and three *S*) are incompatible for the three earthquakes combined. For earthquake 47, six *P* and three *S* phase pairs are found to be incompatible. In this case, a steep dip slip orientation is derived, with dip and slip angles very similar to the compatible orientations for RAMP; however, the strike is inconsistent, being around 10° east of that compatible with the RAMP data.

The CMT results also show good agreement for three earthquakes and less good agreement for one. For earthquakes 14, 47 and 49 there is a total of 11 *P* and no *S* phase pairs found to be incompatible. For earthquake 28 there are thirteen *P* phase pairs incompatible, and one *S*. This is an approximately 45^{o} dip slip earthquake, with the majority of stations grouped in the north-west of the focal sphere. Although all the stations show a negative first motion, the CMT solution shows a *P* wave nodal surface passing through the north-western cluster of stations. For all four earthquakes the strong bias toward *S* wave matching is clearly preserved.

The MSE results show a total of fourteen *P* and three *S* wave phase pairs to be incompatible for the four deep earthquakes combined. Most incompatible phase pairs (four *P* and two *S*) are found for earthquake 49, a dip slip earthquake for which few stations may be used, and fewest (two *P* and no *S*) for earthquake 28, also dip slip in character but with many more observations available.

5.5 Concordant solutions

Thirteen of the 51 earthquakes yield solutions which encompass either the CMT, MSE or FM solution, or a combination of these (see table 6). Twelve of these are shallow earthquakes, the exception being number 27, of intermediate depth, for which only the MSE solution is fully compatible. Of the twelve shallow earthquakes, nine fall into group A, and three into group B.

It will be seen from table 6 that all but one of the fully compatible CMT solutions are from group A; the fully compatible MSE and FM solutions are evenly divided between groups A and B. As the major constraint on the RAMP solutions is normally provided in group A by *S* wave observations and in group B by *P* wave observations, these distributions reflect again the bias of the CMT method towards *S* wave domination, and of the MSE and FM methods towards *P* wave domination.

For only one earthquake (number 38) are all three solutions compatible with the observations used for RAMP. By the assessment criteria outlined above, this is one of the least well constrained of the 51 earthquakes, using RAMP.

6. DISCUSSION AND CONCLUSIONS

6.1 RAMP results

It has been clearly shown that the degree of constraint on the source mechanism, and particularly on the source type, is directly related to the capacity of the seismograms to yield well defined relative amplitude measurements. With very few exceptions, the shallow earthquakes yield the least constraint and the deep earthquakes the most.

The constraint on the shallow earthquakes is very much in line with what is to be expected from the nature of the data; that is, the group B earthquakes are much better resolved in both orientation and source type than the group A earthquakes. Examination of the orientations of the group B earthquakes classed as having "strong" constraint in both source type and orientation shows that all but one of them (number 24) which has a steep dip slip orientation) are strike-slip or near strike-slip type earthquakes. It is not surprising to find that the strike-slip earthquakes tend to be the best resolved in source type at shallow depths. The general impossiblity of reliably observing the surface reflected phases, and consequent virtual "first motion" nature of the solution, means that any source which has both of its *P* wave nodal surfaces passing between the stations on the lower focal hemisphere is almost certain to be better resolved in source type than one which does not.

The intermediate-depth earthquakes, which are all dip-slip in character, are generally better resolved than similarly orientated (normally group A) shallow earthquakes. This is to be expected as increased depth makes possible the use of the surface-reflected phases *pP* and *sP*, though the relative amplitude bounds on these phases are generally widened to allow for the presence of the coda of *P*, and, for *sP*, the coda of *pP*. Furthermore, in some cases the improvement in constraint is not as great as might be expected since source complexity and non-linearity of instrument response further limit the accuracy with which relative amplitude bounds may be measured.

The deep earthquakes as a group yield, as expected, the most tightly constrained solutions: the constraint on both source type and orientation falls into the "strong" category for three out of the four earthquakes. This reflects the fact that the surface-reflected phases are well separated, even on long-period seismograms, for earthquakes at great depth. However, even where the surface-reflected phases may be measured with confidence, the degree of constraint available may still be dependent upon the relationship of the nodal surfaces to the stations. It is notable that the one earthquake for which the source type constraint is "average" (number 28) is one of the 45^{o} dip-slip type. The similarly oriented earthquake 47 attains "strong" constraint on source type largely by virtue of the constraint offered by *S* wave observations.

Examination of the figures showing the results for the 51 earthquakes shows that in many cases - indeed for a typical result - the source type plot shows poor constraint in T, often allowing at least some solutions for any value of T. However, it is frequently found that the constraint in k is considerably better. This confirms the pattern observed elsewhere (Rogers (5), Pearce and Rogers (4)). Also in agreement with previously observed trends is the usually high degree of constraint on the orientation; only a very small percentage of orientation space is permitted for any given source type, even at the peak of the distribution of compatible solutions. That the constraint on orientation is closer than that on source type is borne out by the qualifying values for the constraint categories "strong" and "average". For source type, the values are 10 and 50%, but for orientation they are 0.1 and 0.6%.

In summary:

(a) In general, he shallow earthquakes are least tightly constrained, and the deep earthquakes most tightly constrained. This reflects differences in the available data. However, it is important to note that for smaller sources, such as lower magnitude earthquakes or explosions, it would be possible to make observations usable in RAMP from short period seismograms, on which the *P*, *pP* and *sP* phases would remain discrete at very much shallower depths. Whole waveform inversion methods, such as the CMT and MSE methods, are designed only to operate on long period records (Dziewonski et al (17), Sipkin (18)).

(b) For the shallow earthquakes, the constraint available in group B is much greater than in group A. This is because for group A there is no direct evidence about the position of either nodal surface, whereas for group B, at least one nodal surface may be constrained.

(c) At intermediate depth, measurements of the relative amplitudes of P, pP and sP can generally be made, and these increase the constraint on the solutions. However, the bounds must generally be widened to take account of the presence of signal coda.

(d) The deep earthquakes, for which the surface-reflected phases are not subject to interference with the direct P coda, are generally well constrained in both orientation and source type. However, constraint appears still to be partly dependent upon the orientation of the source.

(e) As found in other studies, the constraint on orientation is usually much tighter than that on source type. For source type, there is generally stronger constraint on k than on T.

6.2 Comparison of RAMP and other results

Comparison of the RAMP results with those obtained by other authors shows that the observed data used in RAMP agree most closely with the most heavily weighted part of the data used in other methods - P observations for the FM and MSE techniques, and S observations in the case of the CMT method. This is particularly illustrated by the differences in compatibility found between the group A and group B shallow earthquakes. For most earthquakes, the solutions obtained by other methods lie outside the region of fully compatible RAMP solutions.

It may at first appear surprising that, for the intermediate-depth and deep earthquakes, the MSE and FM solutions show more incompatibility with P phases than with S phases, as this runs against the pattern found for the shallow earthquakes. However, the nature of the RAMP data for the deeper earthquakes is somewhat different; whereas for shallow earthquakes it is normally only possible to observe the polarity of the direct P and S waves, for deeper earthquakes it is also possible to determine the relative amplitudes of P, pP and sP. Therefore, for a mechanism to be compatible, it must satisfy not only the polarity observations, but also the relative amplitude measurements, which will reduce considerably the range of compatible mechanisms. The nature of S wave data is the same for earthquakes at all depths. For deep earthquakes, this effect will also exaggerate the tendency of the CMT method to match S wave preferentially.

Sipkin (16) carried out a comparison of the results obtained using CMT and FM methods with MSE results (differences between CMT and FM solutions were not presented). Differences in orientation were measured by deriving a unit vector representation of the source moment tensor, and computing the differences between the vector directions. (Clearly, such a technique cannot be used for measuring differences between RAMP and other solutions, since RAMP does not yield a single "best" mechanism). It was concluded from this study that the agreement between the different methods was generally good, but that for shallow earthquakes, there was closer agreement for strike-slip than for dip-slip earthquakes. This was ascribed to lack of constraint on the FM dip-slip solutions and poor resolution of the vertical dip-slip components of faulting by the CMT method. It was acknowledged, however, that the MSE results for shallow strike-slip earthquakes may be poorly resolved.

There would thus appear to be a discrepancy between the expectations of Sipkin and the results of testing CMT, MSE and FM solutions against RAMP data, discussed above. This may be explained by two factors. Firstly, Sipkin made comparisons between waveform inversion solutions and FM solutions, which do not include *S* wave data, as RAMP solutions do. This means that the comparison is often made against a solution which embodies an assumed position for an unconstrained nodal plane. Secondly, the comparisons have been made in different ways, and the correlation between the vector difference and the "number of observation incompatibilities" will in general be subject to station distribution. This difference may be increased by the fact that the RAMP solutions frequently occupy regions of irregular shape in solution space. Thus a mechanism which lies just outside the limit of compatibility may be further from the centroid of the compatible region than one lying well outside it (figure 8).

To summarise:

(a) Other authors' solutions generally agree most closely with the part of the RAMP data which is weighted most heavily by the other methods; *P* waves for FM and MSE, and *S* waves for CMT.

(b) For most of the earthquakes, the results obtained by other authors lie outside the region of fully compatible mechanisms found using RAMP.

(c) When relative amplitudes can be measured for the surface-reflected phases, all other methods show an increase in the number of incompatible *P* phase pairs. This reflects the greater constraint imposed on the RAMP solution when relative amplitude bounds can be measured.

(d) There is an apparent discrepancy between the findings of Sipkin (16) and this study. Sipkin found that better resolution was achieved by the CMT method for shallow strike-slip earthquakes, and by the MSE method for shallow dip-slip earthquakes. However, it is found here that the CMT results are more compatible with the RAMP observations for the shallow group A earthquakes, and MSE results are more compatible for the shallow group B earthquakes.

APPENDIX A

RELATIVE AMPLITUDE MEASUREMENTS

Azores Islands 01.01.80 ias01 NEIS depth 10.0km

Latitude 38.81500
Longitude -27.78000

	P			pP			sP			S(N)			S(E)		
	Pol	Min	Max	Pol	Min	Max	Pol	Min	Max	Pol	Min	Max	Pol	Min	Max
BCAO	-	0.500	100.000	U	0.500	100.000				U	0.500	100.000	O	0.500	100.000
KONO	+	0.500	100.000	U	0.500	100.000				+	0.500	100.000	-	0.500	100.000
ZOBO	+	0.500	100.000	U	0.500	100.000				U	0.500	100.000	+	0.500	100.000
ANMO	-	0.500	100.000	U	0.500	100.000				U	0.500	100.000	S	0.500	100.000
GRFO	-	0.500	100.000	U	0.500	100.000				+	0.500	100.000	U	0.500	100.000
ANTO	-	0.500	100.000	U	0.500	100.000				+	0.500	100.000	+	0.500	100.000
BOCO	-	0.500	100.000	U	0.500	100.000				-	0.500	100.000	+	0.500	100.000
KAAO	-	0.500	100.000	U	0.500	100.000				U	0.500	100.000	+	0.500	100.000

California - Nevada border region   25.05.80   ias02   NEIS depth 5.0km

Latitude 37.60000
Longitude -118.84000

	P			pP			sP			S(N)			S(E)		
	Pol	Min	Max	Pol	Min	Max	Pol	Min	Max	Pol	Min	Max	Pol	Min	Max
GRFO	-	1.000	100.000	U	1.000	100.000									
MAJO	-	1.000	100.000	U	1.000	100.000				U	1.000	100.000	O	1.000	100.000
GUMO	-	1.000	100.000	U	1.000	100.000				U	1.000	100.000	+	1.000	100.000
BOCO										+	1.000	100.000	+	1.000	100.000
ZOBO										U	1.000	100.000	S	1.000	100.000

Near South coast of Honshu, Japan 29.06.80 las03 NEIS depth 15km

Latitude 34.80800
Longitude 139.18100

	P			pP			sP			S(N)			S(E)		
	Pol	Min	Max	Pol	Min	Max	Pol	Min	Max	Pol	Min	Max	Pol	Min	Max
CTAO	-	1.000	100.000	U	1.000	100.000				-	1.000	100.000	-	1.000	100.000
NWAO	+	1.000	100.000	U	1.000	100.000				+	1.000	100.000	-	1.000	100.000
ANTO	-	1.000	100.000	U	1.000	100.000				U	1.000	100.000	-	1.000	100.000
ANMO	+	1.000	100.000	U	1.000	100.000				+	1.000	100.000	U	1.000	100.000
SNZO	-	1.000	100.000	U	1.000	100.000				-	1.000	100.000	U	1.000	100.000

Nepal 29.07.80 ias04 NEIS depth 18km

Latitude 29.59800
Longitude 81.09200

	P			pP			sP			S(N)			S(E)		
	Pol	Min	Max	Pol	Min	Max	Pol	Min	Max	Pol	Min	Max	Pol	Min	Max
NWAO	+	1.000	100.000	U	1.000	100.000				U	1.000	100.000	+	1.000	100.000
ANTO	+	1.000	100.000	U	1.000	100.000				+	1.000	100.000	U	1.000	100.000
BCAO	+	1.000	100.000	U	1.000	100.000				+	1.000	100.000	-	1.000	100.000
GRFO	+	1.000	100.000	U	1.000	100.000				+	1.000	100.000	-	1.000	100.000
CTAO	+	1.000	100.000	U	1.000	100.000				+	1.000	100.000	+	1.000	100.000
MAJO	+	1.000	100.000	U	1.000	100.000				+	1.000	100.000	+	1.000	100.000
TATO	+	1.000	100.000	U	1.000	100.000				U	1.000	100.000	S	1.000	100.000
GUMO	+	1.000	100.000	U	1.000	100.000				+	1.000	100.000	+	1.000	100.000

Algeria 10.10.80 ias05 NEIS depth 10.0km

Latitude 36.19500
Longitude 1.35400

	P			pP			sP			S(N)			S(E)		
	Pol	Min	Max	Pol	Min	Max	Pol	Min	Max	Pol	Min	Max	Pol	Min	Max
ANMO	+	1.000	100.000	U	1.000	100.000				U	1.000	100.000	S	1.000	100.000
BOCO	+	1.000	100.000	U	1.000	100.000				-	1.000	100.000	U	1.000	100.000
BCAO	+	1.000	100.000	U	1.000	100.000				U	1.000	100.000	O	1.000	100.000
ZOBO	+	1.000	100.000	U	1.000	100.000				U	1.000	100.000	S	1.000	100.000
JAS	+	1.000	100.000	U	1.000	100.000				-	1.000	100.000	-	1.000	100.000

Central Mexico 24.10.80 ias06 NEIS depth 72km

Latitude 18.21100
Longitude -98.24000

	P			pP			sP			S(N)			S(E)		
	Pol	Min	Max	Pol	Min	Max	Pol	Min	Max	Pol	Min	Max	Pol	Min	Max
LON	-	1.000	100.000	U	1.000	100.000				-	1.000	100.000	+	1.000	100.000
KONO	-	1.000	100.000	U	1.000	100.000				U	1.000	100.000	O	1.000	100.000
GRFO	-	1.000	100.000	U	1.000	100.000									
ZOBO	-	1.000	100.000	U	1.000	100.000				U	1.000	100.000	-	1.000	100.000

Near coast of Northern California 08.11.80 ias07 NEIS depth 19km

Latitude 41.11700
Longitude -124.25300

	P			pP			sP			S(N)			S(E)		
	Pol	Min	Max	Pol	Min	Max	Pol	Min	Max	Pol	Min	Max	Pol	Min	Max
KONO	-	1.000	100.000	U	1.000	100.000				-	1.000	100.000	-	1.000	100.000
ZOBO	+	1.000	100.000	U	1.000	100.000									
GRFO	-	1.000	100.000	U	1.000	100.000									
BOCO	+	1.000	100.000	U	1.000	100.000				+	1.000	100.000	U	1.000	100.000
GUMO	+	1.000	100.000	U	1.000	100.000				+	1.000	100.000	+	1.000	100.000
MAJO	+	1.000	100.000	U	1.000	100.000				U	1.000	100.000	+	1.000	100.000
TATO	+	1.000	100.000	U	1.000	100.000				+	1.000	100.000	+	1.000	100.000

Southern Italy 23.11.80 ias08 NEIS depth 10km

Latitude 40.91400
Longitude 15.36600

	------- P --------			------- pP -------			------- sP -------			------ S(N) ------			------ S(E) ------		
	Pol	Min	Max	Pol	Min	Max	Pol	Min	Max	Pol	Min	Max	Pol	Min	Max
LON	-	1.000	100.000	U	1.000	100.000				+	1.000	100.000	U	1.000	100.000
MAJO	-	1.000	100.000	U	1.000	100.000				+	1.000	100.000	-	1.000	100.000
TATO	-	1.000	100.000	U	1.000	100.000				+	1.000	100.000	-	1.000	100.000
BCAO	-	1.000	100.000	U	1.000	100.000				+	1.000	100.000	-	1.000	100.000
ANMO	-	1.000	100.000	U	1.000	100.000				+	1.000	100.000	U	1.000	100.000
CHTO	-	1.000	100.000	U	1.000	100.000				U	1.000	100.000	O	1.000	100.000
KAAO	-	1.000	100.000	U	1.000	100.000				U	1.000	100.000	O	1.000	100.000

Near East Coast of Honshu, Japan 18.01.81 ias09 NEIS depth 33km

Latitude 38.64000
Longitude 142.75000

	P			pP			sP			S(N)			S(E)		
	Pol	Min	Max	Pol	Min	Max	Pol	Min	Max	Pol	Min	Max	Pol	Min	Max
KONO	+	1.000	100.000	U	1.000	100.000				-	1.000	100.000	+	1.000	100.000
CTAO	-	1.000	100.000	U	1.000	100.000				-	1.000	100.000	-	1.000	100.000
SNZO	-	1.000	100.000	U	1.000	100.000				U	1.000	100.000	-	1.000	100.000
GRFO	+	1.000	100.000	U	1.000	100.000				U	1.000	100.000	+	1.000	100.000
NWAO	+	1.000	100.000	U	1.000	100.000				U	1.000	100.000	-	1.000	100.000
ANTO	+	1.000	100.000	U	1.000	100.000				+	1.000	100.000			

Sichuan Province, China 23.01.81 iasl0 NEIS depth 33km

Latitude 30.92700
Longitude 101.09800

	P			pP			sP			S(N)			S(E)		
	Pol	Min	Max	Pol	Min	Max	Pol	Min	Max	Pol	Min	Max	Pol	Min	Max
KONO	+	1.000	100.000	U	1.000	100.000				+	1.000	100.000	U	1.000	100.000
MAJO	-	1.000	100.000	U	1.000	100.000				+	1.000	100.000	+	1.000	100.000
CTAO	+	1.000	100.000	U	1.000	100.000				-	1.000	100.000	-	1.000	100.000
NWAO	+	1.000	100.000	U	1.000	100.000				U	1.000	100.000	-	1.000	100.000
BCAO	-	1.000	100.000	U	1.000	100.000				U	1.000	100.000	S	1.000	100.000
GUMO	-	1.000	100.000	U	1.000	100.000				-	1.000	100.000	+	1.000	100.000
ANTO	-	1.000	100.000	U	1.000	100.000				+	1.000	100.000	-	1.000	100.000
GRFO										+	1.000	100.000	-	1.000	100.000

Loyalty Islands Region 06.07.81 iasll 33km

Latitude -22.29300
Longitude 171.74200

	P			pP			sP			S(N)			S(E)		
	Pol	Min	Max	Pol	Min	Max	Pol	Min	Max	Pol	Min	Max	Pol	Min	Max
JAS	+	0.100	100.000	U	0.100	100.000				+	0.100	100.000	-	0.100	100.000
LON	+	0.100	100.000	U	0.100	100.000				+	0.100	100.000	-	0.100	100.000
MAJO	+	0.100	100.000	U	0.100	100.000									
GUMO	+	0.100	100.000	U	0.100	100.000									
TATO	+	0.100	100.000	U	0.100	100.000				+	0.100	100.000	-	0.100	100.000
NWAO	+	0.100	100.000	U	0.100	100.000				+	0.100	100.000	U	0.100	100.000

Easter Island region 28.10.81 ias12 NEIS depth 10.0km

Latitude -37.27200
Longitude -110.64900

	P			pP			sP			S(N)			S(E)		
	Pol	Min	Max	Pol	Min	Max	Pol	Min	Max	Pol	Min	Max	Pol	Min	Max
JAS	-	1.000	100.000	U	1.000	100.000				+	1.000	100.000	-	1.000	100.000
SNZO	+	1.000	100.000	U	1.000	100.000				+	1.000	100.000	+	1.000	100.000
SCP	-	1.000	100.000	U	1.000	100.000				+	1.000	100.000	+	1.000	100.000
AFI	+	1.000	100.000	U	1.000	100.000				U	1.000	100.000	O	1.000	100.000
ALQ	-	1.000	100.000	U	1.000	100.000				+	1.000	100.000	U	1.000	100.000
ZOBO	+	1.000	100.000	U	1.000	100.000				U	1.000	100.000	S	1.000	100.000
ANMO	-	1.000	100.000	U	1.000	100.000				+	1.000	100.000	U	1.000	100.000
CTAO	+	1.000	100.000	U	1.000	100.000				+	1.000	100.000	+	1.000	100.000
BOCO										-	1.000	100.000	+	1.000	100.000
LON										+	1.000	100.000	-	1.000	100.000

Luzon, Philippine Islands 22.11.81 ias13 NEIS depth 24.0km

Latitude 18.75200
Longitude 120.83900

	P			pP			sP			S(N)			S(E)		
	Pol	Min	Max	Pol	Min	Max	Pol	Min	Max	Pol	Min	Max	Pol	Min	Max
ANTO	-	1.000	100.000	U	1.000	100.000				U	1.000	100.000	O	1.000	100.000
NWAO	-	1.000	100.000	U	1.000	100.000				+	1.000	100.000	-	1.000	100.000
GRFO	-	1.000	100.000	U	1.000	100.000									
CTAO	-	1.000	100.000	U	1.000	100.000				+	1.000	100.000	-	1.000	100.000
KONO	-	1.000	100.000	U	1.000	100.000				U	1.000	100.000	+	1.000	100.000
TAU	-	1.000	100.000	U	1.000	100.000				+	1.000	100.000	-	1.000	100.000
SNZO	-	1.000	100.000	U	1.000	100.000				+	1.000	100.000	-	1.000	100.000

E USSR - NE China border region 27.11.81 ias14 NEIS depth 543km

Latitude 42.91300
Longitude 131.07600

	P			pP			sP			S(N)			S(E)		
	Pol	Min	Max	Pol	Min	Max	Pol	Min	Max	Pol	Min	Max	Pol	Min	Max
NWAO	-	6.000	8.000	-	6.000	10.000	+	5.000	9.000	-	1.000	100.000	+	1.000	100.000
ANTO	-	5.000	8.000	-	2.000	6.000	U	1.000	8.000	+	1.000	100.000	-	1.000	100.000
ANMO	+	4.000	6.000	+	2.000	4.000	U	2.000	8.000	U	1.000	100.000	O	1.000	100.000
LON	+	6.000	10.000	+	1.000	8.000	U	2.000	15.000						
CTAO	+	1.000	5.000	-	5.000	13.000	-	2.000	20.000	U	1.000	100.000	+	1.000	100.000
GRFO										+	1.000	100.000	-	1.000	100.000
SNZO										+	1.000	100.000	+	1.000	100.000
ALQ										U	1.000	100.000	O	1.000	100.000
KONO										+	1.000	100.000	-	1.000	100.000
KEV										+	1.000	100.000	-	1.000	100.000
TAU										U	1.000	100.000	+	1.000	100.000

Central Mid-Atlantic Ridge 03.01.82 ias15 NEIS depth 10.0km

Latitude -0.97200
Longitude -21.87000

	P			pP			sP			S(N)			S(E)		
	Pol	Min	Max	Pol	Min	Max	Pol	Min	Max	Pol	Min	Max	Pol	Min	Max
ANMO	-	1.000	100.000	U	1.000	100.000				U	1.000	100.000	S	1.000	100.000
KEV	+	1.000	100.000	U	1.000	100.000									
BOCO	-	1.000	100.000	U	1.000	100.000				-	1.000	100.000	-	1.000	100.000
GRFO	+	1.000	100.000	U	1.000	100.000				U	1.000	100.000	S	1.000	100.000
KONO	+	1.000	100.000	U	1.000	100.000				U	1.000	100.000	S	1.000	100.000
SCP	-	1.000	100.000	U	1.000	100.000				U	1.000	100.000	O	1.000	100.000
TOL	+	1.000	100.000	U	1.000	100.000				U	1.000	100.000	S	1.000	100.000

New Brunswick 09.01.82 ias16 NEIS depth 10.1km

Latitude 46.98400
Longitude -66.65600

	P			pP			sP			S(N)			S(E)		
	Pol	Min	Max	Pol	Min	Max	Pol	Min	Max	Pol	Min	Max	Pol	Min	Max
TOL	+	1.000	100.000	U	1.000	100.000									
KEV	+	1.000	100.000	U	1.000	100.000									
KONO	+	1.000	100.000	U	1.000	100.000				U	1.000	100.000	S	1.000	100.000
GRFO	+	1.000	100.000	U	1.000	100.000									
JAS										U	1.000	100.000	S	1.000	100.000
LON										U	1.000	100.000	S	1.000	100.000
ALQ										U	1.000	100.000	S	1.000	100.000
ANMO										U	1.000	100.000	S	1.000	100.000

Santa Cruz Islands 05.08.82 las17 NEIS depth 30.7km

Latitude -15.59700
Longitude 165.93100

	P			pP			sP			S(N)			S(E)		
	Pol	Min	Max	Pol	Min	Max	Pol	Min	Max	Pol	Min	Max	Pol	Min	Max
TAU	+	1.000	100.000	U	1.000	100.000									
NWAO	-	1.000	100.000	U	1.000	100.000				U	1.000	100.000	S	1.000	100.000
JAS	+	1.000	100.000	U	1.000	100.000				+	1.000	100.000	+	1.000	100.000
LON	+	1.000	100.000	U	1.000	100.000				+	1.000	100.000	+	1.000	100.000
SNZO	+	1.000	100.000	U	1.000	100.000				U	1.000	100.000	O	1.000	100.000
TATO	+	1.000	100.000	U	1.000	100.000				+	1.000	100.000	U	1.000	100.000
GUMO	+	1.000	100.000	U	1.000	100.000				+	1.000	100.000	U	1.000	100.000

South of Honshu, Japan   06.09.82   ias18   NEIS depth 176km : depth used 120km

Latitude 29.32500
Longitude 140.36000

	P			pP			sP			S(N)			S(E)		
	Pol	Min	Max	Pol	Min	Max	Pol	Min	Max	Pol	Min	Max	Pol	Min	Max
SNZO	+	0.000	4.500	+	10.000	15.000	U	0.000	80.000	U	0.000	1.000	S	0.000	1.000
ANMO	-	2.000	30.000	+	2.000	10.000	U	0.000	30.000						
ANTO	-	3.500	45.000	U	0.000	12.000	U	0.000	10.000						
COL	-	1.500	22.000	+	0.000	3.000	+	0.000	5.000	U	0.000	1.000	S	0.000	1.000
CTAO	+	0.000	6.000	+	8.000	25.000	U	0.000	50.000						
GAC	-	4.500	65.000	U	0.000	12.000	U	0.000	10.000						
GDH	-	8.000	100.000	U	0.000	6.000	U	0.000	15.000	U	0.000	1.000	-	0.000	1.000
JAS	-	1.000	40.000	+	5.000	30.000	U	0.000	100.000	U	0.000	1.000	-	0.000	1.000
KEV	-	13.000	150.000	U	0.000	10.000	+	2.000	10.000	U	0.000	1.000	O	0.000	1.000
KONO	-	19.000	210.000	U	0.000	30.000	U	0.000	20.000	U	0.000	1.000	O	0.000	1.000
LON	-	0.500	12.000	U	0.000	1.800	U	0.000	15.000	U	0.000	1.000	S	0.000	1.000

Western Arabian Peninsula 13.12.82 ias19 NEIS depth 5km

Latitude 14.70100
Longitude 44.37900

	P			pP			sP			S(N)			S(E)		
	Pol	Min	Max	Pol	Min	Max	Pol	Min	Max	Pol	Min	Max	Pol	Min	Max
TATO	+	1.000	100.000	U	1.000	100.000				+	1.000	100.000	-	1.000	100.000
NWAO	-	1.000	100.000	U	1.000	100.000				+	1.000	100.000	-	1.000	100.000
MAJO	-	1.000	100.000	U	1.000	100.000				+	1.000	100.000	-	1.000	100.000
SLR	-	1.000	100.000	U	1.000	100.000				U	1.000	100.000	S	1.000	100.000
BCAO	-	1.000	100.000	U	1.000	100.000				U	1.000	100.000	S	1.000	100.000

Southern Xinjiang, China 13.02.83 ias20 NEIS depth 16.1km

Latitude 39.94500
Longitude 75.13500

	P			pP			sP			S(N)			S(E)		
	Pol	Min	Max	Pol	Min	Max	Pol	Min	Max	Pol	Min	Max	Pol	Min	Max
GUMO	+	1.000	100.000	U	1.000	100.000				U	0.100	100.000	O	0.100	100.000
NWAO	-	1.000	100.000	U	1.000	100.000				+	0.100	100.000	+	0.100	100.000
BCAO	+	1.000	100.000	U	1.000	100.000				U	0.100	100.000	O	0.100	100.000
GRFO	+	1.000	100.000	U	1.000	100.000				U	0.100	100.000	O	0.100	100.000
TATO	+	1.000	100.000	U	1.000	100.000				U	0.100	100.000	O	0.100	100.000
CTAO	+	1.000	100.000	U	1.000	100.000				+	0.100	100.000	U	0.100	100.000
MAJO	+	1.000	100.000	U	1.000	100.000									
KONO	+	1.000	100.000	U	1.000	100.000				-	0.100	100.000	+	0.100	100.000
COL										-	0.100	100.000	-	0.100	100.000
RSNT										U	0.100	100.000	S	0.100	100.000

Costa Rica 03.04.83 las21 NEIS depth 37km

Latitude 8.71700
Longitude -83.12300

	P			pP			sP			S(N)			S(E)		
	Pol	Min	Max	Pol	Min	Max	Pol	Min	Max	Pol	Min	Max	Pol	Min	Max
GRFO	+	1.000	100.000	U	1.000	100.000				-	1.000	100.000	+	1.000	100.000
HON	+	1.000	100.000	U	1.000	100.000				+	1.000	100.000	-	1.000	100.000
LON	+	1.000	100.000	U	1.000	100.000				+	1.000	100.000	-	1.000	100.000
KEV	+	1.000	100.000	U	1.000	100.000				-	1.000	100.000	+	1.000	100.000
RSSD	+	1.000	100.000	U	1.000	100.000				U	1.000	100.000	0	1.000	100.000
BER	+	1.000	100.000	U	1.000	100.000				U	1.000	100.000	+	1.000	100.000
TOL	+	1.000	100.000	U	1.000	100.000				U	1.000	100.000	+	1.000	100.000
AFI	+	1.000	100.000	U	1.000	100.000				U	1.000	100.000	S	1.000	100.000
COL	+	1.000	100.000	U	1.000	100.000				U	1.000	100.000	-	1.000	100.000
KONO	+	1.000	100.000	U	1.000	100.000				U	1.000	100.000	+	1.000	100.000
ZOBO	+	1.000	100.000	U	1.000	100.000				U	1.000	100.000	0	1.000	100.000
ANMO	+	1.000	100.000	U	1.000	100.000				U	1.000	100.000	0	1.000	100.000
RSON	+	1.000	100.000	U	1.000	100.000									
RSNY	+	1.000	100.000	U	1.000	100.000									
SCP	+	1.000	100.000	U	1.000	100.000									
GAC	+	1.000	100.000	U	1.000	100.000									

Northern Sumatera 04.04.83 ias22 NEIS depth 78.5km

Latitude 5.72300
Longitude 94.72200

	P			pP			sP			S(N)			S(E)		
	Pol	Min	Max	Pol	Min	Max	Pol	Min	Max	Pol	Min	Max	Pol	Min	Max
ANTO	+	1.000	100.000	U	1.000	100.000				+	1.000	100.000	-	1.000	100.000
GUMO	+	1.000	100.000	U	1.000	100.000				+	1.000	100.000	U	1.000	100.000
BCAO	+	1.000	100.000	U	1.000	100.000				U	1.000	100.000	S	1.000	100.000
NWAO	+	1.000	100.000	U	1.000	100.000				-	1.000	100.000	+	1.000	100.000
GRFO	+	1.000	100.000	U	1.000	100.000				+	1.000	100.000	U	1.000	100.000
SNZO	+	1.000	100.000	U	1.000	100.000				U	1.000	100.000	S	1.000	100.000
CTAO	+	1.000	100.000	U	1.000	100.000				+	1.000	100.000	+	1.000	100.000
KONO	+	1.000	100.000	U	1.000	100.000				+	1.000	100.000	-	1.000	100.000
KEV	+	1.000	100.000	U	1.000	100.000				+	1.000	100.000	-	1.000	100.000
BER	+	1.000	100.000	U	1.000	100.000				+	1.000	100.000	U	1.000	100.000
TATO	+	1.000	100.000	U	1.000	100.000									
MAJO	+	1.000	100.000	U	1.000	100.000									

Near Coast of Venezuela 11.04.83 ias23 NEIS depth 40km

Latitude 10.41900
Longitude -62.76400

	P			pP			sP			S(N)			S(E)		
	Pol	Min	Max	Pol	Min	Max	Pol	Min	Max	Pol	Min	Max	Pol	Min	Max
ANTO	-	1.000	100.000	U	1.000	100.000				-	1.000	100.000	-	1.000	100.000
BCAO	-	1.000	100.000	U	1.000	100.000				U	1.000	100.000	S	1.000	100.000
GRFO	-	1.000	100.000	U	1.000	100.000				-	1.000	100.000	U	1.000	100.000
GAC										U	1.000	100.000	O	1.000	100.000
KONO	-	1.000	100.000	U	1.000	100.000				-	1.000	100.000	U	1.000	100.000
KEV	-	1.000	100.000	U	1.000	100.000				-	1.000	100.000	-	1.000	100.000
TOL	-	1.000	100.000	U	1.000	100.000				-	1.000	100.000	U	1.000	100.000
BER	-	1.000	100.000	U	1.000	100.000				-	1.000	100.000	U	1.000	100.000
ANMO	-	1.000	100.000	U	1.000	100.000									
SCP	-	1.000	100.000	U	1.000	100.000									
COL	-	1.000	100.000	U	1.000	100.000									
LON	-	1.000	100.000	U	1.000	100.000									
HON	-	1.000	100.000	U	1.000	100.000									
RSSD	-	1.000	100.000	U	1.000	100.000									

Southern Iran 18.04.83 ias24 NEIS depth 64 km

Latitude 27.79300
Longitude 62.05400

	P			pP			sP			S(N)			S(E)		
	Pol	Min	Max	Pol	Min	Max	Pol	Min	Max	Pol	Min	Max	Pol	Min	Max
COL	+	1.000	100.000	U	1.000	100.000				+	1.000	100.000	+	1.000	100.000
MAJO	-	1.000	100.000	U	1.000	100.000				+	1.000	100.000	U	1.000	100.000
BCAO	-	1.000	100.000	U	1.000	100.000				+	1.000	100.000	U	1.000	100.000
TOL	+	1.000	100.000	U	1.000	100.000				U	1.000	100.000	S	1.000	100.000
BER	+	1.000	100.000	U	1.000	100.000									
KEV	+	1.000	100.000	U	1.000	100.000				U	1.000	100.000	O	1.000	100.000
KONO	+	1.000	100.000	U	1.000	100.000				-	1.000	100.000	+	1.000	100.000
TATO	-	1.000	100.000	U	1.000	100.000				+	1.000	100.000	U	1.000	100.000
GRFO	+	1.000	100.000	U	1.000	100.000				U	1.000	100.000	O	1.000	100.000
NWAO	-	1.000	100.000	U	1.000	100.000				U	1.000	100.000	O	1.000	100.000
GUMO	-	1.000	100.000	U	1.000	100.000				+	1.000	100.000	U	1.000	100.000

Central California 02.05.83 ias25 NEIS depth 10.2km

Latitude 36.21900
Longitude -120.31700

	P			pP			sP			S(N)			S(E)		
	Pol	Min	Max	Pol	Min	Max	Pol	Min	Max	Pol	Min	Max	Pol	Min	Max
COL	+	1.000	100.000	U	1.000	100.000				U	1.000	100.000	O	1.000	100.000
SCP	-	1.000	100.000	U	1.000	100.000									
KONO	+	1.000	100.000	U	1.000	100.000				U	1.000	100.000	O	1.000	100.000
HON	+	1.000	100.000	U	1.000	100.000				U	1.000	100.000	O	1.000	100.000
MAJO	+	1.000	100.000	U	1.000	100.000				U	1.000	100.000	O	1.000	100.000
ZOBO	+	1.000	100.000	U	1.000	100.000				-	1.000	100.000	-	1.000	100.000
GAC	-	1.000	100.000	U	1.000	100.000				U	1.000	100.000	O	1.000	100.000
AFI	+	1.000	100.000	U	1.000	100.000									
KEV	+	1.000	100.000	U	1.000	100.000				-	1.000	100.000	+	1.000	100.000
RSNY	-	1.000	100.000	U	1.000	100.000									
GUMO										U	1.000	100.000	O	1.000	100.000

Near West Coast of Honshu, Japan 26.05.83 ias26 NEIS depth 23.7km

Latitude 40.46200
Longitude 139.10200

	P			pP			sP			S(N)			S(E)		
	Pol	Min	Max	Pol	Min	Max	Pol	Min	Max	Pol	Min	Max	Pol	Min	Max
COL	+	1.000	100.000	U	1.000	100.000									
RSON	+	1.000	100.000	U	1.000	100.000									
RSNY	+	1.000	100.000	U	1.000	100.000									
RSSD	+	1.000	100.000	U	1.000	100.000									
RSNT	+	1.000	100.000	U	1.000	100.000									
BER	+	1.000	100.000	U	1.000	100.000									
TAU	+	1.000	100.000	U	1.000	100.000				U	1.000	100.000	S	1.000	100.000
AFI	+	1.000	100.000	U	1.000	100.000				U	1.000	100.000	O	1.000	100.000
KEV	+	1.000	100.000	U	1.000	100.000									
HON	+	1.000	100.000	U	1.000	100.000									
JAS	+	1.000	100.000	U	1.000	100.000				U	1.000	100.000	O	1.000	100.000
LON	+	1.000	100.000	U	1.000	100.000				U	1.000	100.000	O	1.000	100.000
CTAO	+	1.000	100.000	U	1.000	100.000				U	1.000	100.000	S	1.000	100.000
KONO	+	1.000	100.000	U	1.000	100.000				U	1.000	100.000	S	1.000	100.000
GAC	+	1.000	100.000	U	1.000	100.000				U	1.000	100.000	S	1.000	100.000
SNZO	+	1.000	100.000	U	1.000	100.000				U	1.000	100.000	O	1.000	100.000
GRFO	+	1.000	100.000	U	1.000	100.000				U	1.000	100.000	S	1.000	100.000
NWAO	+	1.000	100.000	U	1.000	100.000				U	1.000	100.000	O	1.000	100.000
ANTO	+	1.000	100.000	U	1.000	100.000				U	1.000	100.000	S	1.000	100.000
ANMO	+	1.000	100.000	U	1.000	100.000				U	1.000	100.000	S	1.000	100.000

Tonga Islands 01.06.83 las27 NEIS depth 180km

Latitude -17.03800
Longitude -174.60500

	P			pP			sP			S(N)			S(E)		
	Pol	Min	Max	Pol	Min	Max	Pol	Min	Max	Pol	Min	Max	Pol	Min	Max
CTAO	-	5.000	8.000	U	0.000	2.000	+	7.000	16.000	U	0.000	1.000	O	0.000	1.000
ANMO	-	27.000	33.000	+	19.000	43.000	U	0.000	60.000	-	0.000	1.000	U	0.000	1.000
LON	-	20.000	29.000	+	2.000	15.000	U	0.000	40.000						
HON	-	8.000	11.000	U	0.000	10.000	+	7.000	16.000						
LEM	-	18.000	26.000	+	8.000	17.000	U	0.000	60.000						
RSCP	-	20.000	40.000	+	30.000	60.000	U	0.000	120.000						
RSNT	-	11.000	22.000	+	1.000	17.000	U	0.000	30.000						
JAS	-	19.000	27.000	+	0.000	15.000	U	0.000	50.000	-	0.000	1.000	U	0.000	1.000
MAJO	-	12.000	18.000	U	0.000	8.000	+	10.000	40.000						
ZOBO	U	0.000	10.000	+	13.000	27.000	U	0.000	60.000						
NWAO	-	13.000	28.000	+	7.000	28.000	U	0.000	40.000	-	0.000	1.000	+	0.000	1.000

Peru - Brazil Border Region 02.06.83 ias28 NEIS depth 598.6km

Latitude -9.51200
Longitude -71.25900

	P			pP			sP			S(N)			S(E)		
	Pol	Min	Max	Pol	Min	Max	Pol	Min	Max	Pol	Min	Max	Pol	Min	Max
RSCP	-	15.000	20.000	U	1.000	15.000	+	5.000	15.000	-	0.010	100.000	U	0.010	100.000
RSNY	-	9.000	12.000	+	2.000	5.000	+	2.000	12.000	-	0.010	100.000	+	0.010	100.000
GAC	-	20.000	25.000	+	2.000	10.000	+	2.000	40.000	-	0.010	100.000	U	0.010	100.000
ANMO	-	8.000	12.000	+	4.000	8.000	+	1.000	12.000						
RSSD	-	11.000	15.000	+	4.000	7.000	U	2.000	20.000	-	0.010	100.000	+	0.010	100.000
JAS	-	8.000	12.000	+	4.000	7.000	U	1.000	20.000	-	0.010	100.000	+	0.010	100.000
LON	-	5.000	8.000	U	2.000	10.000	U	1.000	10.000	-	0.010	100.000	+	0.010	100.000
TOL	-	7.000	11.000	+	1.000	8.000	+	5.000	12.000	-	0.010	100.000	-	0.010	100.000
RSNT	-	10.000	14.000	+	5.000	8.000	+	2.000	25.000	-	0.010	100.000	+	0.010	100.000
HON	-	1.000	8.000	+	1.000	12.000	U	0.000	10.000						
GRFO	-	5.000	10.000	+	5.000	8.000	+	1.000	8.000						
RSON	-	9.000	12.000	+	2.000	5.000	U	0.000	20.000						
KONO	-	5.000	12.000	+	4.000	7.000	+	2.000	5.000						
AFI	-	1.000	3.000	+	1.000	7.000	U	0.000	22.000						
SNZO	-	9.000	20.000	+	8.000	15.000	U	0.000	20.000						
SLR	-	3.000	6.000	+	5.000	10.000	U	0.000	20.000						

Andreanof Islands, Aleutian Is.   09.06.83   ias29   NEIS depth 20.8km

Latitude 51.41400
Longitude -174.11100

	P			pP			sP			S(N)			S(E)		
	Pol	Min	Max	Pol	Min	Max	Pol	Min	Max	Pol	Min	Max	Pol	Min	Max
RSSD	+	1.000	100.000	U	1.000	100.000				U	1.000	100.000	S	1.000	100.000
JAS	-	1.000	100.000	U	1.000	100.000									
HON	-	1.000	100.000	U	1.000	100.000									
GUMO	+	1.000	100.000	U	1.000	100.000				U	1.000	100.000	O	1.000	100.000
RSNY	+	1.000	100.000	U	1.000	100.000				U	1.000	100.000	S	1.000	100.000
RSNT	+	1.000	100.000	U	1.000	100.000				U	1.000	100.000	S	1.000	100.000
RSCP	+	1.000	100.000	U	1.000	100.000				U	1.000	100.000	S	1.000	100.000
BER	+	1.000	100.000	U	1.000	100.000				U	1.000	100.000	S	1.000	100.000
TOL	+	1.000	100.000	U	1.000	100.000									
KEV	+	1.000	100.000	U	1.000	100.000				U	1.000	100.000	S	1.000	100.000
SCP	+	1.000	100.000	U	1.000	100.000				U	1.000	100.000	+	1.000	100.000
KONO	+	1.000	100.000	U	1.000	100.000									
MAJO	+	1.000	100.000	U	1.000	100.000									
GAC	+	1.000	100.000	U	1.000	100.000				U	1.000	100.000	S	1.000	100.000
TATO	+	1.000	100.000	U	1.000	100.000									
GRFO	+	1.000	100.000	U	1.000	100.000									
LEM										U	1.000	100.000	O	1.000	100.000

Hokkaido, Japan Region   21.06.83   ias30   NEIS depth 9.9km

Latitude   41.34600
Longitude   139.09900

	P			pP			sP			S(N)			S(E)		
	Pol	Min	Max	Pol	Min	Max	Pol	Min	Max	Pol	Min	Max	Pol	Min	Max
RSSD	+	1.000	100.000	U	1.000	100.000				U	1.000	100.000	+	1.000	100.000
RSNT	+	1.000	100.000	U	1.000	100.000				+	1.000	100.000	+	1.000	100.000
LEM	+	1.000	100.000	U	1.000	100.000									
TAU	+	1.000	100.000	U	1.000	100.000				-	1.000	100.000	-	1.000	100.000
KEV	+	1.000	100.000	U	1.000	100.000				U	1.000	100.000	O	1.000	100.000
HON	+	1.000	100.000	U	1.000	100.000									
JAS	+	1.000	100.000	U	1.000	100.000				U	1.000	100.000	+	1.000	100.000
LON	+	1.000	100.000	U	1.000	100.000				+	1.000	100.000	+	1.000	100.000
COL	+	1.000	100.000	U	1.000	100.000				+	1.000	100.000	U	1.000	100.000
CTAO	+	1.000	100.000	U	1.000	100.000									
GAC	+	1.000	100.000	U	1.000	100.000				U	1.000	100.000	O	1.000	100.000
SNZO	+	1.000	100.000	U	1.000	100.000									
NWAO	+	1.000	100.000	U	1.000	100.000									
ANMO	+	1.000	100.000	U	1.000	100.000				+	1.000	100.000	+	1.000	100.000
RSNY	+	1.000	100.000	U	1.000	100.000									
BER	+	1.000	100.000	U	1.000	100.000									
SCP	+	1.000	100.000	U	1.000	100.000									
KONO	+	1.000	100.000	U	1.000	100.000									
GRFO	+	1.000	100.000	U	1.000	100.000									

Taiwan Region 24.06.83 ias31 NEIS depth 44.1km

Latitude 24.17600
Longitude 122.40200

	P			pP			sP			S(N)			S(E)		
	Pol	Min	Max	Pol	Min	Max	Pol	Min	Max	Pol	Min	Max	Pol	Min	Max
KEV	+	1.000	100.000	U	1.000	100.000				U	1.000	100.000	S	1.000	100.000
LEM	-	1.000	100.000	U	1.000	100.000				U	1.000	100.000	S	1.000	100.000
RSNT	+	1.000	100.000	U	1.000	100.000									
BER	+	1.000	100.000	U	1.000	100.000									
TAU	-	1.000	100.000	U	1.000	100.000				U	1.000	100.000	O	1.000	100.000
HON	+	1.000	100.000	U	1.000	100.000				U	1.000	100.000	S	1.000	100.000
LON	+	1.000	100.000	U	1.000	100.000									
COL	+	1.000	100.000	U	1.000	100.000									
KONO	+	1.000	100.000	U	1.000	100.000				U	1.000	100.000	S	1.000	100.000
CTAO	-	1.000	100.000	U	1.000	100.000				U	1.000	100.000	O	1.000	100.000
GRFO	+	1.000	100.000	U	1.000	100.000				U	1.000	100.000	+	1.000	100.000
NWAO	-	1.000	100.000	U	1.000	100.000									
SNZO										-	1.000	100.000	U	1.000	100.000

Southern Alaska 12.07.83 ias32 NEIS depth 37km

Latitude 61.03100
Longitude -147.28600

	P			pP			sP			S(N)			S(E)		
	Pol	Min	Max	Pol	Min	Max	Pol	Min	Max	Pol	Min	Max	Pol	Min	Max
KEV	-	1.000	10.000	U	1.000	100.000				+	1.000	100.000	+	1.000	100.000
RSNY	-	1.000	100.000	U	1.000	100.000				U	1.000	100.000	O	1.000	100.000
RSSD	-	1.000	100.000	U	1.000	100.000				U	1.000	100.000	O	1.000	100.000
RSCP	-	1.000	100.000	U	1.000	100.000				+	1.000	100.000	-	1.000	100.000
BER	-	1.000	100.000	U	1.000	100.000				+	1.000	100.000	+	1.000	100.000
HON	-	1.000	100.000	U	1.000	100.000				U	1.000	100.000	+	1.000	100.000
JAS	-	1.000	100.000	U	1.000	100.000									
KONO	-	1.000	100.000	U	1.000	100.000				+	1.000	100.000	+	1.000	100.000
MAJO	-	1.000	100.000	U	1.000	100.000				U	1.000	100.000	O	1.000	100.000
GAC	-	1.000	100.000	U	1.000	100.000				+	1.000	100.000	U	1.000	100.000
TATO	-	1.000	100.000	U	1.000	100.000				+	1.000	100.000	U	1.000	100.000
GRFO	-	1.000	100.000	U	1.000	100.000				+	1.000	100.000	+	1.000	100.000
ANMO	-	1.000	100.000	U	1.000	100.000				+	1.000	100.000	U	1.000	100.000

Aegean Sea 06.08.83 ias33 NEIS depth 2.4km

Latitude 40.14200
Longitude 24.76600

	P			pP			sP			S(N)			S(E)		
	Pol	Min	Max	Pol	Min	Max	Pol	Min	Max	Pol	Min	Max	Pol	Min	Max
RSNY	-	1.000	100.000	U	1.000	100.000				+	1.000	100.000	-	1.000	100.000
RSSD	+	1.000	100.000	U	1.000	100.000				+	1.000	100.000	-	1.000	100.000
RSCP	-	1.000	100.000	U	1.000	100.000				+	1.000	100.000	-	1.000	100.000
RSNT	+	1.000	100.000	U	1.000	100.000				+	1.000	100.000	-	1.000	100.000
SLR	+	1.000	100.000	U	1.000	100.000				U	1.000	100.000	O	1.000	100.000
KEV	+	1.000	100.000	U	1.000	100.000									
LON	+	1.000	100.000	U	1.000	100.000				U	1.000	100.000	O	1.000	100.000
COL	+	1.000	100.000	U	1.000	100.000				+	1.000	100.000	-	1.000	100.000
SCP	-	1.000	100.000	U	1.000	100.000				+	1.000	100.000	-	1.000	100.000
MAJO	+	1.000	100.000	U	1.000	100.000				+	1.000	100.000	U	1.000	100.000
GAC	-	1.000	100.000	U	1.000	100.000				+	1.000	100.000	-	1.000	100.000
TATO	+	1.000	100.000	U	1.000	100.000				U	1.000	100.000	+	1.000	100.000

Near East Coast of Kamchatka 17.08.83 ias34 NEIS depth 62.6km

Latitude 55.86700
Longitude 161.28700

	P			pP			sP			S(N)			S(E)		
	Pol	Min	Max	Pol	Min	Max	Pol	Min	Max	Pol	Min	Max	Pol	Min	Max
RSSD	+	1.000	100.000	U	1.000	100.000									
RSNT	+	1.000	100.000	U	1.000	100.000									
HON	+	1.000	100.000	U	1.000	100.000				U	1.000	100.000	O	1.000	100.000
SCP	+	1.000	100.000	U	1.000	100.000									
RSNY	+	1.000	100.000	U	1.000	100.000									
BER	+	1.000	100.000	U	1.000	100.000				U	1.000	100.000	S	1.000	100.000
LEM	+	1.000	100.000	U	1.000	100.000				U	1.000	100.000	S	1.000	100.000
TOL	+	1.000	100.000	U	1.000	100.000				-	1.000	100.000	-	1.000	100.000
AFI	+	1.000	100.000	U	1.000	100.000				U	1.000	100.000	O	1.000	100.000
JAS	+	1.000	100.000	U	1.000	100.000				U	1.000	100.000	+	1.000	100.000
LON	+	1.000	100.000	U	1.000	100.000				U	1.000	100.000	+	1.000	100.000
KONO	+	1.000	100.000	U	1.000	100.000				U	1.000	100.000	S	1.000	100.000
CTAO	+	1.000	100.000	U	1.000	100.000				-	1.000	100.000	U	1.000	100.000
GAC	+	1.000	100.000	U	1.000	100.000									
TATO	+	1.000	100.000	U	1.000	100.000				U	1.000	100.000	S	1.000	100.000
GRFO	+	1.000	100.000	U	1.000	100.000				U	1.000	100.000	S	1.000	100.000
ANMO	+	1.000	100.000	U	1.000	100.000				U	1.000	100.000	S	1.000	100.000

Southern Alaska 07.09.83 ias35 NEIS depth 45km

Latitude 60.97600
Longitude -147.50000

	------- P --------			------- pP -------			------- sP -------			------ S(N) ------			------ S(E) ------		
	Pol	Min	Max	Pol	Min	Max	Pol	Min	Max	Pol	Min	Max	Pol	Min	Max
RSCP	-	1.000	100.000	+	1.000	100.000				+	1.000	100.000	-	1.000	100.000
KONO	-	1.000	100.000	U	1.000	100.000				+	1.000	100.000	+	1.000	100.000
GAC	-	1.000	100.000	U	1.000	100.000				+	1.000	100.000	-	1.000	100.000
BOCO	-	1.000	100.000	U	1.000	100.000				+	1.000	100.000	-	1.000	100.000
RSSD	-	1.000	100.000	U	1.000	100.000				U	1.000	100.000	O	1.000	100.000
BER	-	1.000	100.000	U	1.000	100.000				+	1.000	100.000	U	1.000	100.000
TOL	-	1.000	100.000	+	1.000	100.000				+	1.000	100.000	U	1.000	100.000
JAS	-	1.000	100.000	U	1.000	100.000				U	1.000	100.000	O	1.000	100.000
MAJO	-	1.000	100.000	U	1.000	100.000				U	1.000	100.000	O	1.000	100.000
TATO	-	1.000	100.000	U	1.000	100.000				+	1.000	100.000	U	1.000	100.000
ANMO	-	1.000	100.000	U	1.000	100.000				U	1.000	100.000	O	1.000	100.000
AFI	-	1.000	100.000	U	1.000	100.000									
HON	-	1.000	100.000	U	1.000	100.000									

Afghanistan - USSR border   12.09.83   ias36   Depth (NEIS) 208.8km

Latitude 36.50200
Longitude 71.08200

	P			pP			sP			S(N)			S(E)		
	Pol	Min	Max	Pol	Min	Max	Pol	Min	Max	Pol	Min	Max	Pol	Min	Max
COL	+	18.000	20.000	-	12.000	25.000	U	0.000	40.000	-	0.000	1.000	U	0.000	1.000
SLR	+	12.000	17.000	-	2.000	16.000	U	0.000	8.000						
RSNT	+	15.000	17.000	-	8.000	22.000	U	0.000	60.000	-	0.000	1.000	-	0.000	1.000
GAC	+	9.000	11.000	-	0.000	16.000	U	0.000	15.000						
MAJO	+	28.000	30.000	U	0.000	20.000	U	0.000	30.000	-	0.000	1.000	+	0.000	1.000
TOL	+	5.000	9.000	-	0.000	17.000	U	0.000	8.000						
LEM	+	9.000	14.000	U	0.000	8.000	-	15.000	40.000						
TATO	+	14.000	16.000	-	0.000	15.000	-	11.000	34.000	+	0.000	1.000	+	0.000	1.000
KONO	+	4.000	6.000	U	0.000	30.000	U	0.000	100.000						
BCAO										-	0.000	1.000	-	0.000	1.000
LON										-	0.000	1.000	-	0.000	1.000

Near Coat of Northern Chile 04.10.83 ias37 Depth (NEIS) 14.8km

Latitude -26.53500
Longitude -70.56300

	P			pP			sP			S(N)			S(E)		
	Pol	Min	Max	Pol	Min	Max	Pol	Min	Max	Pol	Min	Max	Pol	Min	Max
RSCP	+	1.000	100.000	U	1.000	100.000				+	1.000	100.000	+	1.000	100.000
JAS	+	1.000	100.000	U	1.000	100.000				+	1.000	100.000	+	1.000	100.000
SCP	+	1.000	100.000	U	1.000	100.000				+	1.000	100.000	+	1.000	100.000
BOCO	+	1.000	100.000	U	1.000	100.000				+	1.000	100.000	+	1.000	100.000
ANMO	+	1.000	100.000	U	1.000	100.000				+	1.000	100.000	+	1.000	100.000
SNZO	+	1.000	100.000	U	1.000	100.000				U	1.000	100.000	O	1.000	100.000
RSON	+	1.000	100.000	U	1.000	100.000				U	1.000	100.000	S	1.000	100.000
RSNY	+	1.000	100.000	U	1.000	100.000				U	1.000	100.000	S	1.000	100.000
RSSD	+	1.000	100.000	U	1.000	100.000				U	1.000	100.000	S	1.000	100.000
LON	+	1.000	100.000	U	1.000	100.000				U	1.000	100.000	S	1.000	100.000
TOL	+	1.000	100.000	U	1.000	100.000									
SLR	+	1.000	100.000	U	1.000	100.000									
GAC	+	1.000	100.000	U	1.000	100.000									

Near Coast of Northern Chile   04.10.83   las38   Depth (NEIS) 16.1km

Latitude   -26.13500
Longitude   -70.51800

	P			pP			sP			S(N)			S(E)		
	Pol	Min	Max	Pol	Min	Max	Pol	Min	Max	Pol	Min	Max	Pol	Min	Max
JAS	+	1.000	100.000	U	1.000	100.000				+	1.000	100.000	+	1.000	100.000
SCP	+	1.000	100.000	U	1.000	100.000				+	1.000	100.000	+	1.000	100.000
BOCO	+	1.000	100.000	U	1.000	100.000				U	1.000	100.000	S	1.000	100.000
ANMO	+	1.000	100.000	U	1.000	100.000				+	1.000	100.000	+	1.000	100.000
RSNY	+	1.000	100.000	U	1.000	100.000				+	1.000	100.000	+	1.000	100.000
RSSD	+	1.000	100.000	U	1.000	100.000				U	1.000	100.000	S	1.000	100.000
LON	+	1.000	100.000	U	1.000	100.000				+	1.000	100.000	U	1.000	100.000
RSCP	+	1.000	100.000	U	1.000	100.000				U	1.000	100.000	S	1.000	100.000
SLR	+	1.000	100.000	U	1.000	100.000				+	1.000	100.000	U	1.000	100.000
GAC	+	1.000	100.000	U	1.000	100.000				U	1.000	100.000	S	1.000	100.000
TOL	+	1.000	100.000	U	1.000	100.000									
SNZO	+	1.000	100.000	U	1.000	100.000									

North Atlantic Ocean 17.10.83 ias39 NEIS depth 10km

Latitude 37.58800
Longitude -17.52000

	P			pP			sP			S(N)			S(E)		
	Pol	Min	Max	Pol	Min	Max	Pol	Min	Max	Pol	Min	Max	Pol	Min	Max
GDH	-	1.000	100.000	U	1.000	100.000				+	1.000	100.000	U	1.000	100.000
KONO	+	1.000	100.000	U	1.000	100.000									
ZOBO	+	1.000	100.000	U	1.000	100.000				U	1.000	100.000	+	1.000	100.000
SLR	-	1.000	100.000	U	1.000	100.000				-	1.000	100.000	+	1.000	100.000
BDF	+	1.000	100.000	U	1.000	100.000				U	1.000	100.000	S	1.000	100.000
RSNY	-	1.000	100.000	U	1.000	100.000				U	1.000	100.000	S	1.000	100.000
RSSD	-	1.000	100.000	U	1.000	100.000				U	1.000	100.000	S	1.000	100.000
RSNT	-	1.000	100.000	U	1.000	100.000				U	1.000	100.000	S	1.000	100.000
RSCP	-	1.000	100.000	U	1.000	100.000				U	1.000	100.000	S	1.000	100.000
JAS	-	1.000	100.000	U	1.000	100.000									
LON	-	1.000	100.000	U	1.000	100.000				U	1.000	100.000	S	1.000	100.000
COL	-	1.000	100.000	U	1.000	100.000				U	1.000	100.000	-	1.000	100.000
SCP	-	1.000	100.000	U	1.000	100.000				U	1.000	100.000	S	1.000	100.000
GAC	-	1.000	100.000	U	1.000	100.000				U	1.000	100.000	S	1.000	100.000
ANMO	-	1.000	100.000	U	1.000	100.000				U	1.000	100.000	S	1.000	100.000

South Sandwich Islands Region 22.10.83 ias 40 NEIS depth 24km

Latitude -60.66500
Longitude -25.45100

	P			pP			sP			S(N)			S(E)		
	Pol	Min	Max	Pol	Min	Max	Pol	Min	Max	Pol	Min	Max	Pol	Min	Max
BDF	+	1.000	100.000	U	1.000	100.000				U	1.000	100.000	+	1.000	100.000
SLR	-	1.000	100.000	U	1.000	100.000				+	1.000	100.000	+	1.000	100.000
ZOBO	+	1.000	100.000	U	1.000	100.000									
NWAO	-	1.000	100.000	U	1.000	100.000				U	1.000	100.000	S	1.000	100.000

Turkey 30.10.83 ias41 NEIS depth 11.6km

Latitude 40.33000
Longitude 42.18700

	P			pP			sP			S(N)			S(E)		
	Pol	Min	Max	Pol	Min	Max	Pol	Min	Max	Pol	Min	Max	Pol	Min	Max
KONO	-	1.000	100.000	U	1.000	100.000									
TOL	+	1.000	100.000	U	1.000	100.000				U	1.000	100.000	O	1.000	100.000
SLR	-	1.000	100.000	U	1.000	100.000				-	1.000	100.000	-	1.000	100.000
MAJO	+	1.000	100.000	U	1.000	100.000				-	1.000	100.000	-	1.000	100.000
COL	-	1.000	100.000	U	1.000	100.000									
LEM	+	1.000	100.000	U	1.000	100.000									
RSCP	-	1.000	100.000	U	1.000	100.000									
TATO	+	1.000	100.000	U	1.000	100.000				U	1.000	100.000	-	1.000	100.000
RSNY	-	1.000	100.000	U	1.000	100.000				-	1.000	100.000	+	1.000	100.000
RSSD	-	1.000	100.000	U	1.000	100.000									
RSNT	-	1.000	100.000	U	1.000	100.000				-	1.000	100.000	U	1.000	100.000
BER	-	1.000	100.000	U	1.000	100.000				U	1.000	100.000	-	1.000	100.000
GDH	-	1.000	100.000	U	1.000	100.000				-	1.000	100.000	-	1.000	100.000
SCP	-	1.000	100.000	U	1.000	100.000				-	1.000	100.000	+	1.000	100.000
GAC	-	1.000	100.000	U	1.000	100.000				-	1.000	100.000	U	1.000	100.000

Hawaii 16.11.83 ias42 NEIS depth 12km

Latitude 19.43000
Longitude -155.45400

	P			pP			sP			S(N)			S(E)		
	Pol	Min	Max	Pol	Min	Max	Pol	Min	Max	Pol	Min	Max	Pol	Min	Max
RSNY	-	1.000	100.000	U	1.000	100.000				+	1.000	100.000	U	1.000	100.000
RSNT	+	1.000	100.000	U	1.000	100.000				+	1.000	100.000	-	1.000	100.000
TAU	+	1.000	100.000	U	1.000	100.000				U	1.000	100.000	O	1.000	100.000
SNZO	-	1.000	100.000	U	1.000	100.000				U	1.000	100.000	O	1.000	100.000
RSSD	-	1.000	100.000	U	1.000	100.000				+	1.000	100.000	U	1.000	100.000
GDH	+	1.000	100.000	U	1.000	100.000				+	1.000	100.000	U	1.000	100.000
AFI	-	1.000	100.000	U	1.000	100.000				U	1.000	100.000	O	1.000	100.000
COL	+	1.000	100.000	U	1.000	100.000				U	1.000	100.000	S	1.000	100.000
SCP	-	1.000	100.000	U	1.000	100.000				+	1.000	100.000	U	1.000	100.000
MAJO	+	1.000	100.000	U	1.000	100.000				+	1.000	100.000	U	1.000	100.000
ZOBO	-	1.000	100.000	U	1.000	100.000									
CTAO	+	1.000	100.000	U	1.000	100.000				U	1.000	100.000	O	1.000	100.000
GAC	-	1.000	100.000	U	1.000	100.000				+	1.000	100.000	+	1.000	100.000
TATO	+	1.000	100.000	U	1.000	100.000				+	1.000	100.000	+	1.000	100.000
GUMO	+	1.000	100.000	U	1.000	100.000				U	1.000	100.000	S	1.000	100.000
BOCO	-	1.000	100.000	U	1.000	100.000				+	1.000	100.000	+	1.000	100.000
ANMO	-	1.000	100.000	U	1.000	100.000				+	1.000	100.000	U	1.000	100.000
LON										+	1.000	100.000	-	1.000	100.000

Banda Sea 24.11.83 ias43 NEIS depth 178.5km

Latitude -7.48100
Longitude 128.16700

	P			pP			sP			S(N)			S(E)		
	Pol	Min	Max	Pol	Min	Max	Pol	Min	Max	Pol	Min	Max	Pol	Min	Max
TATO	+	10.000	20.000	U	0.100	30.000	-	5.000	50.000	U	1.000	100.000	O	1.000	100.000
HON	+	1.000	10.000	-	10.000	20.000				U	1.000	100.000	S	1.000	100.000
TAU	+	1.000	100.000	U	1.000	100.000				U	1.000	100.000	O	1.000	100.000
AFI	+	1.000	100.000	-	1.000	100.000									
MAJO	+	1.000	100.000	U	1.000	100.000				+	1.000	100.000	U	1.000	100.000
SNZO	+	1.000	100.000	U	1.000	100.000				U	1.000	100.000	O	1.000	100.000
NWAO	+	1.000	100.000	U	1.000	100.000									
GUMO	+	1.000	100.000	U	1.000	100.000									

Chagos Archipelago Region 30.11.83 ias44 NEIS depth 10km

Latitude -6.85200
Longitude 72.11000

	P			pP			sP			S(N)			S(E)		
	Pol	Min	Max	Pol	Min	Max	Pol	Min	Max	Pol	Min	Max	Pol	Min	Max
KEV	-	1.000	100.000	U	1.000	100.000				-	1.000	100.000	+	1.000	100.000
MAJO	-	1.000	100.000	U	1.000	100.000				+	1.000	100.000	-	1.000	100.000
KONO	-	1.000	100.000	U	1.000	100.000				U	1.000	100.000	+	1.000	100.000
GUMO	-	1.000	100.000	U	1.000	100.000				+	1.000	100.000	U	1.000	100.000
GRFO	-	1.000	100.000	U	1.000	100.000				U	1.000	100.000	+	1.000	100.000
TAU	-	1.000	100.000	U	1.000	100.000				U	1.000	100.000	S	1.000	100.000
SLR	-	1.000	100.000	U	1.000	100.000				U	1.000	100.000	O	1.000	100.000
TATO	-	1.000	100.000	U	1.000	100.000				U	1.000	100.000	O	1.000	100.000
BCAO	-	1.000	100.000	U	1.000	100.000				U	1.000	100.000	O	1.000	100.000
CTAO	-	1.000	100.000	U	1.000	100.000									
NWAO	-	1.000	100.000	U	1.000	100.000									

Northwest Africa 22.12.83 ias45 NEIS depth 11.3km

Latitude 11.86600
Longitude -13.52900

	P			pP			sP			S(N)			S(E)		
	Pol	Min	Max	Pol	Min	Max	Pol	Min	Max	Pol	Min	Max	Pol	Min	Max
KEV	-	1.000	100.000	U	1.000	100.000				-	1.000	100.000	-	1.000	100.000
BCAO	-	1.000	100.000	U	1.000	100.000				+	1.000	100.000	-	1.000	100.000
RSSD	-	1.000	100.000	U	1.000	100.000				U	1.000	100.000	S	1.000	100.000
BDF	-	1.000	100.000	U	1.000	100.000				U	1.000	100.000	S	1.000	100.000
KONO	-	1.000	100.000	U	1.000	100.000				U	1.000	100.000	S	1.000	100.000
RSCP	-	1.000	100.000	U	1.000	100.000				U	1.000	100.000	S	1.000	100.000
GRFO	-	1.000	100.000	U	1.000	100.000				U	1.000	100.000	S	1.000	100.000
ANMO	-	1.000	100.000	U	1.000	100.000				U	1.000	100.000	S	1.000	100.000
RSNT	-	1.000	100.000	U	1.000	100.000									
GDH	-	1.000	100.000	U	1.000	100.000									
SCP	-	1.000	100.000	U	1.000	100.000									

Hindu Kush Region 30.12.83 ias46 NEIS depth 214.5km

Latitude 36.37200
Longitude 70.73800

	P			pP			sP			S(N)			S(E)		
	Pol	Min	Max	Pol	Min	Max	Pol	Min	Max	Pol	Min	Max	Pol	Min	Max
KONO	+	10.000	100.000	U	0.000	10.000	U	10.000	100.000	U	1.000	100.000	O	1.000	100.000
GUMO	+	6.000	10.000	-	7.000	18.000				+	1.000	100.000	+	1.000	100.000
RSNT	+	10.000	100.000	U	0.000	10.000	U	10.000	100.000	U	1.000	100.000	-	1.000	100.000
GDH	+	10.000	100.000	U	0.000	10.000	U	10.000	100.000	U	1.000	100.000	O	1.000	100.000
KEV	+	10.000	100.000	U	0.000	10.000	U	10.000	100.000	U	1.000	100.000	O	1.000	100.000
COL	+	10.000	100.000	U	0.000	10.000	U	10.000	100.000						
TATO	+	1.000	100.000	U	1.000	100.000				U	1.000	100.000	S	1.000	100.000
GRFO	+	1.000	100.000	U	1.000	100.000									
NWAO	+	1.000	100.000	U	1.000	100.000				U	1.000	100.000	+	1.000	100.000
BCAO	+	1.000	100.000	U	1.000	100.000									

Near S Coast of Honshu, Japan 01.01.84 las47 NEIS depth 374.2km

Latitude 33.40400
Longitude 137.32200

	P			pP			sP			S(N)			S(E)		
	Pol	Min	Max	Pol	Min	Max	Pol	Min	Max	Pol	Min	Max	Pol	Min	Max
KONO	+	8.000	12.000	-	4.000	7.000	U	0.000	25.000	+	1.000	100.000	-	1.000	100.000
RSSD	+	11.000	14.000	+	2.000	7.000	U	0.000	35.000	U	1.000	100.000	0	1.000	100.000
RSNT	+	9.000	12.000	+	1.000	3.000	U	0.000	30.000	U	1.000	100.000	S	1.000	100.000
KEV	+	10.000	14.000	-	2.000	5.000	U	1.500	20.000	+	1.000	100.000	-	1.000	100.000
HON	+	5.000	8.000	+	1.000	2.500	U	1.000	25.000						
JAS	+	5.000	8.000	+	1.500	4.000	U	0.000	25.000	+	1.000	100.000	-	1.000	100.000
LON	+	6.000	8.000	+	1.000	6.000	U	2.000	25.000						
CTAO	+	6.000	10.000	U	1.000	30.000	U	1.000	20.000	U	1.000	100.000	+	1.000	100.000
GRFO										+	1.000	100.000	-	1.000	100.000
NWAO										-	1.000	100.000	+	1.000	100.000
COL										-	1.000	100.000	U	1.000	100.000
SNZO										U	1.000	100.000	+	1.000	100.000
ANMO										U	1.000	100.000	0	1.000	100.000

Solomon Islands 07.02.84 ias48 NEIS depth 14.2km

Latitude -9.92400
Longitude 160.45500

	P			pP			sP			S(N)			S(E)		
	Pol	Min	Max	Pol	Min	Max	Pol	Min	Max	Pol	Min	Max	Pol	Min	Max
TAU	+	1.000	100.000	U	1.000	100.000				U	1.000	100.000	O	1.000	100.000
TATO	-	1.000	100.000	U	1.000	100.000				U	1.000	100.000	S	1.000	100.000
COL	+	1.000	100.000	U	1.000	100.000				U	1.000	100.000	O	1.000	100.000
NWAO	-	1.000	100.000	U	1.000	100.000				U	1.000	100.000	S	1.000	100.000
HON	+	1.000	100.000	U	1.000	100.000									
GUMO	-	1.000	100.000	U	1.000	100.000									
JAS	+	1.000	100.000	U	1.000	100.000				U	1.000	100.000	O	1.000	100.000
LON	+	1.000	100.000	U	1.000	100.000				U	1.000	100.000	O	1.000	100.000
SNZO	+	1.000	100.000	U	1.000	100.000									

Mindanao, Philippine Islands 05.03.84 ias49 NEIS depth 650.6km

Latitude 8.13600
Longitude 123.76500

	------- P --------			------- pP -------			------- sP -------			------ S(N) ------			------ S(E) ------		
	Pol	Min	Max	Pol	Min	Max	Pol	Min	Max	Pol	Min	Max	Pol	Min	Max
KONO	-	9.000	11.000	+	2.000	5.000	+	5.000	12.000						
GRFO	-	9.000	12.000	+	1.000	5.000	+	2.000	10.000						
SNZO	+	4.000	6.000	+	5.000	12.000	U	0.000	45.000	U	1.000	100.000	O	1.000	100.000
NWAO	+	10.000	30.000	+	10.000	40.000	U	5.000	50.000	U	1.000	100.000	S	1.000	100.000
RSNT	-	8.000	11.000	+	3.000	7.000	+	2.000	10.000						
COL	-	10.000	12.000	+	1.000	3.000	+	4.000	15.000	U	1.000	100.000	S	1.000	100.000

Uzbek SSR 19.03.84 ias50 NEIS depth 25.8km

Latitude 40.28800
Longitude 63.33300

	P			pP			sP			S(N)			S(E)		
	Pol	Min	Max	Pol	Min	Max	Pol	Min	Max	Pol	Min	Max	Pol	Min	Max
TOL	+	1.000	100.000	U	1.000	100.000				+	1.000	100.000	U	1.000	100.000
SLR	+	1.000	100.000	U	1.000	100.000				U	1.000	100.000	S	1.000	100.000
KEV	+	1.000	100.000	U	1.000	100.000				U	1.000	100.000	O	1.000	100.000
GAC	+	1.000	100.000	U	1.000	100.000				U	1.000	100.000	S	1.000	100.000
GRFO	+	1.000	100.000	U	1.000	100.000				U	1.000	100.000	S	1.000	100.000
NWAO	+	1.000	100.000	U	1.000	100.000				U	1.000	100.000	O	1.000	100.000
GUMO	+	1.000	100.000	U	1.000	100.000				U	1.000	100.000	O	1.000	100.000
GDH	+	1.000	100.000	U	1.000	100.000									
COL	+	1.000	100.000	U	1.000	100.000									

Kuril Islands 24.03.84 ias51 NEIS depth 43.0km

Latitude 44.16200
Longitude 148.28900

	P			pP			sP			S(N)			S(E)		
	Pol	Min	Max	Pol	Min	Max	Pol	Min	Max	Pol	Min	Max	Pol	Min	Max
AFI	-	1.000	100.000	U	1.000	100.000									
CTAO	+	1.000	100.000	U	1.000	100.000									
ANMO	+	1.000	100.000	U	1.000	100.000									
SNZO	+	1.000	100.000	U	1.000	100.000									
KEV	+	1.000	100.000	U	1.000	100.000									
NWAO	+	1.000	100.000	U	1.000	100.000									
COL	+	1.000	100.000	U	1.000	100.000									
LON	+	1.000	100.000	U	1.000	100.000									
GRFO	+	1.000	100.000	U	1.000	100.000									
TAU	+	1.000	100.000	U	1.000	100.000									
BER	+	1.000	100.000	U	1.000	100.000									
GDH	+	1.000	100.000	U	1.000	100.000									
RSNY	+	1.000	100.000	U	1.000	100.000									
GAC	+	1.000	100.000	U	1.000	100.000									
RSCP	+	1.000	100.000	U	1.000	100.000									
RSON	+	1.000	100.000	U	1.000	100.000									
RSSD	+	1.000	100.000	U	1.000	100.000									
RSNT	+	1.000	100.000	U	1.000	100.000									

THIS PAGE LEFT BLANK INTENTIONALLY

APPENDIX B

SEISMOGRAMS AND GRAPHICAL SUMMARY OF RESULTS

NOTE

Appendix B presents a graphical summary of the siesmograms available and the results obtained from RAMP for each of the IASPEI list earthquakes. For each earthquake the following graphics are shown:-

(a) The stations used, plotted on a lower focal hemisphere projection, and the relevant portions of the long period seismograms taken from each. The vertical component seismograms (labelled "V") supply *P*, and sometimes *pP* and *sP* observations, while the east-west ("E") and north-south ("N") component seismograms supply observations of the direct *S* wave.

(b) A source type plot, showing the proportion of orientation space in which each source type tested is compatible with all the observations.

(c) A vectorplot, showing those orientations in which the double couple source type is compatible with all the observations.

(d) The fault plane solution of Needham (1985), derived from *P* wave first motion observations.

(e) The solution derived by Ekström et al (1987), using the CMT method. The dashed lines show the nodal planes of their "best double couple"; the solid lines show the nodal surfaces for their "best solution". The shaded areas show regions of positive *P* wave first motion.

(f) The solution derived by Sipkin (1987), using the MSE method. Dashed and solid lines once again represent the nodal surfaces of the "best double couple" and "best solution".

(a)

IASPEI event 1

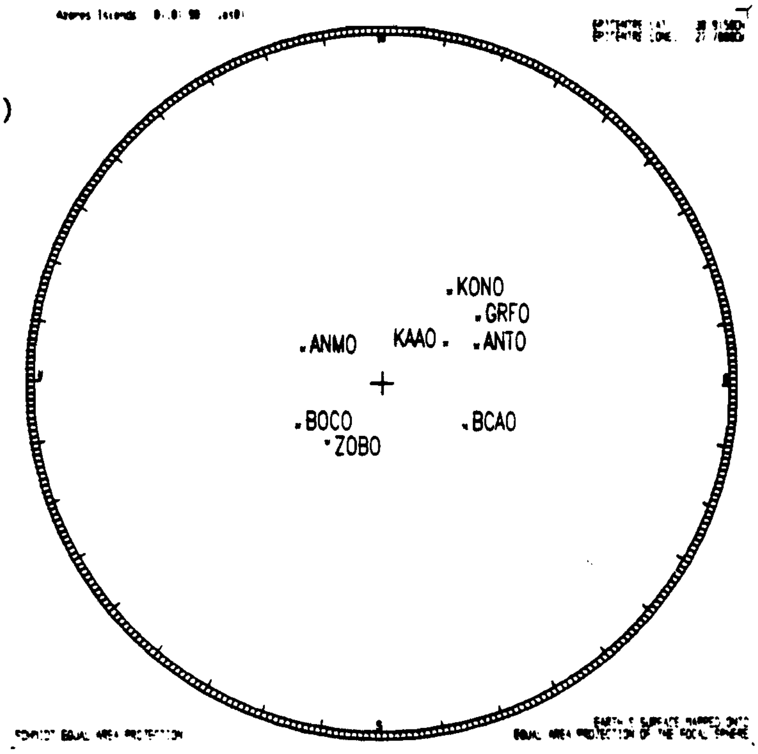

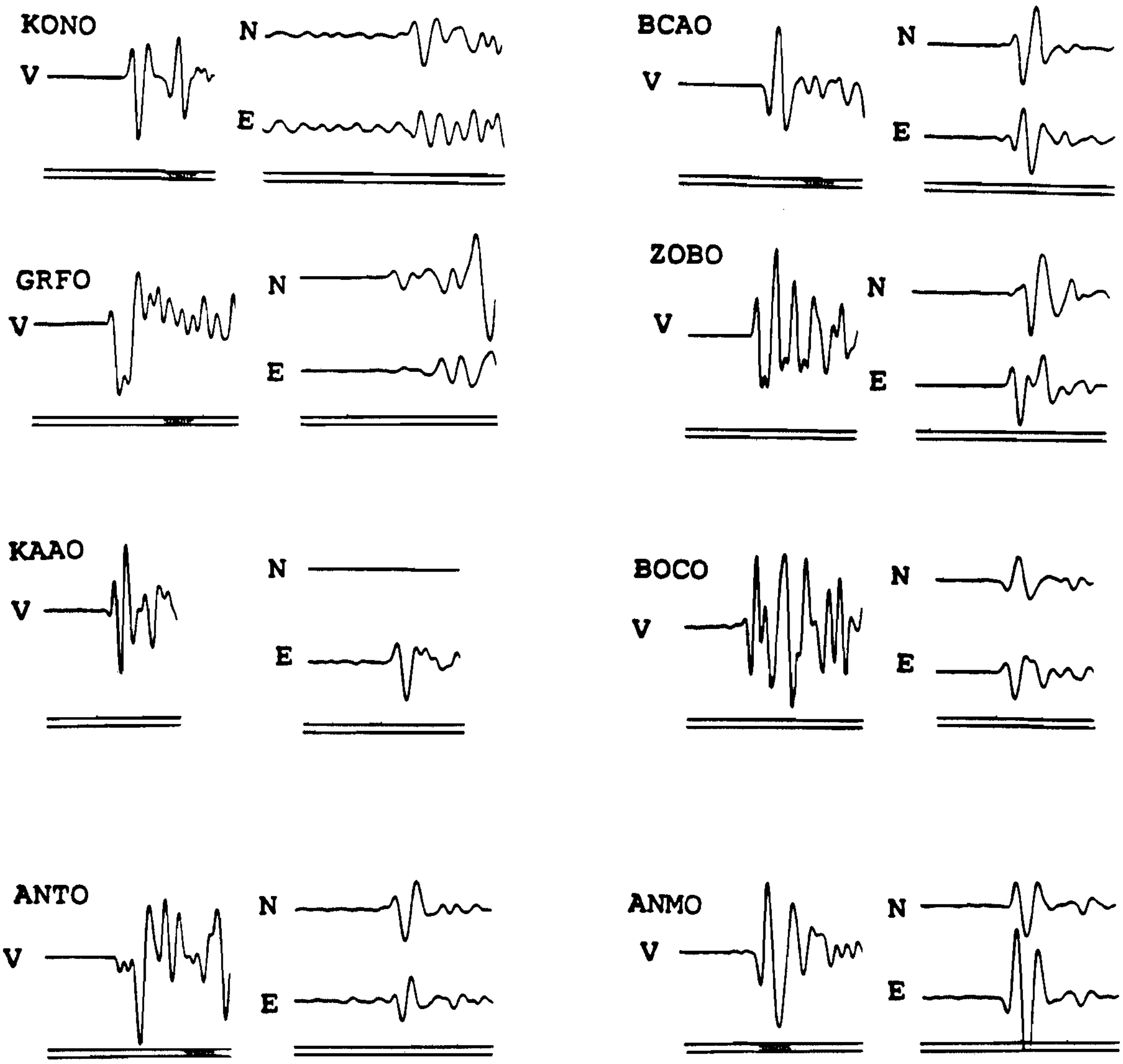

IASPEI
event 1

(b)

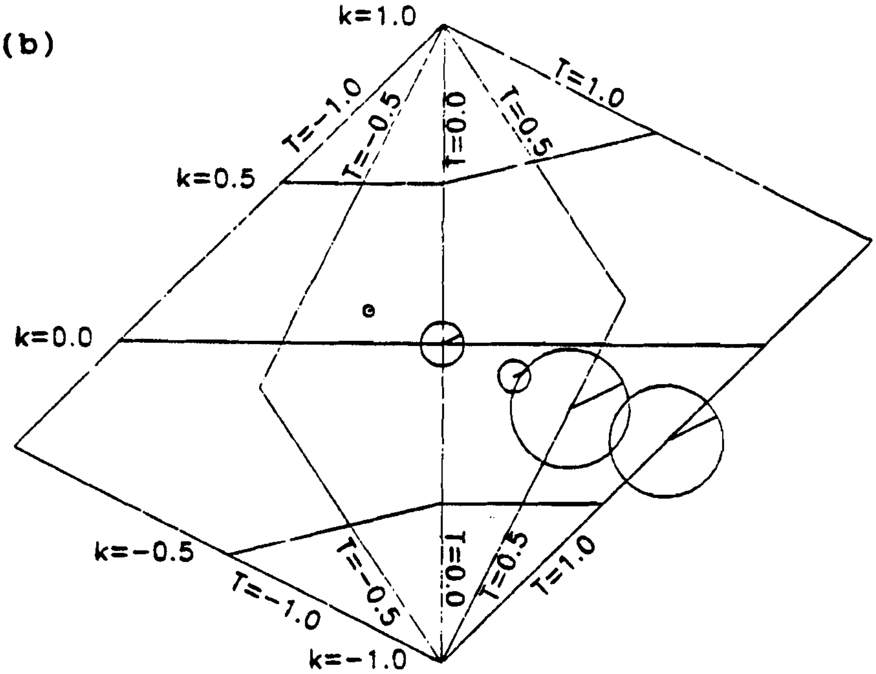

(c)

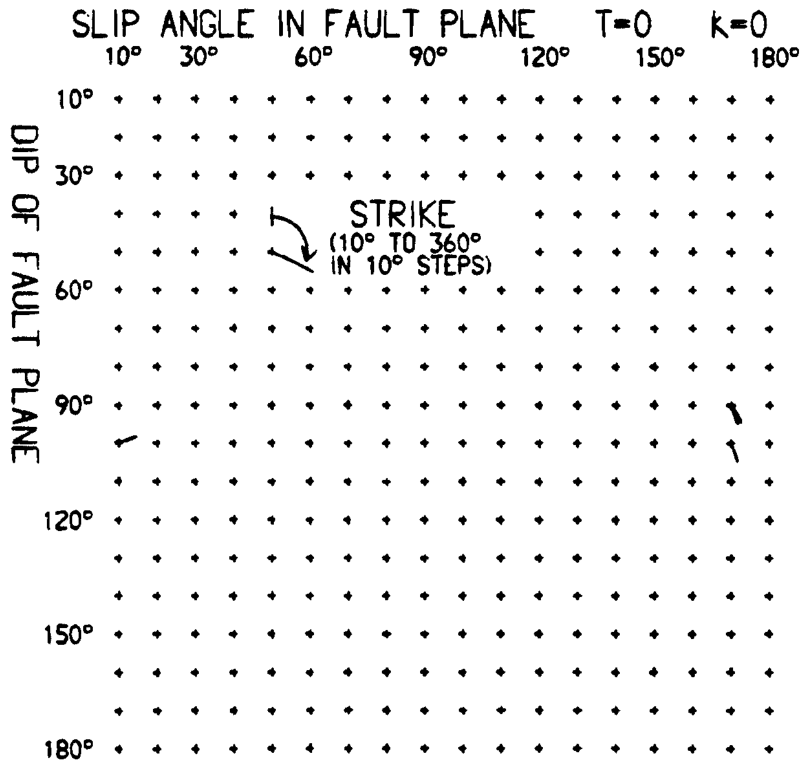

(d)

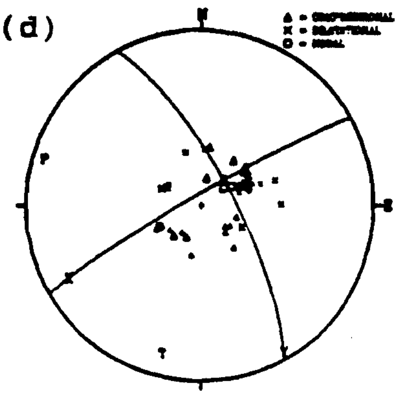

(e)

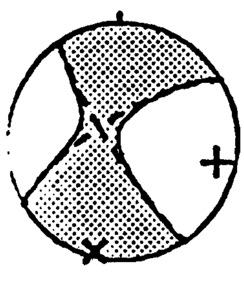

(f)

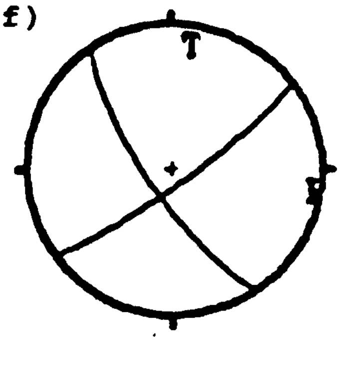

IASPEI
event 2

(a)

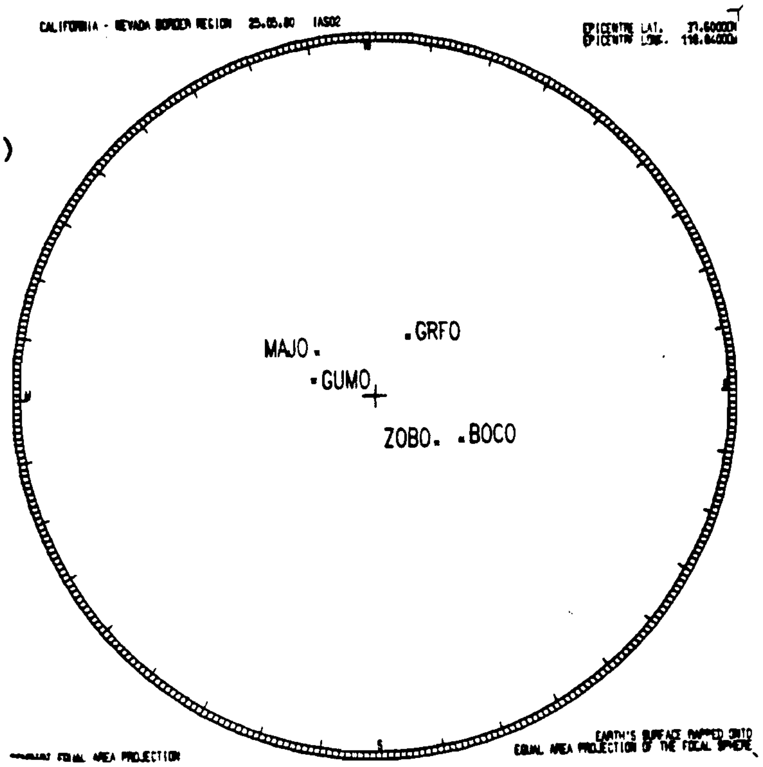

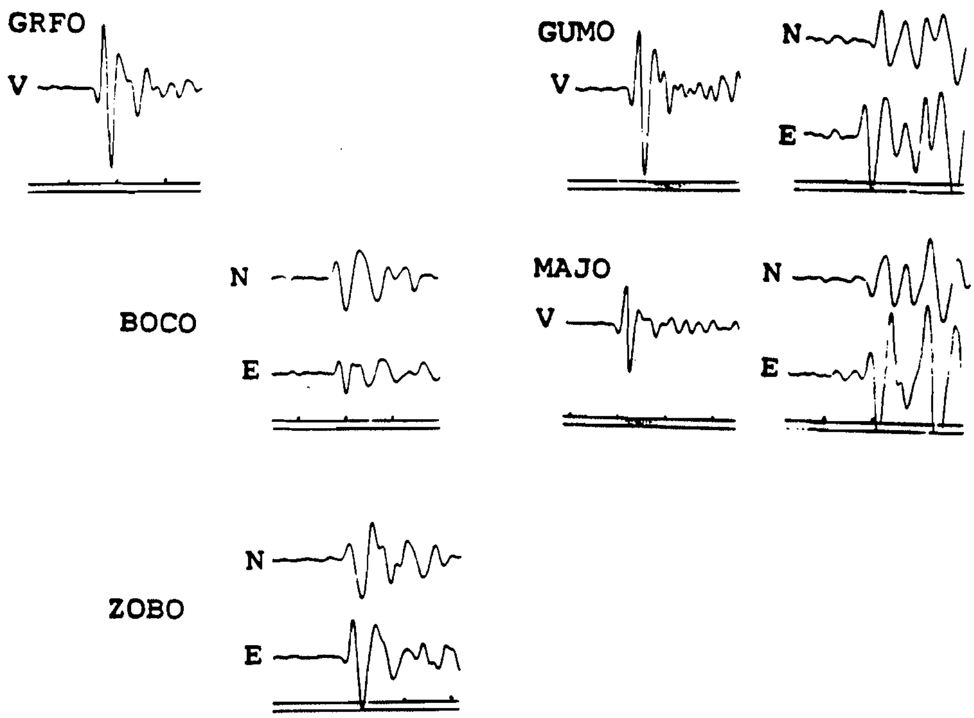

IASPEI
event 2

(b)

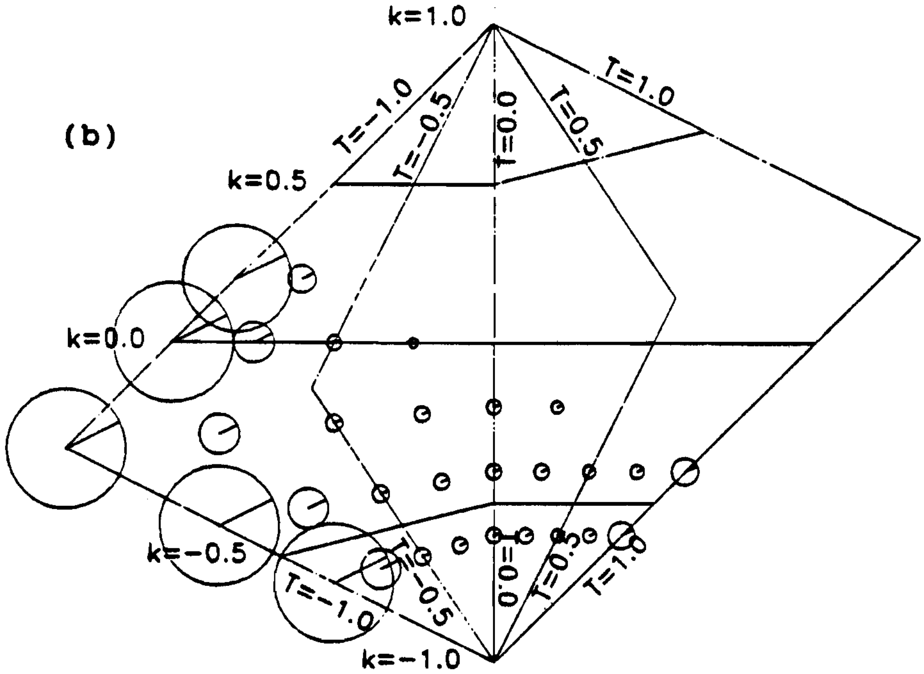

(c)

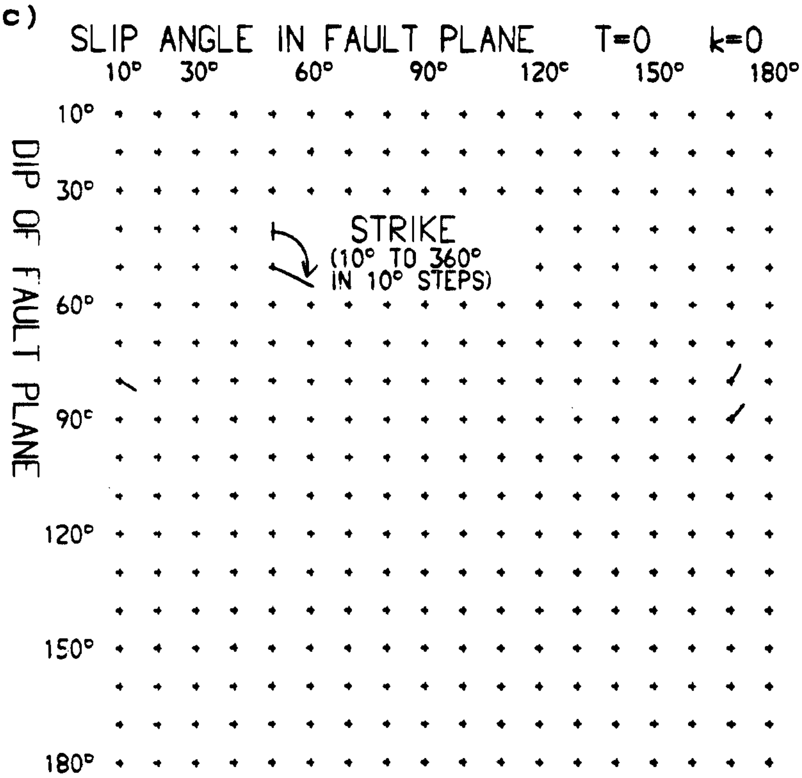

(d)

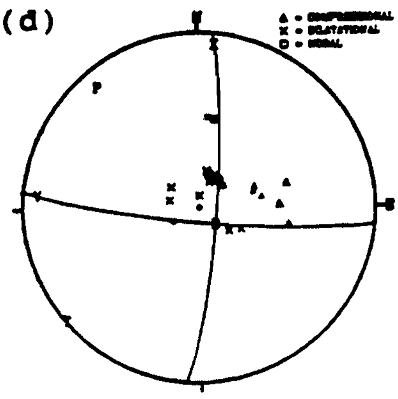

(e)

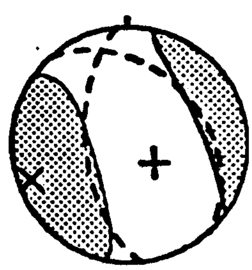

(f)

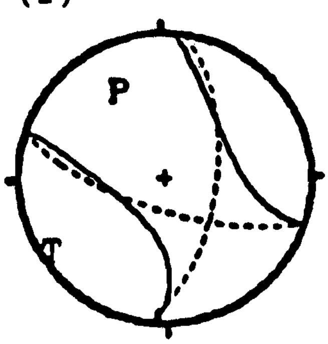

IASPEI event 3

(a)

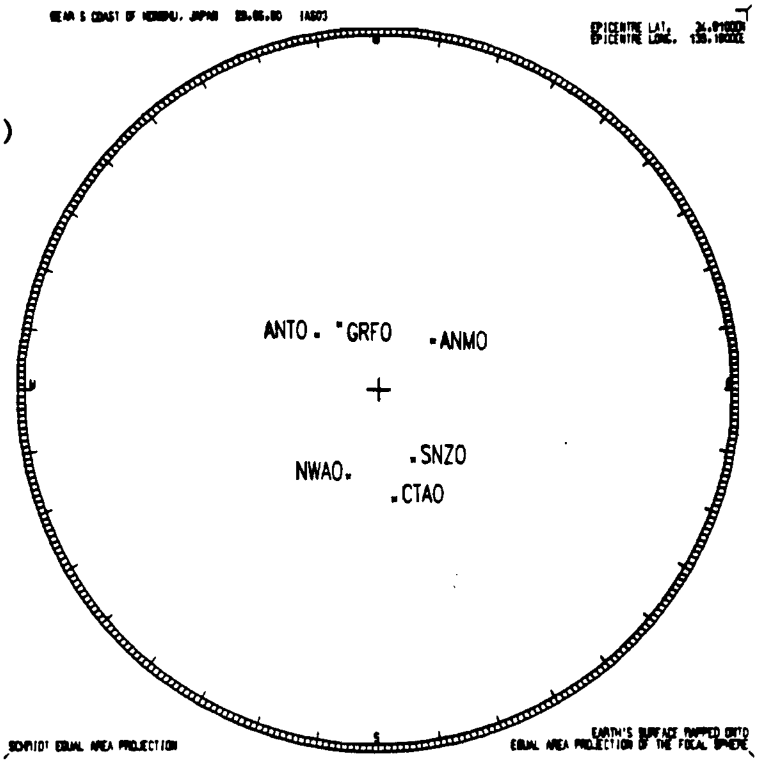

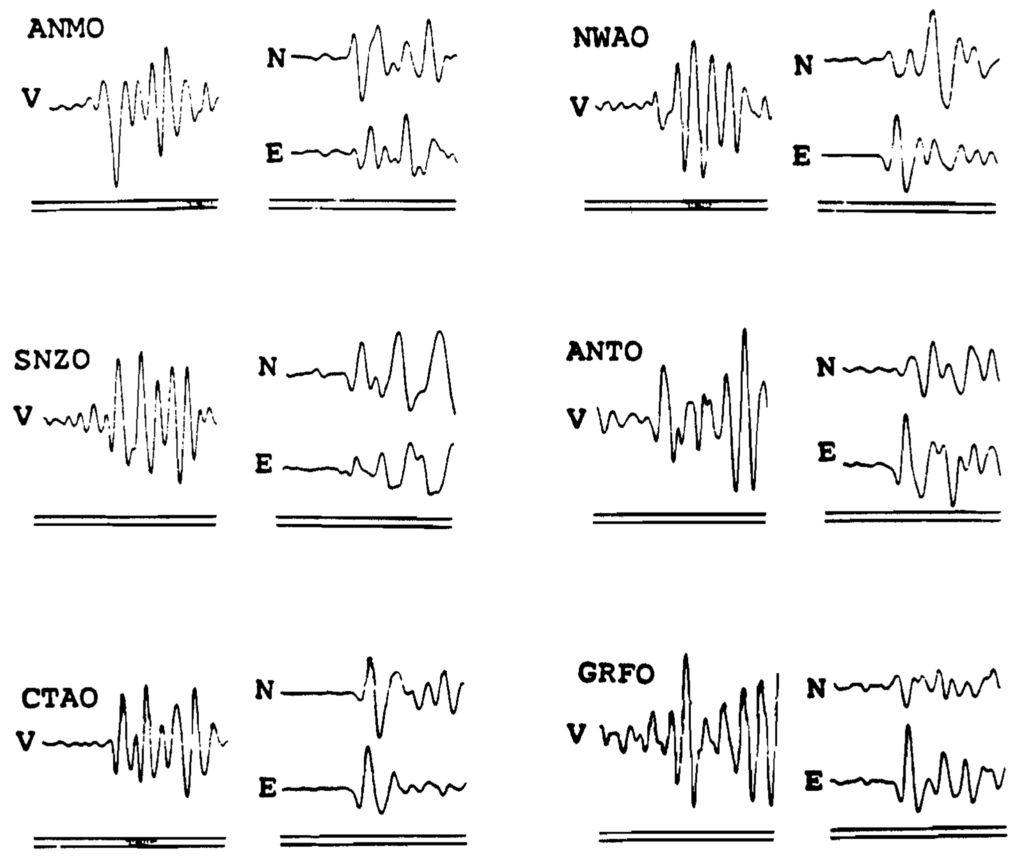

IASPEI
event 3

(b)

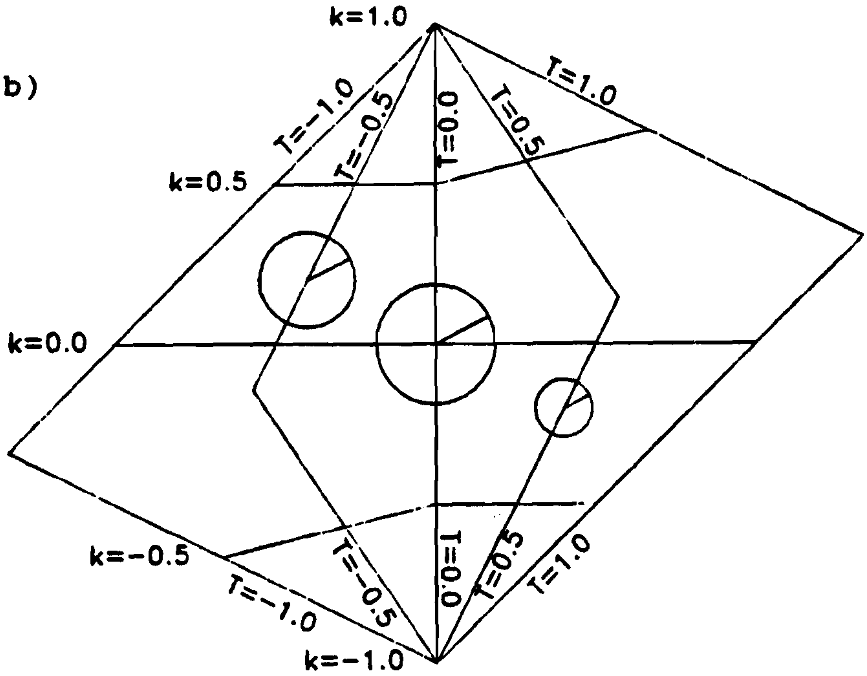

(c)

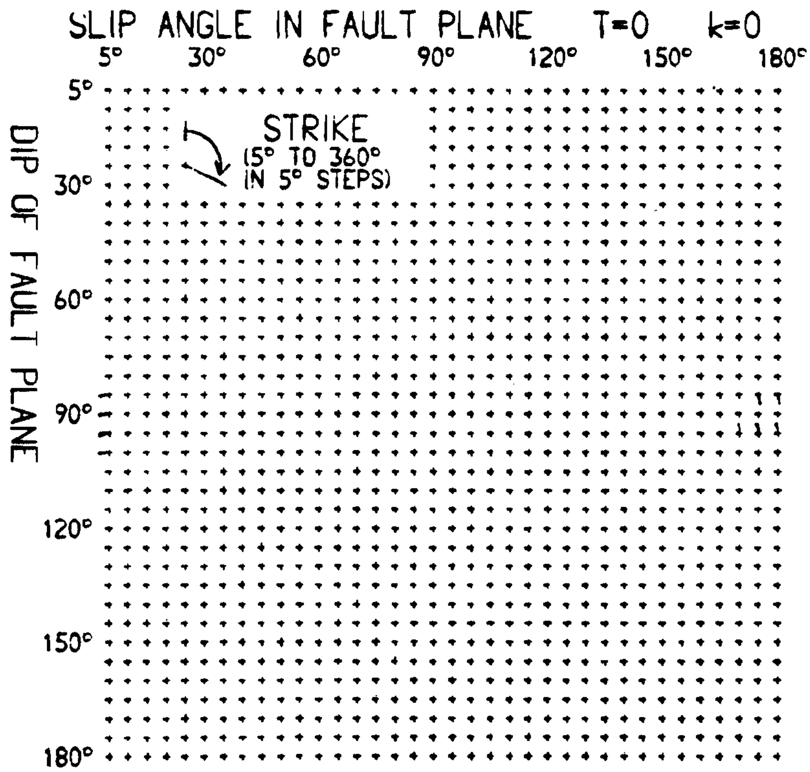

(d)

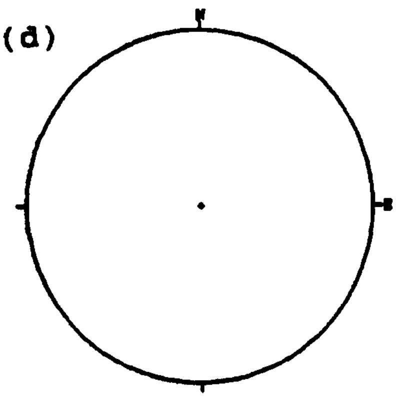

(e)

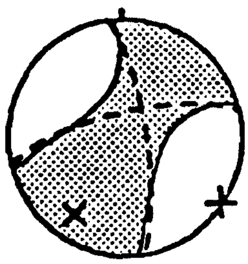

(f)

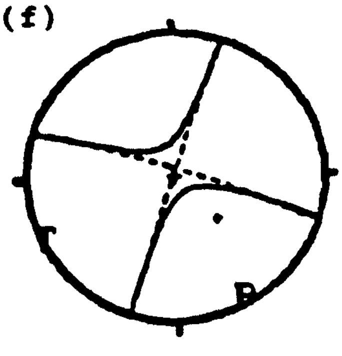

(a)

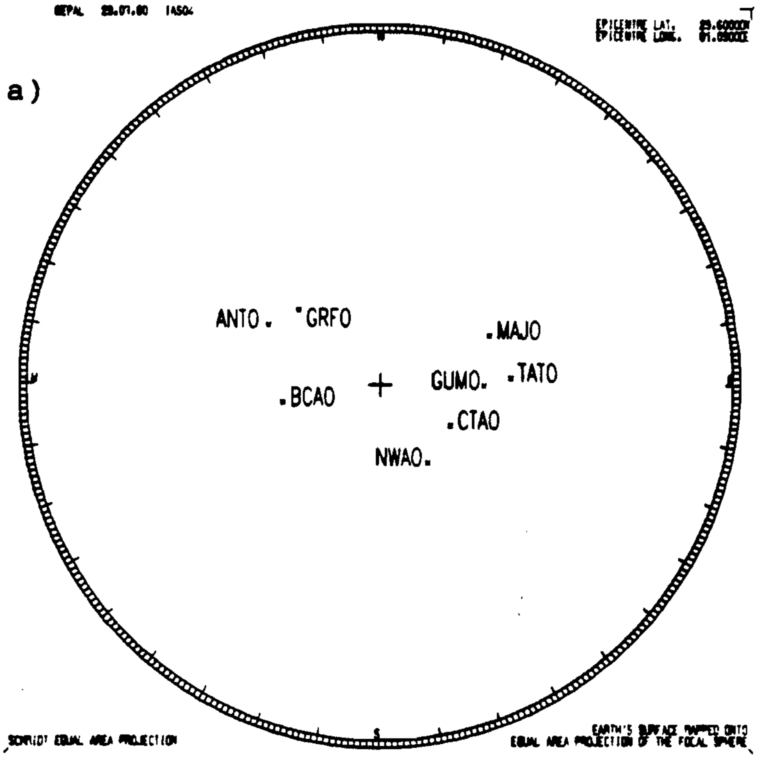

IASPEI
event 4

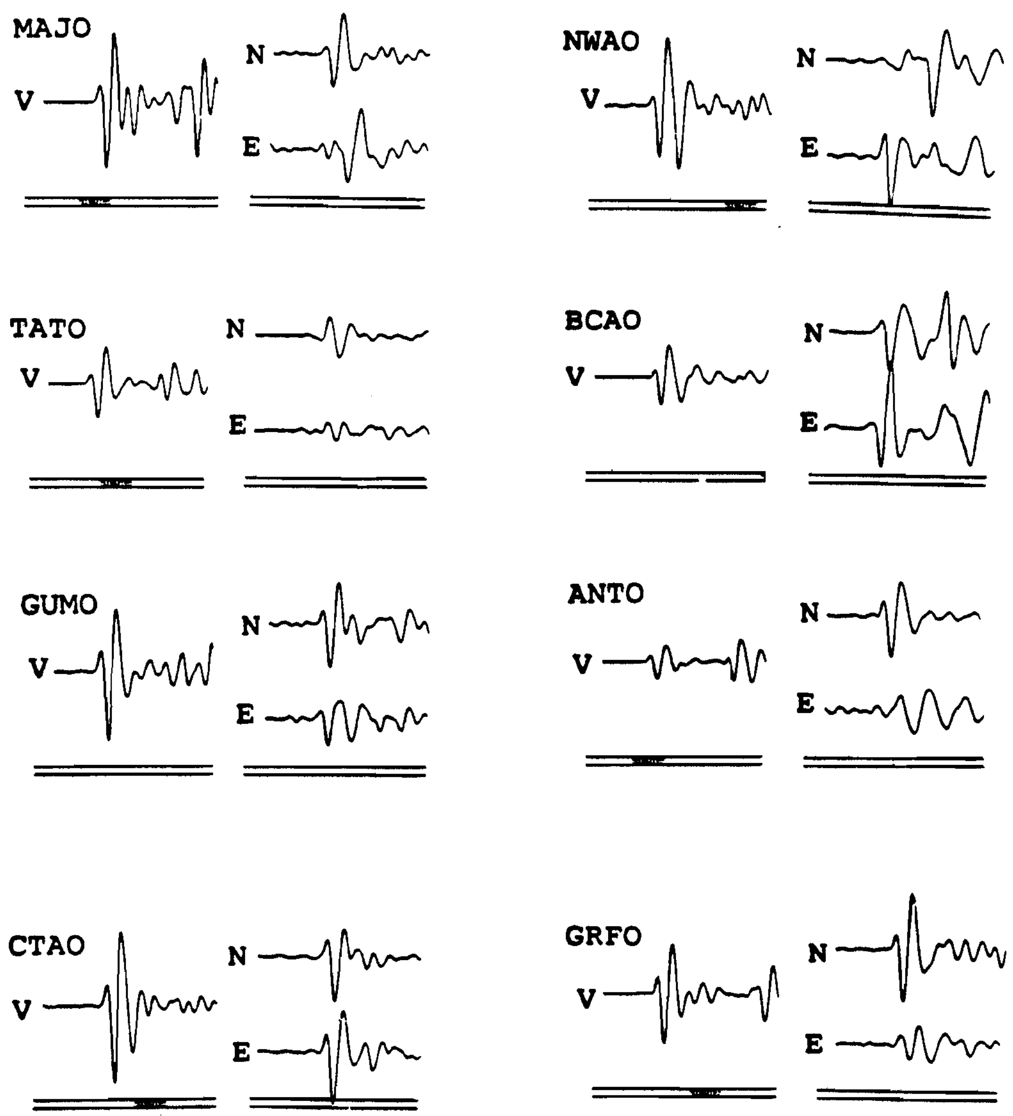

IASPEI
event 4

(b)

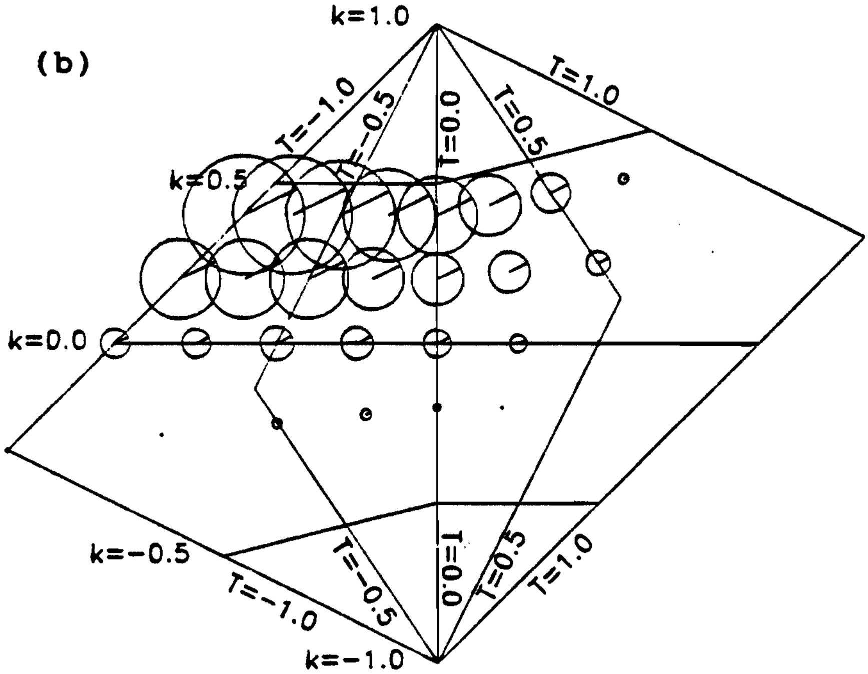

(c) SLIP ANGLE IN FAULT PLANE T=0 k=0

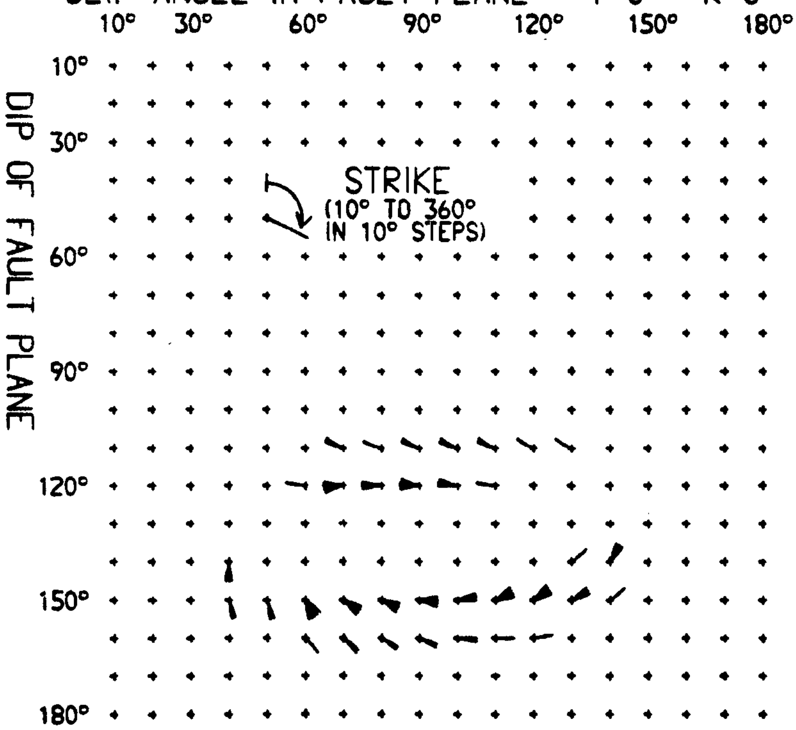

(d)

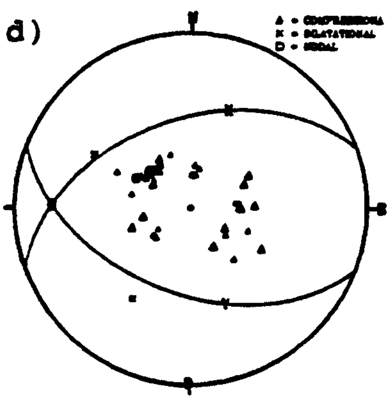

(e)

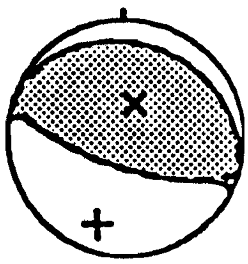

(f)

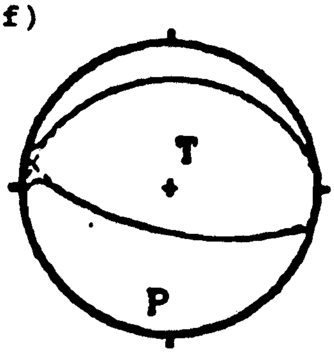

IASPEI event 5

(a)

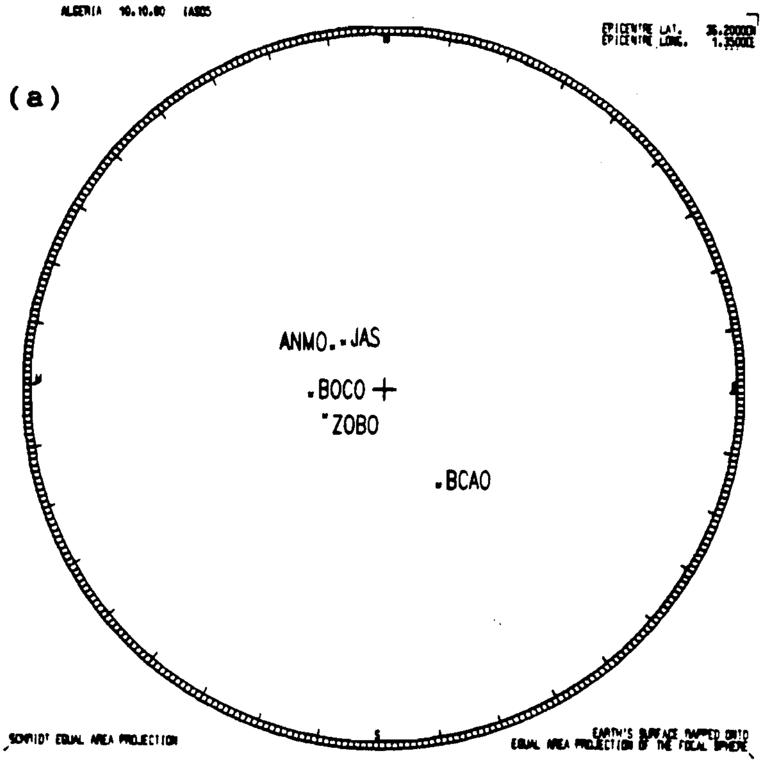

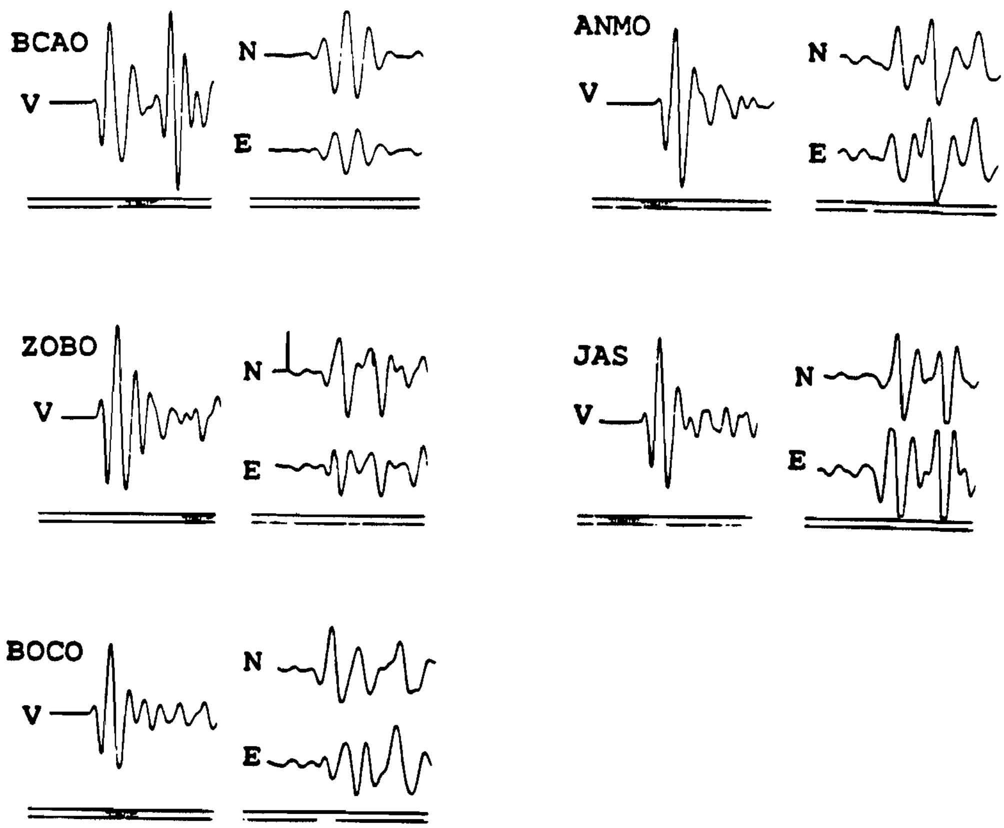

IASPEI
event 5

(b)

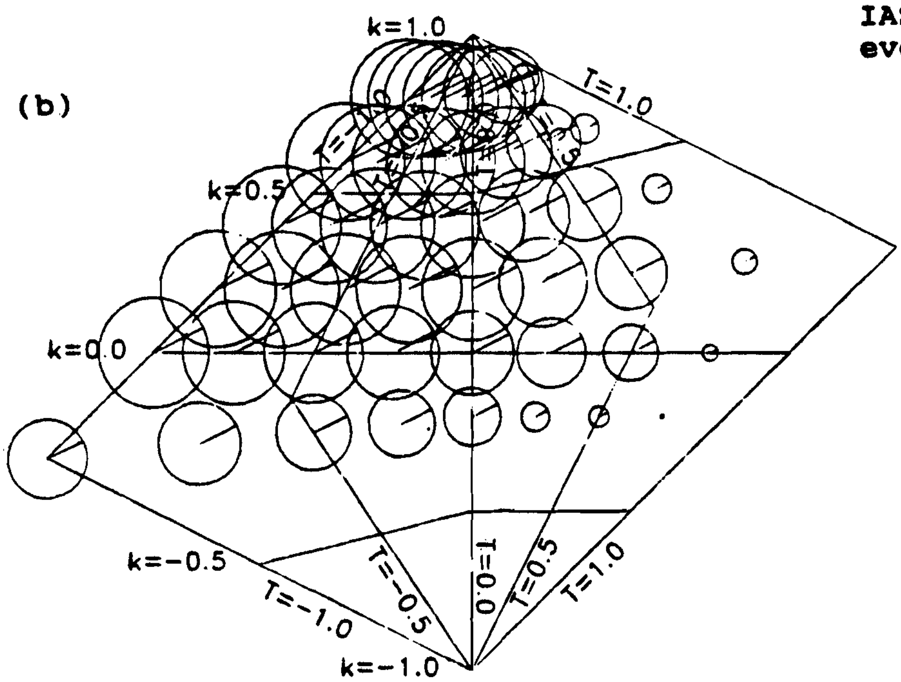

(c)

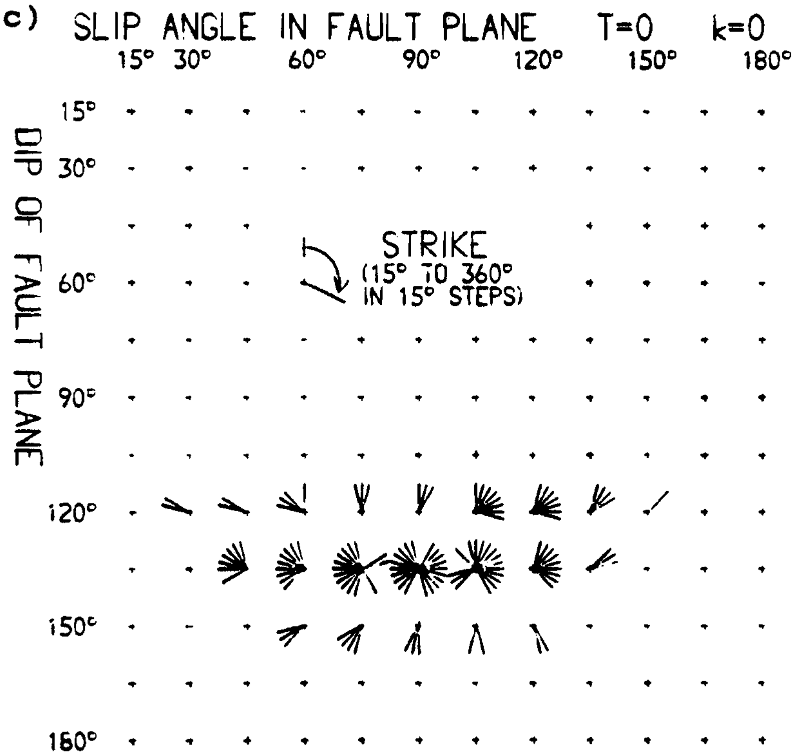

(d)

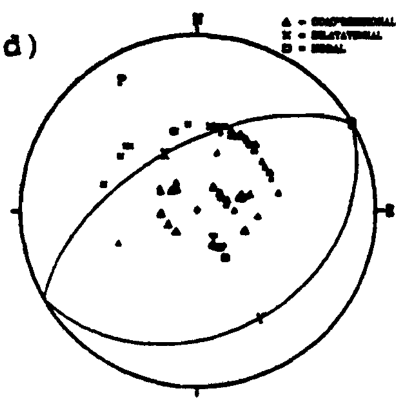

(e)

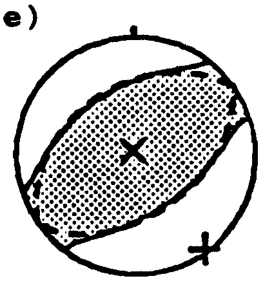

(f)

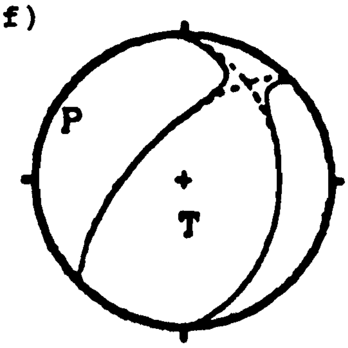

IASPEI
event 6

(a)

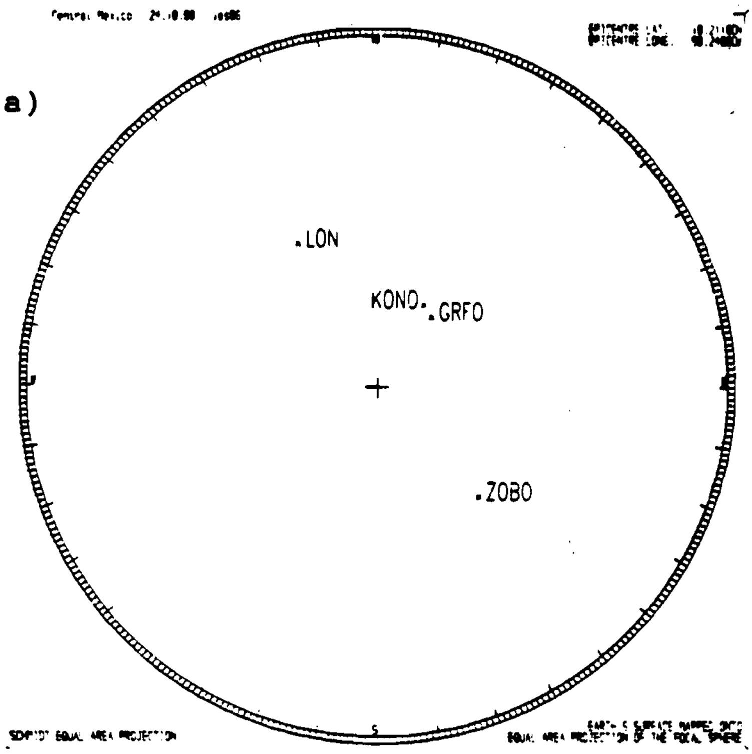

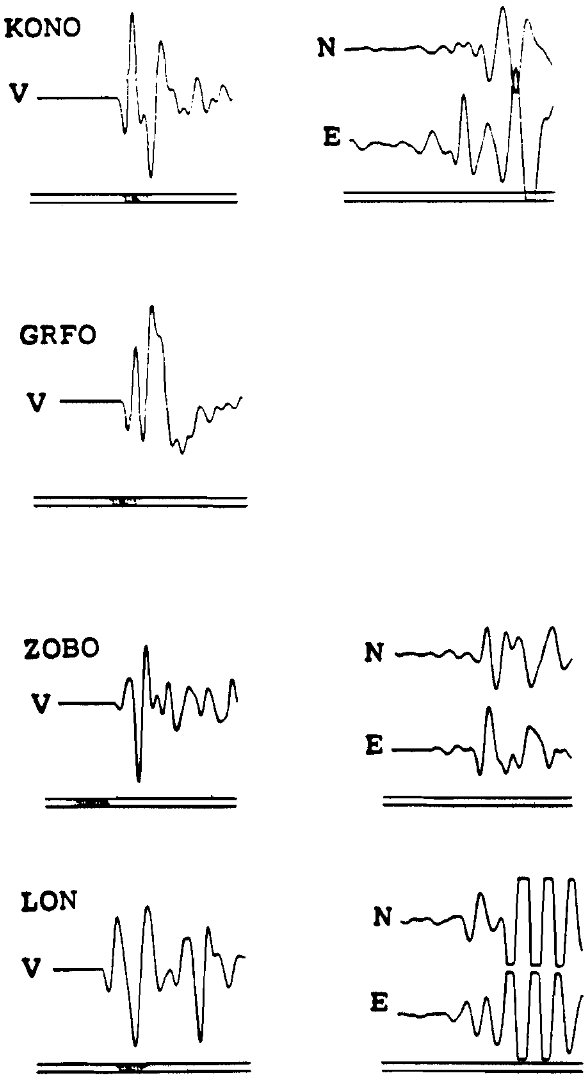

(b)

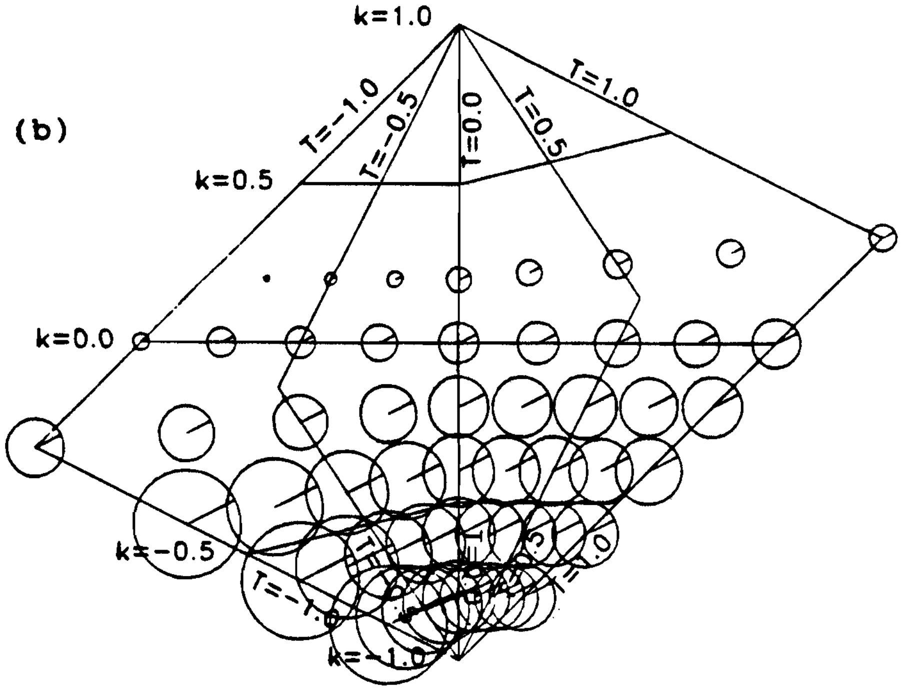

IASPEI event 6

(c)

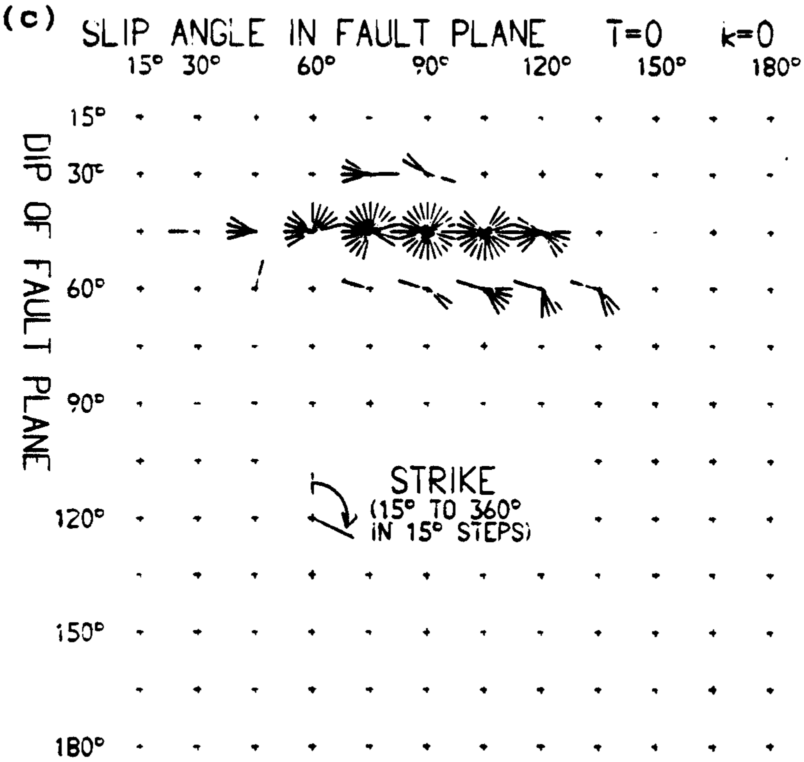

(d)

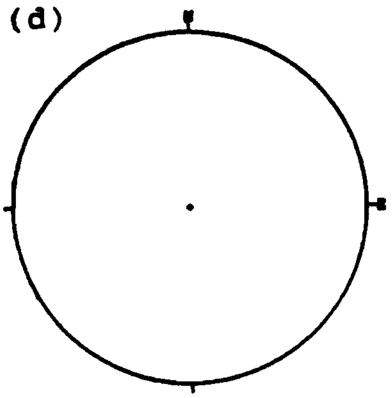

(e)

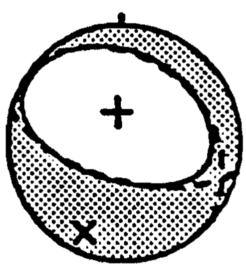

(f)

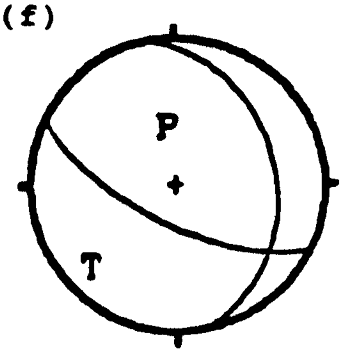

(a)

IASPEI event 7

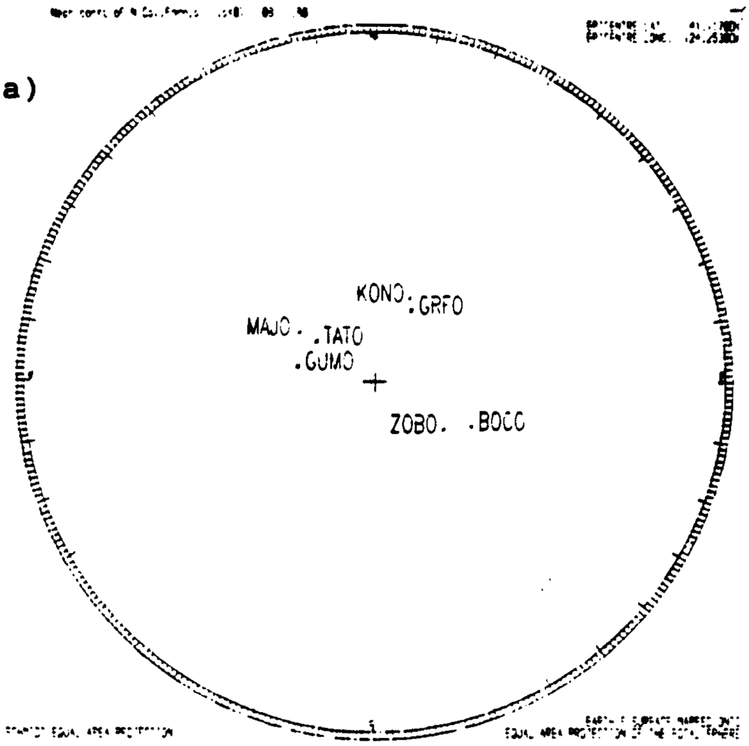

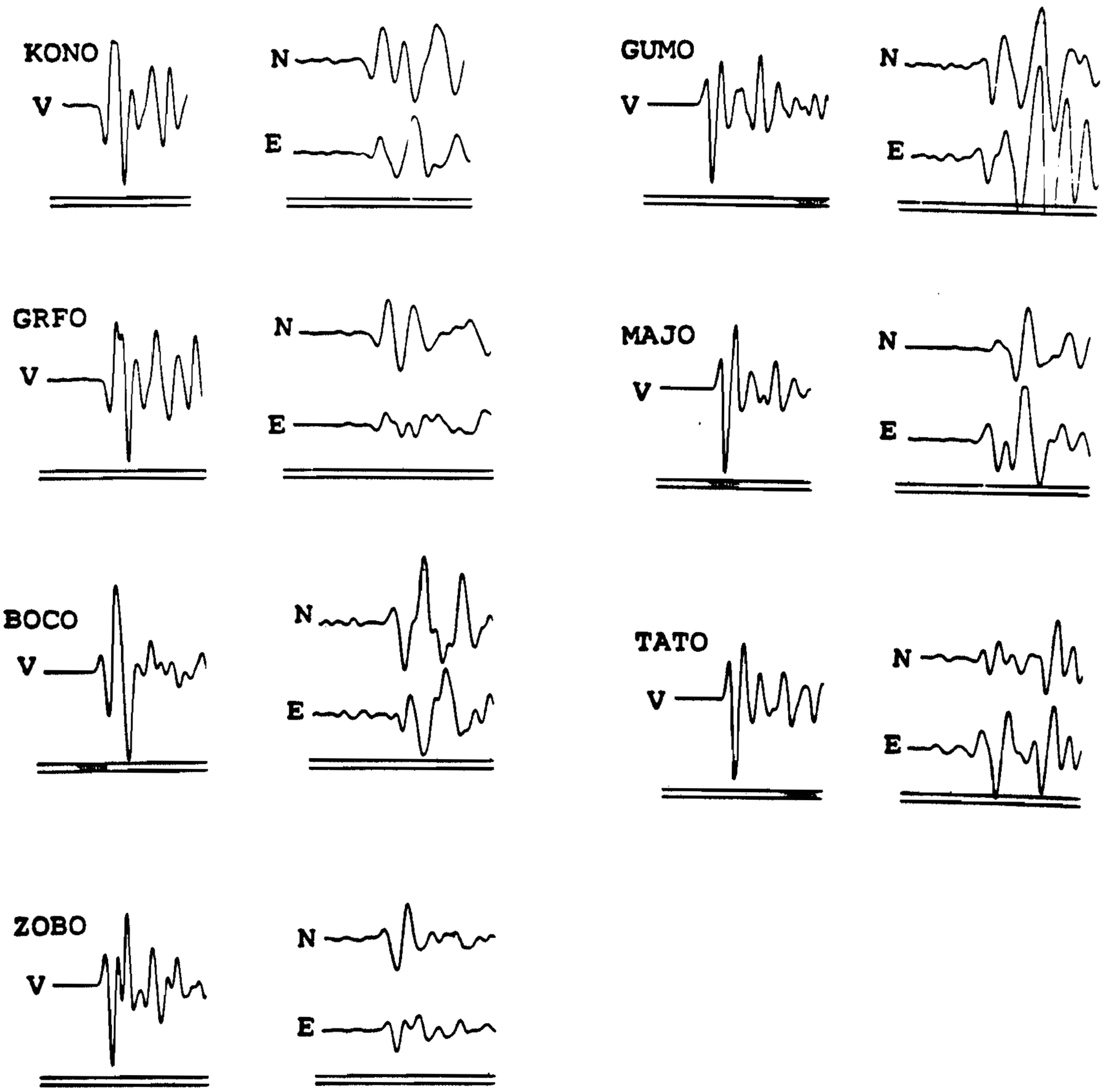

IASPEI event 7

(b)

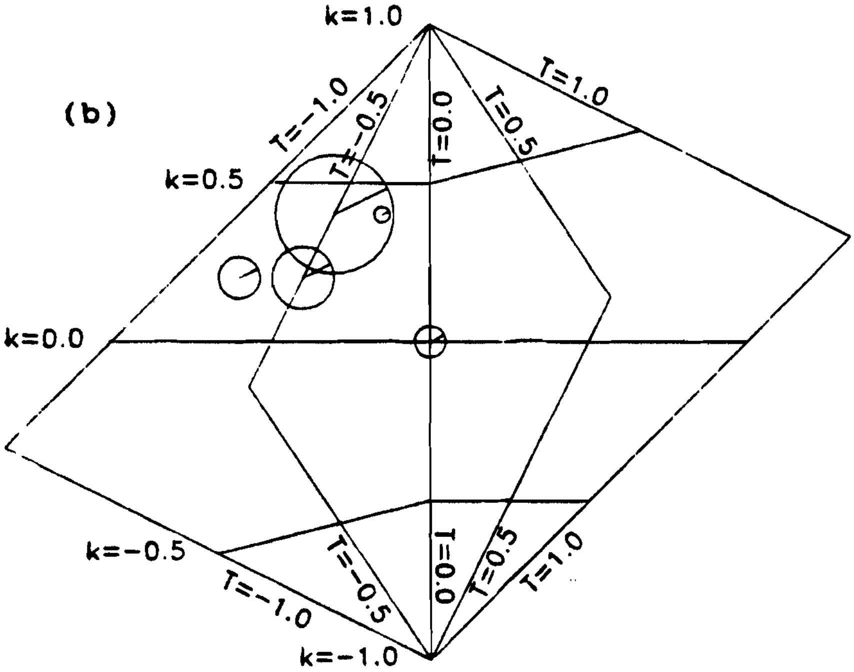

(c)

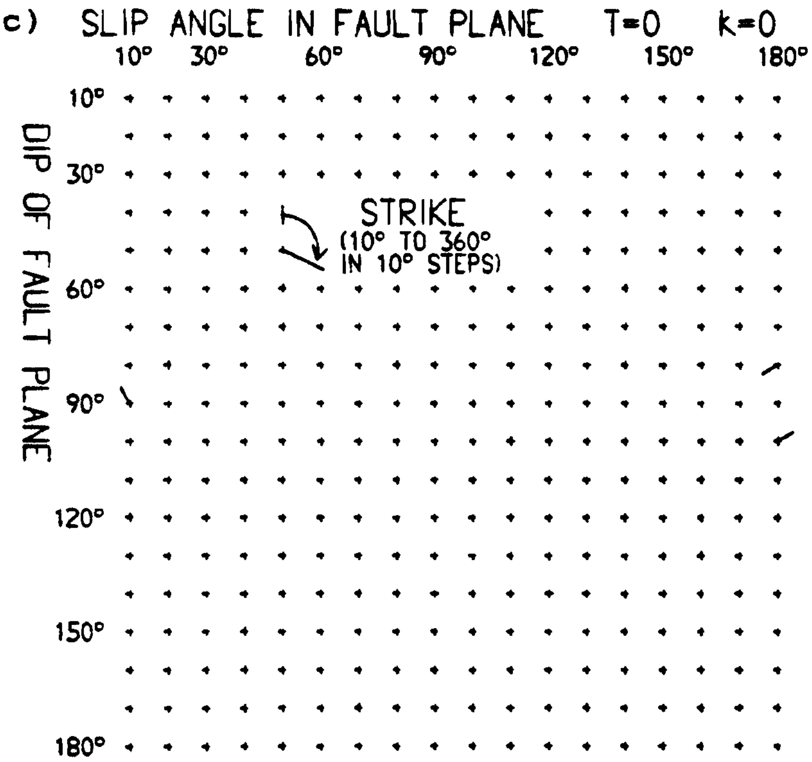

(d)

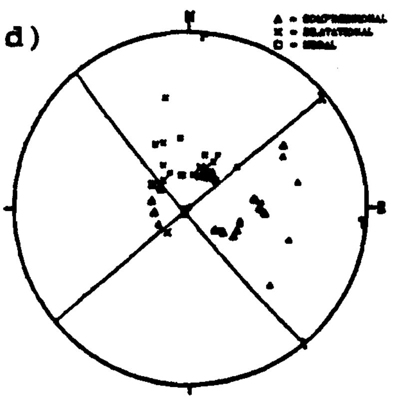

(e)

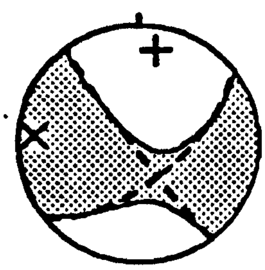

(f)

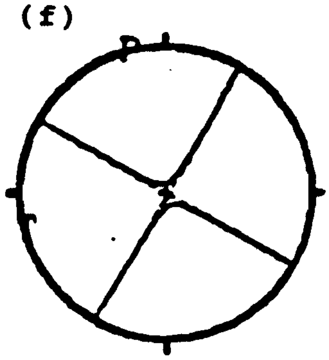

IASPEI
event 8

(a)

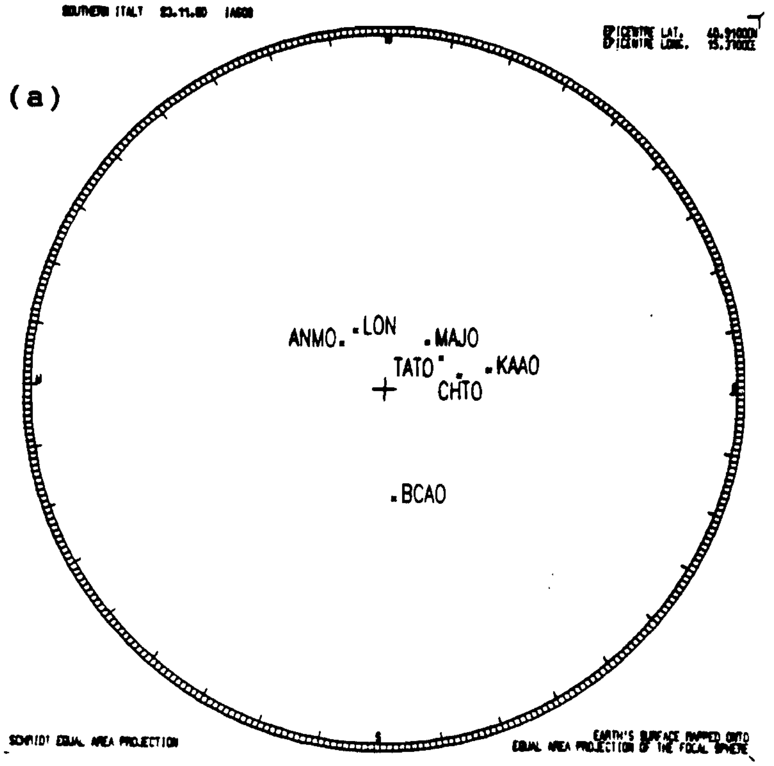

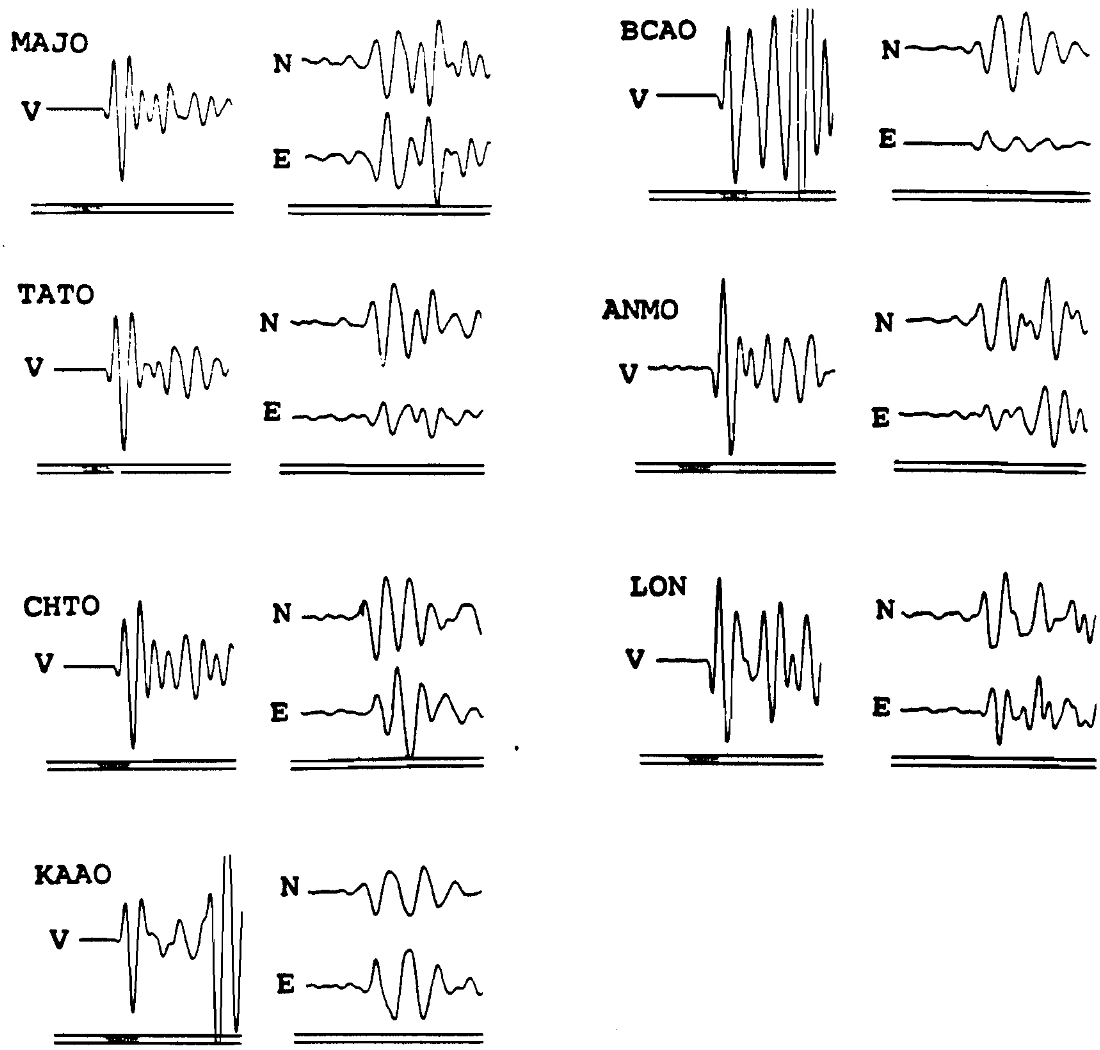

IASPEI
event 8

(b)

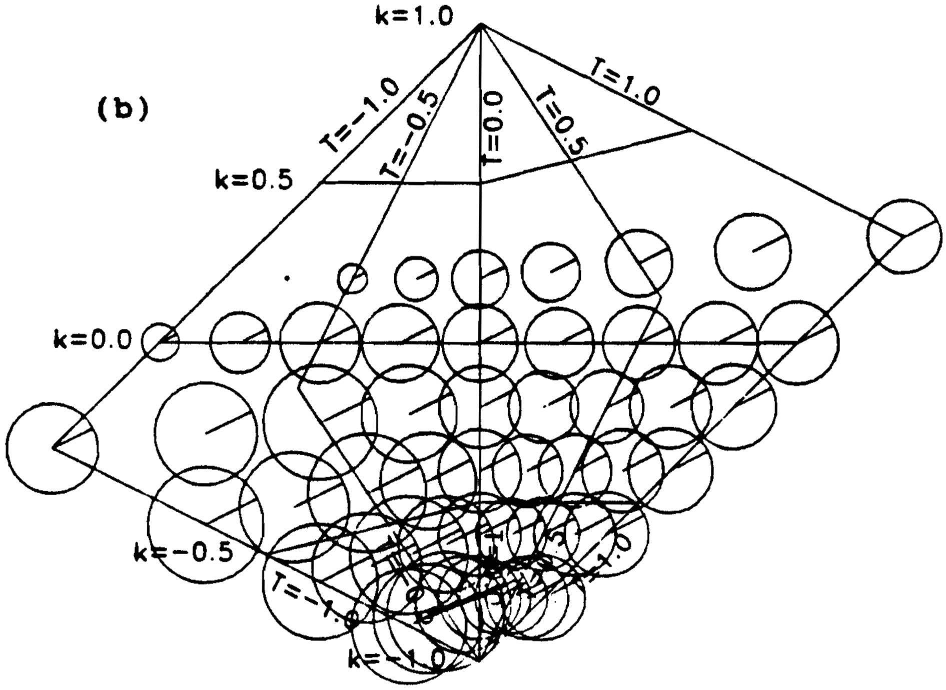

(c)

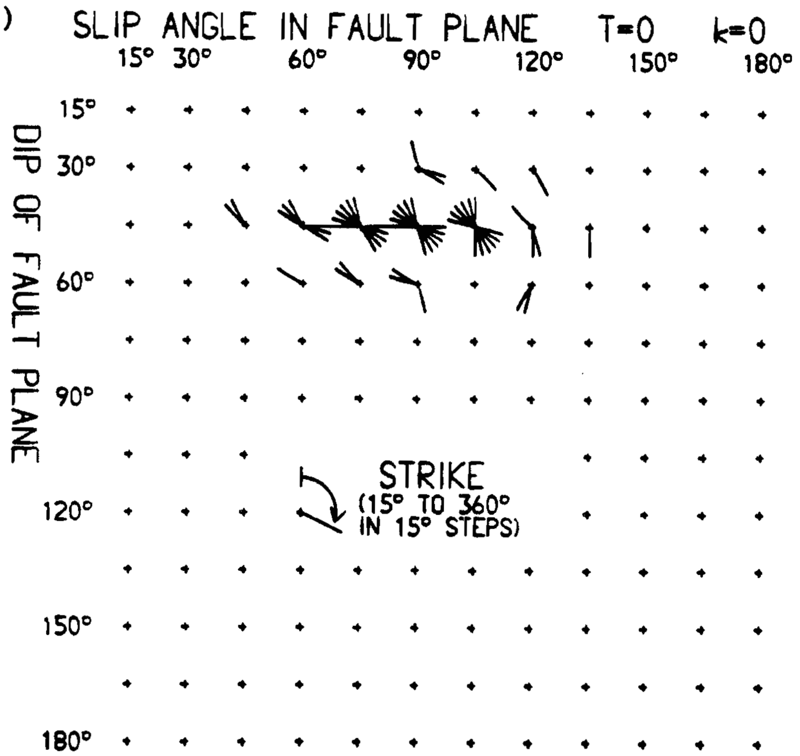

(d)

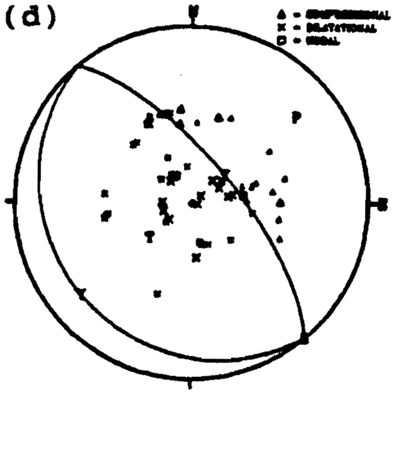

(e)

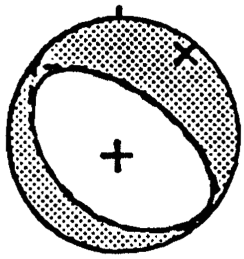

(f)

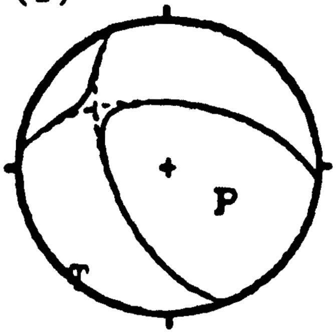

IASPEI
event 9

(a)

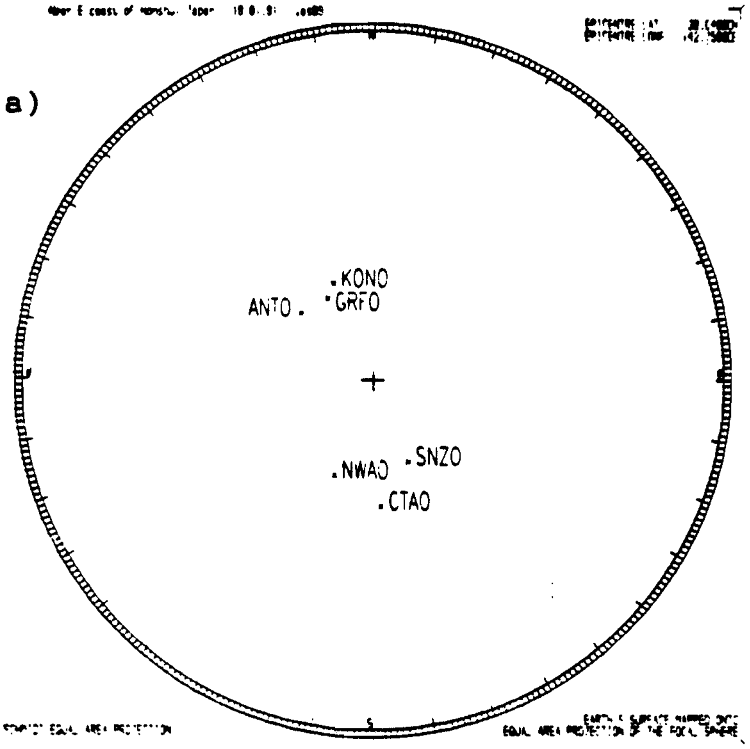

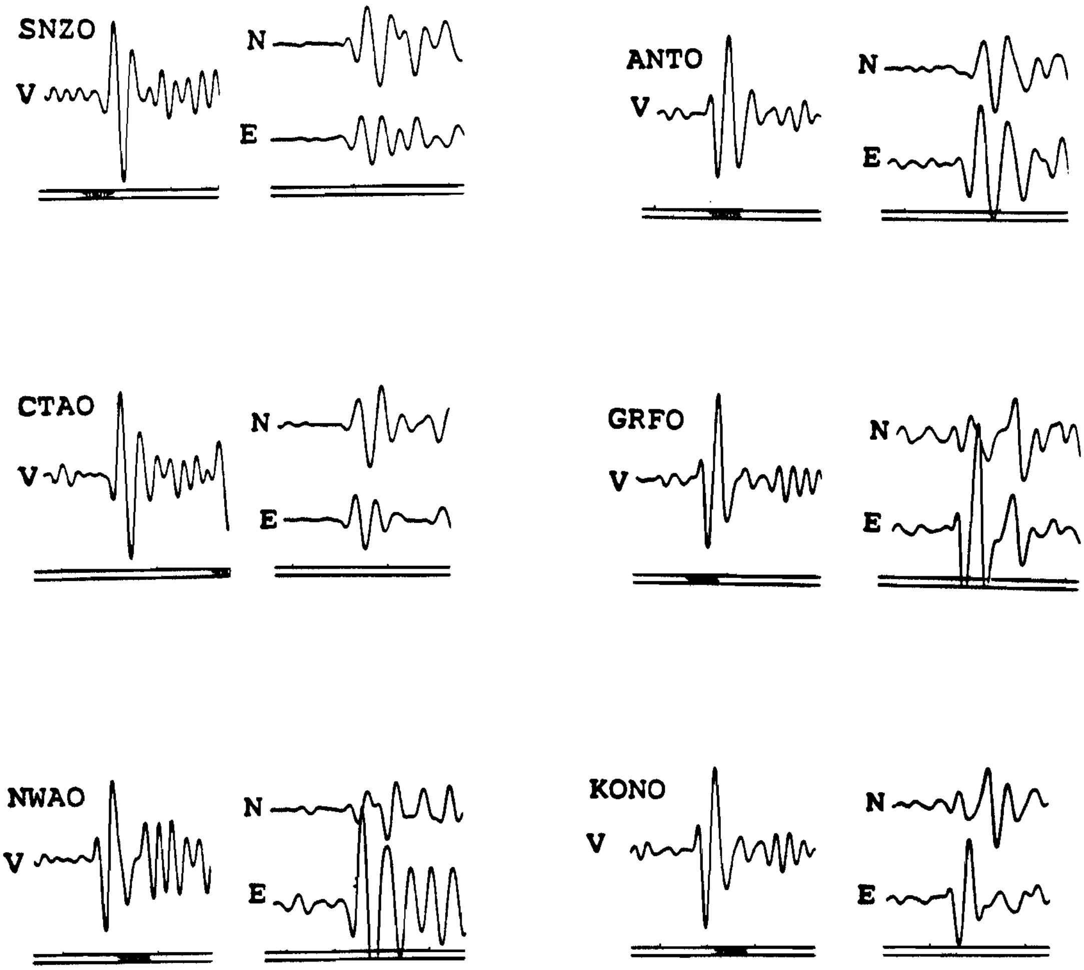

IASPEI
event 9

(b)

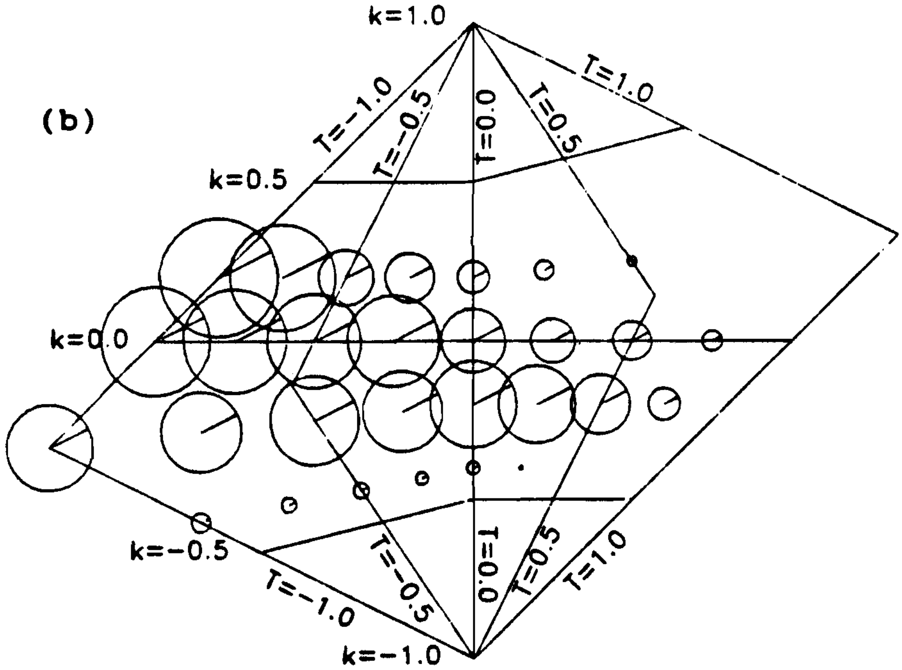

(c)

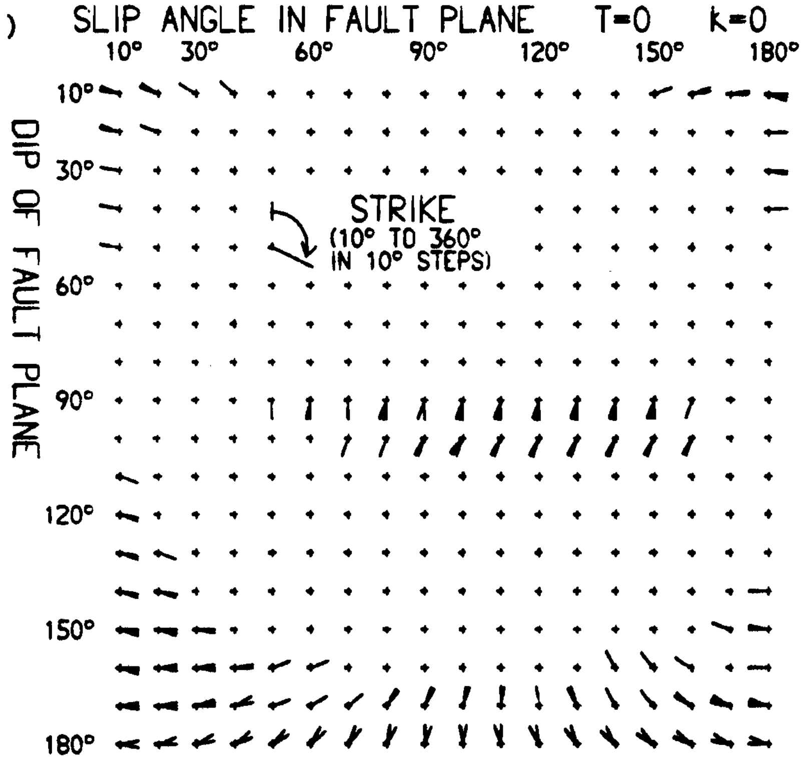

(d)

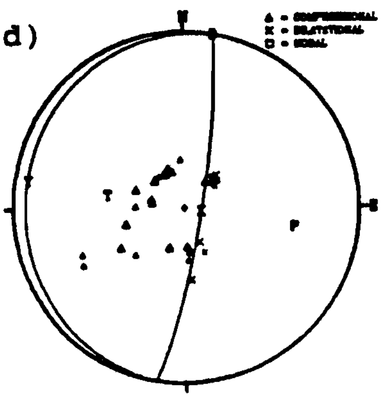

(e)

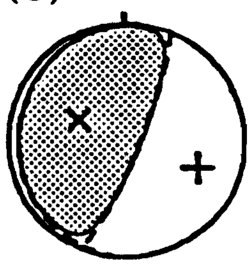

(f)

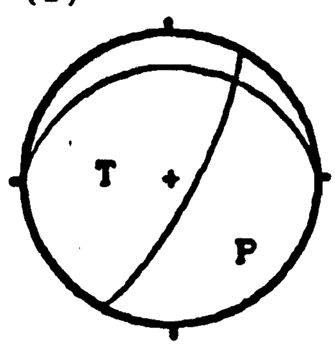

(a)

IASPEI event 10

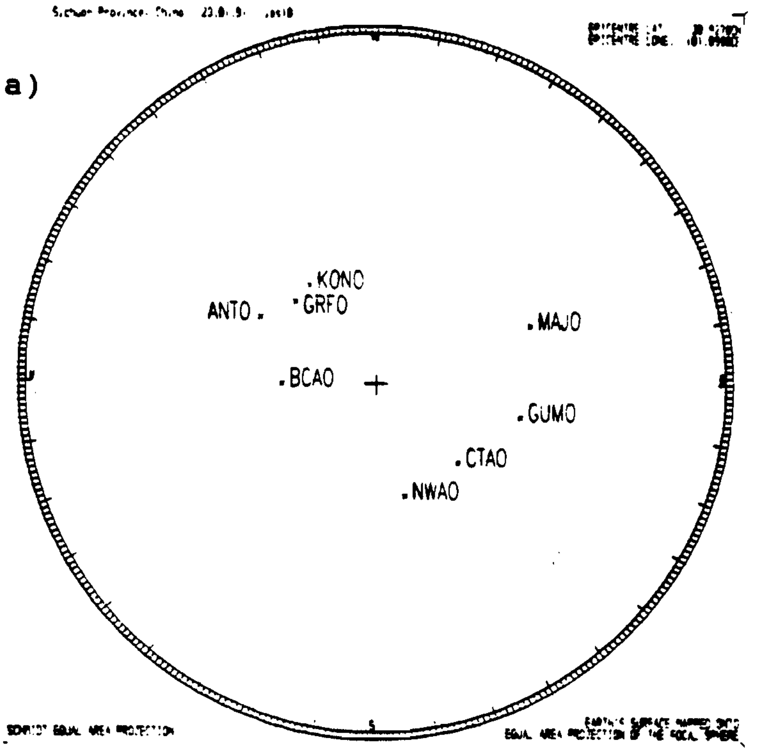

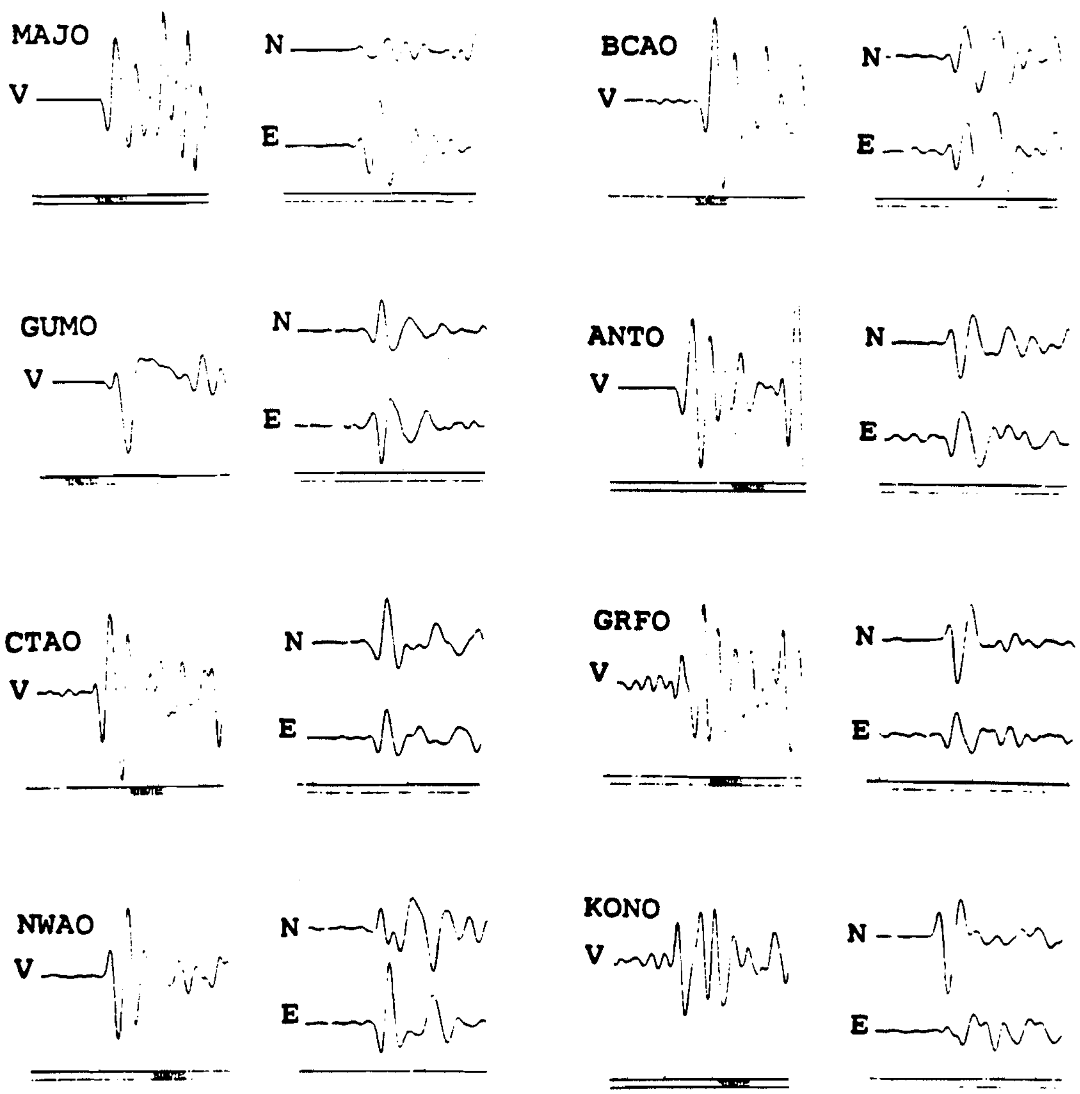

IASPEI
event 10

(b)

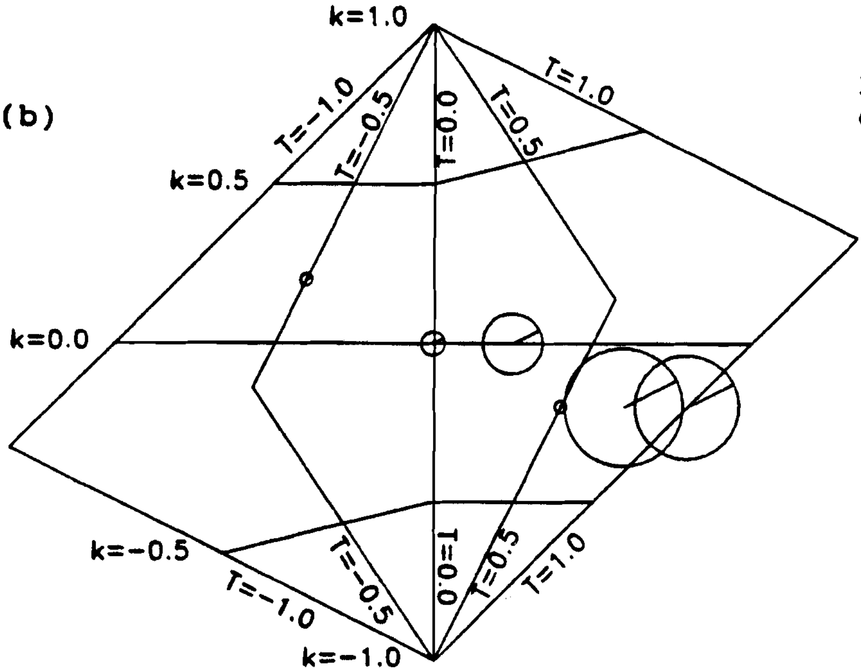

(c)

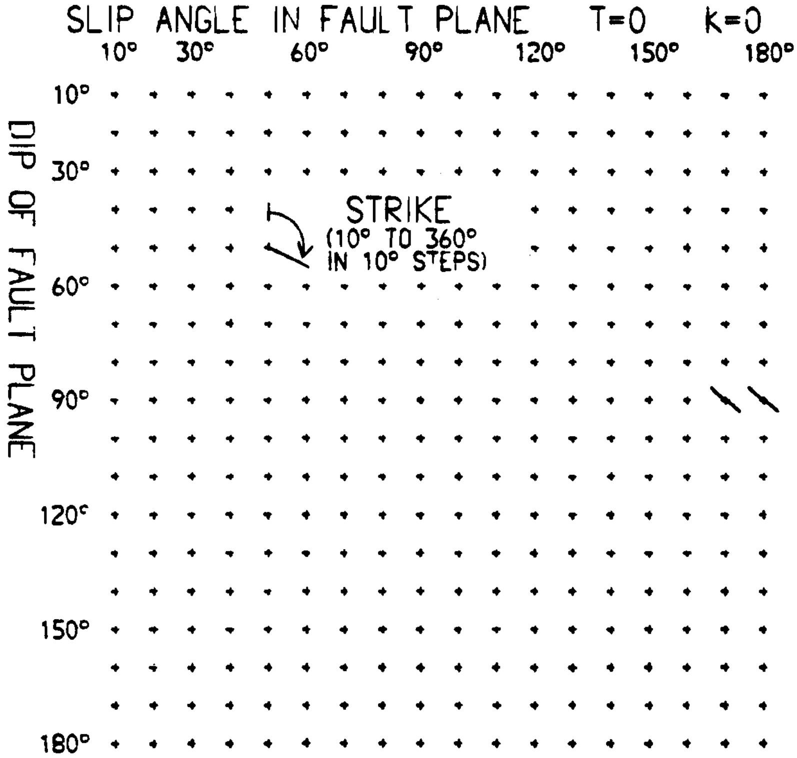

(d)

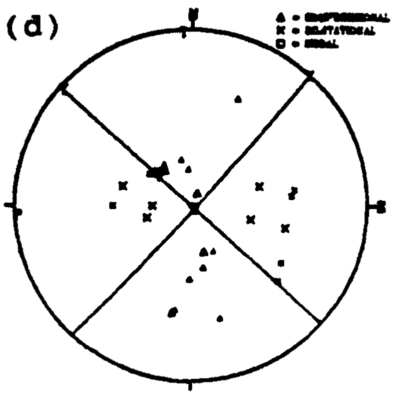

(e)

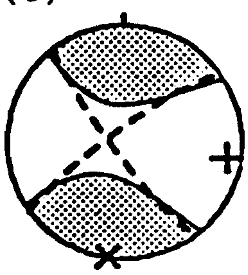

(f)

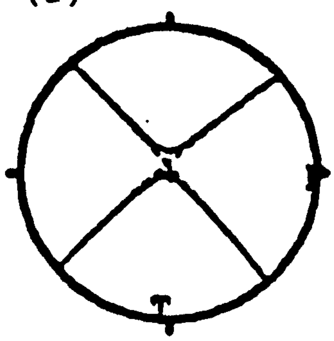

IASPEI event 11

(a)

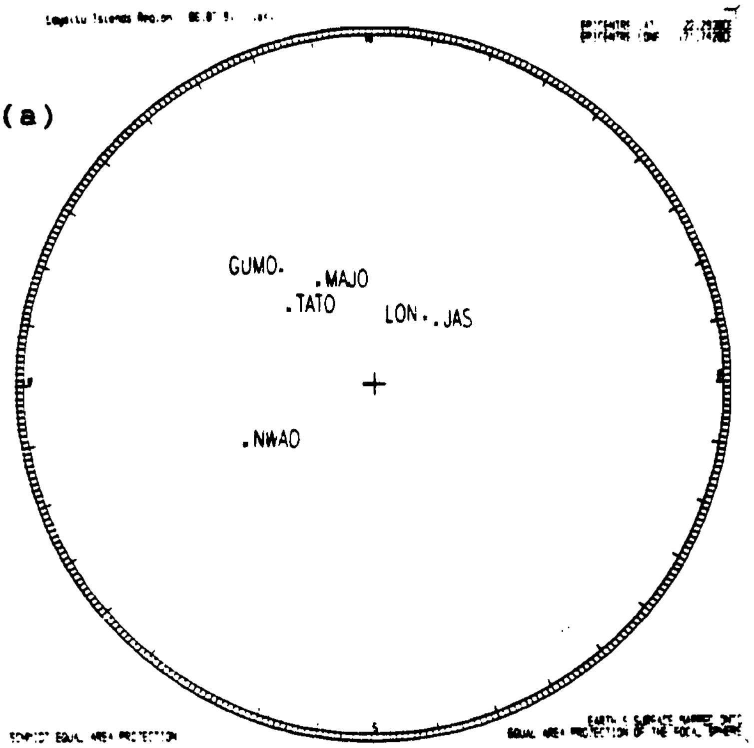

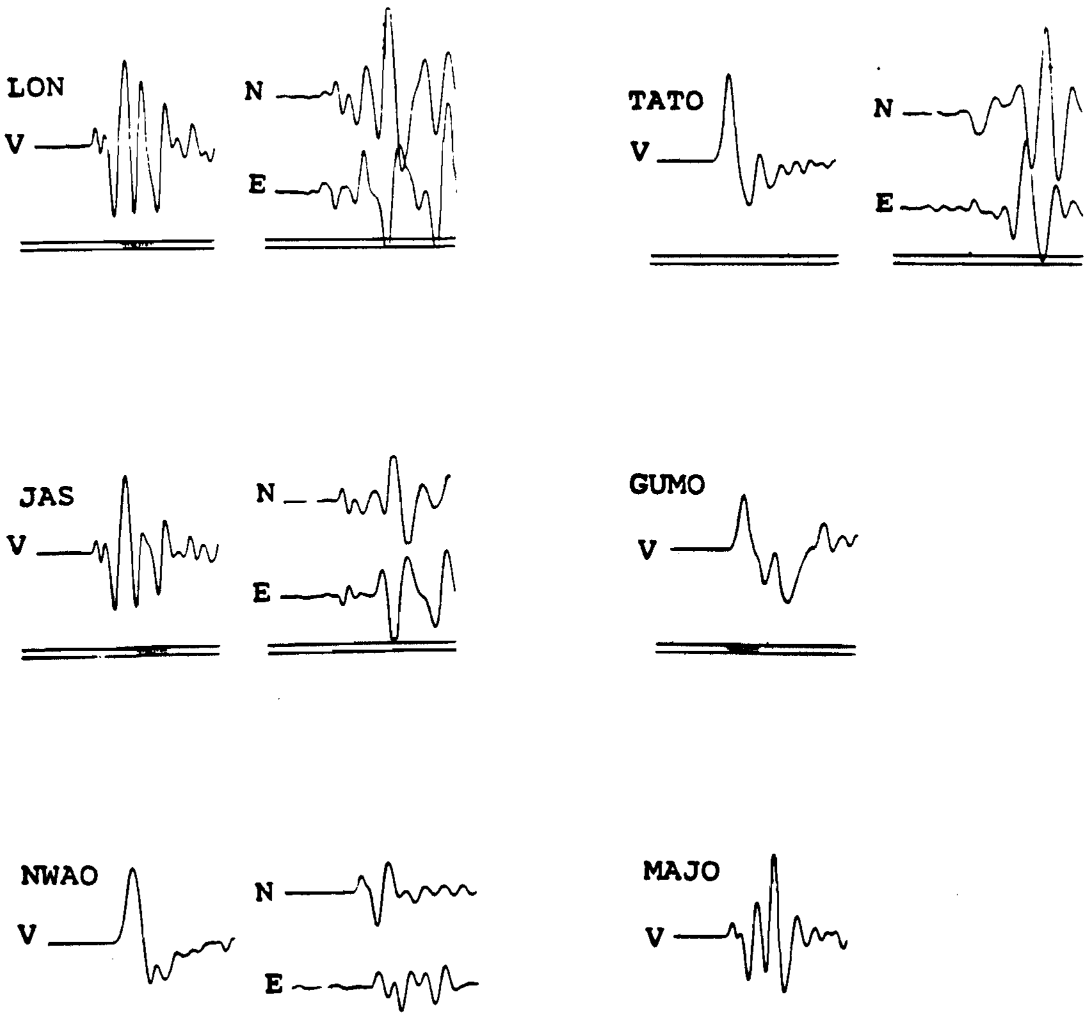

IASPEI
event 11

(b)

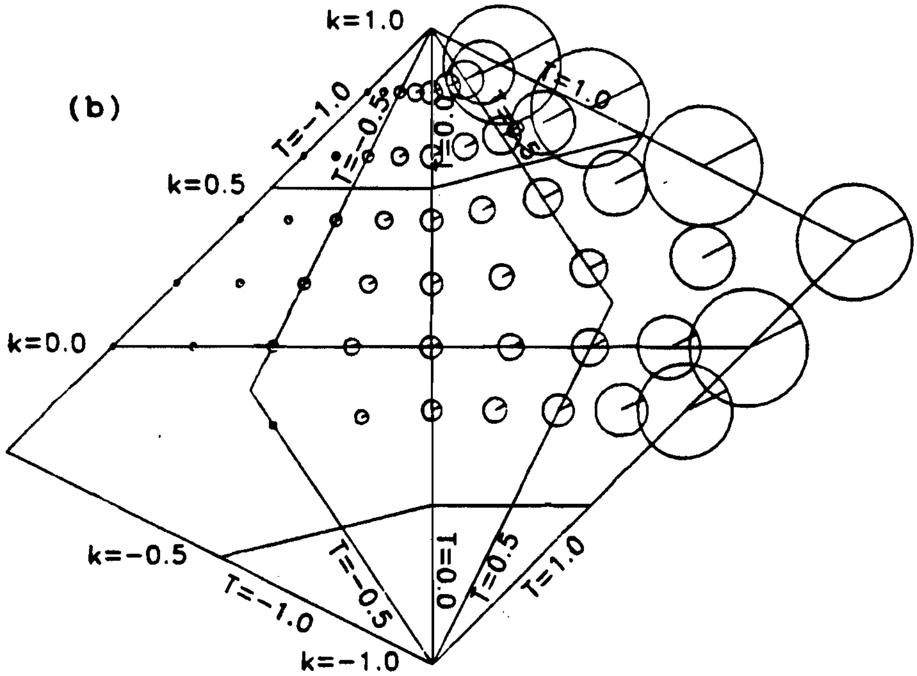

(c)

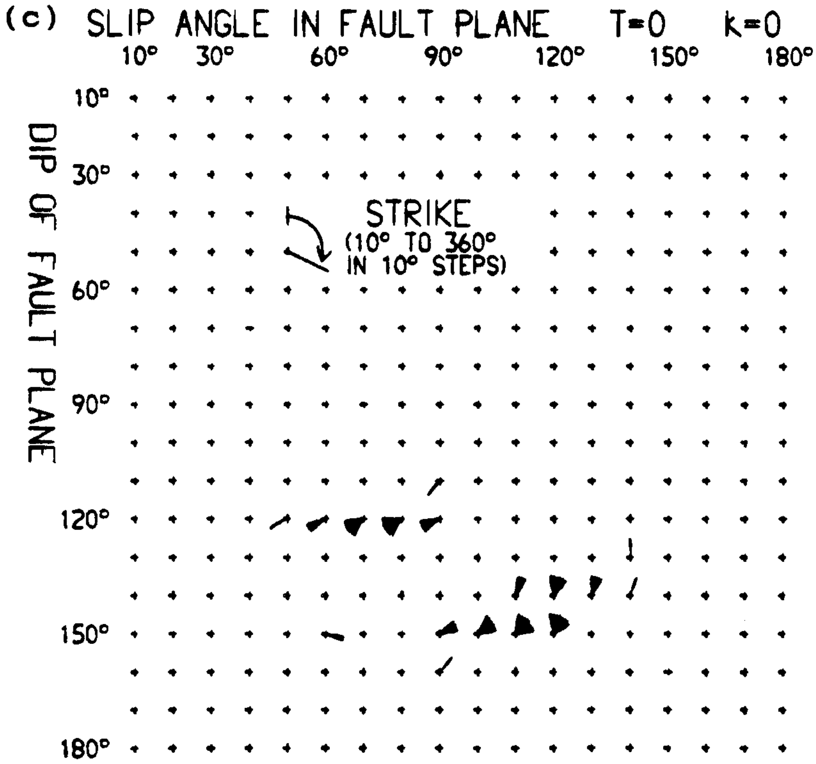

(d)

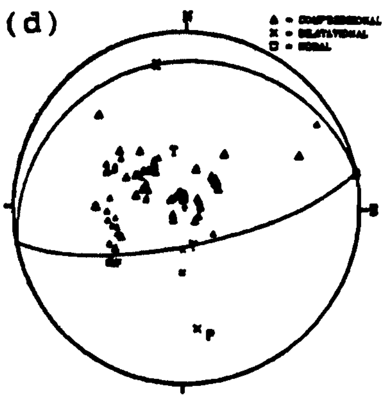

(e)

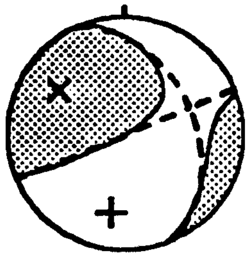

(f)

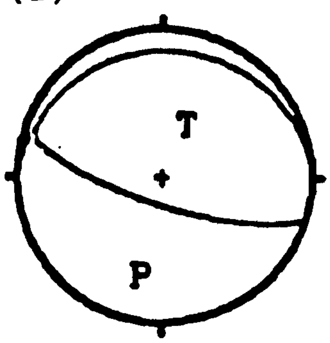

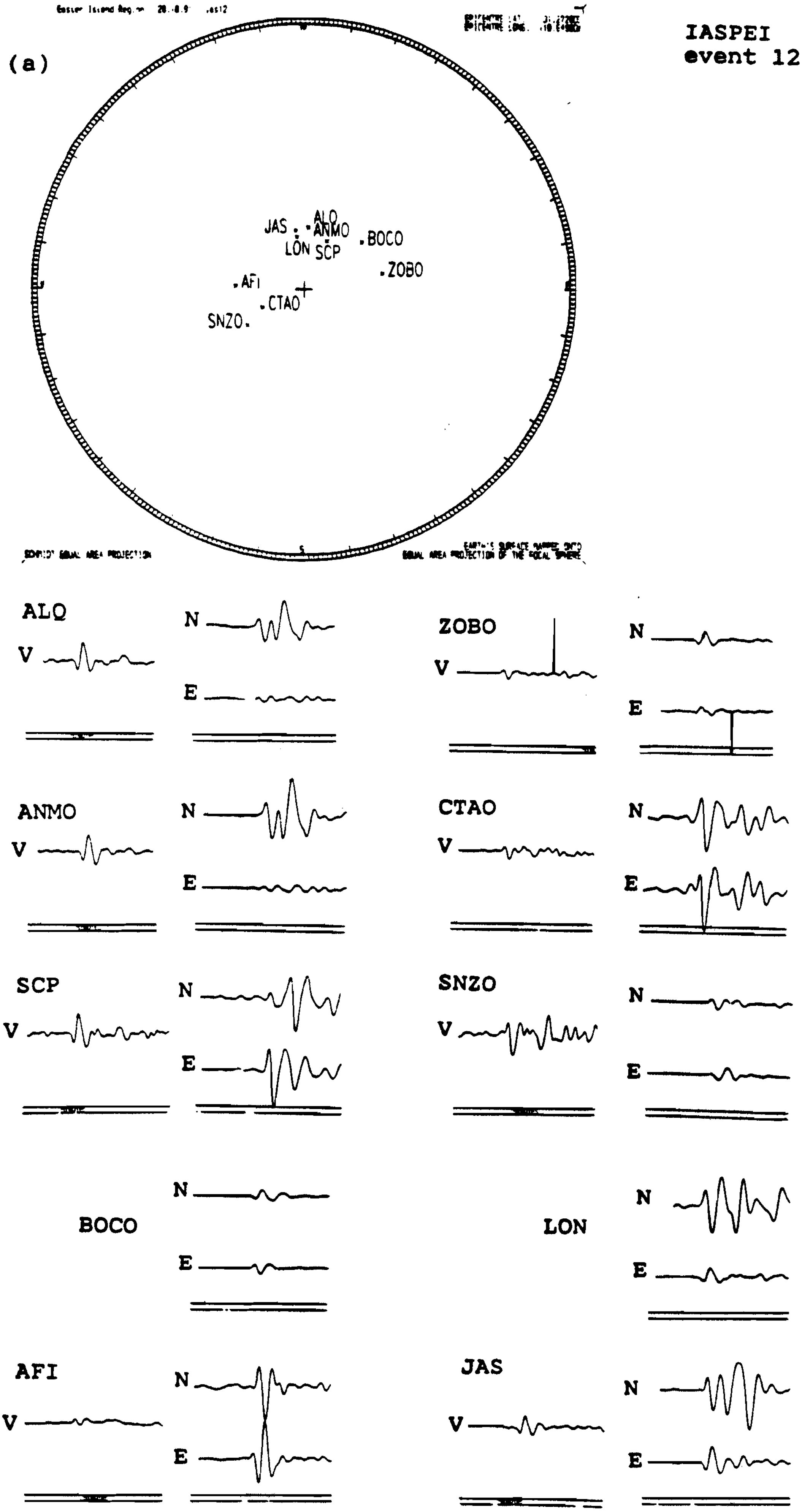

(a)
IASPEI
event 12
JAS
ALQ
ANMO
LON
SCP
BOCO
ZOBO
AFI
CTAO
SNZO
ALQ
V
N
E
ZOBO
V
N
E
ANMO
V
N
E
CTAO
V
N
E
SCP
V
N
E
SNZO
V
N
E
BOCO
N
E
LON
N
E
AFI
V
N
E
JAS
V
N
E

IASPEI
event 12

(b)

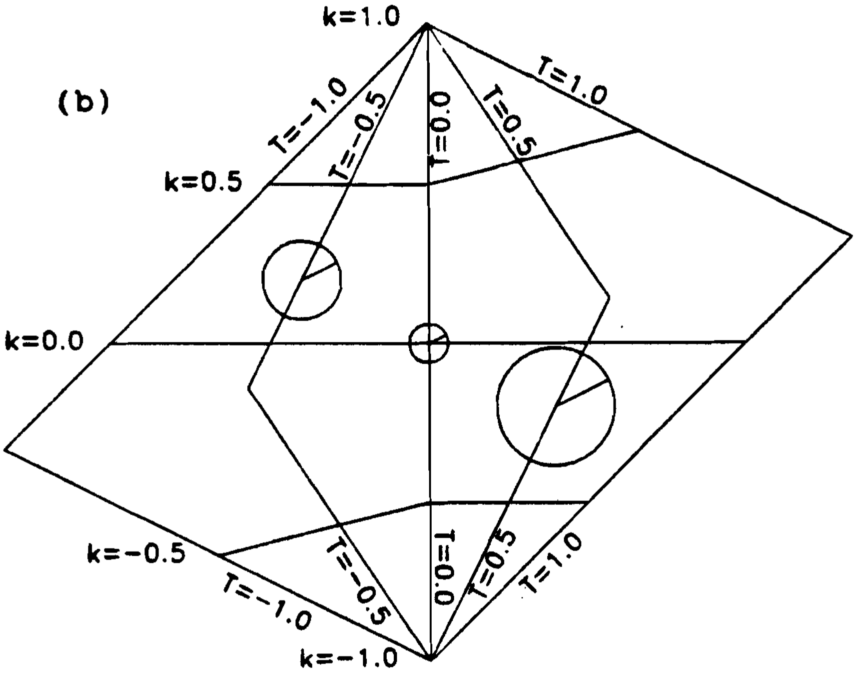

(c)

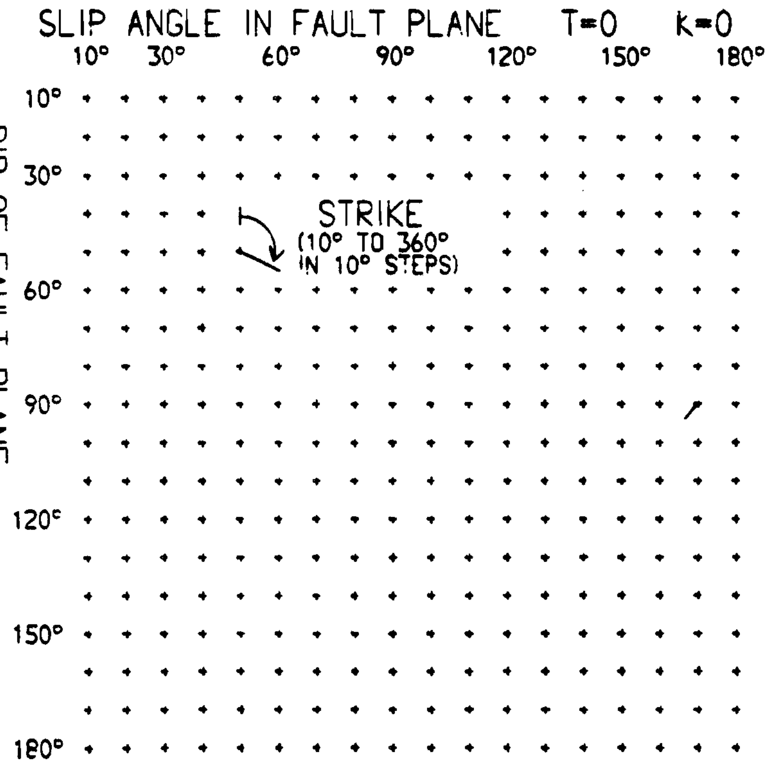

(d)

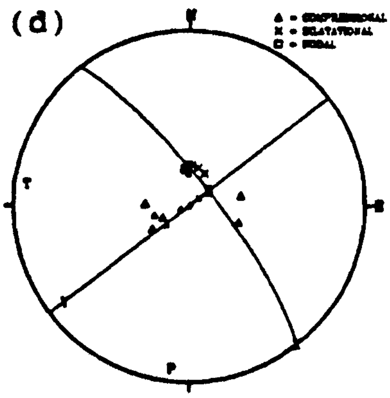

(e)

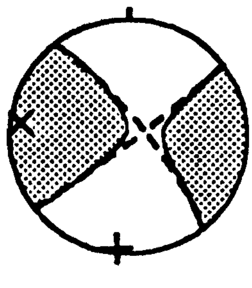

(f)

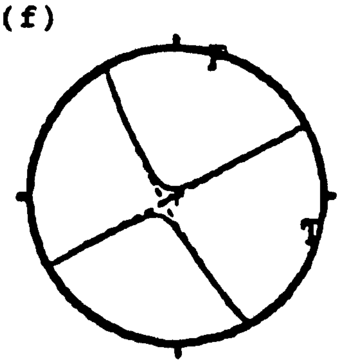

IASPEI
event 13

(a)

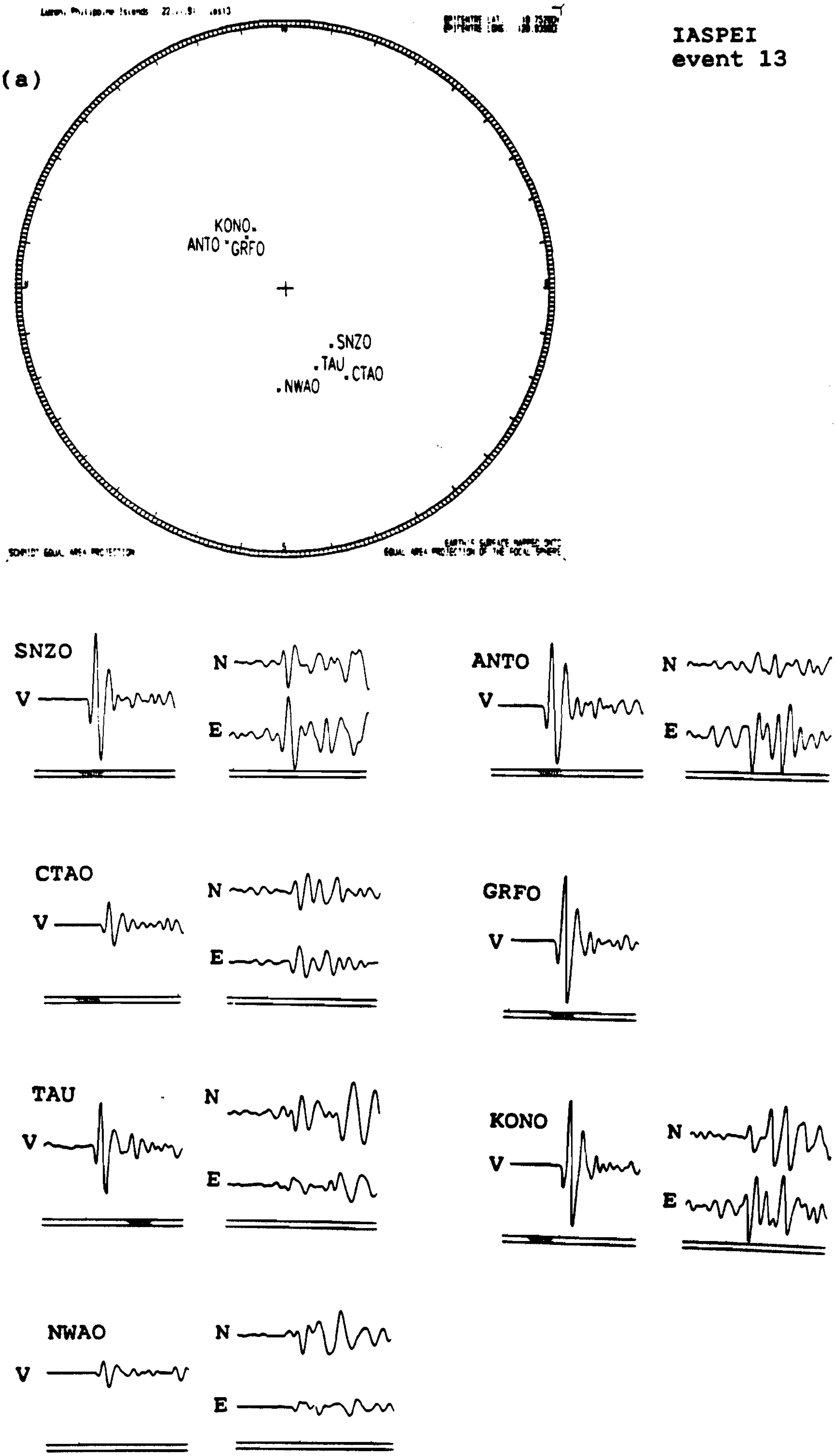

IASPEI
event 13

(b)

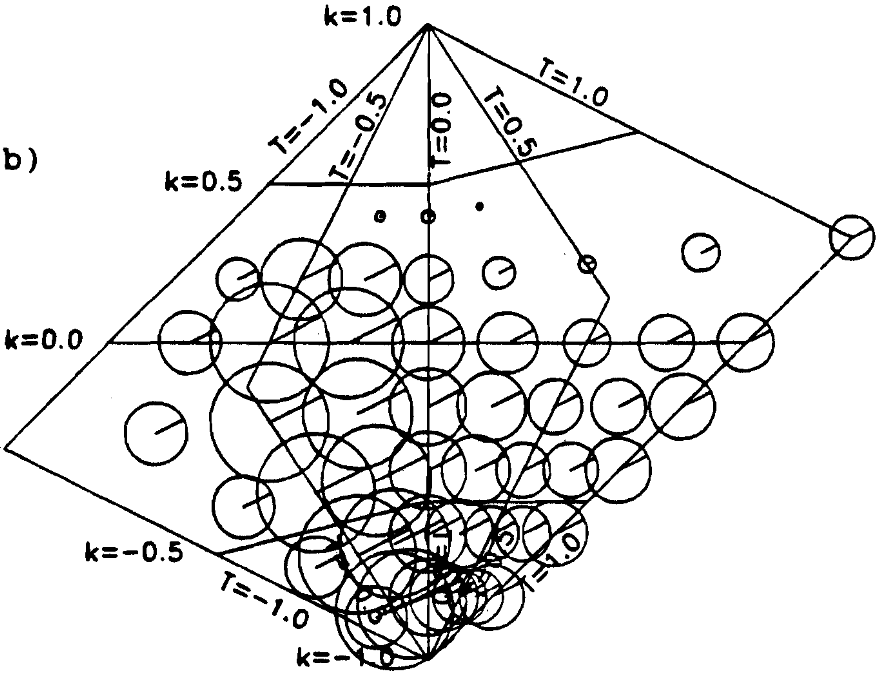

(c)

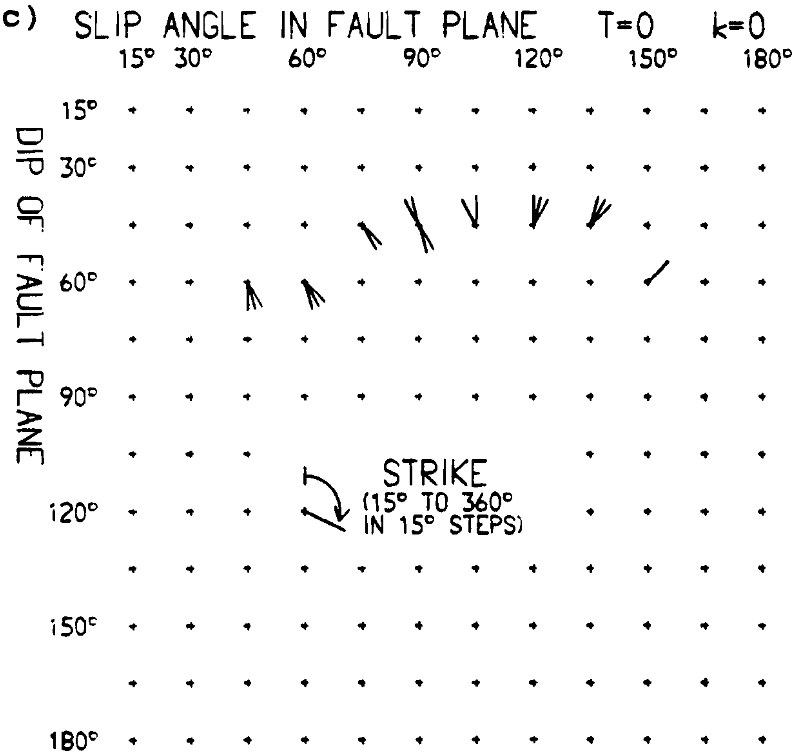

(d)

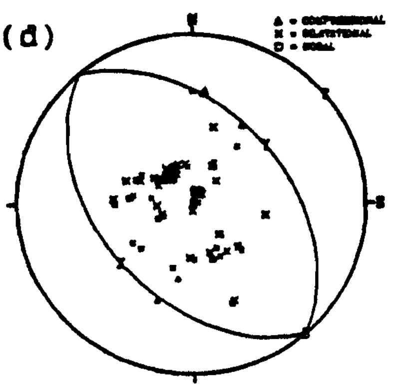

(e)

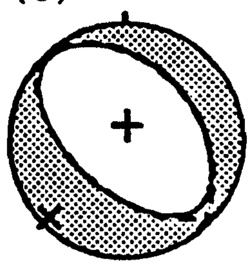

(f)

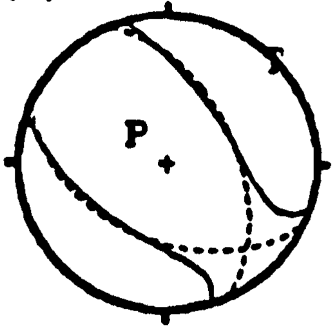

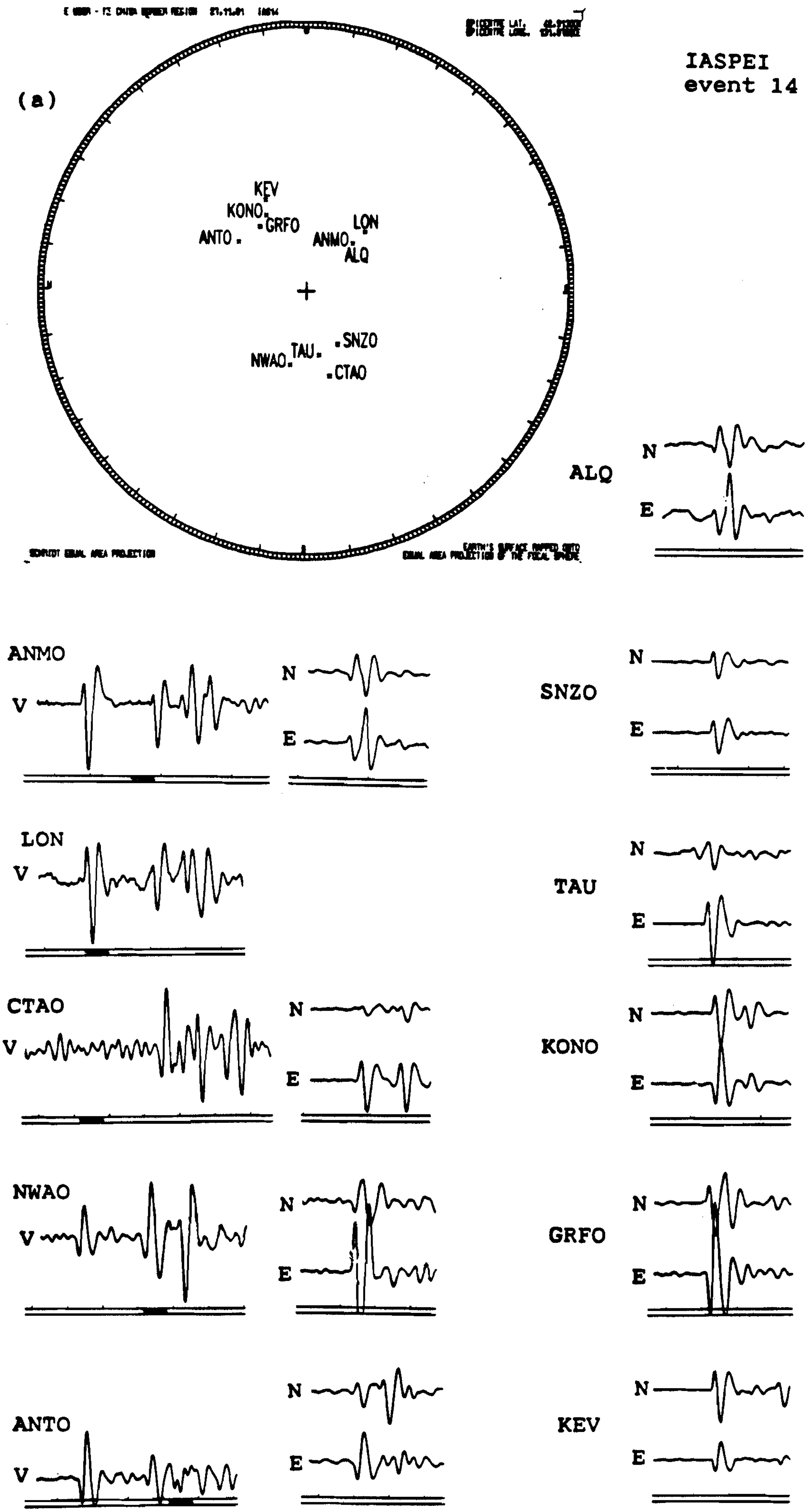
(a)
IASPEI
event 14
KEV
KONO
GRFO
LON
ANTO
ANMO
ALQ
SNZO
NWAO
TAU
CTAO
ALQ N E
ANMO V N E
SNZO N E
LON V
TAU N E
CTAO V N E
KONO N E
NWAO V N E
GRFO N E
ANTO V N E
KEV N E

IASPEI
event 14

(b)

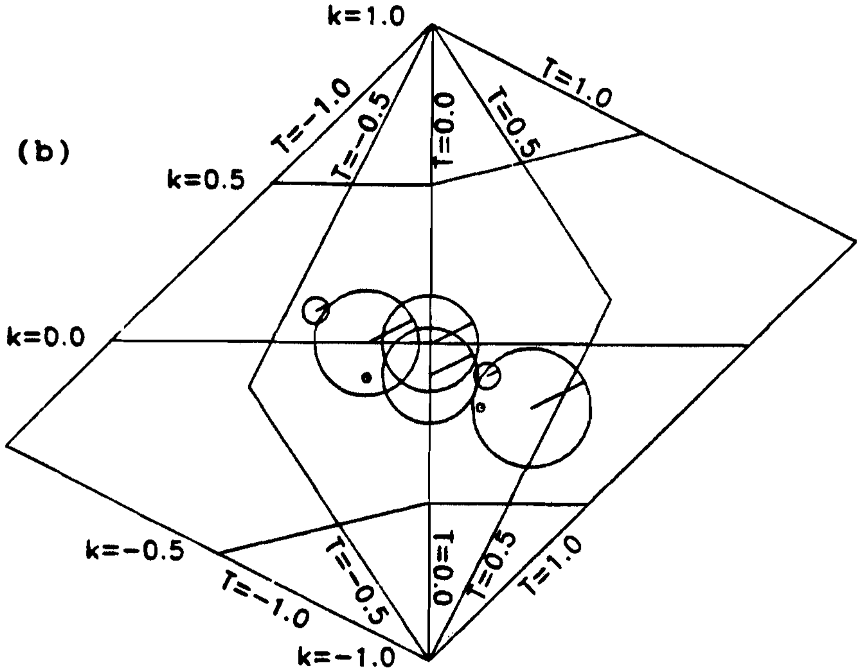

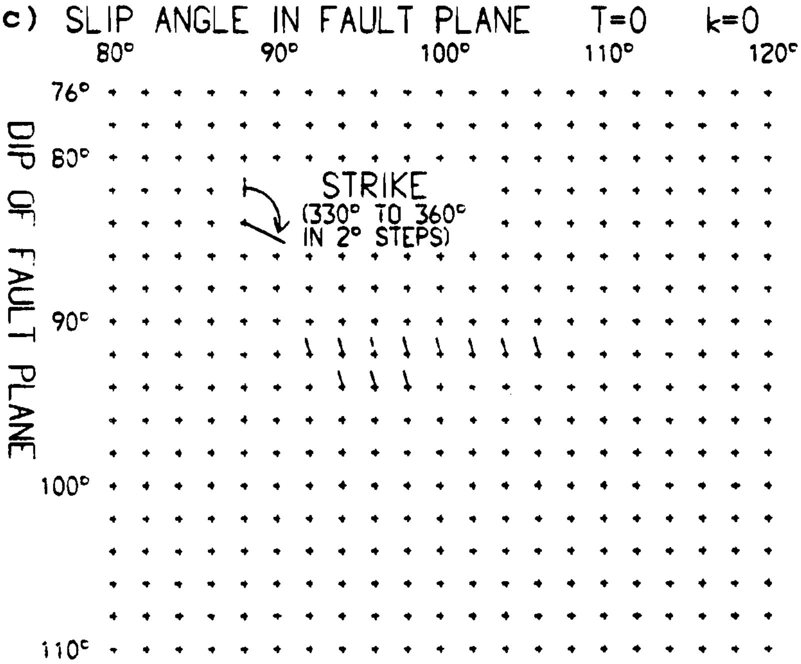

(d)

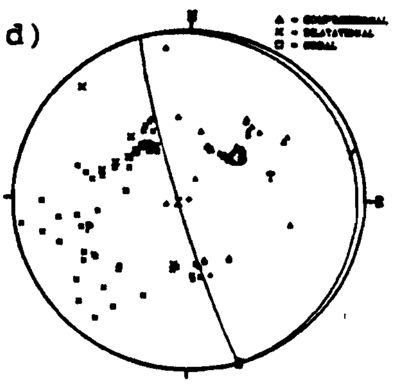

(e)

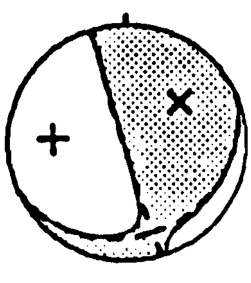

(f)

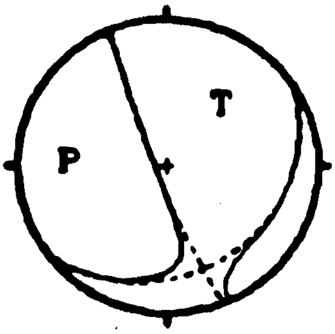

IASPEI
event 15

(a)

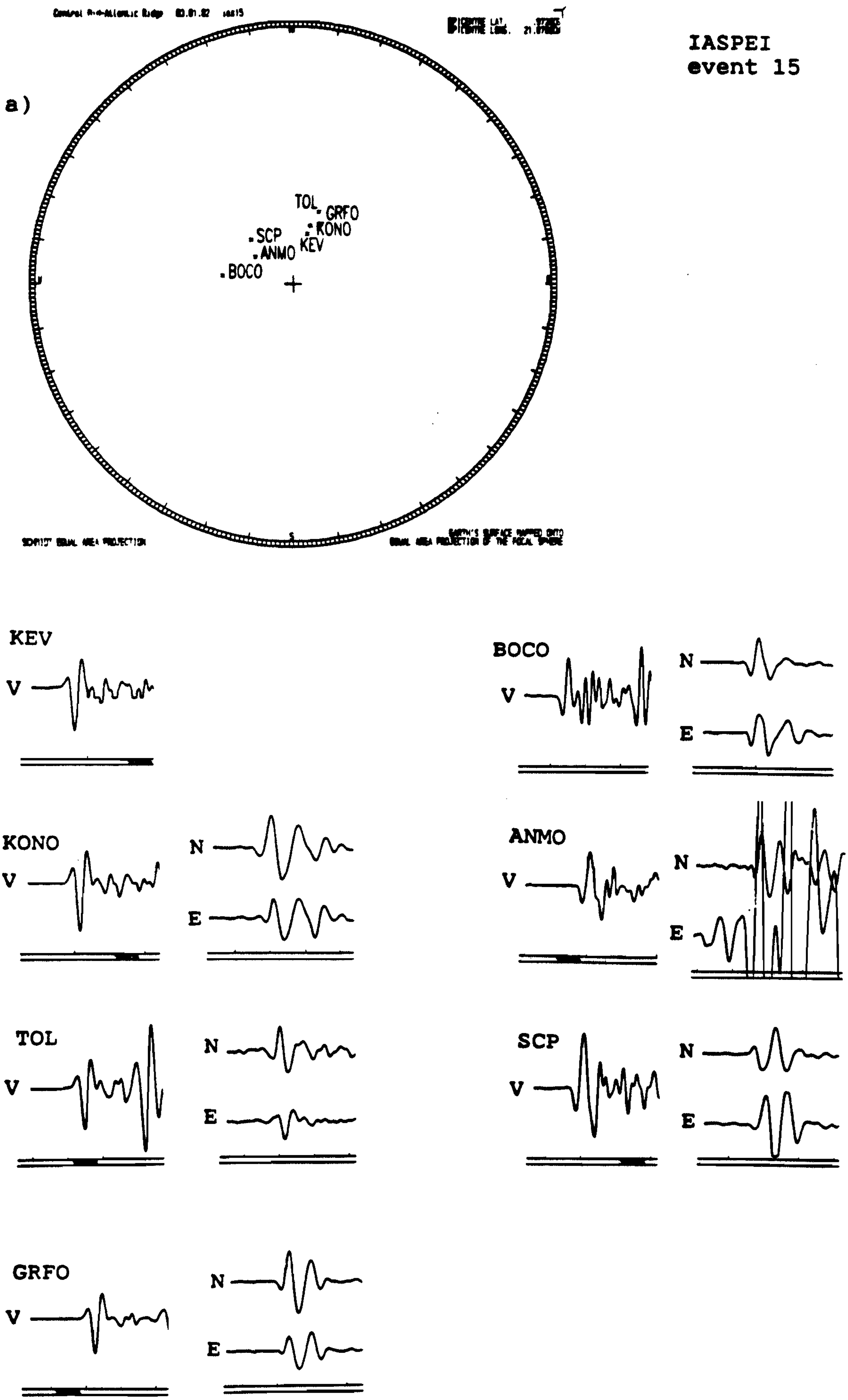

IASPEI
event 15

(b)

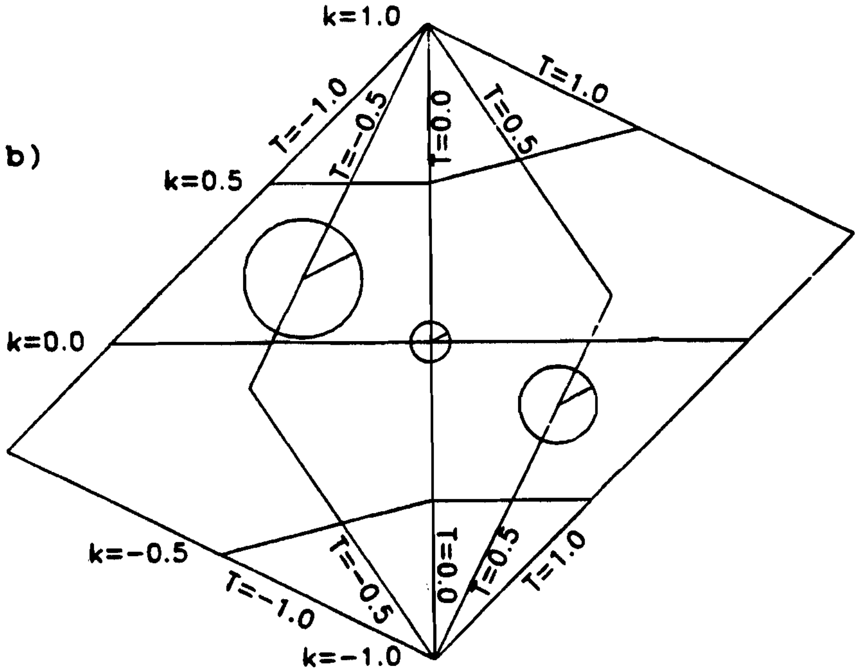

(c)

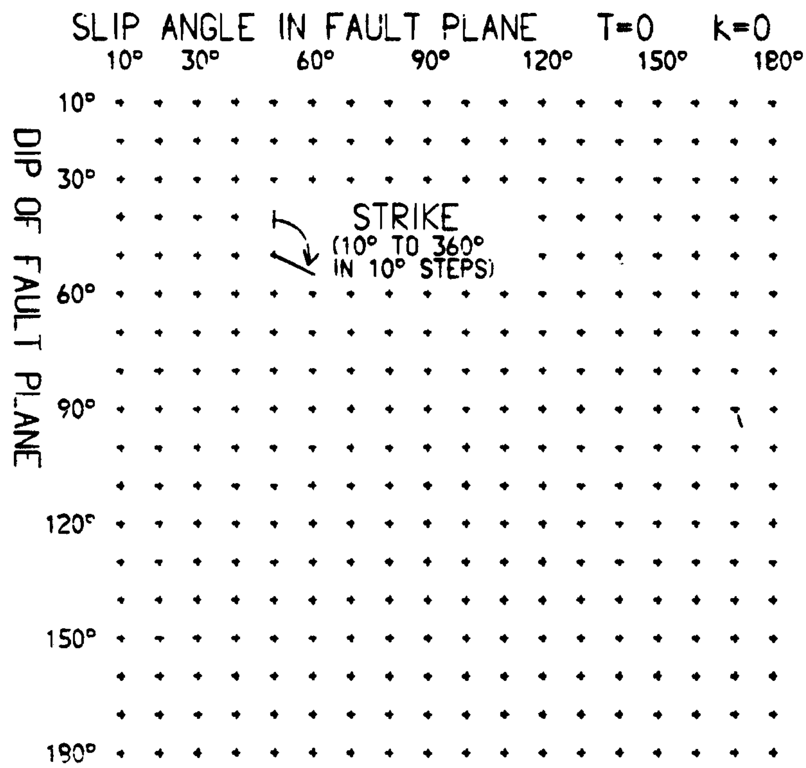

(d)

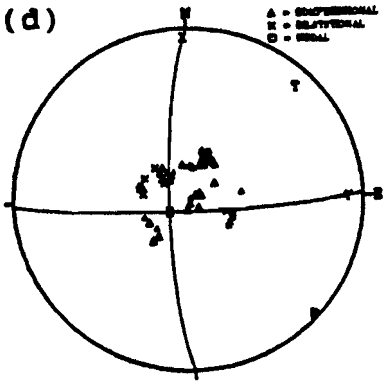

(e)

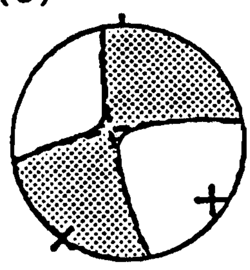

(f)

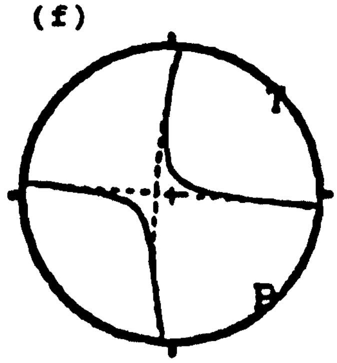

(a)

IASPEI
event 16

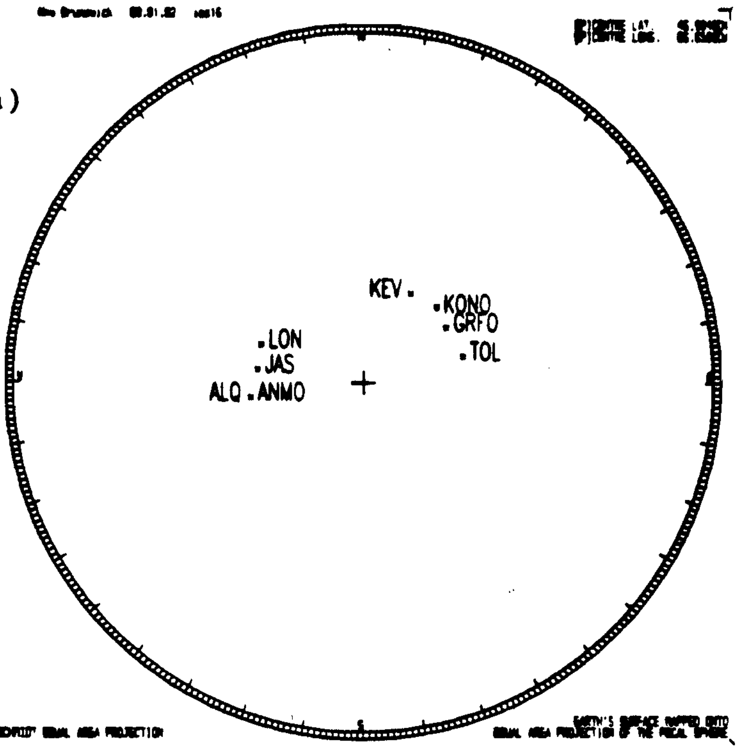

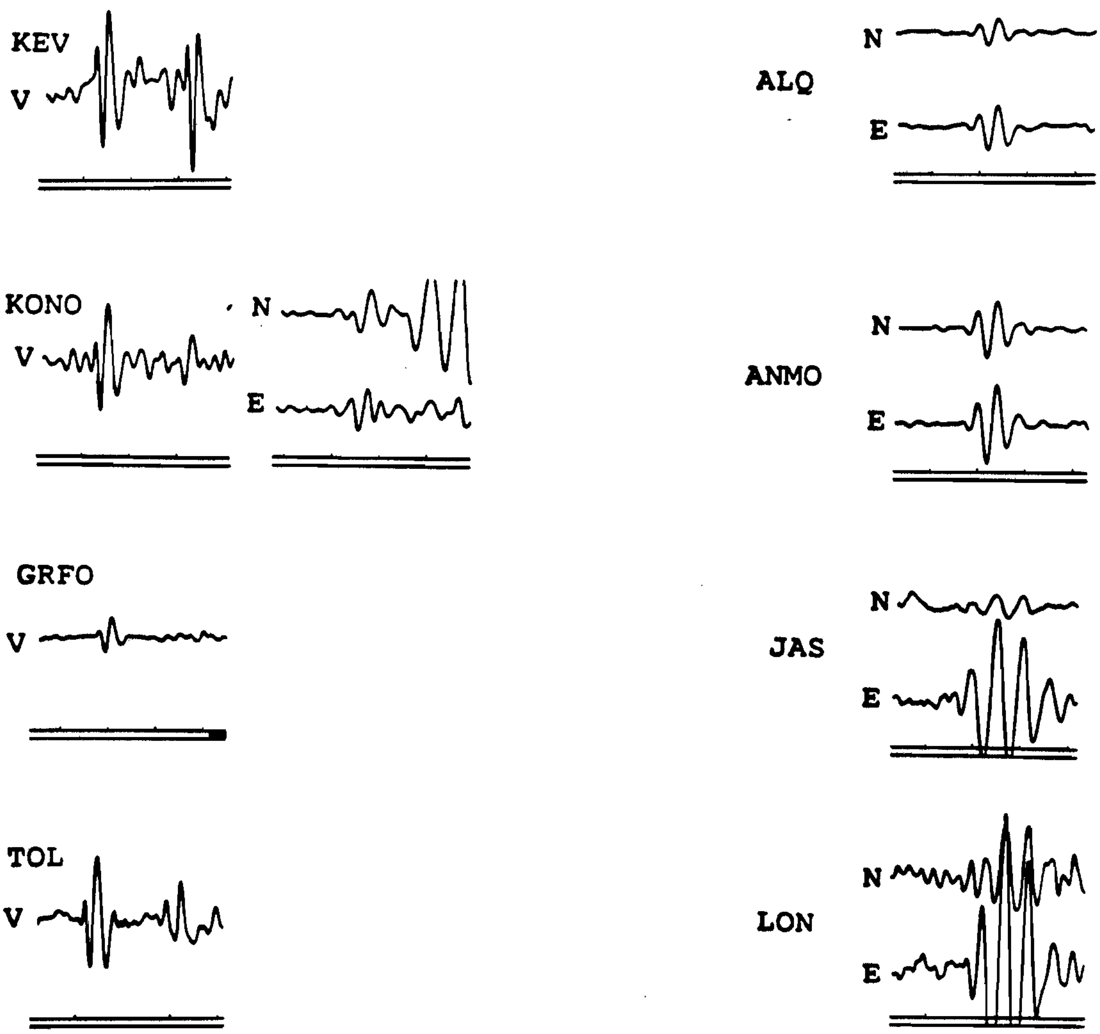

IASPEI
event 16

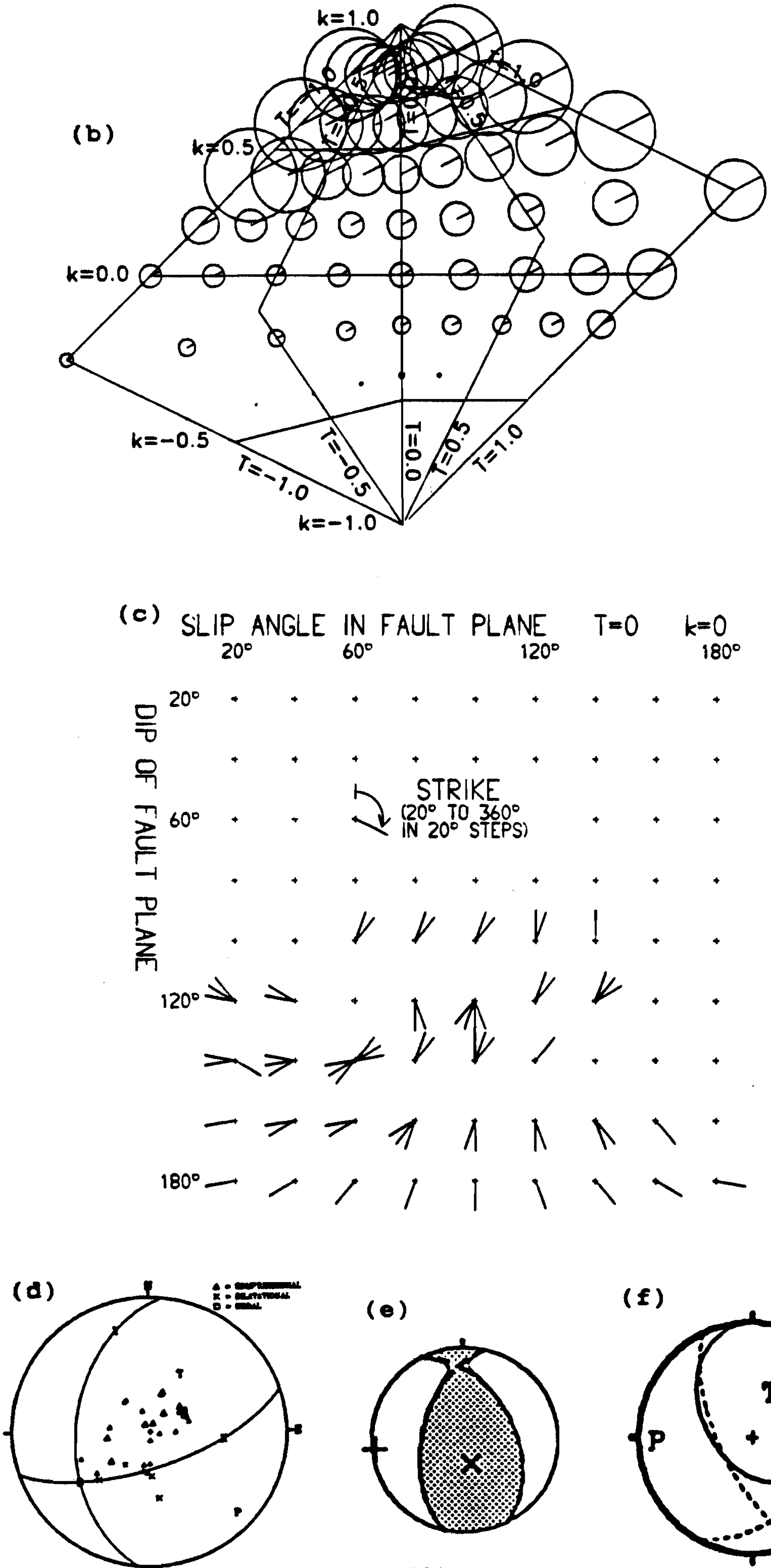

(a)

IASPEI
event 17

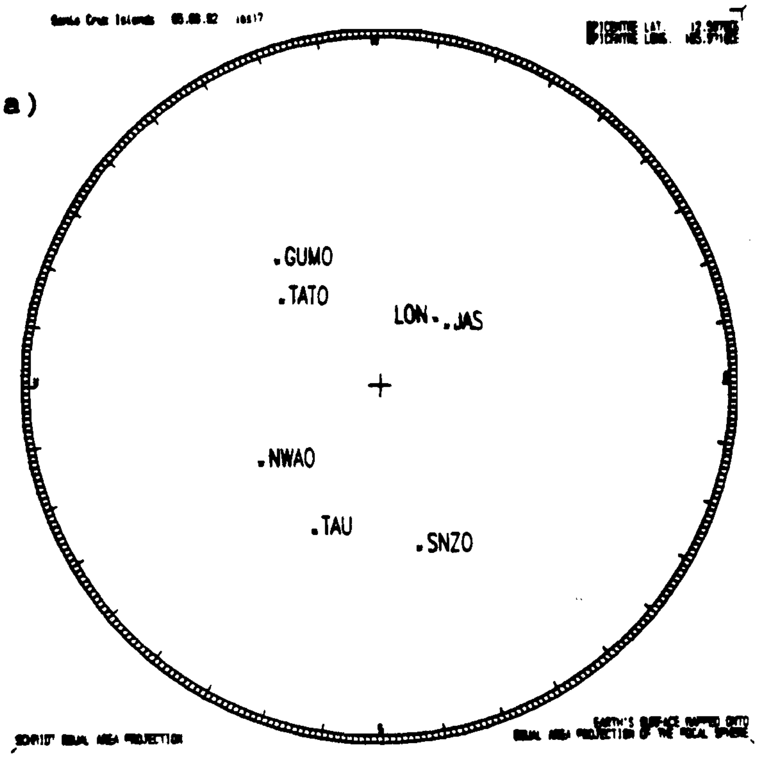

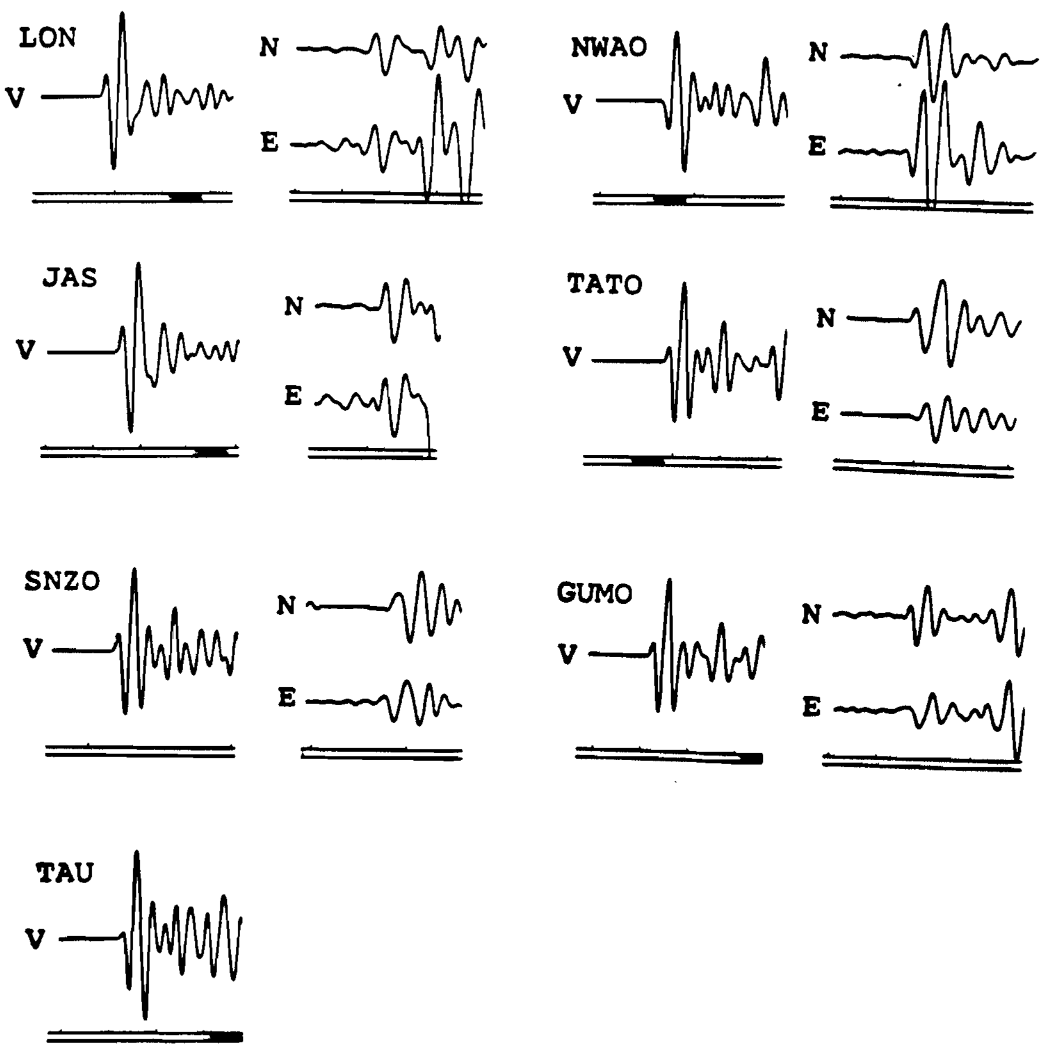

IASPEI
event 17

(b)

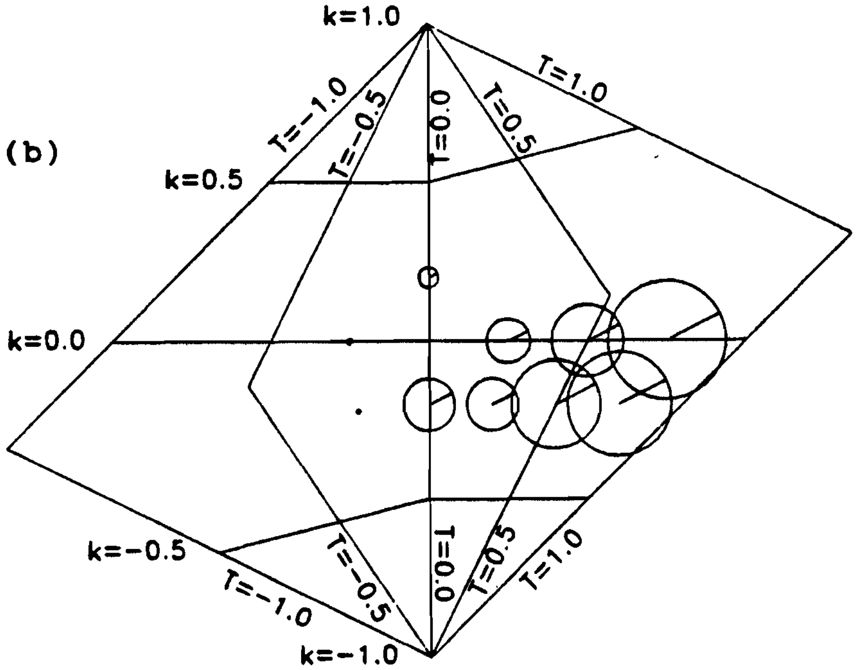

(c)

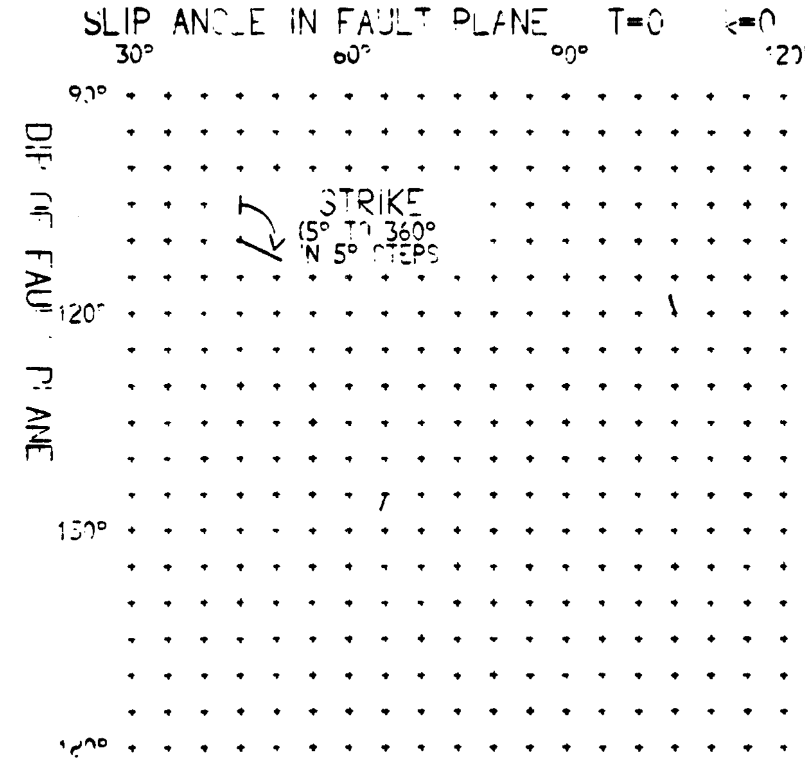

(d)

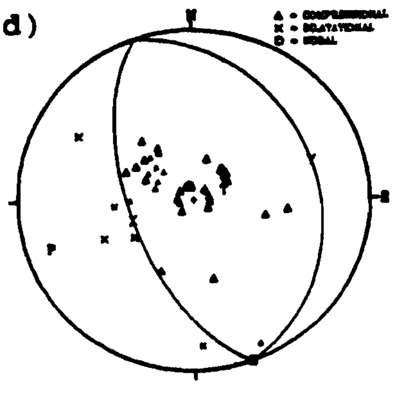

(e)

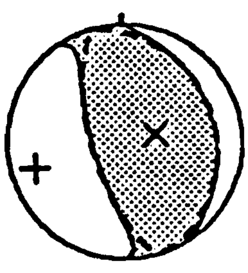

(f)

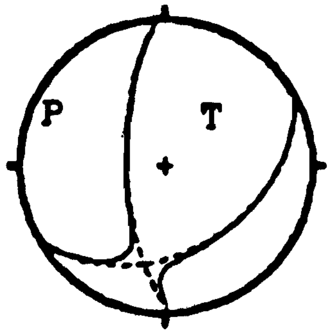

IASPEI
event 18

(a)

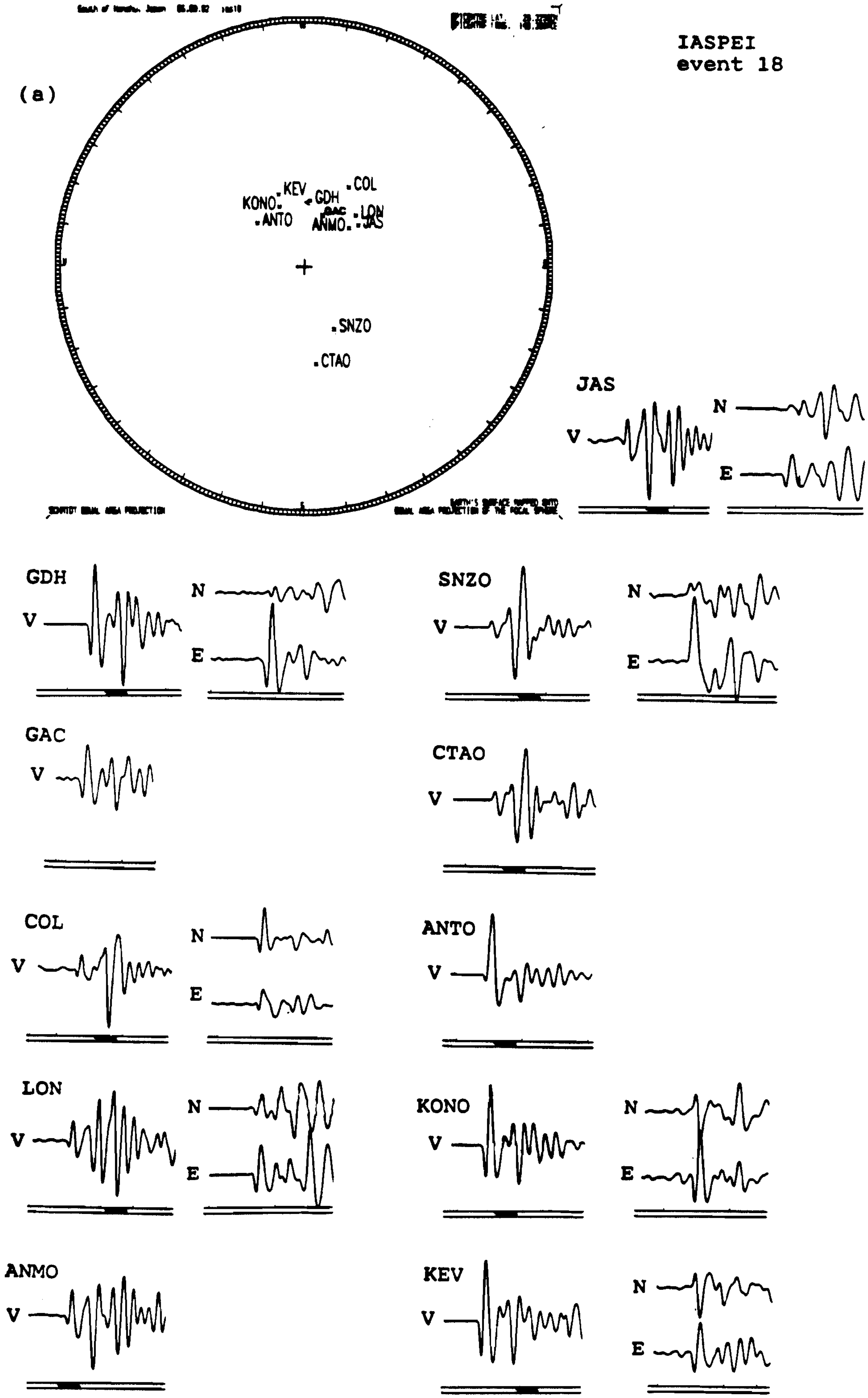

IASPEI
event 18

(b)

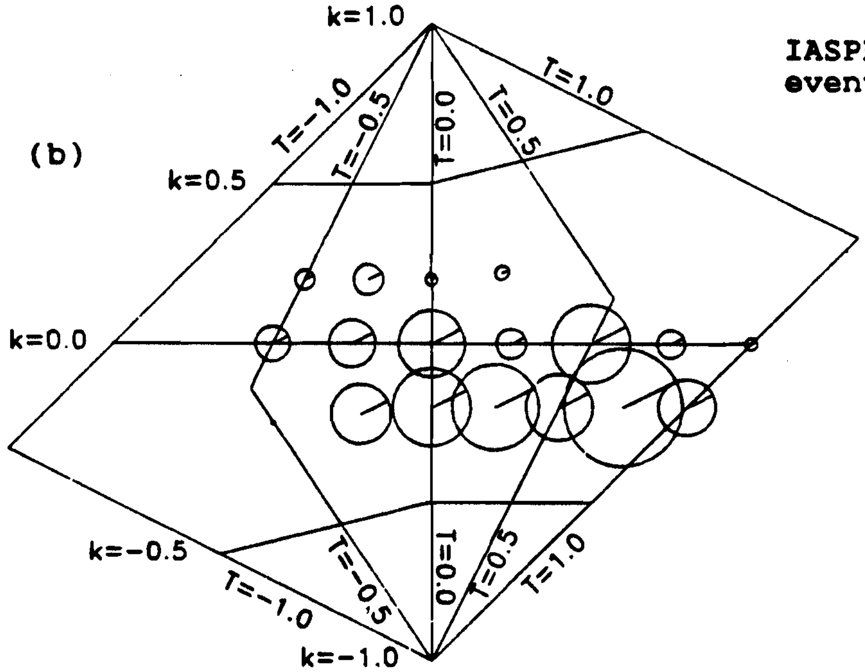

(c)

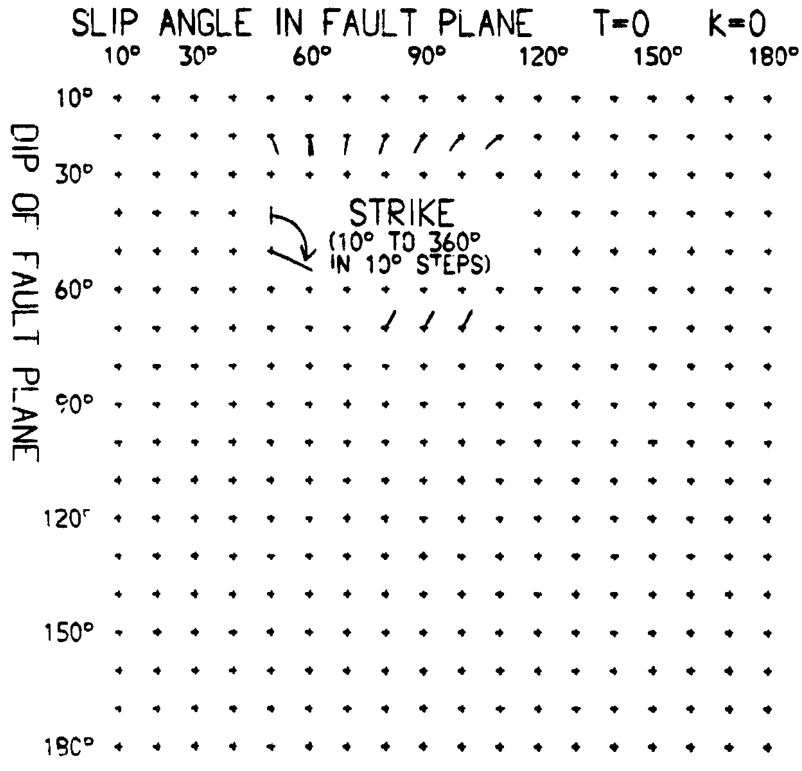

(d)

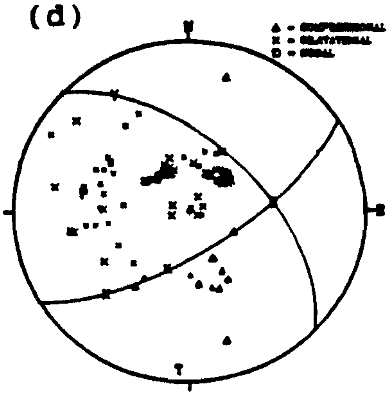

(e)

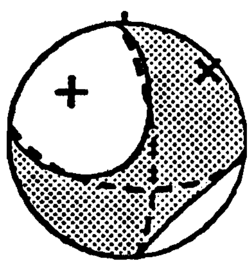

(f)

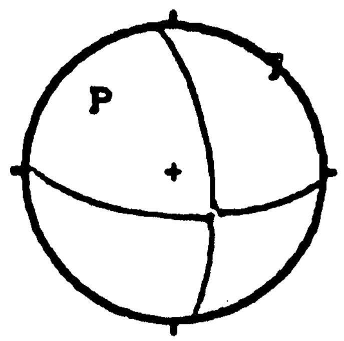

IASPEI
event 19

(a)

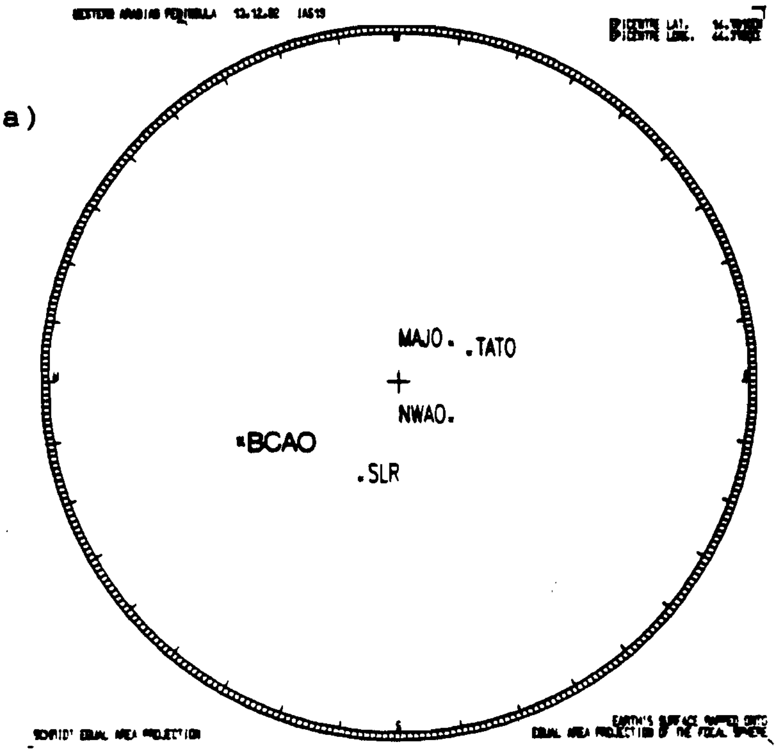

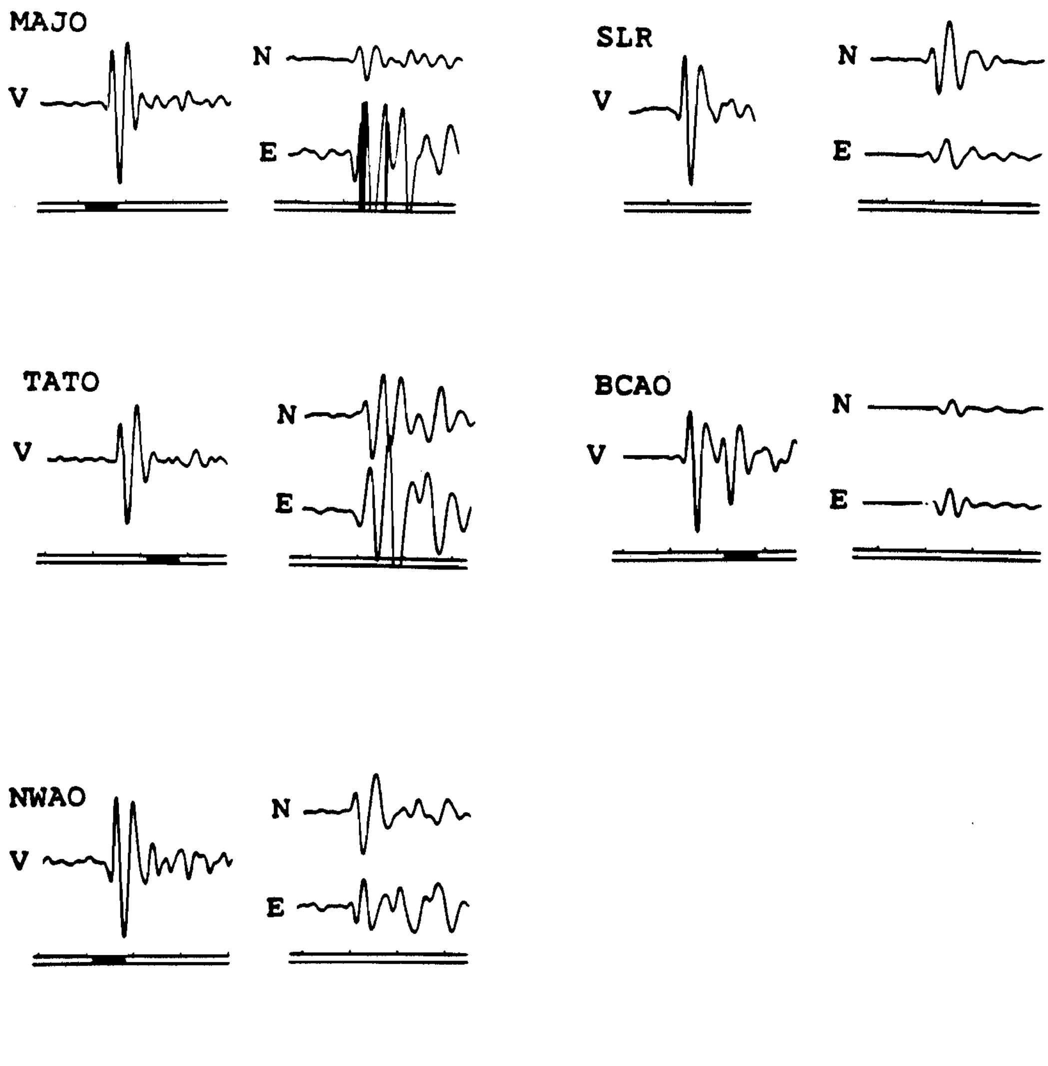

IASPEI
event 19

(b)

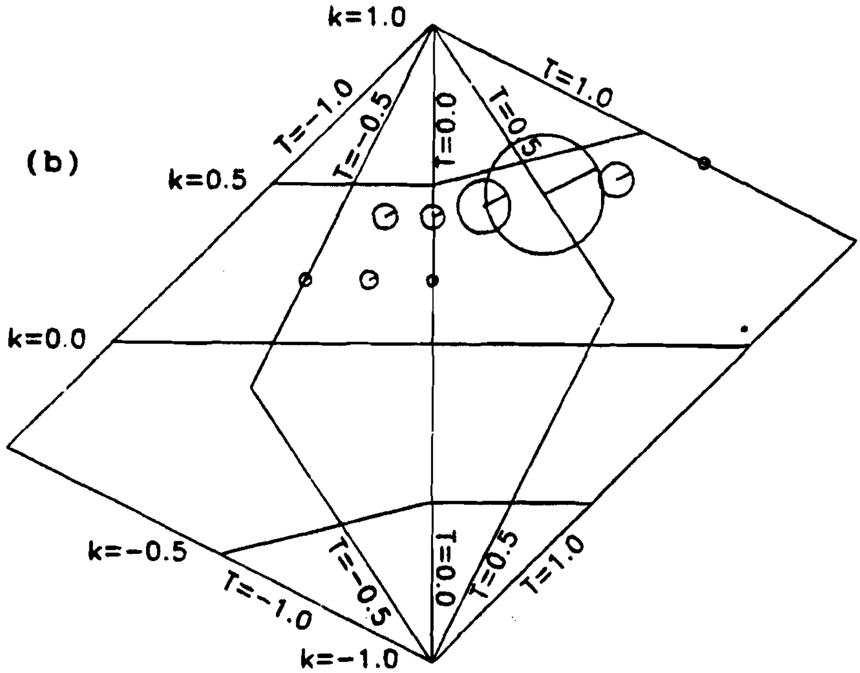

(c)

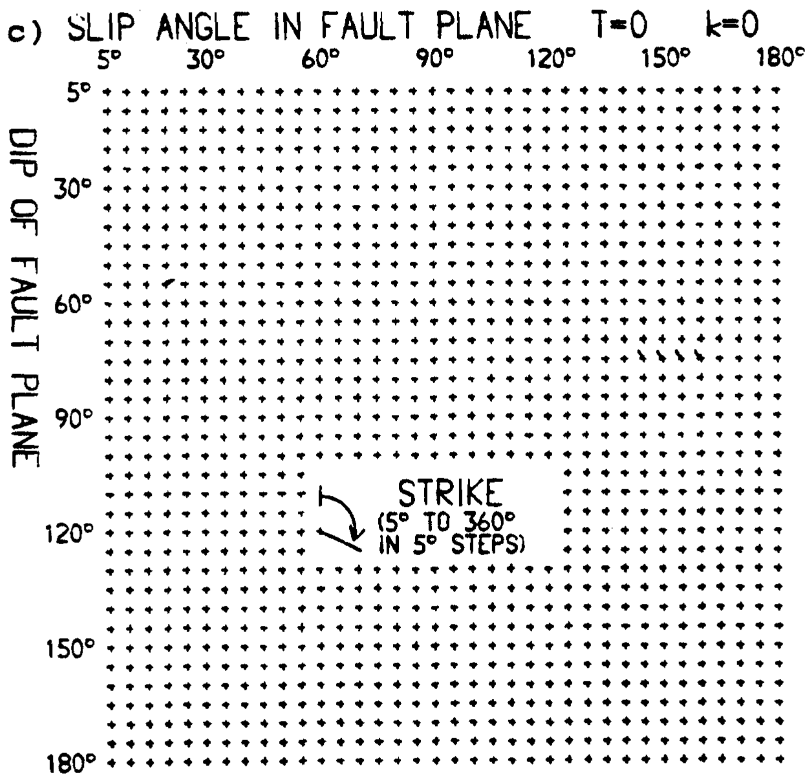

(d) (e) (f)

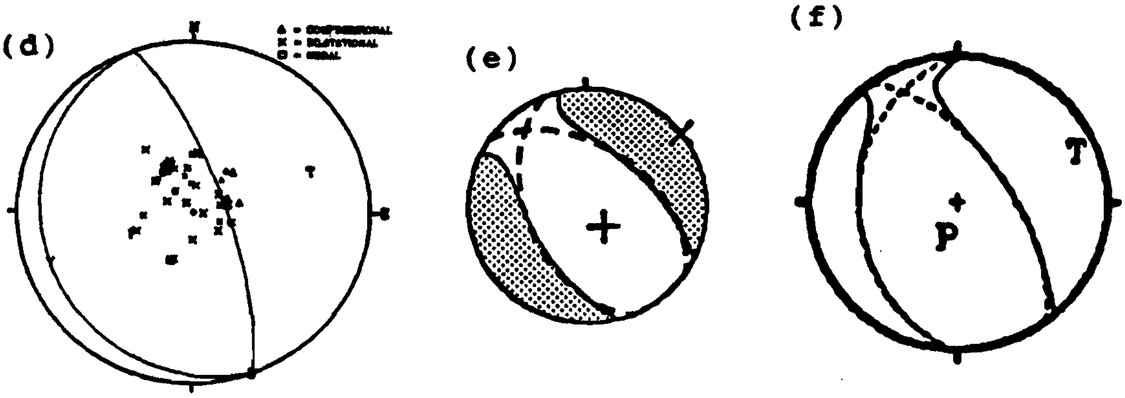

IASPEI
event 20

(a)

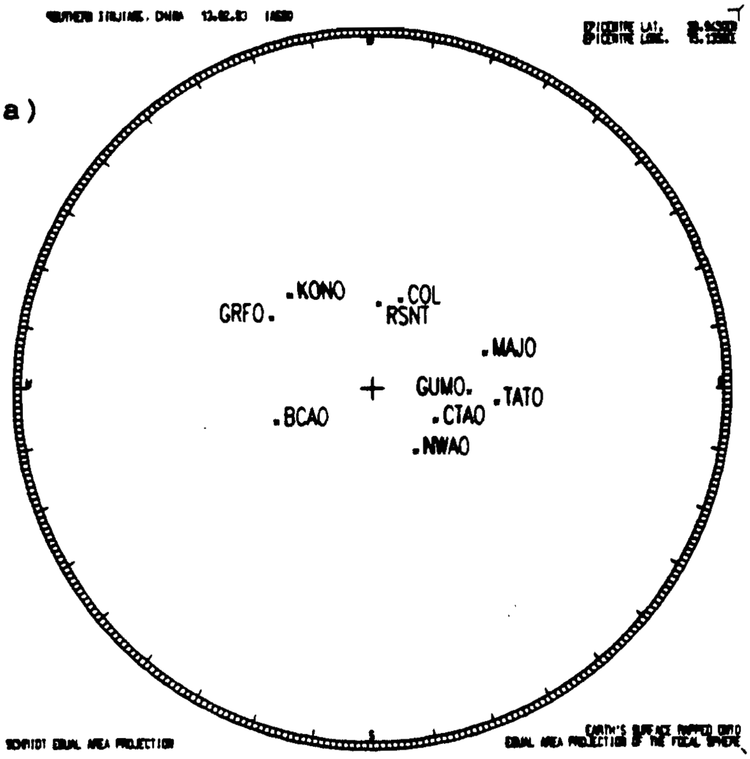

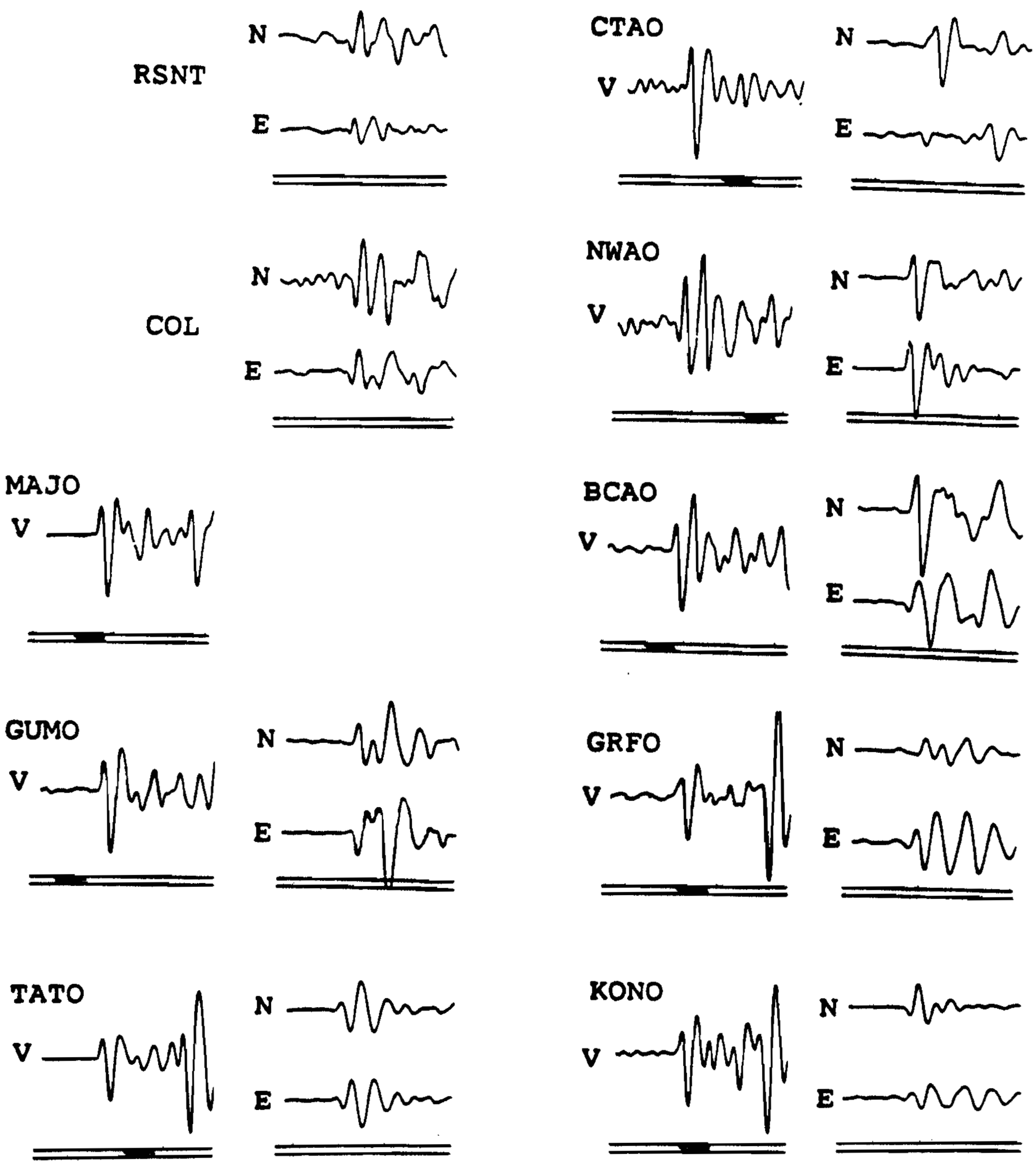

IASPEI
event 20

(b)

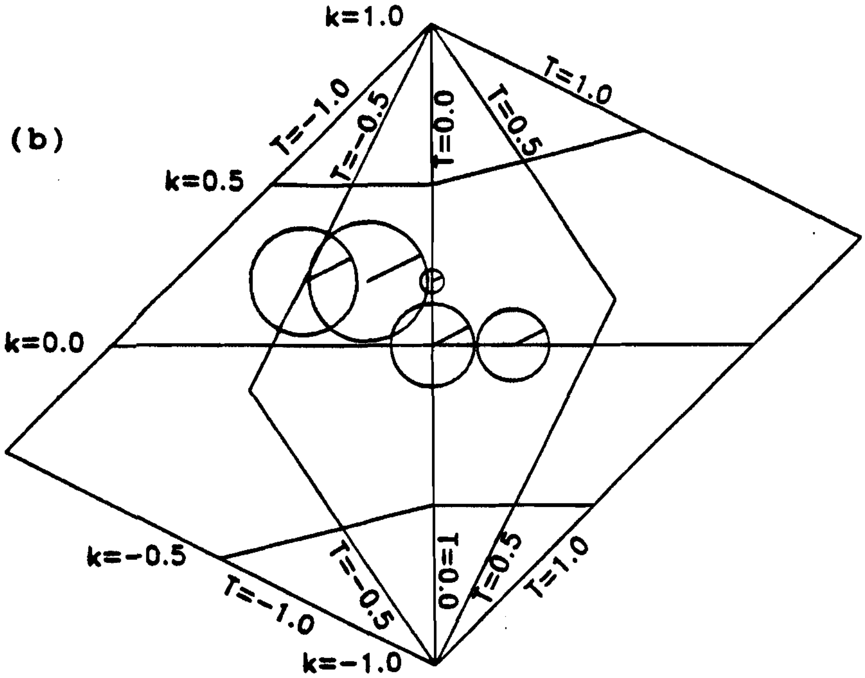

(c)

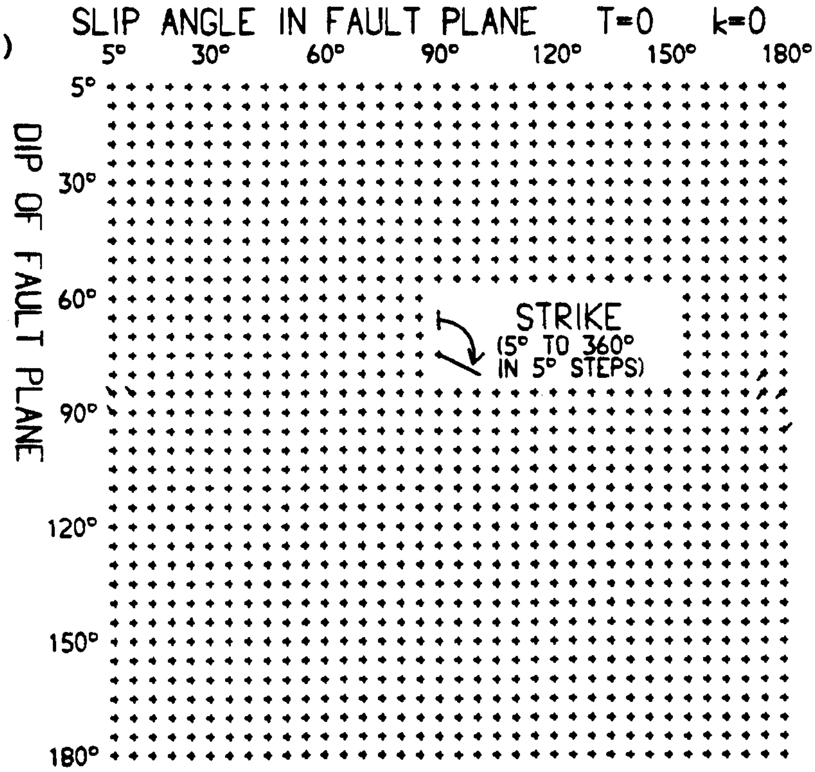

(d)

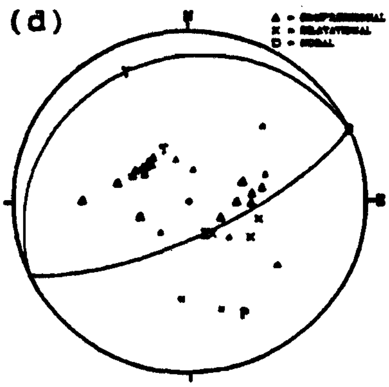

(e)

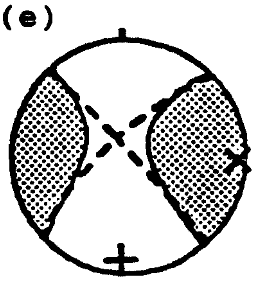

(f)

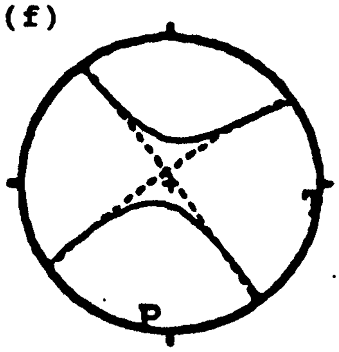

IASPEI
event 21

(a)

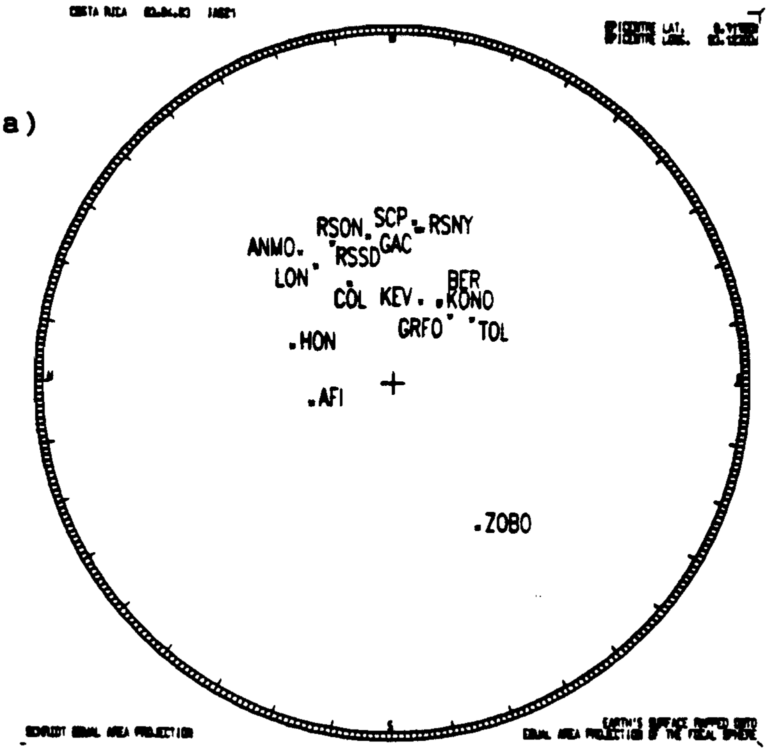

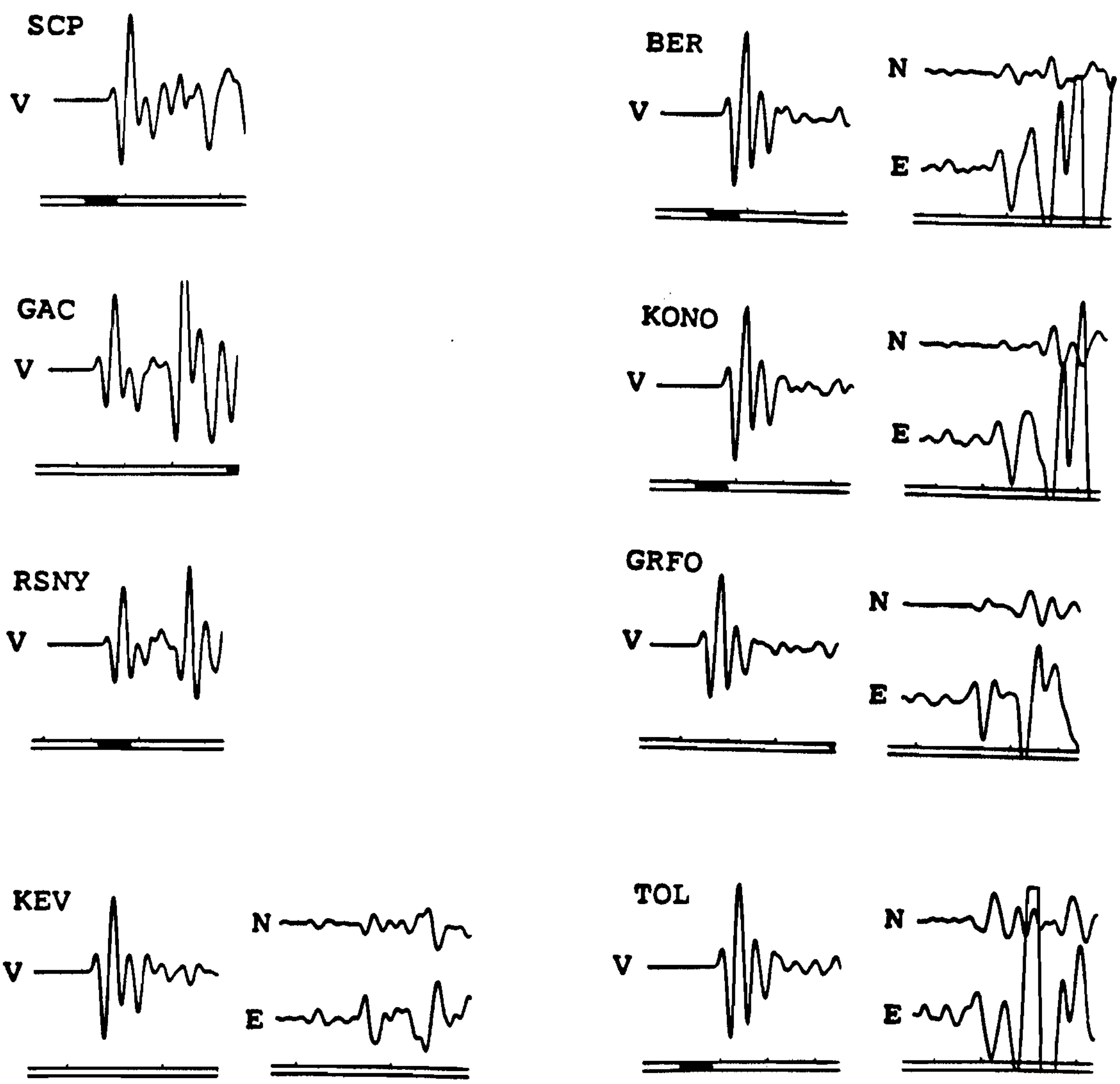

IASPEI
event 21

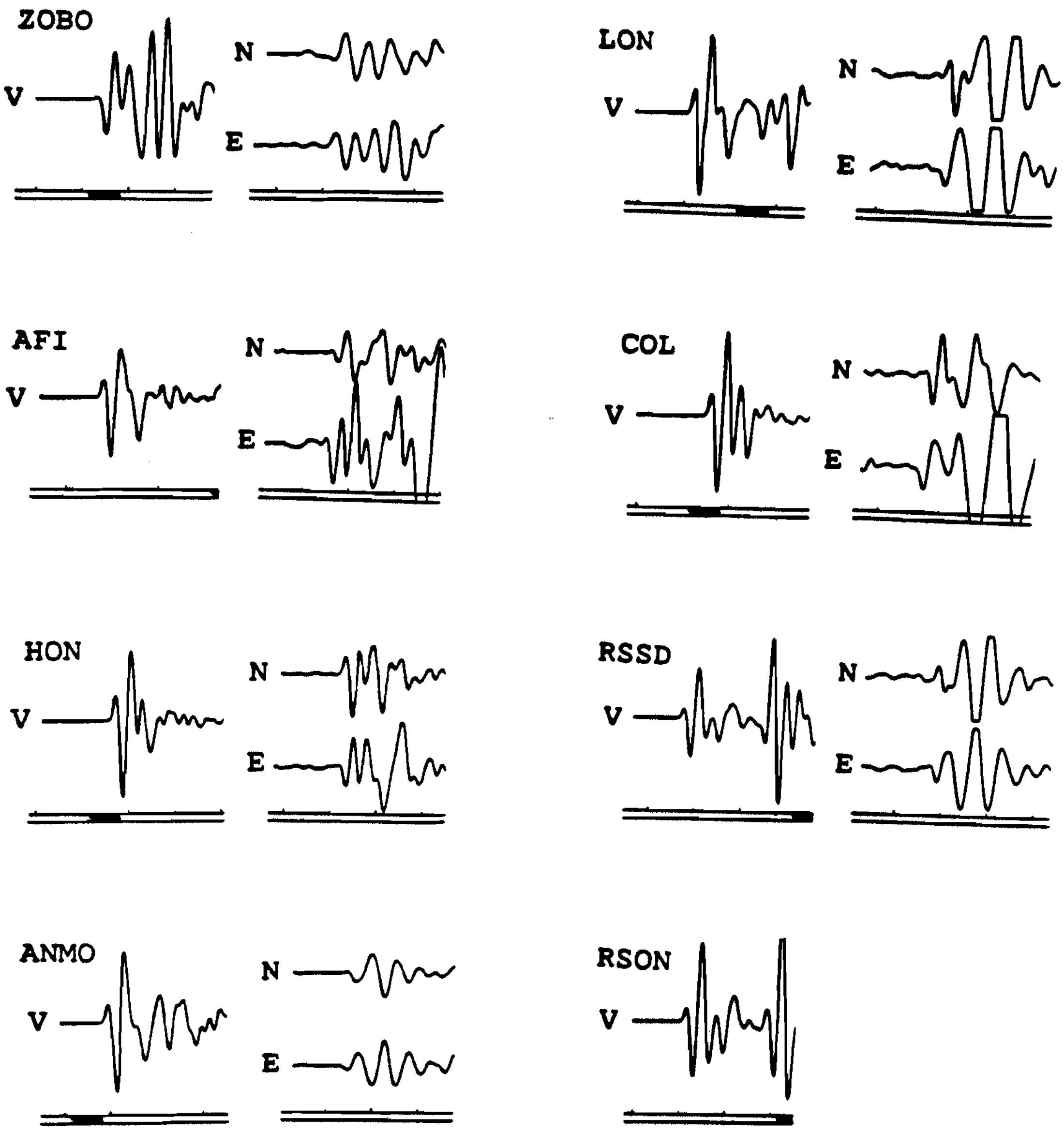

IASPEI
event 21

(b)

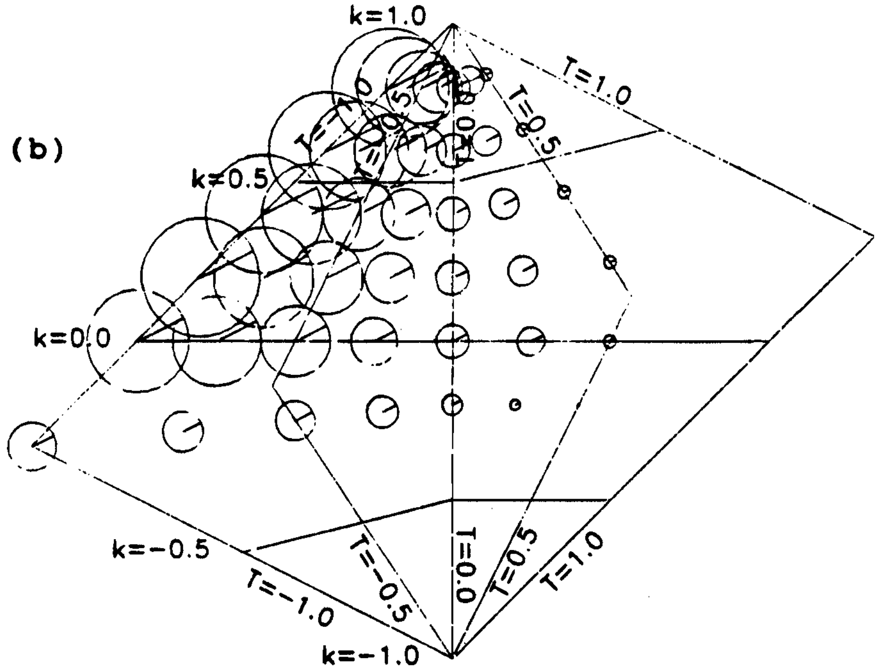

(c)

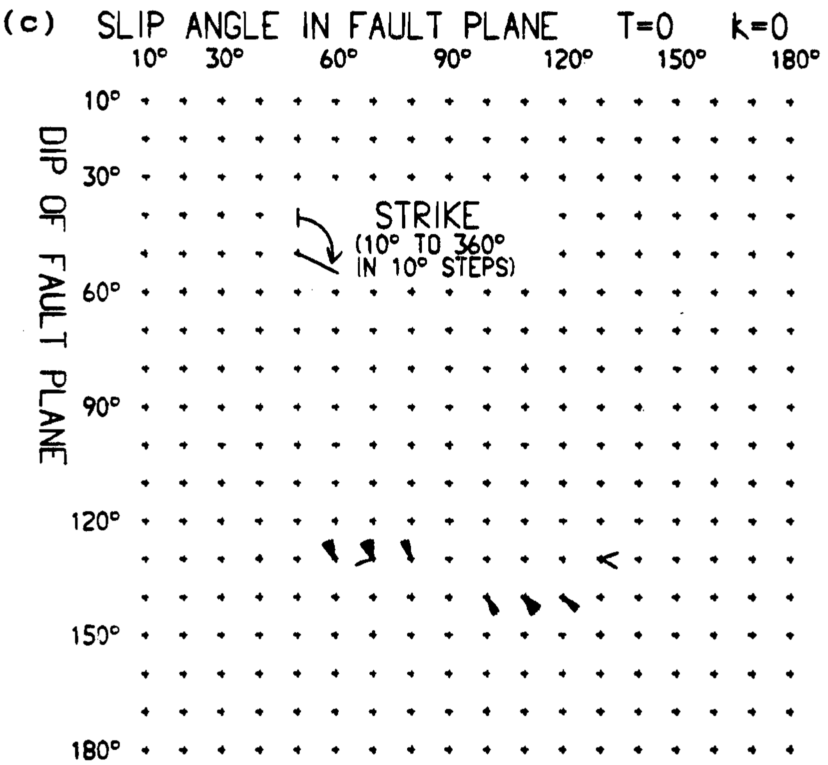

(d)

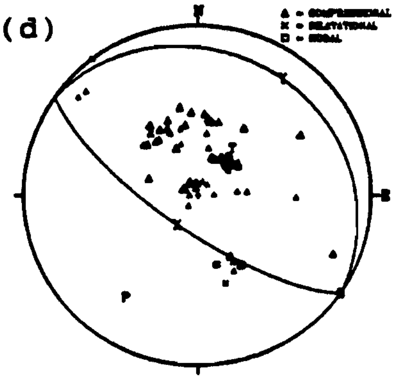

(e)

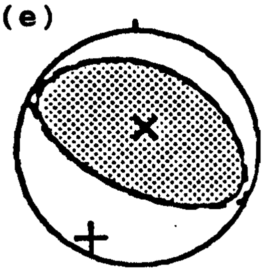

(f)

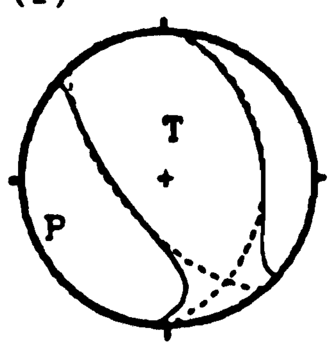

THIS PAGE LEFT BLANK INTENTIONALLY

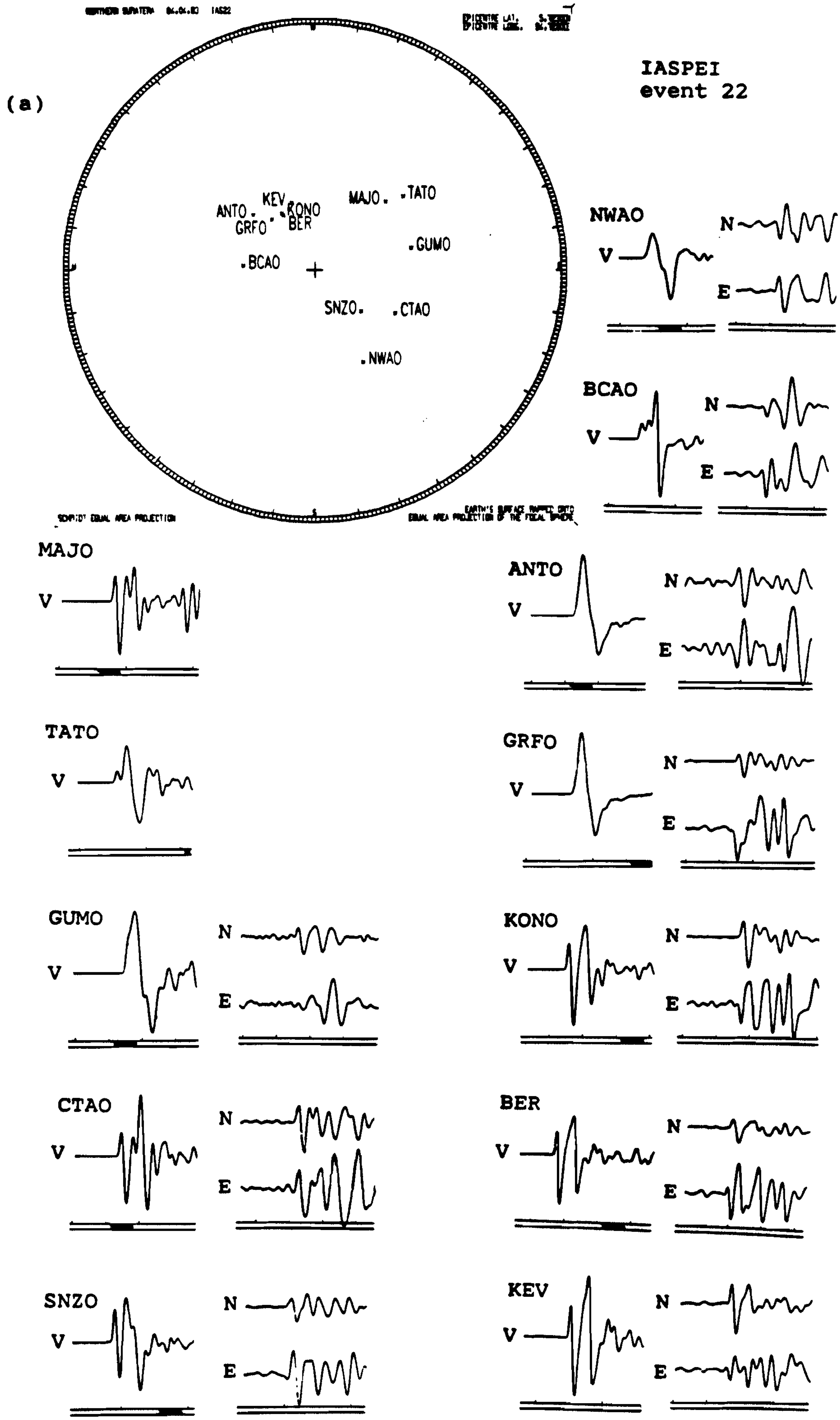

(a)
IASPEI
event 22
ANTO
KEV
KONO
GRFO
BER
MAJO
TATO
GUMO
BCAO
SNZO
CTAO
NWAO
NWAO
BCAO
MAJO
ANTO
TATO
GRFO
GUMO
KONO
CTAO
BER
SNZO
KEV
V
N
E

IASPEI
event 22

(b)

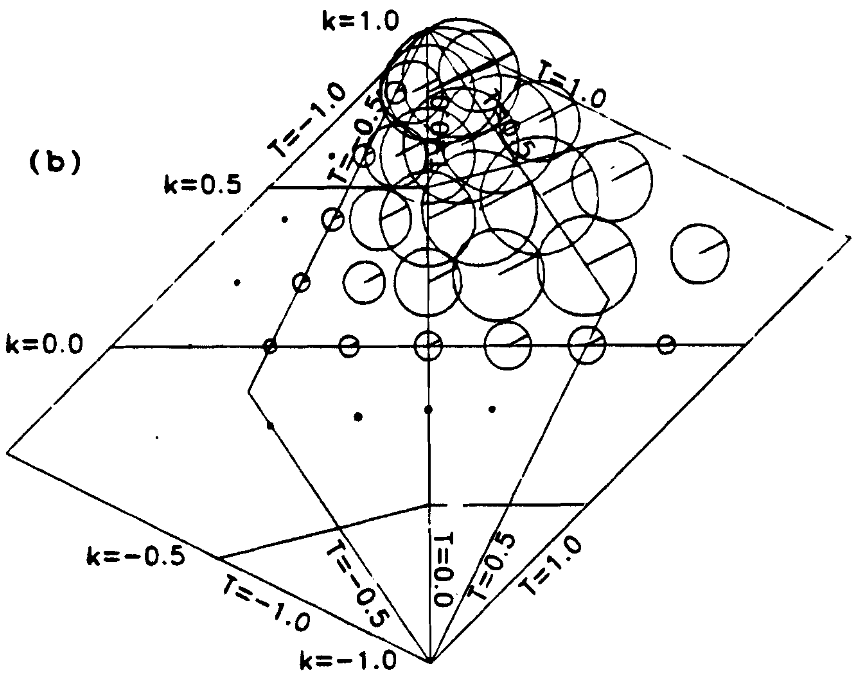

(c)

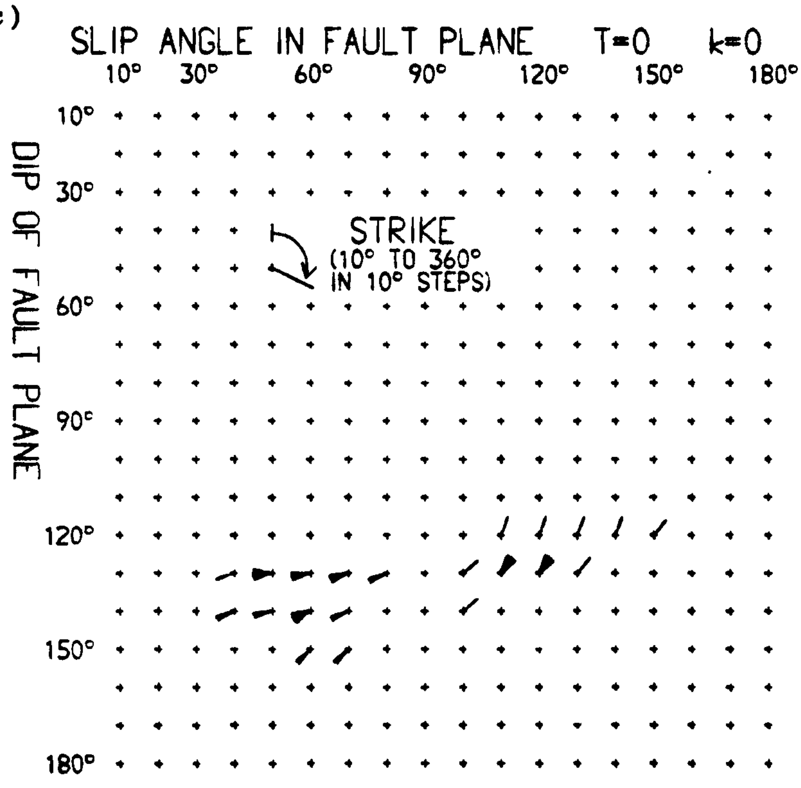

(d)

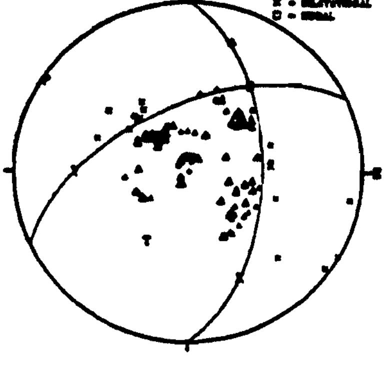

(e)

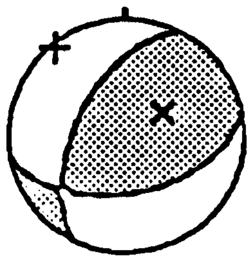

(f)

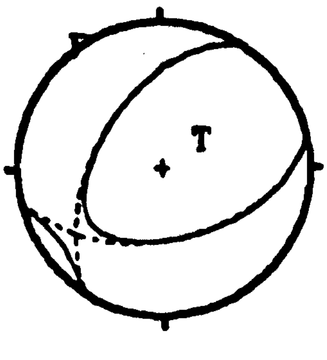

IASPEI
event 23

(a)

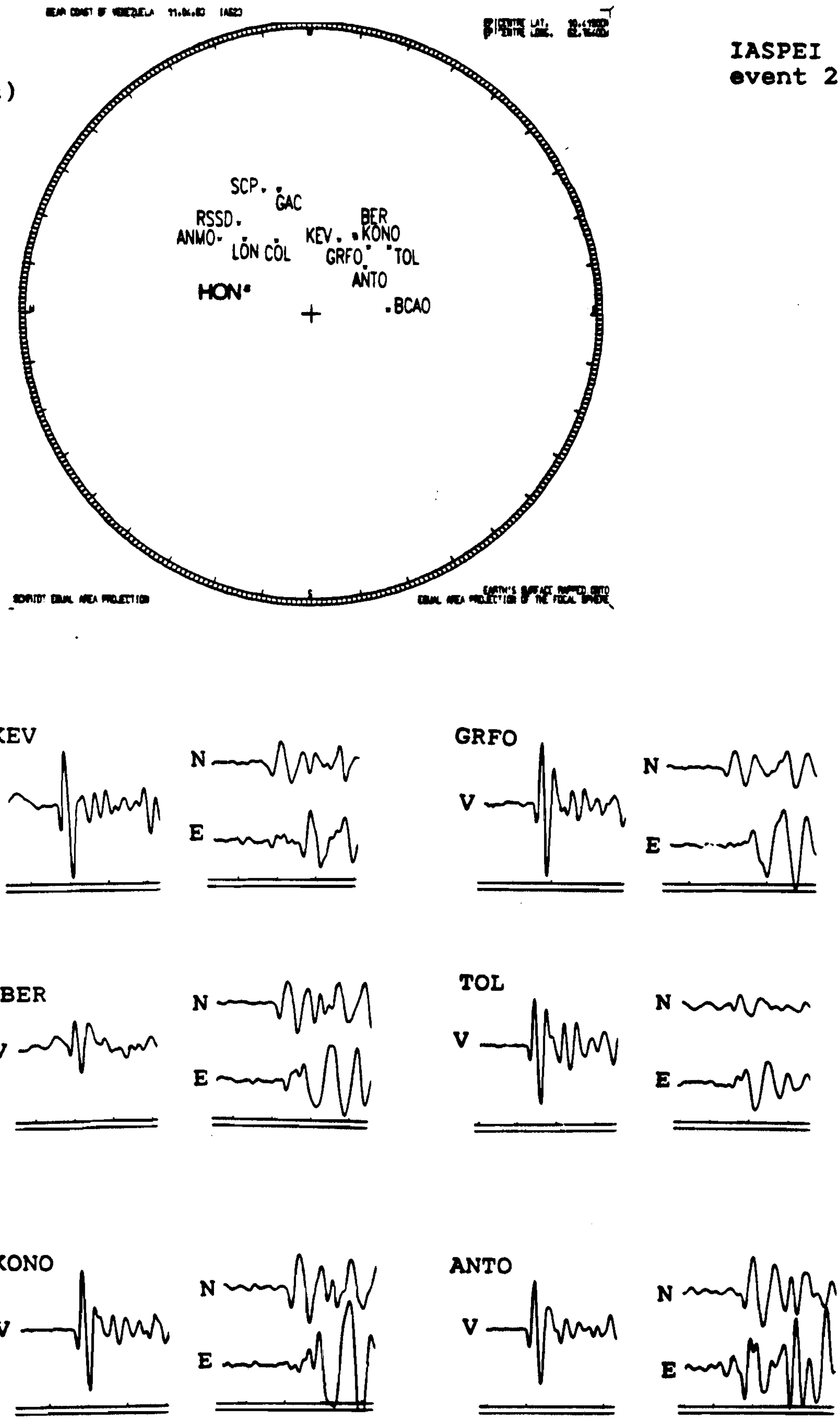

IASPEI
event 23

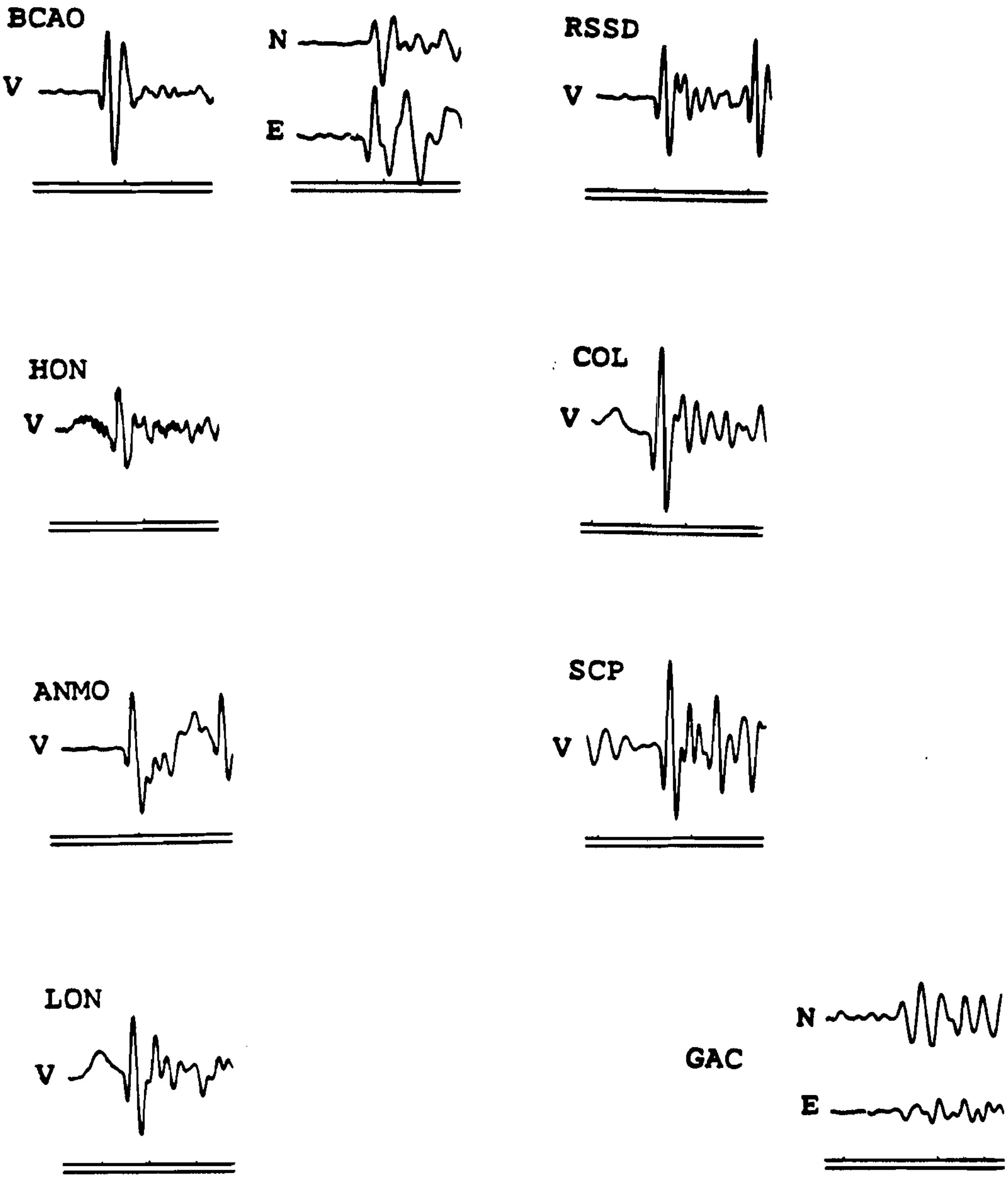

IASPEI
event 23

(b)

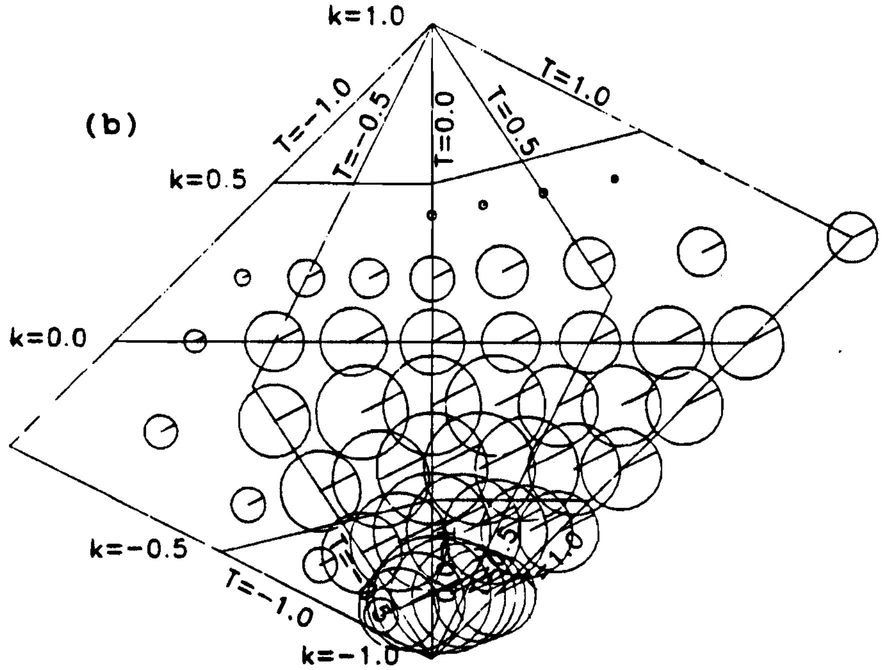

(c)

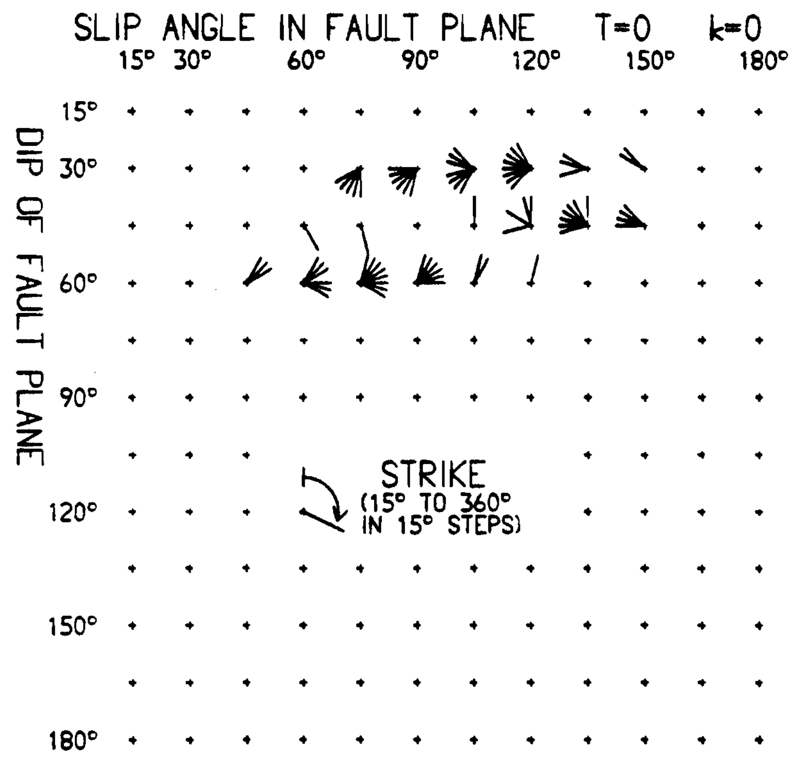

(d)

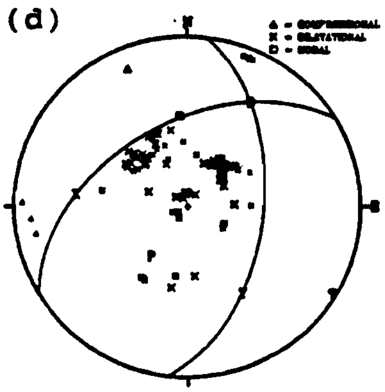

(e)

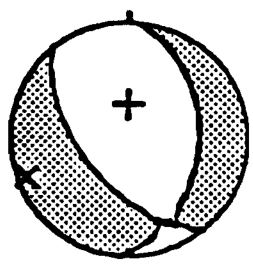

(f)

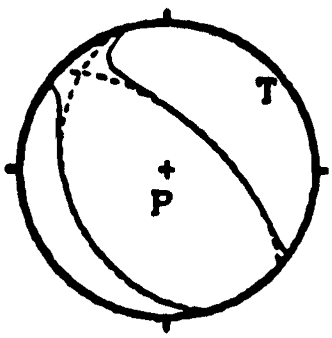

THIS PAGE LEFT BLANK INTENTIONALLY

IASPEI
event 24

(a)

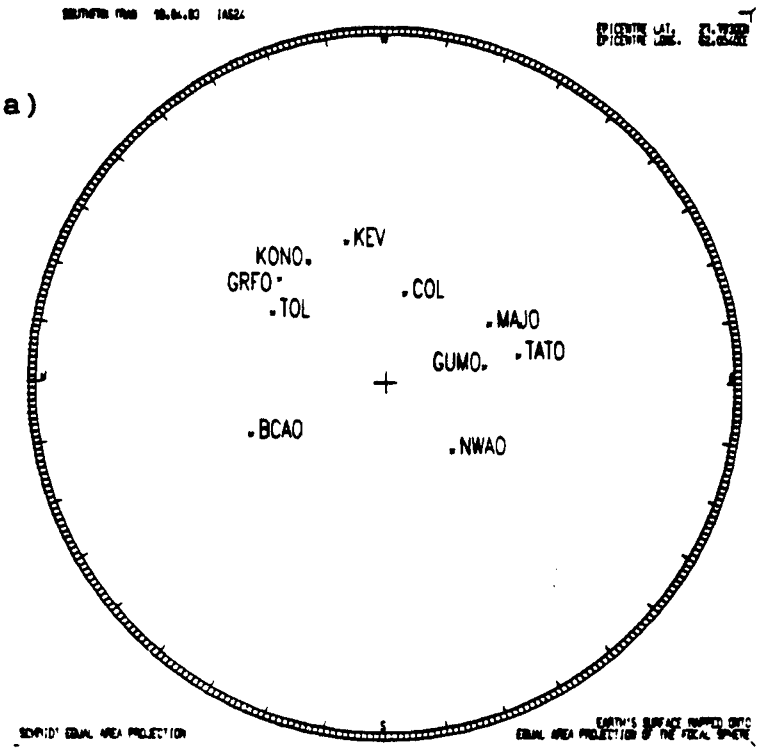

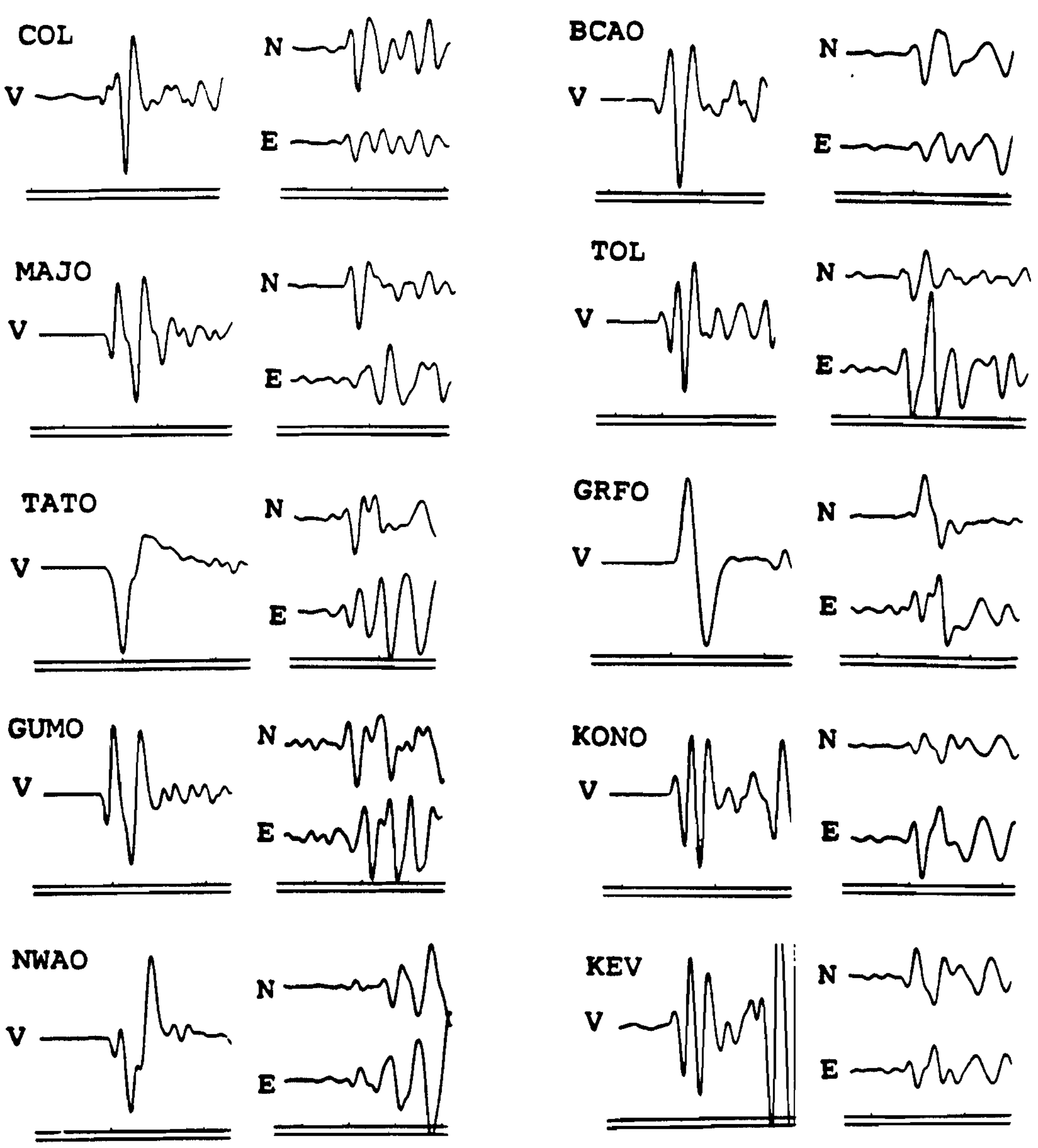

IASPEI
event 24

(b)

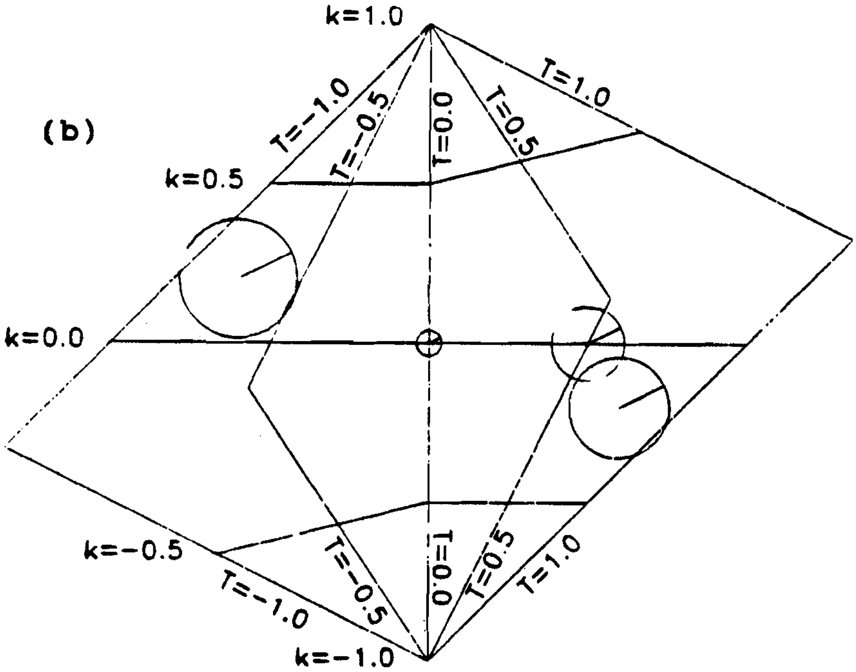

(c)

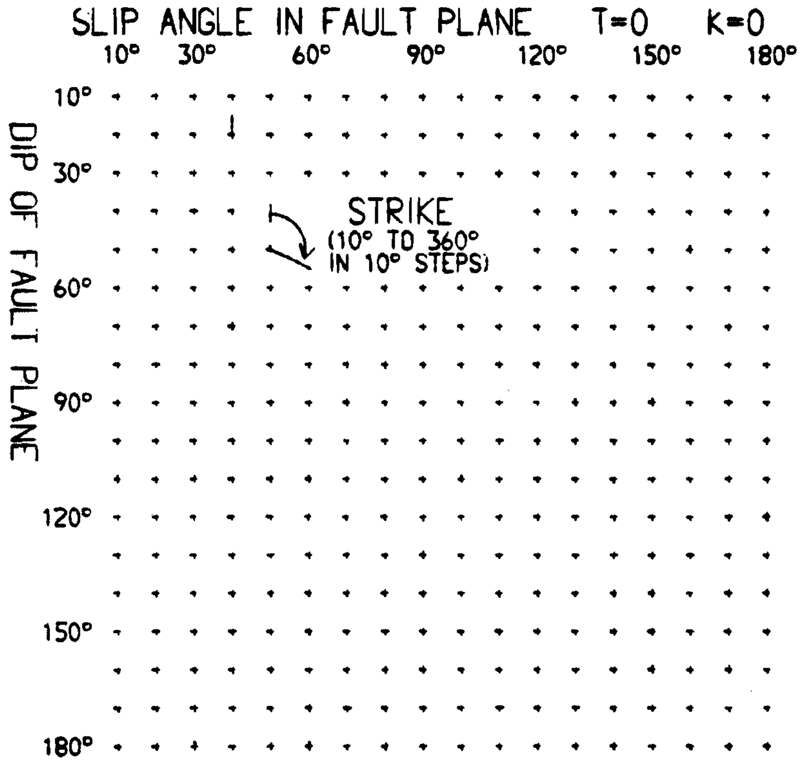

(d)

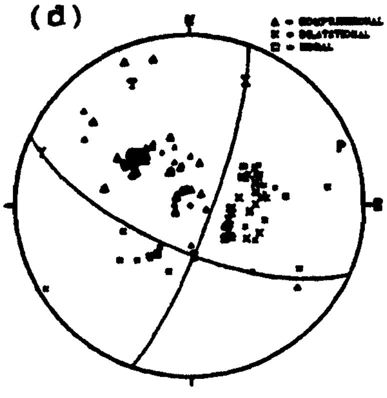

(e)

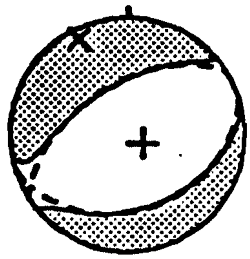

(f)

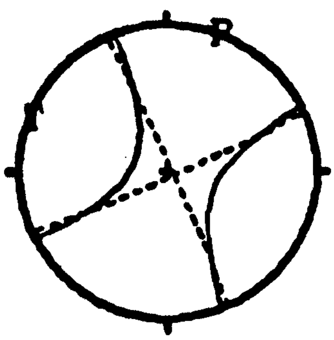

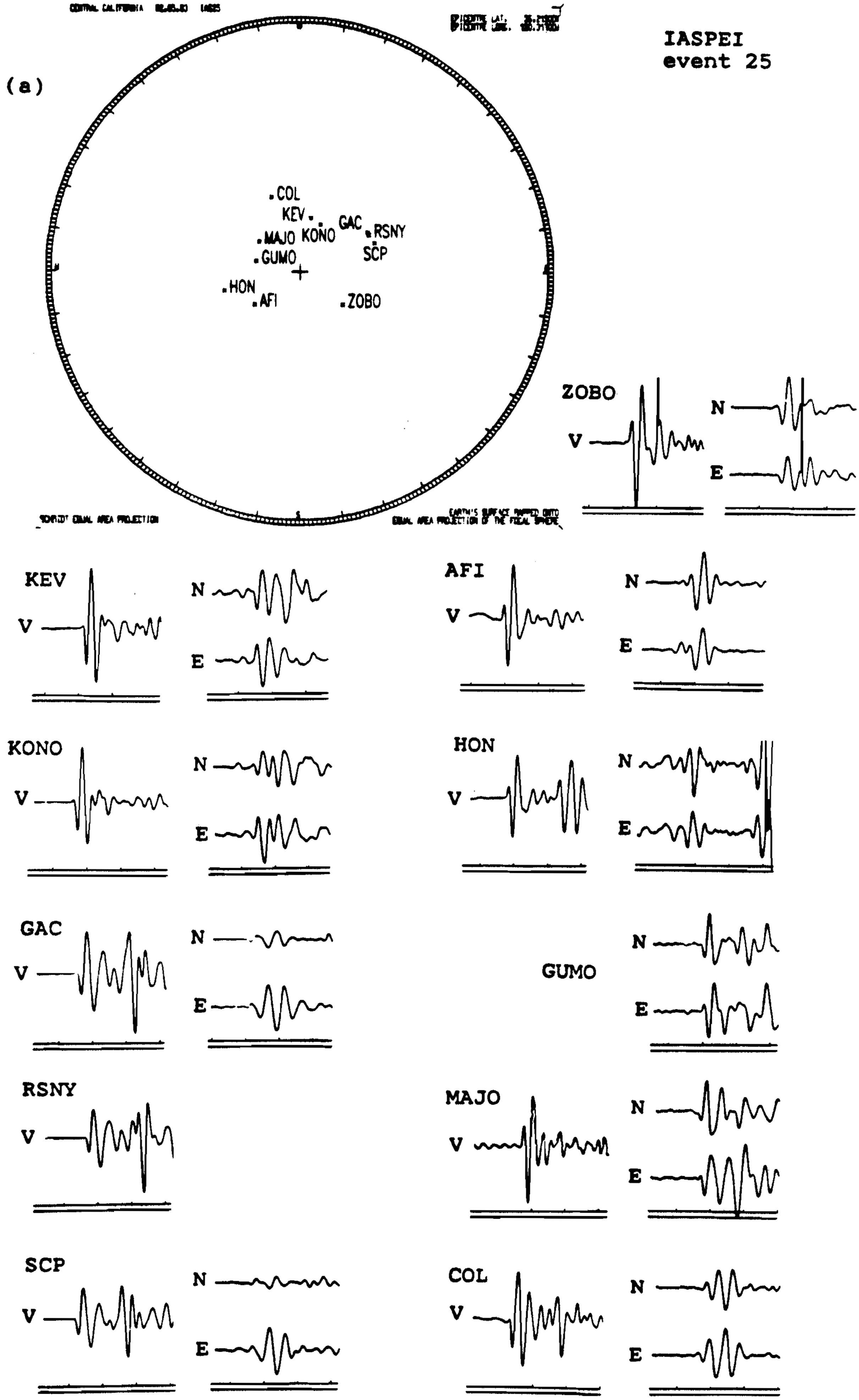
IASPEI
event 25
(a)
COL
KEV
GAC
RSNY
MAJO
KONO
GUMO
SCP
HON
AFI
ZOBO
ZOBO
V
N
E
KEV
V
N
E
AFI
V
N
E
KONO
V
N
E
HON
V
N
E
GAC
V
N
E
GUMO
N
E
RSNY
V
MAJO
V
N
E
SCP
V
N
E
COL
V
N
E

IASPEI
event 25

(b)

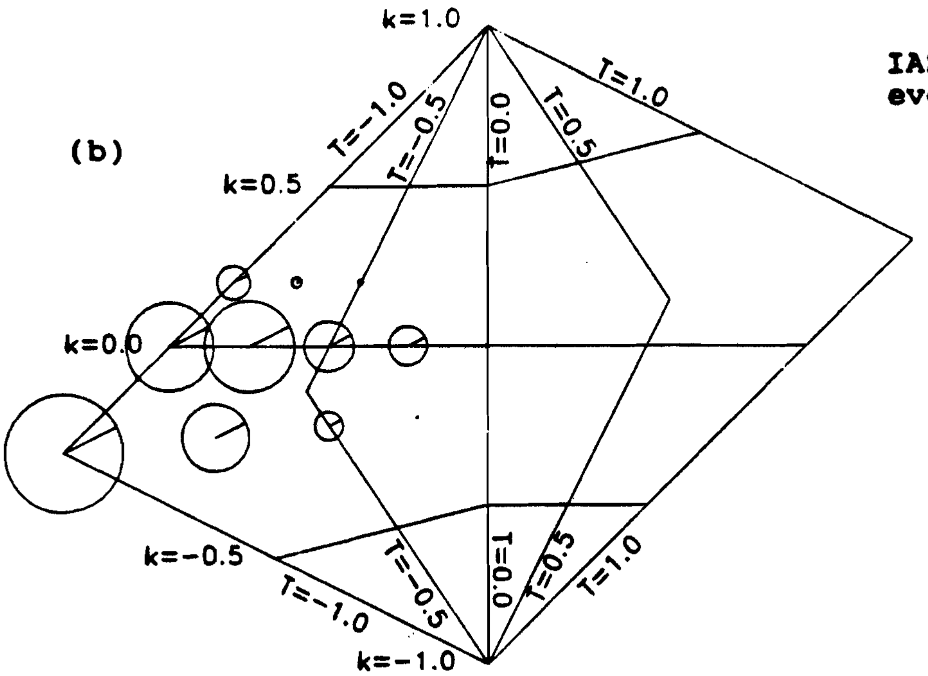

(c)

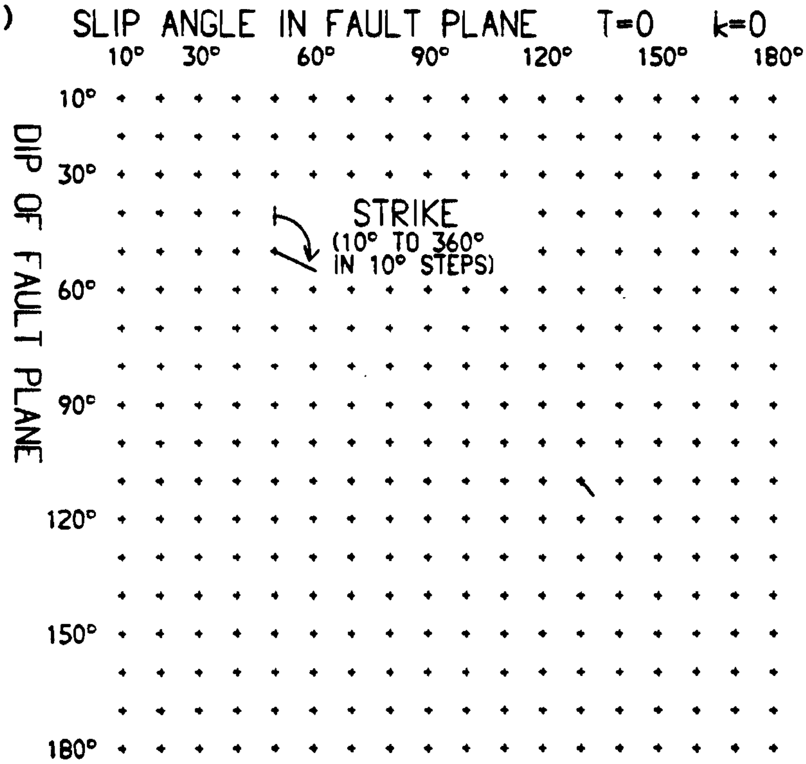

(d)

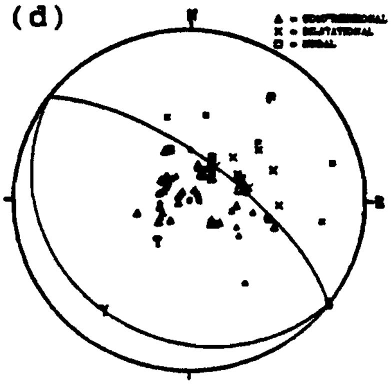

(e)

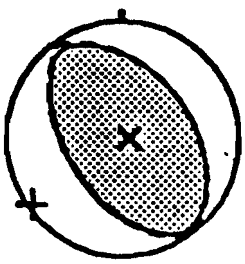

(f)

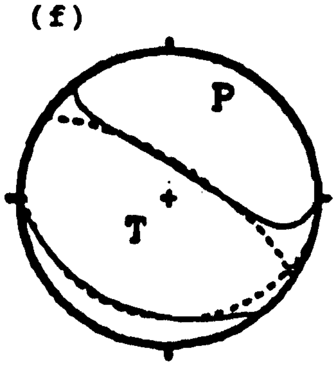

IASPEI
event 26

(a)

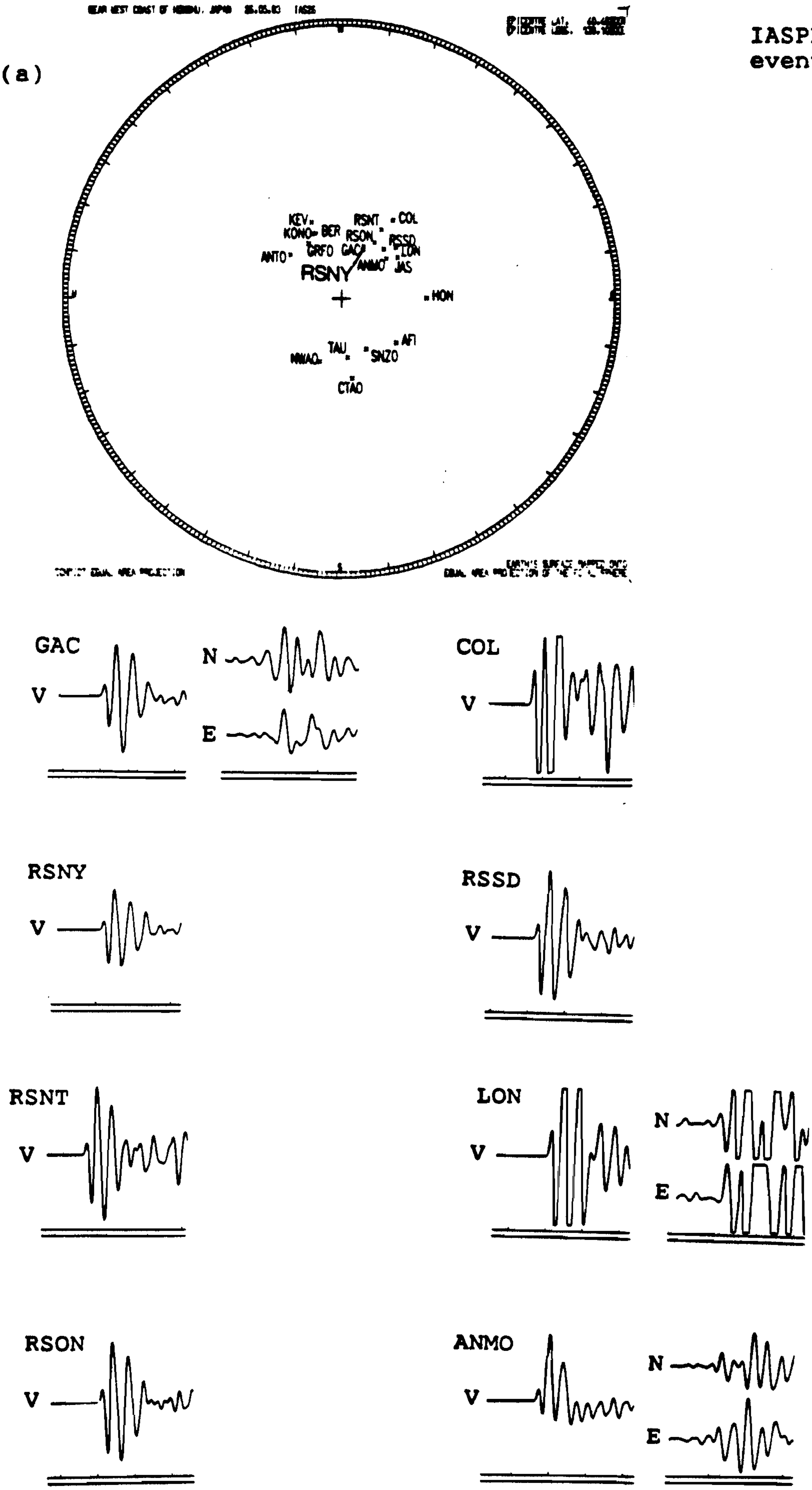

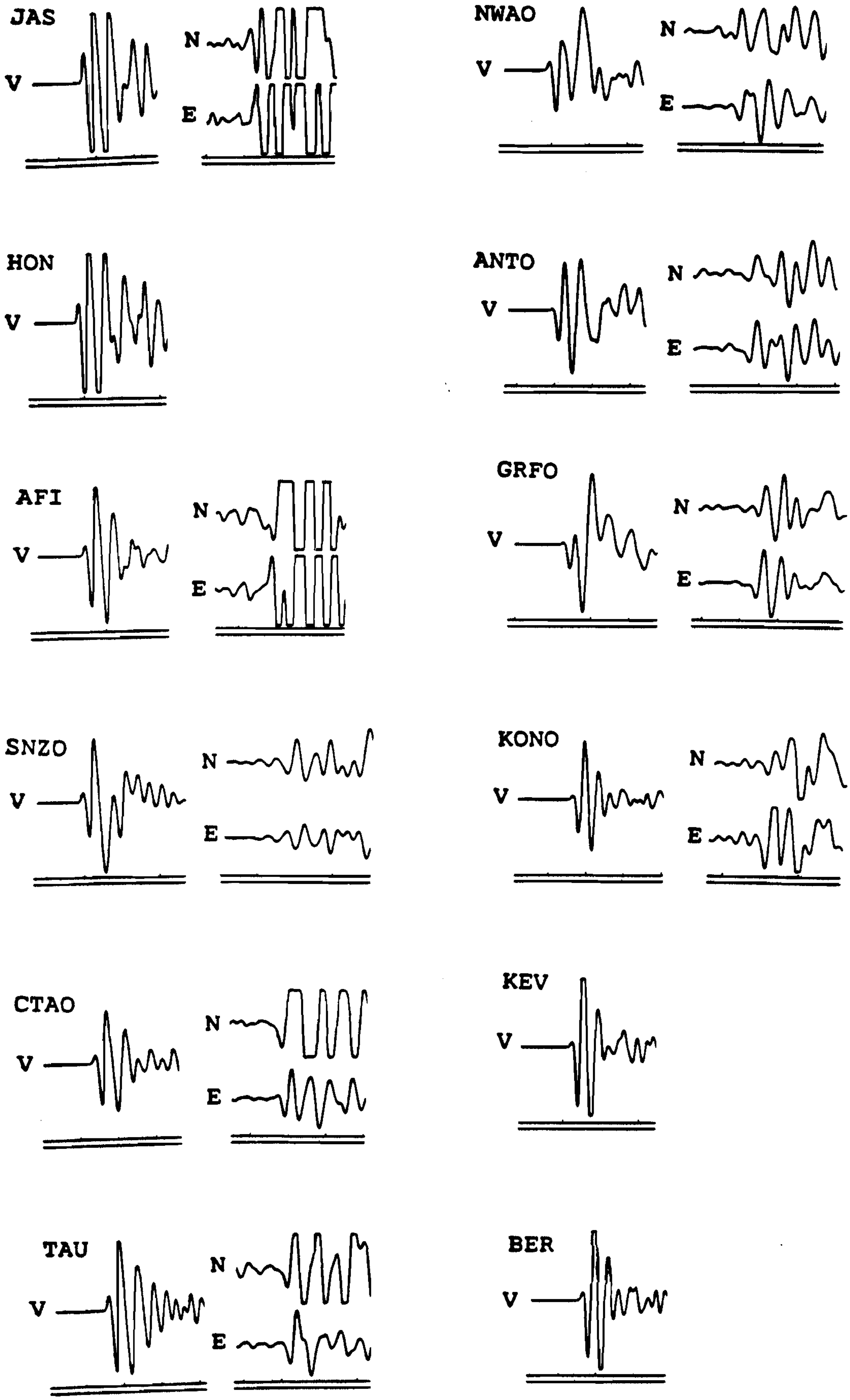
JAS
V
N
E
NWAO
V
N
E
HON
V
ANTO
V
N
E
AFI
V
N
E
GRFO
V
N
E
SNZO
V
N
E
KONO
V
N
E
CTAO
V
N
E
KEV
V
TAU
V
N
E
BER
V

IASPEI
event 26

(b)

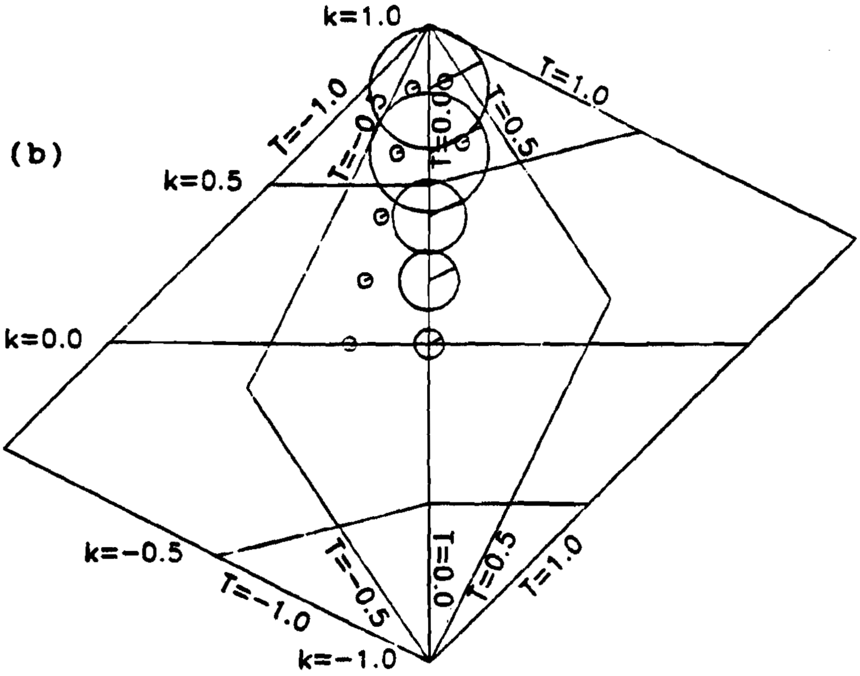

(c)

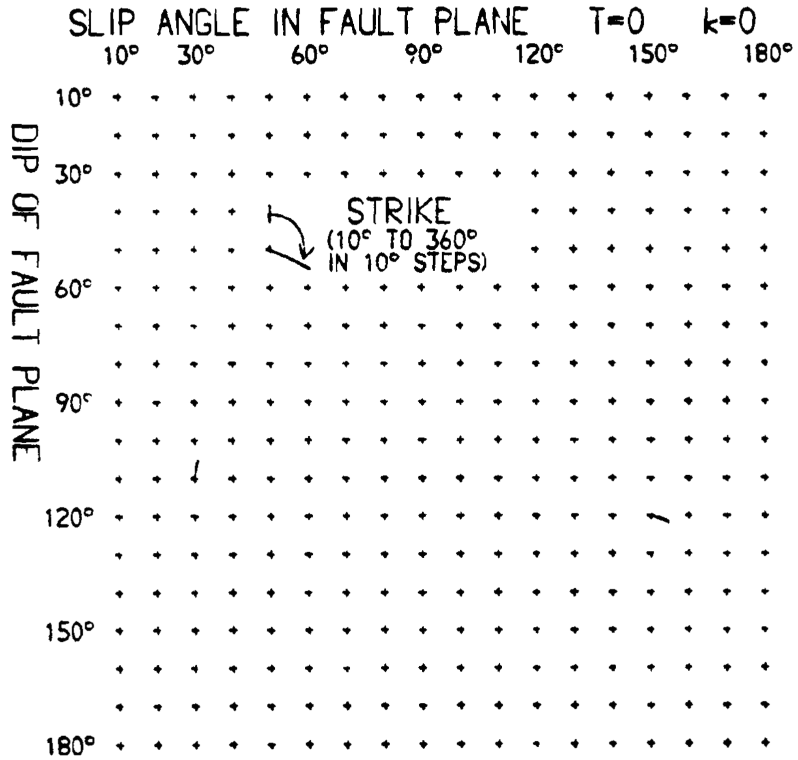

(d)

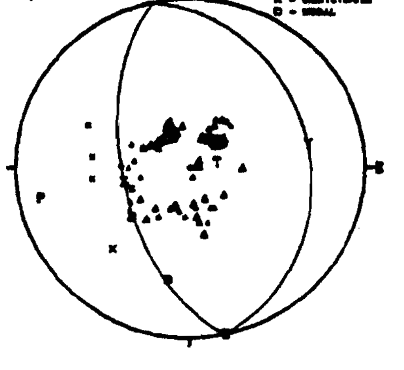

(e)

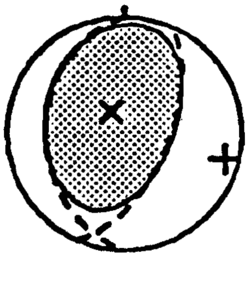

(f)

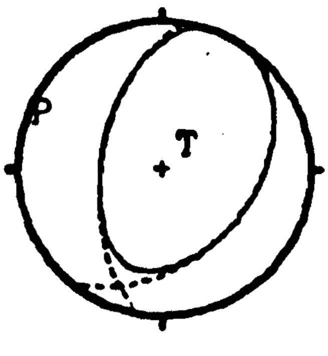

THIS PAGE LEFT BLANK INTENTIONALLY

IASPEI
event 27

(a)

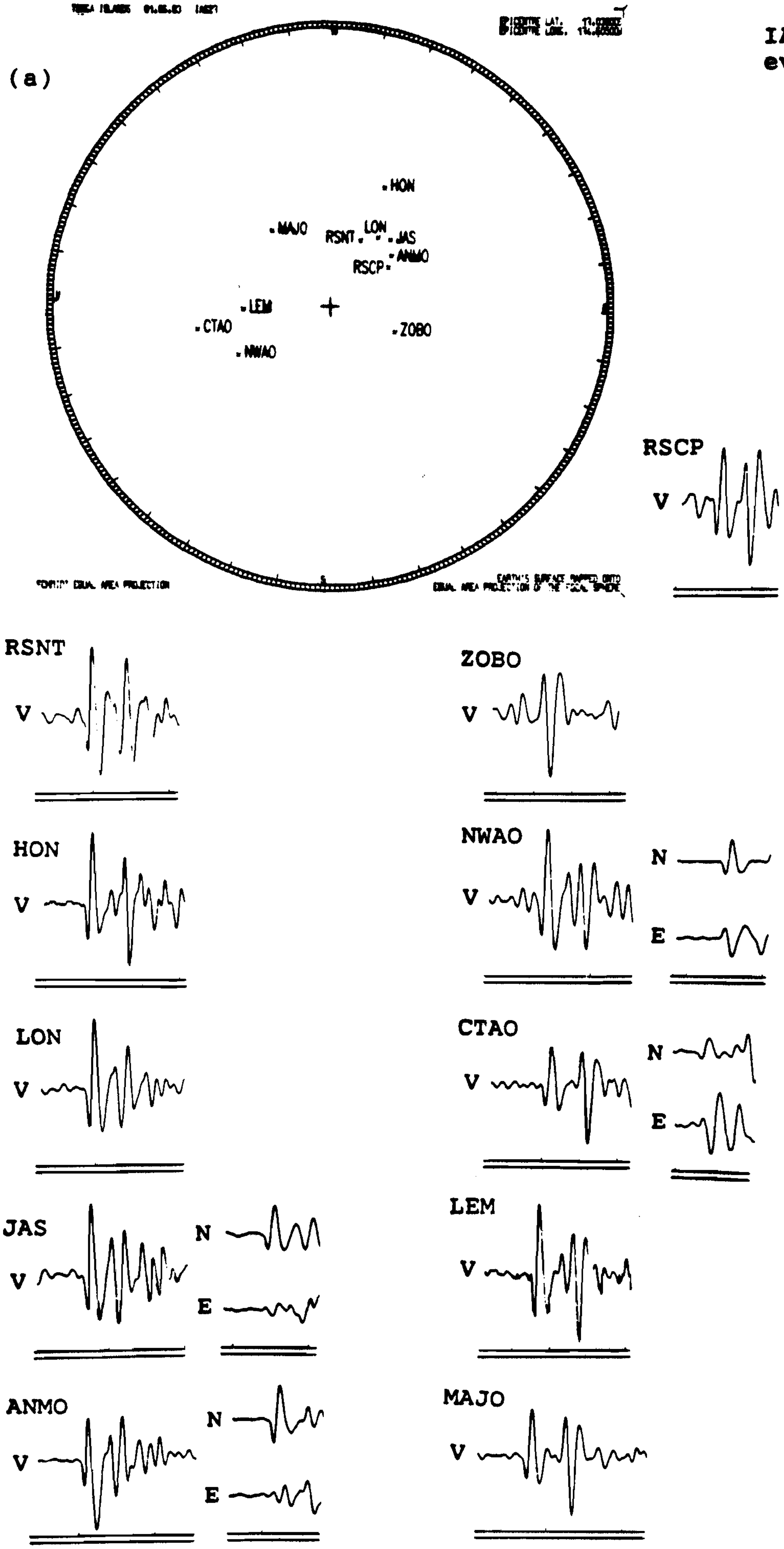

IASPEI
event 27

(b)

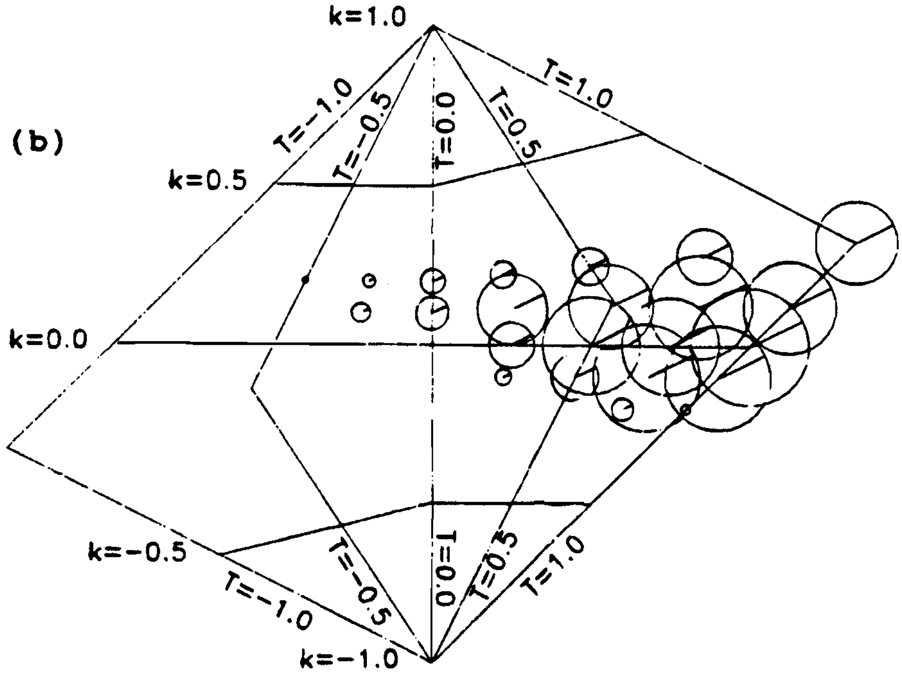

(c)

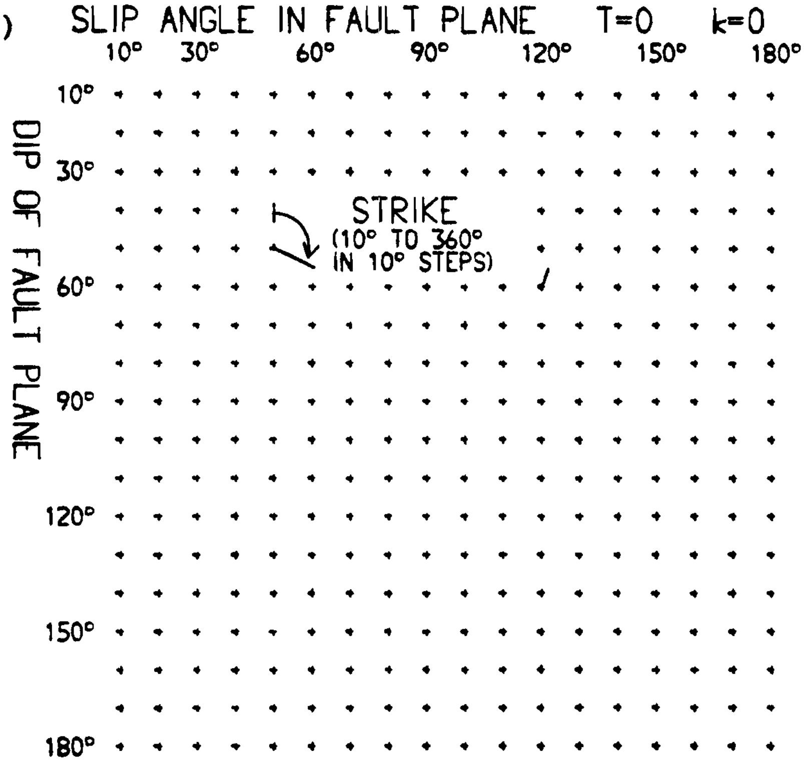

(d)

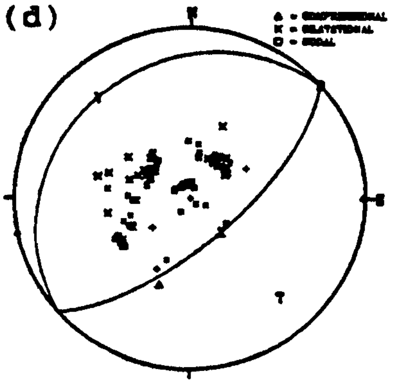

(e)

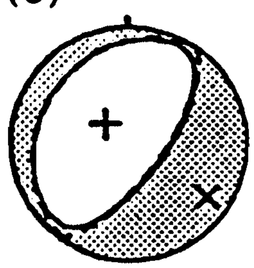

(f)

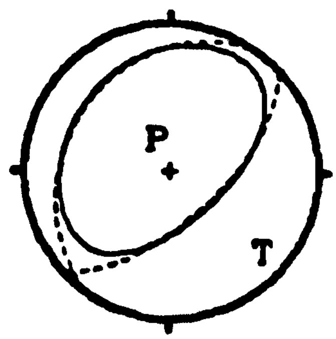

IASPEI
event 28

(a)

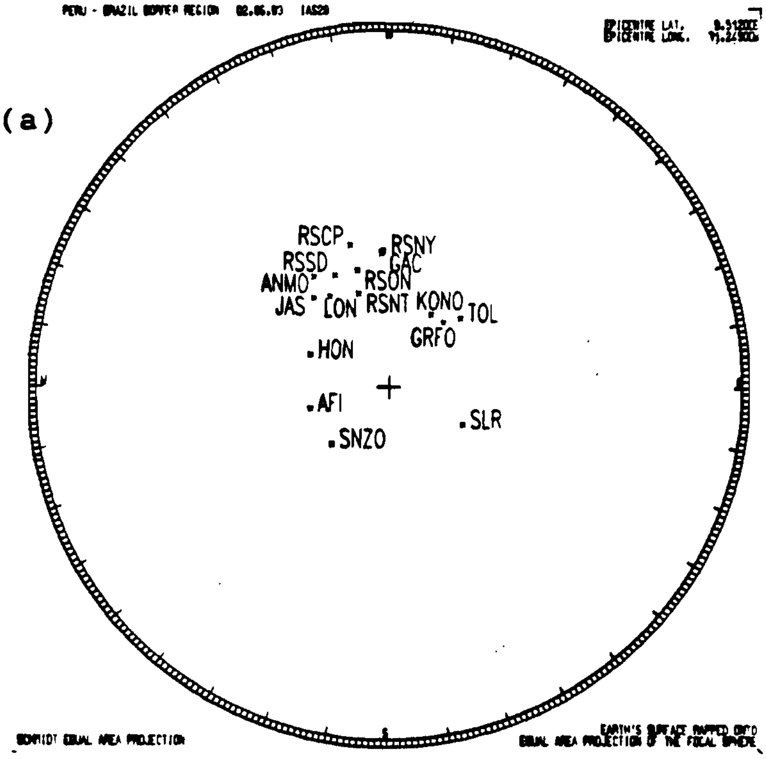

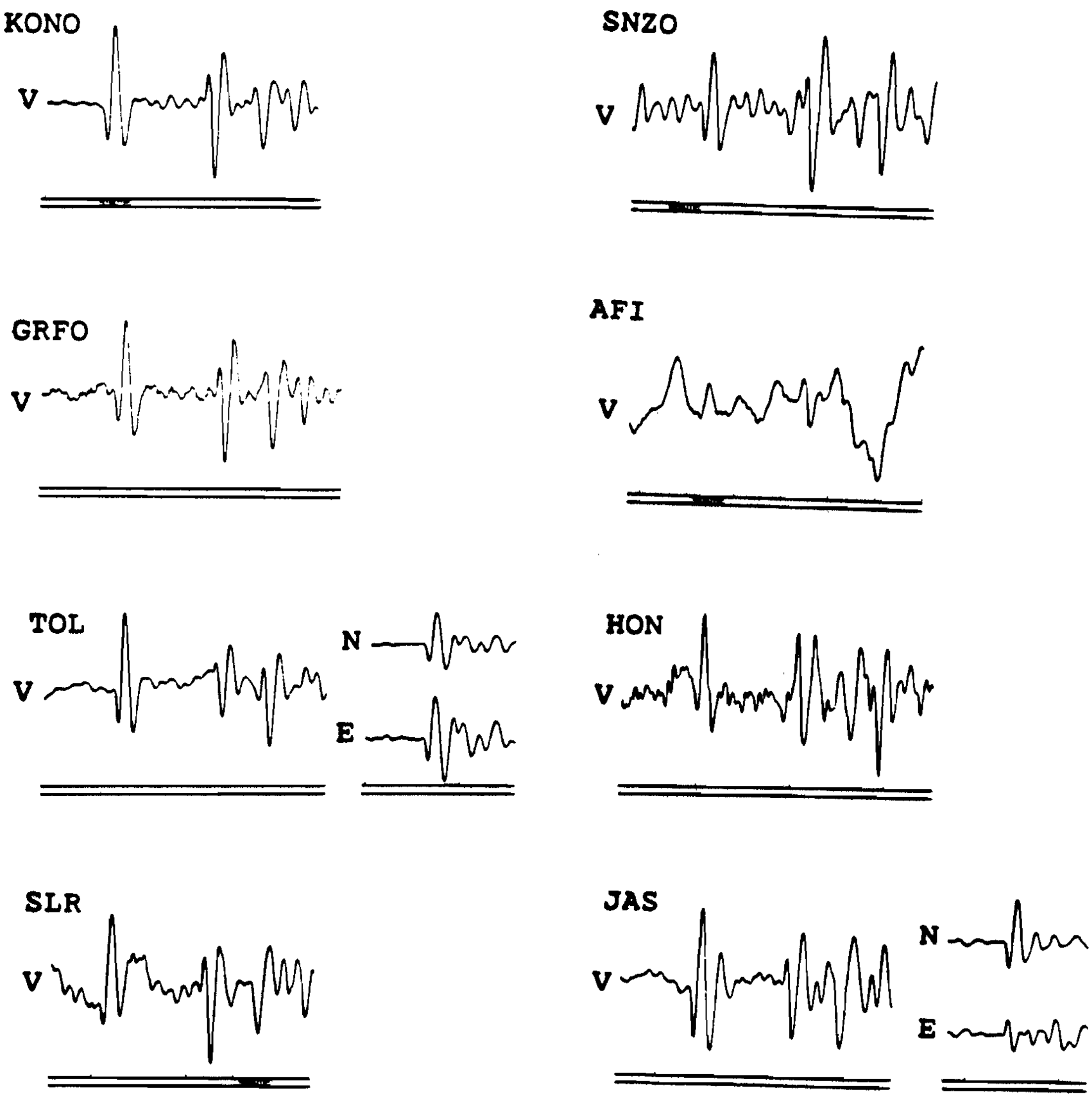

IASPEI
event 28

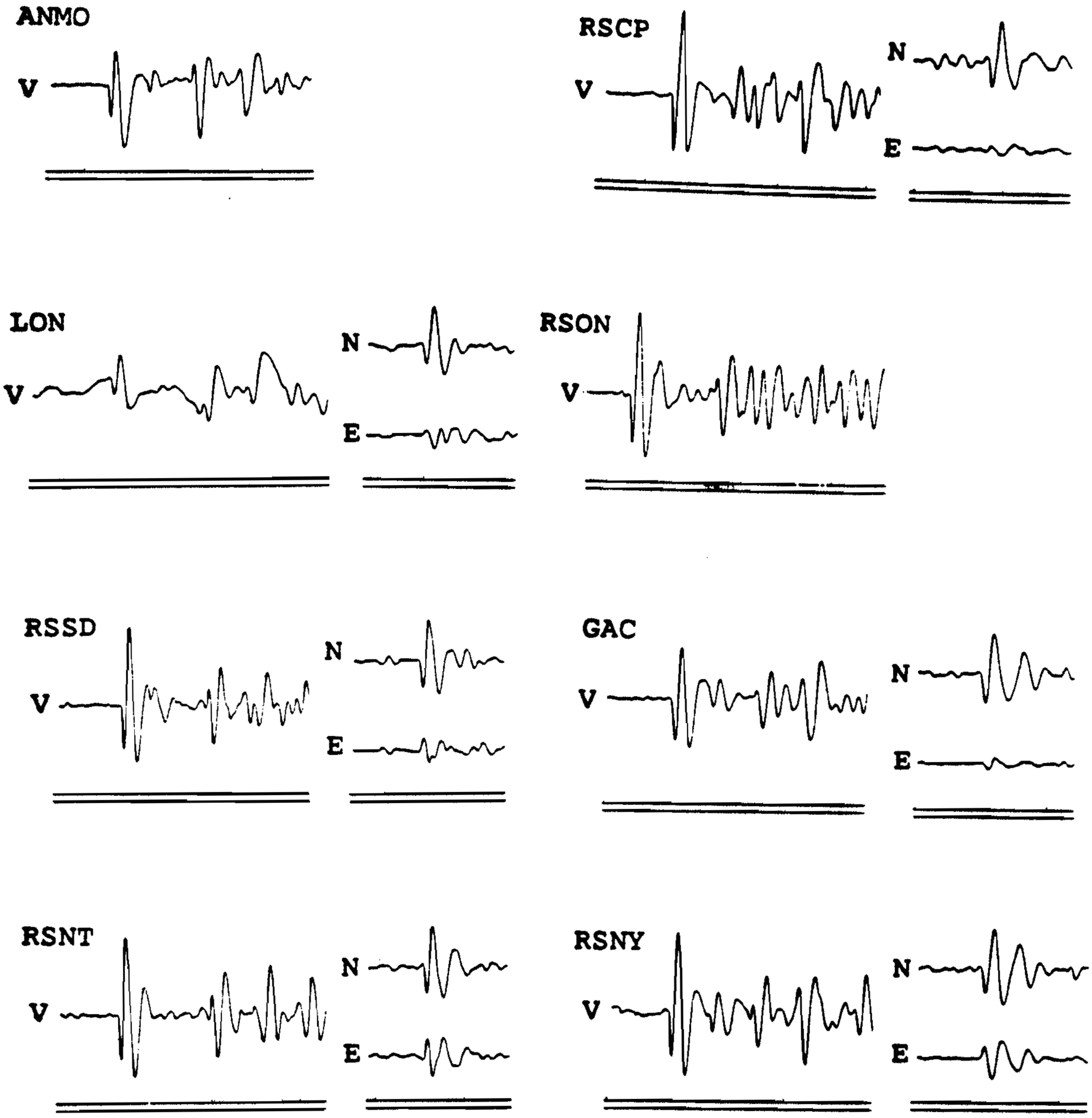

IASPEI
event 28

(b)

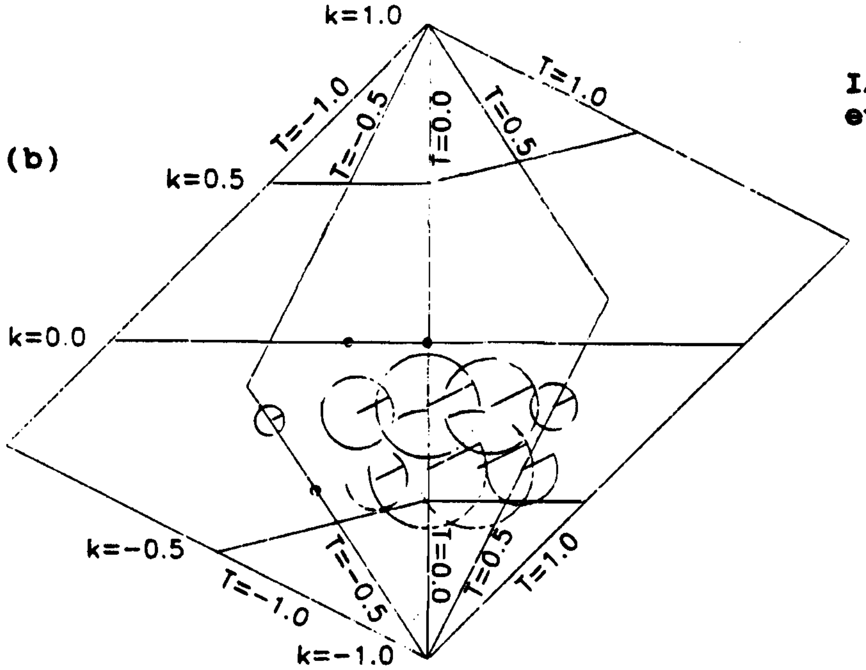

(c)

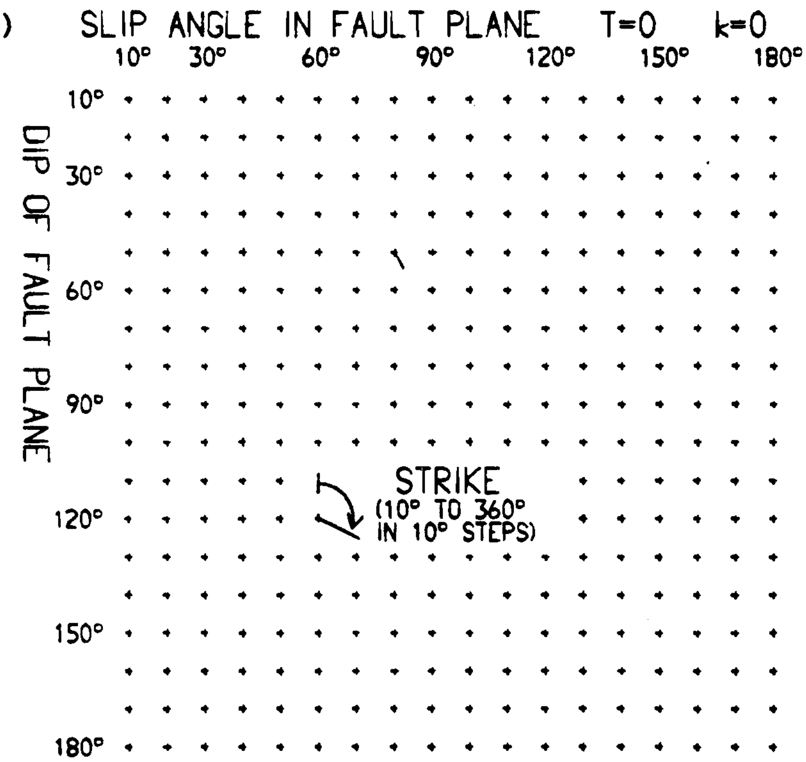

(d)

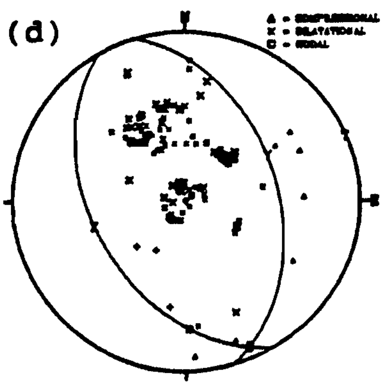

(e)

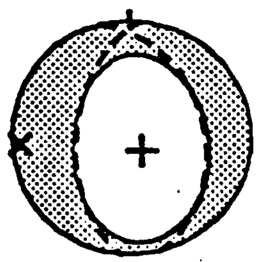

(f)

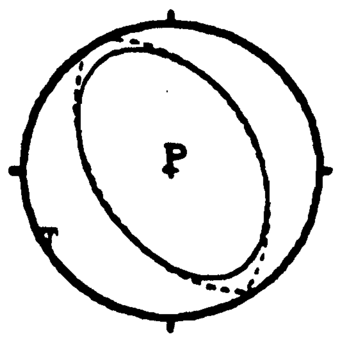

THIS PAGE LEFT BLANK INTENTIONALLY

IASPEI
event 29

(a)

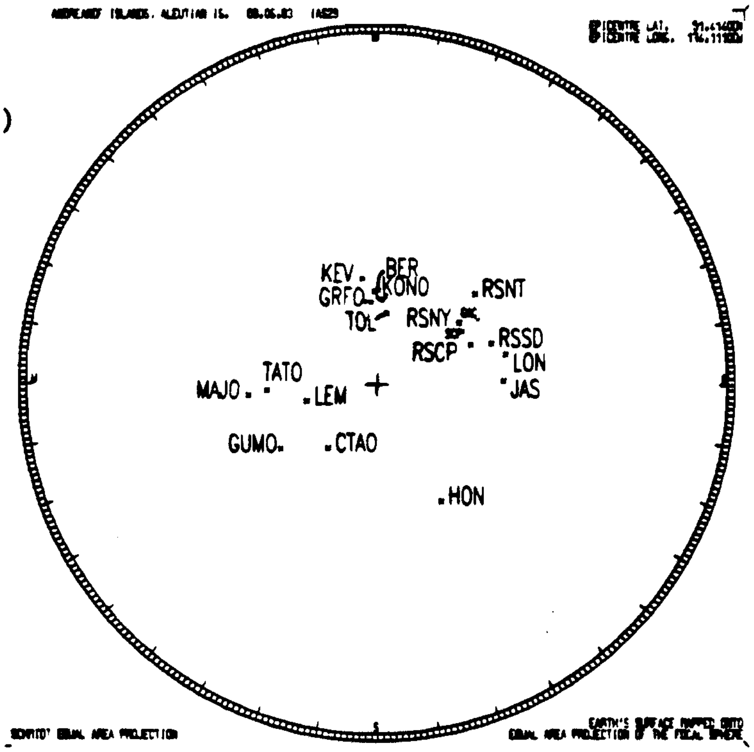

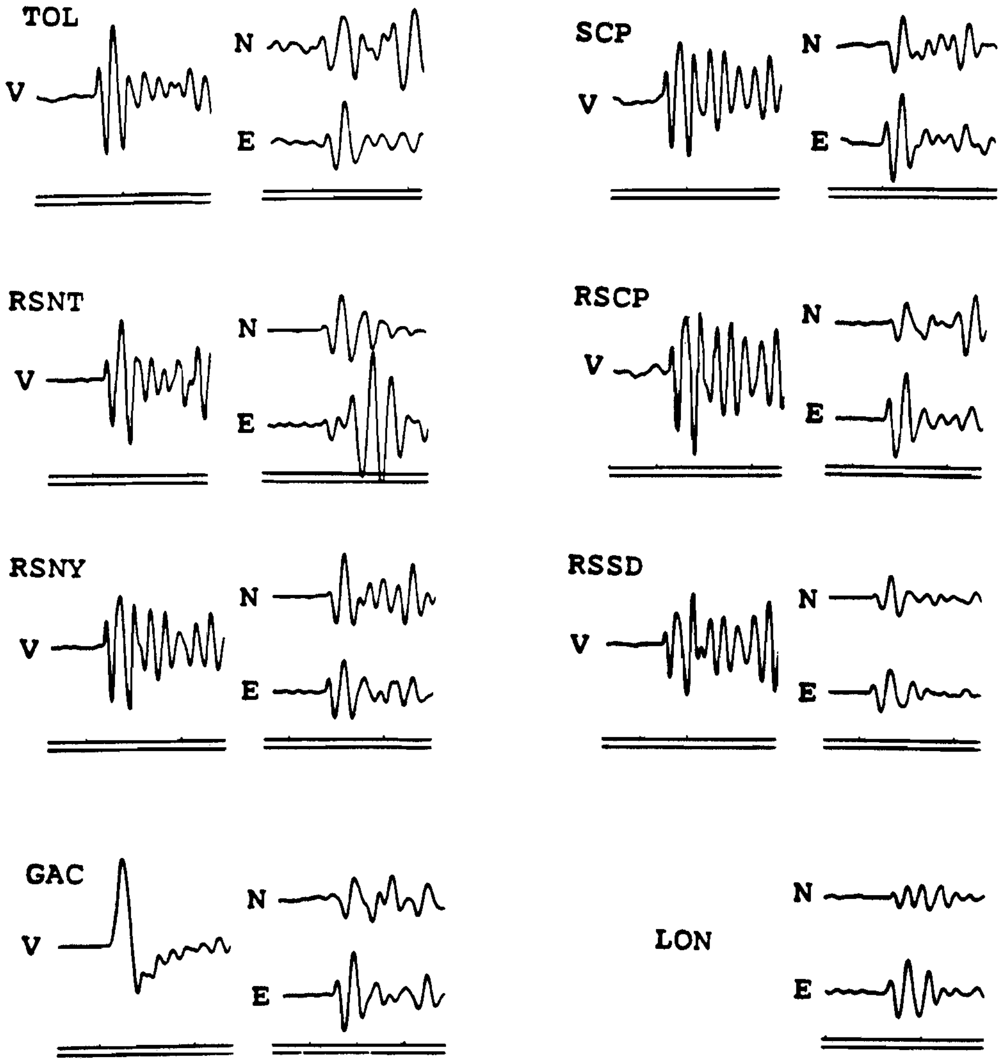

IASPEI
event 29

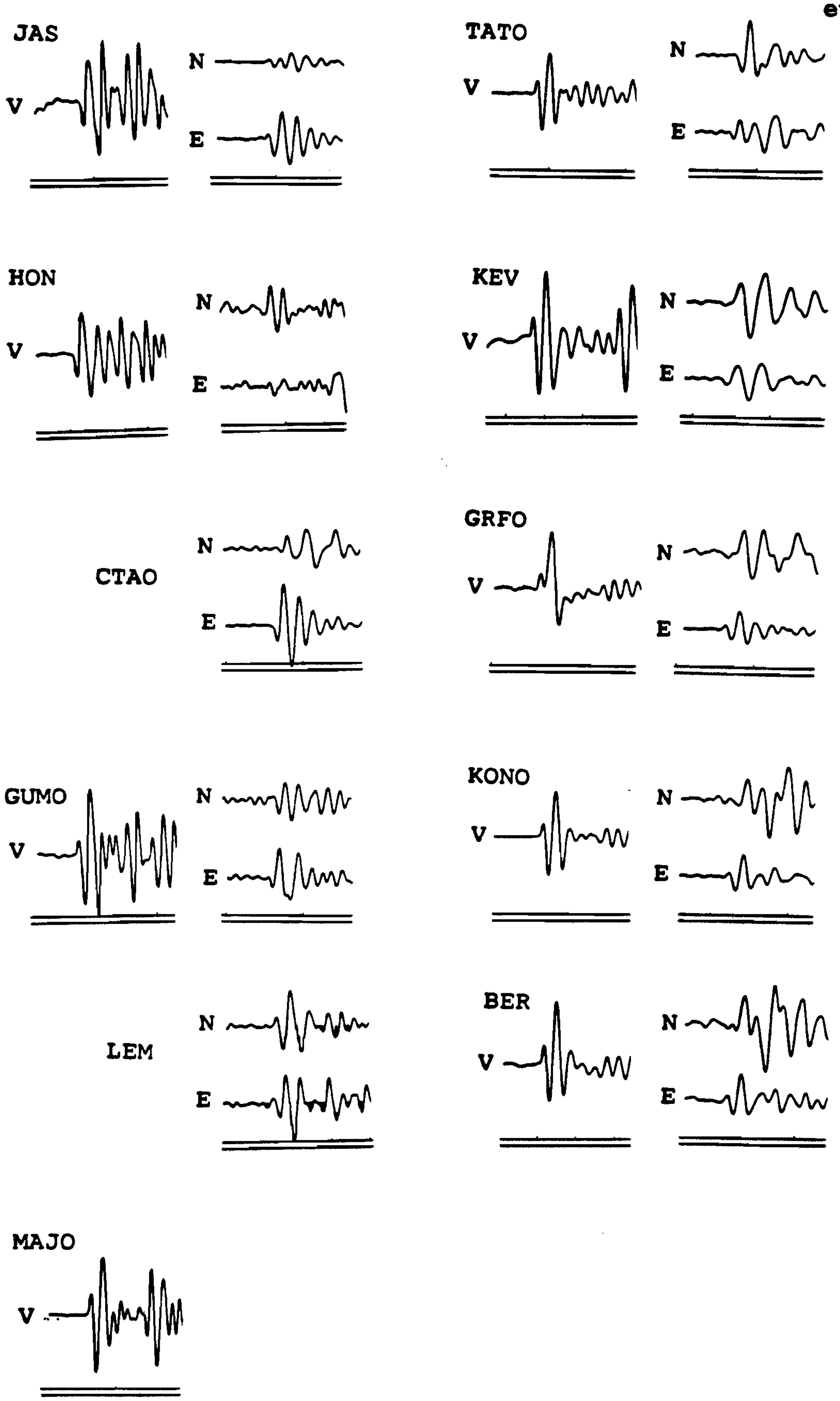

(b)

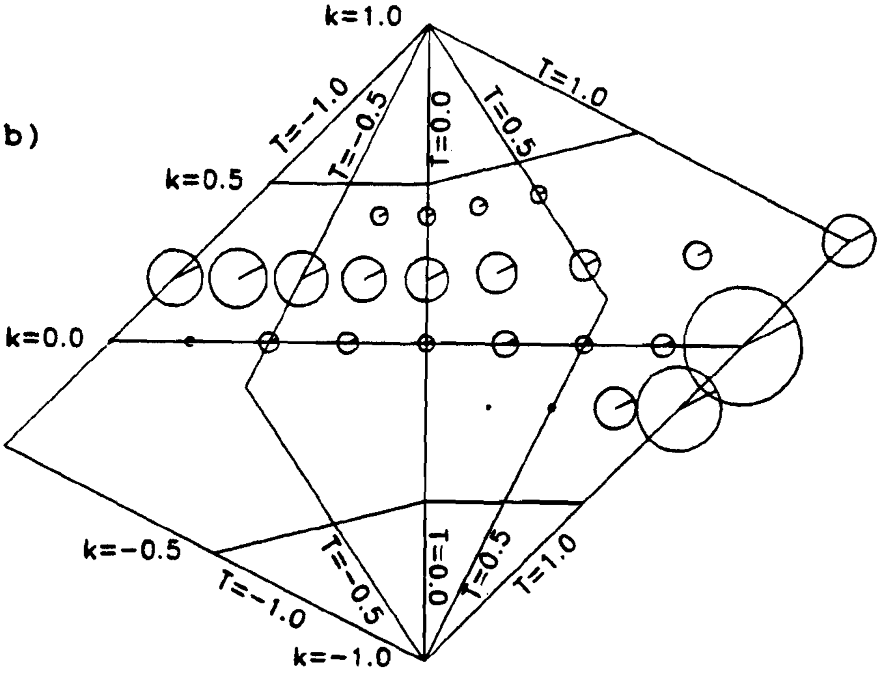
k=1.0
T=-1.0
T=-0.5
T=0.0
T=0.5
T=1.0
k=0.5
k=0.0
k=-0.5
T=-1.0
T=-0.5
T=0.0
T=0.5
T=1.0
k=-1.0

(c)

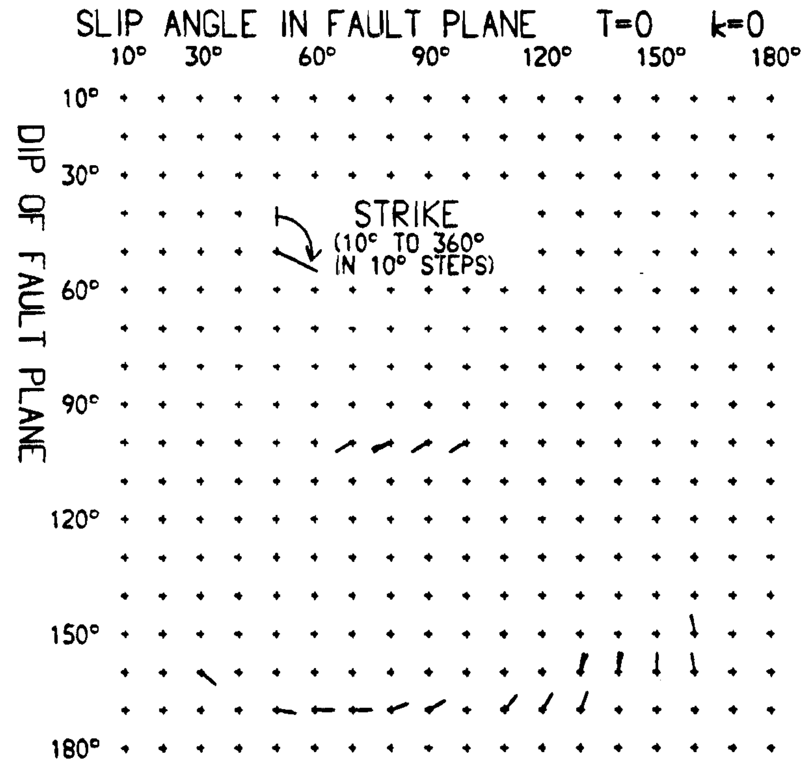
SLIP ANGLE IN FAULT PLANE T=0 k=0
10° 30° 60° 90° 120° 150° 180°
DIP OF FAULT PLANE
10° 30° 60° 90° 120° 150° 180°
STRIKE
(10° TO 360°
IN 10° STEPS)

(d)

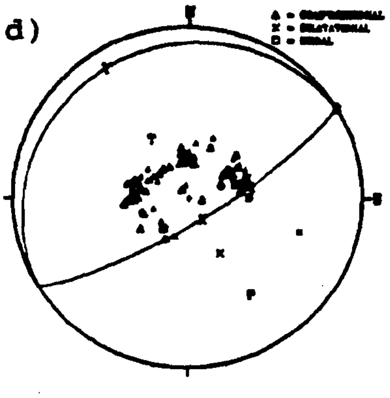

(e)

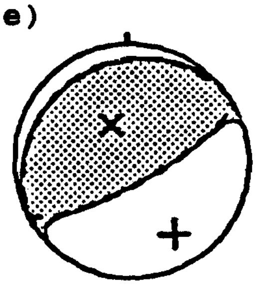

(f)

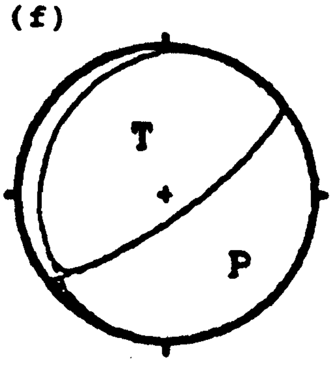
T
P

THIS PAGE LEFT BLANK INTENTIONALLY

(a)

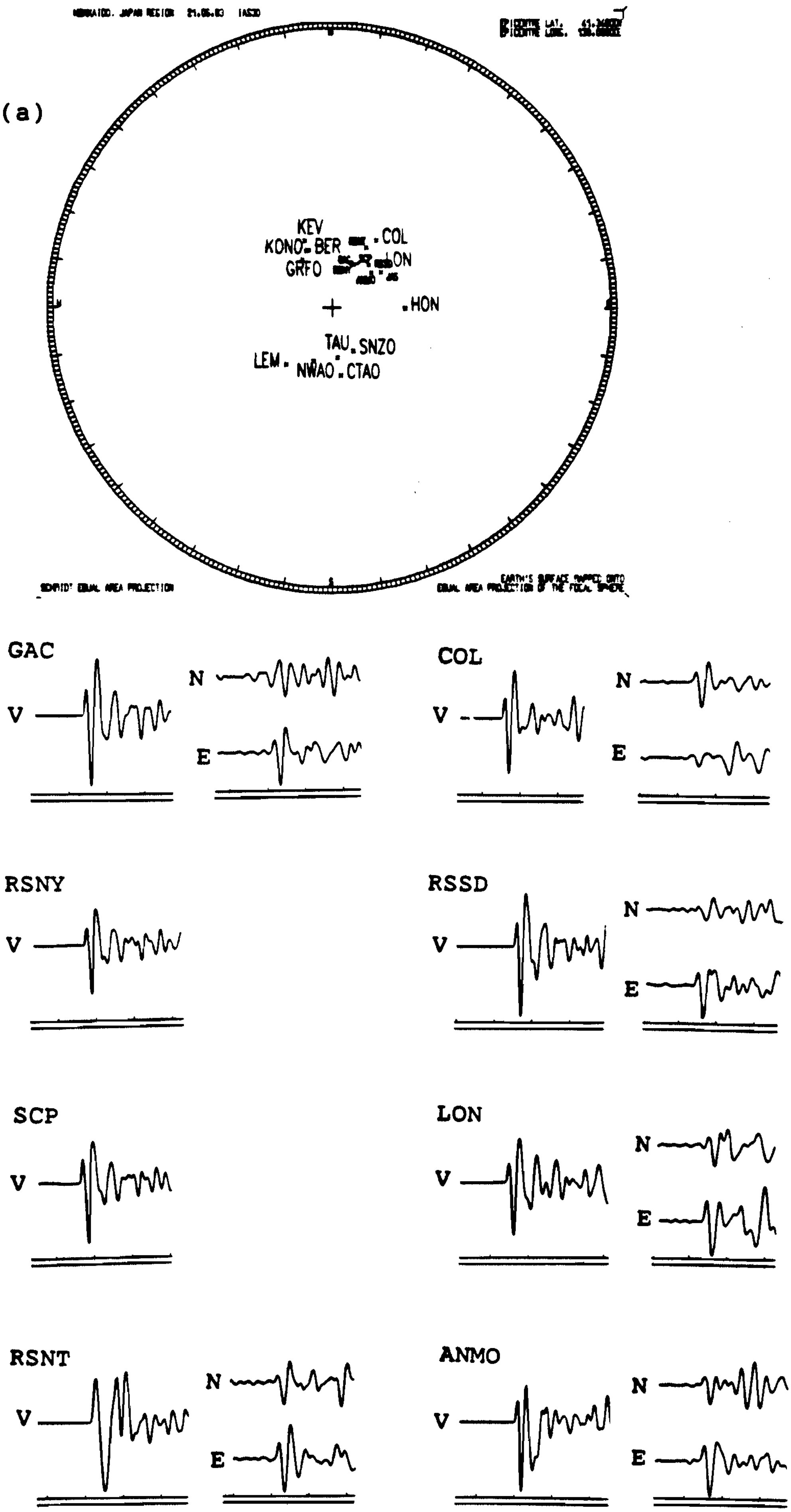
KEV
KONO BER COL
GRFO LON
HON
TAU SNZO
LEM NWAO CTAO
GAC
V
N
E
COL
V
N
E
RSNY
V
RSSD
V
N
E
SCP
V
LON
V
N
E
RSNT
V
N
E
ANMO
V
N
E

IASPEI
event 30

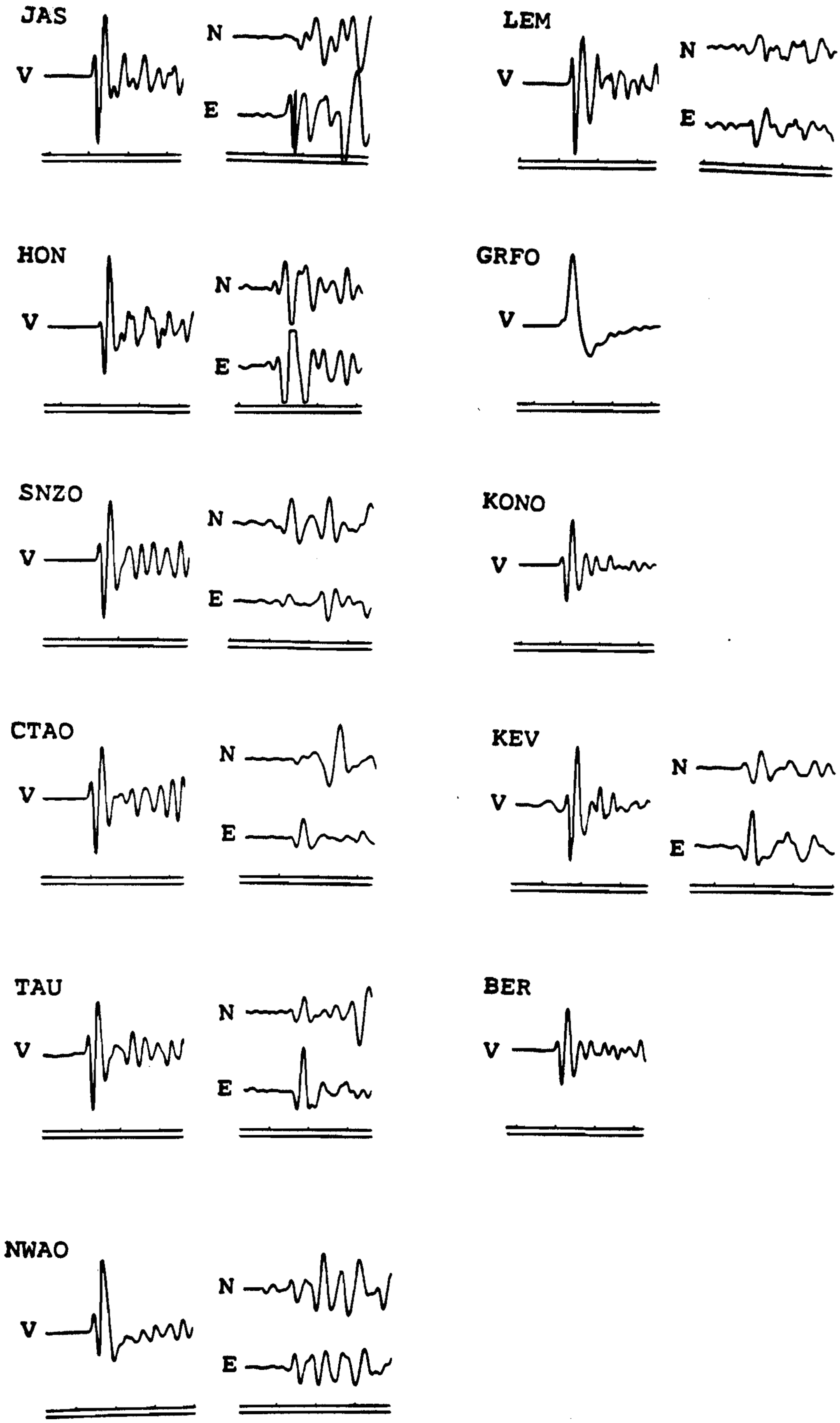

(b)

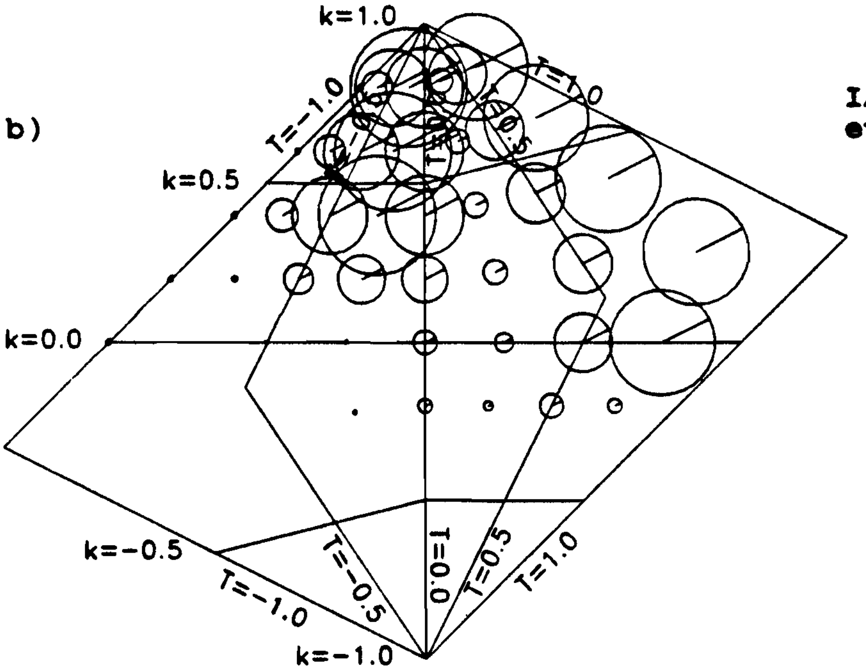

IASPEI event 30

(c)

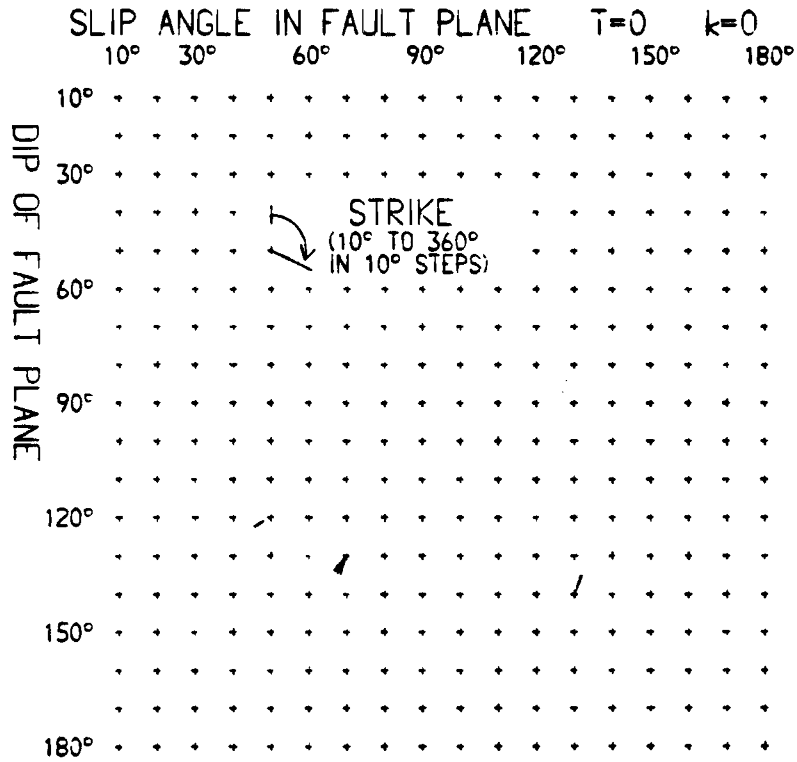

(d)

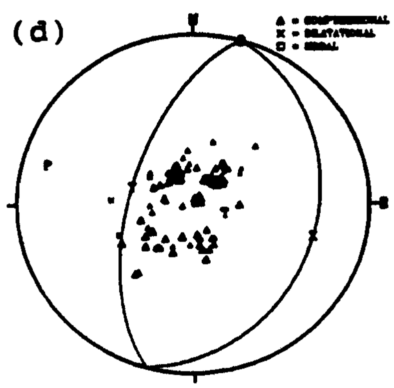

(e)

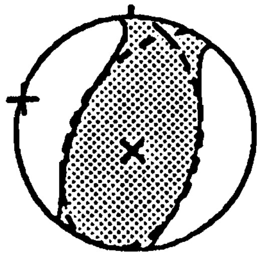

(f)

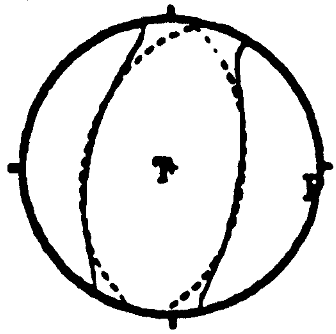

THIS PAGE LEFT BLANK INTENTIONALLY

(a)

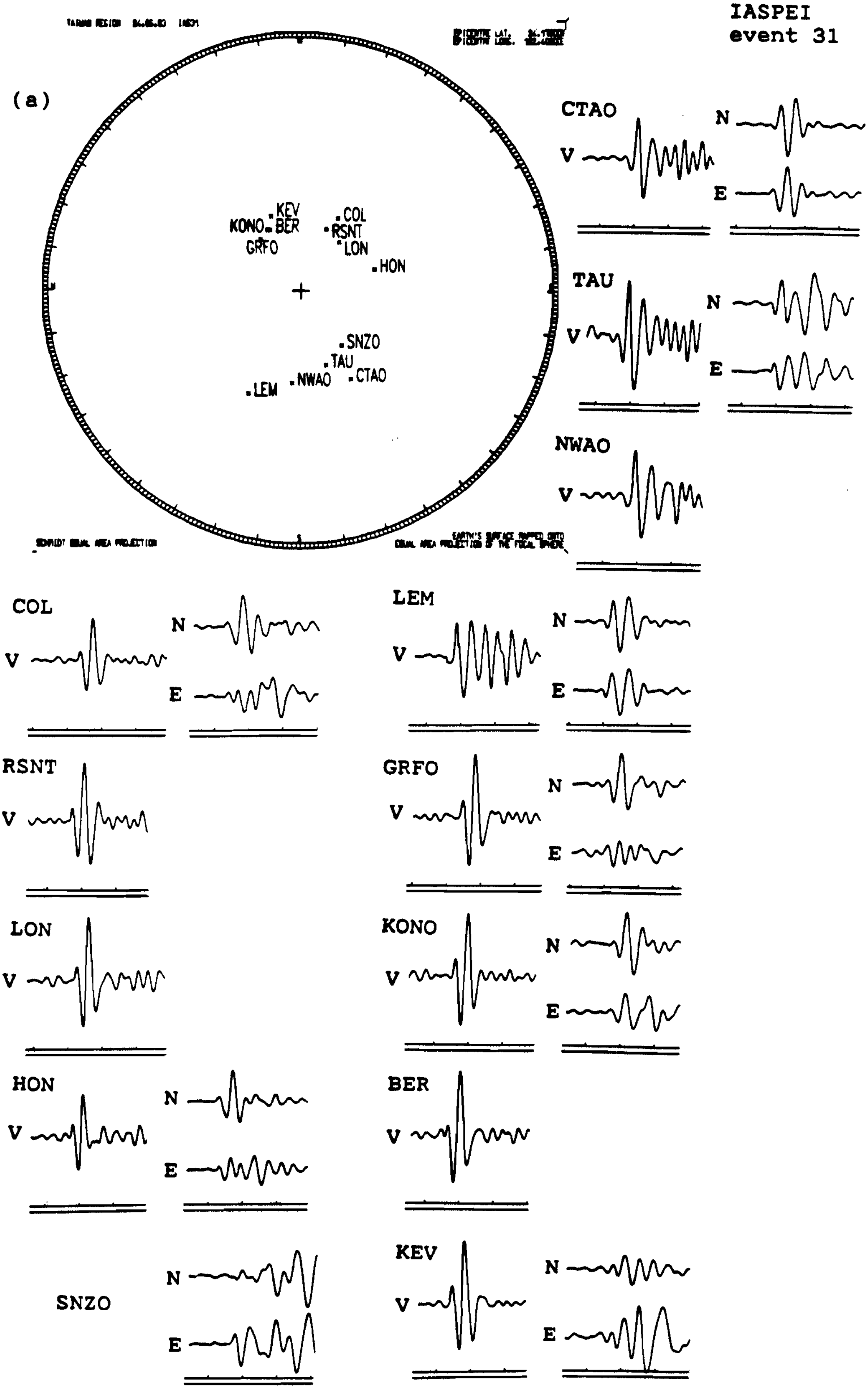
KEV
KONO
BER
GRFO
COL
RSNT
LON
HON
SNZO
TAU
NWAO
CTAO
LEM
CTAO
V
N
E
TAU
V
N
E
NWAO
V
COL
V
N
E
LEM
V
N
E
RSNT
V
GRFO
V
N
E
LON
V
KONO
V
N
E
HON
V
N
E
BER
V
SNZO
N
E
KEV
V
N
E

IASPEI
event 31

(b)

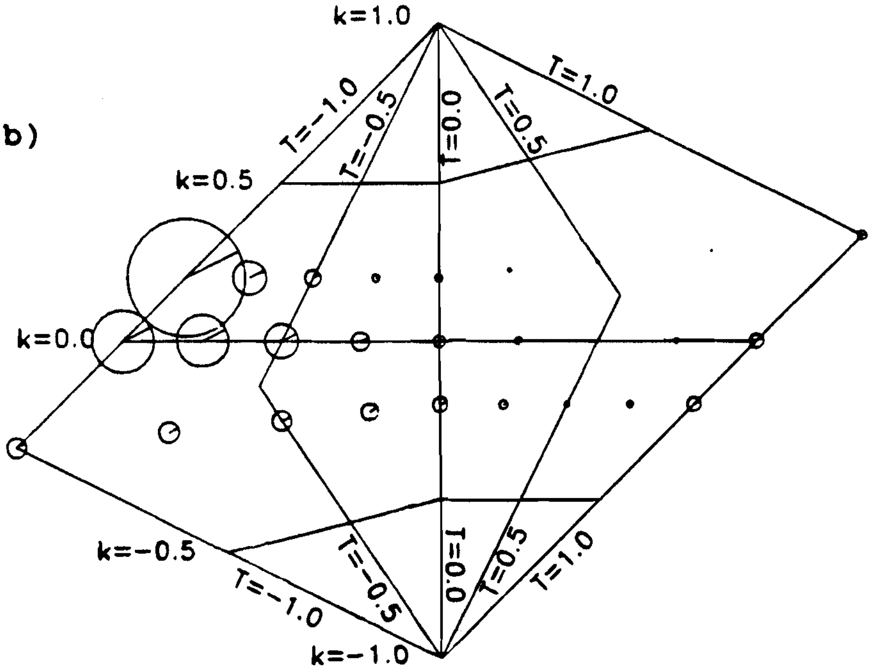

(c)

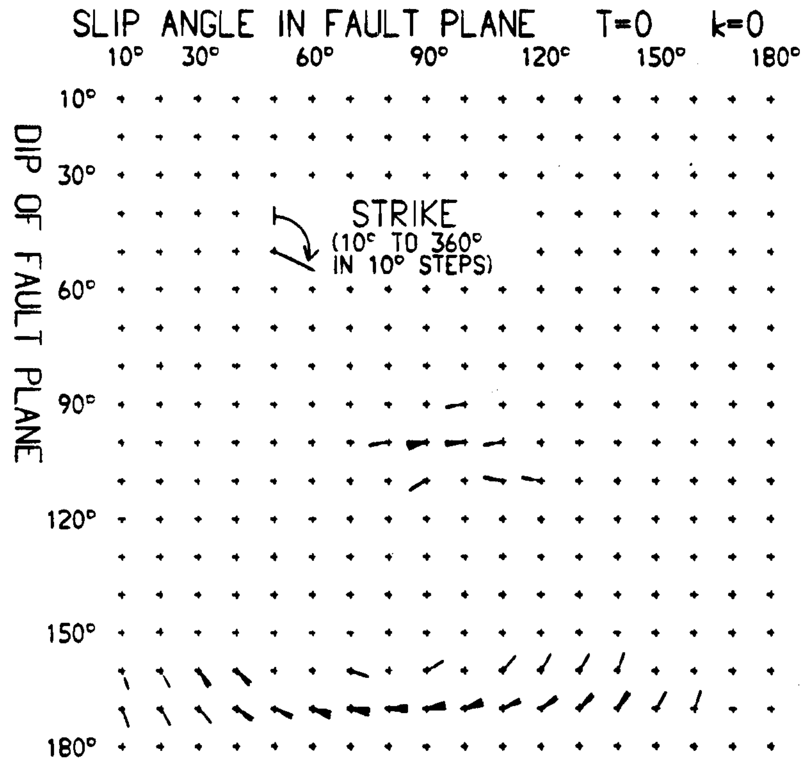

(d)

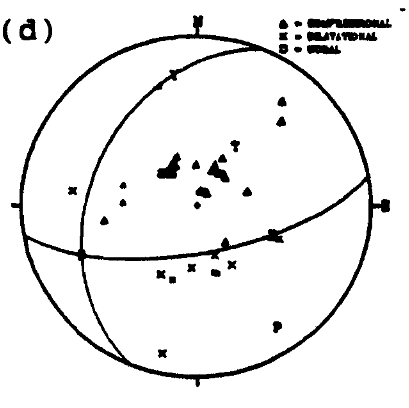

(e)

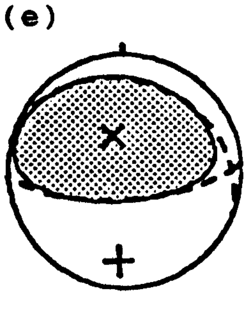

(f)

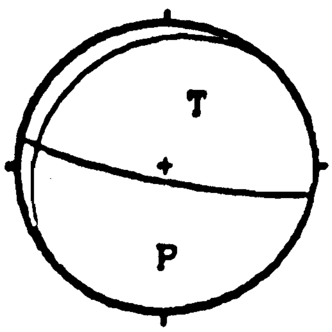

(a)

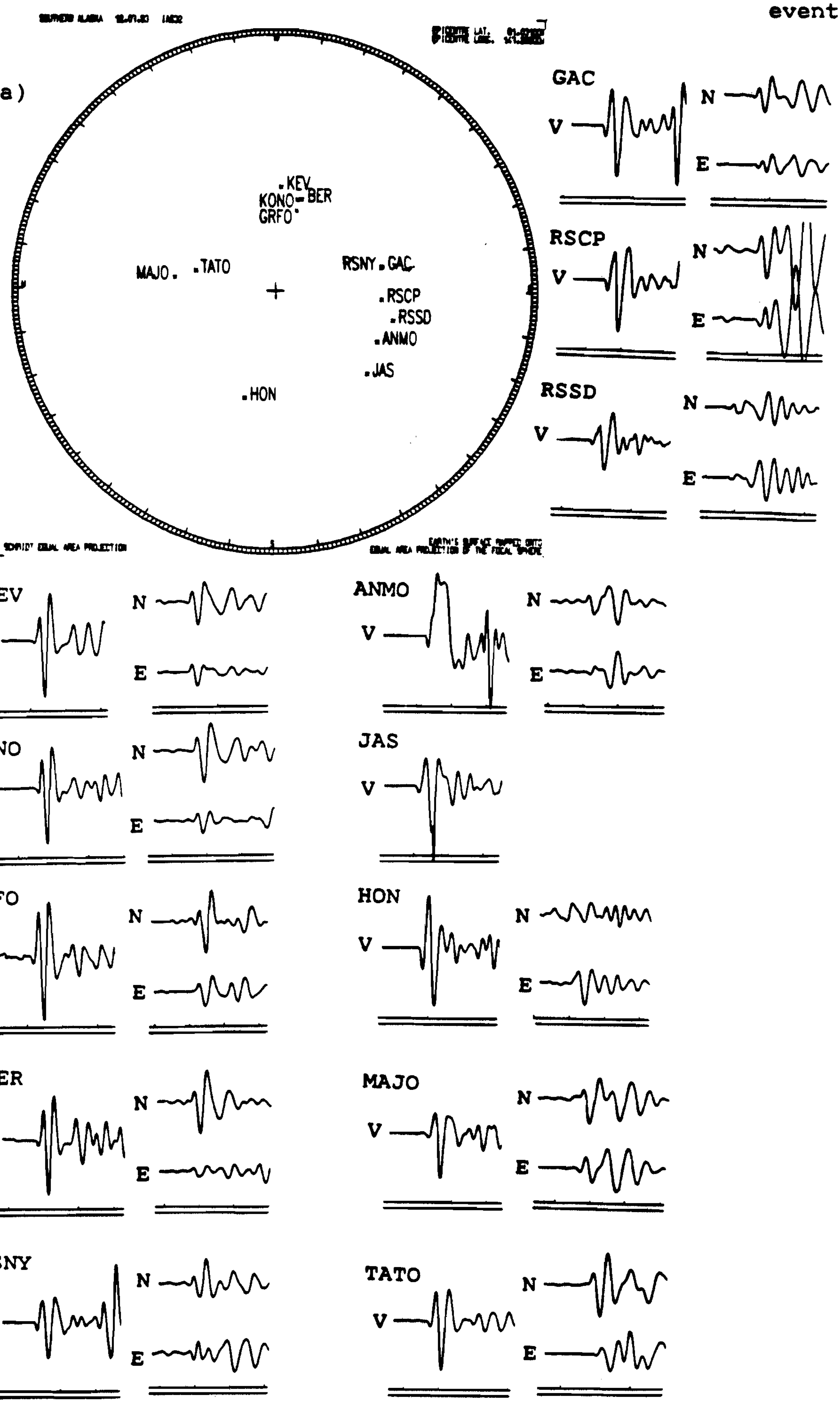
KEV
KONO
BER
GRFO
MAJO
TATO
RSNY
GAC
RSCP
RSSD
ANMO
JAS
HON
V
N
E

IASPEI event 32

(b)

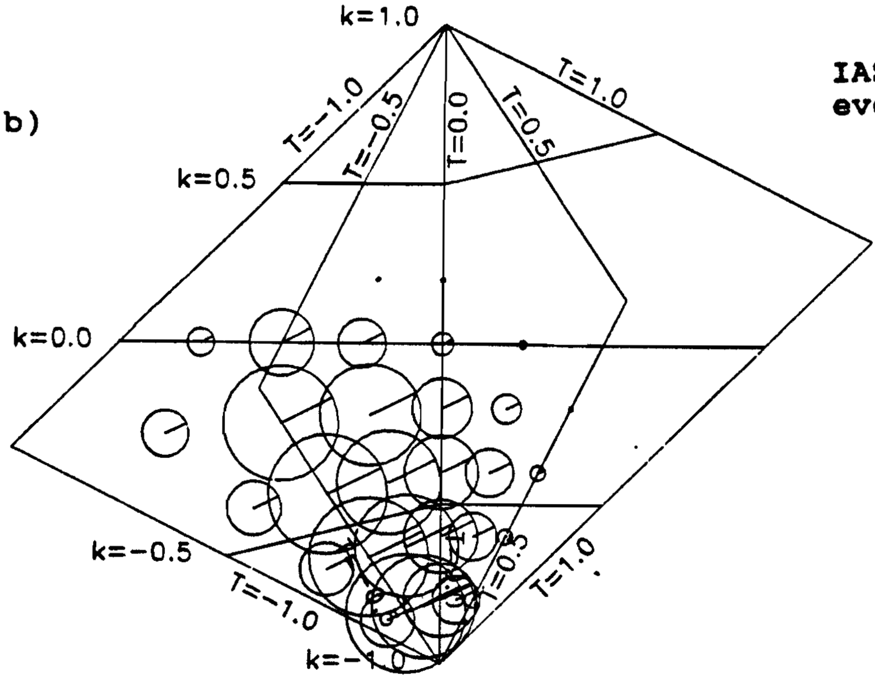

(c)

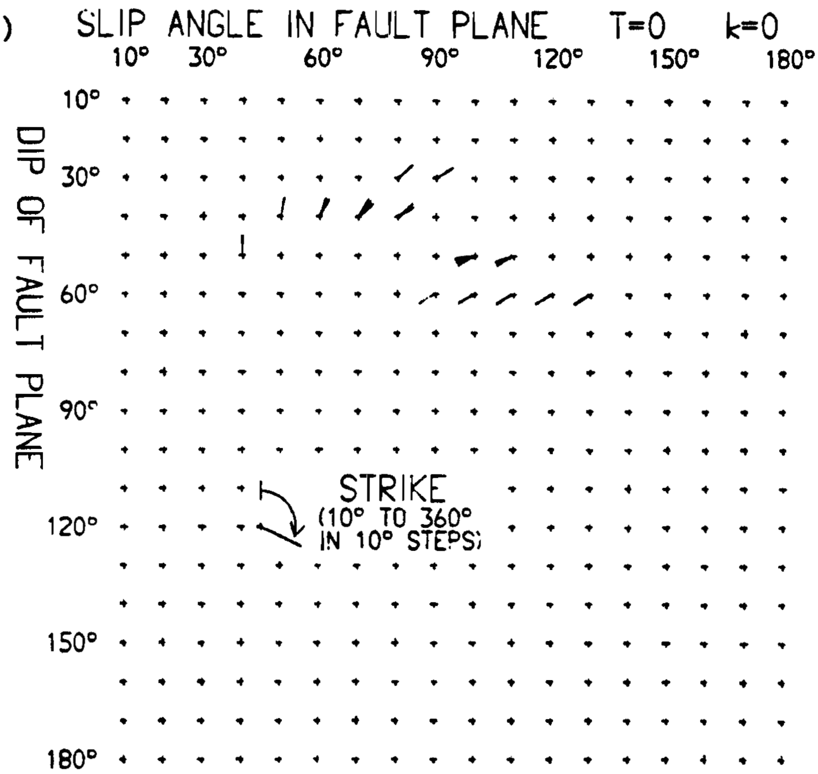

(d)

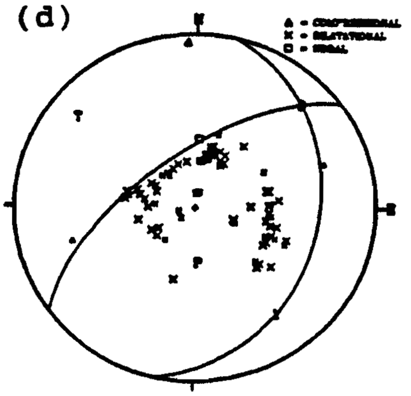

(e)

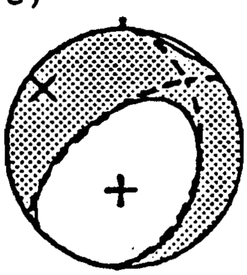

(f)

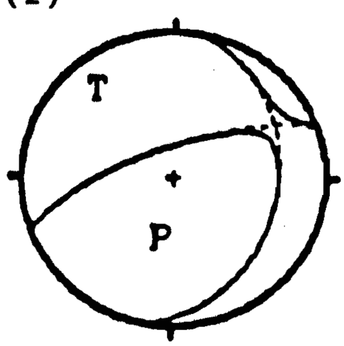

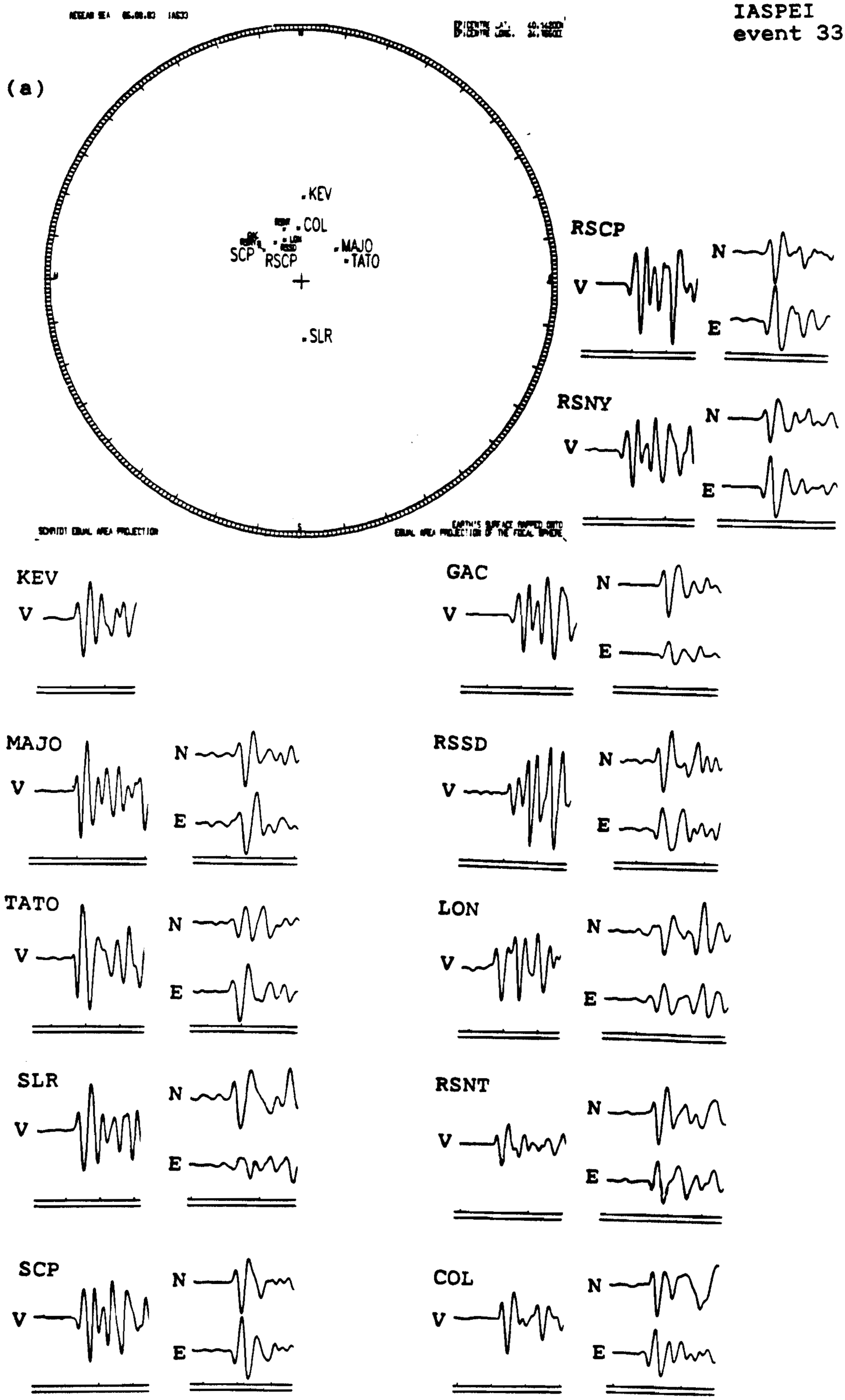
(a)
SCHMIDT EQUAL AREA PROJECTION
KEV
COL
MAJO
TATO
SCP
RSCP
SLR
RSCP
RSNY
KEV
GAC
MAJO
RSSD
TATO
LON
SLR
RSNT
SCP
COL
V
N
E

IASPEI event 33

(b)

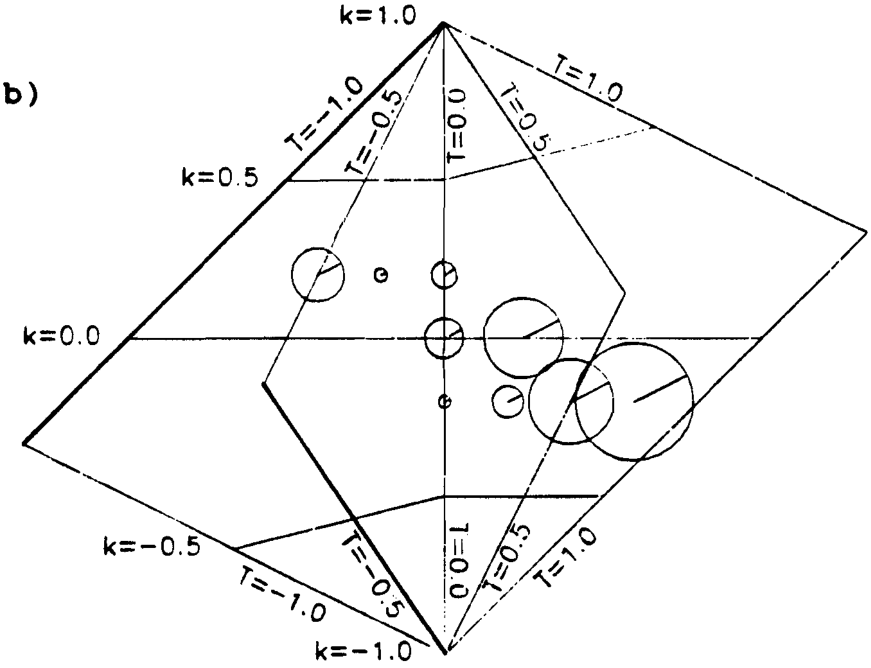

(c)

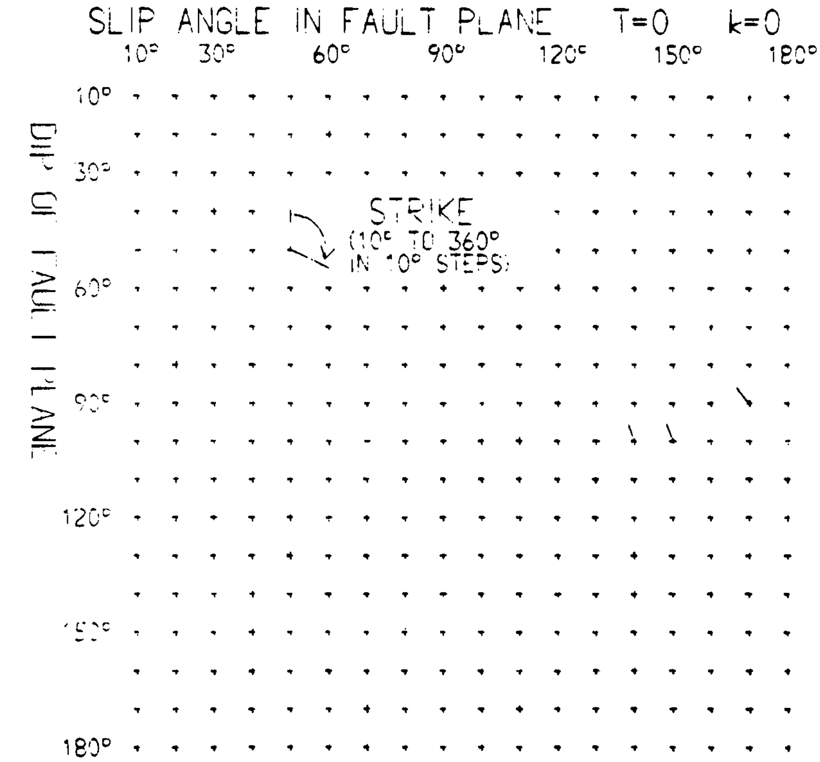

(d)

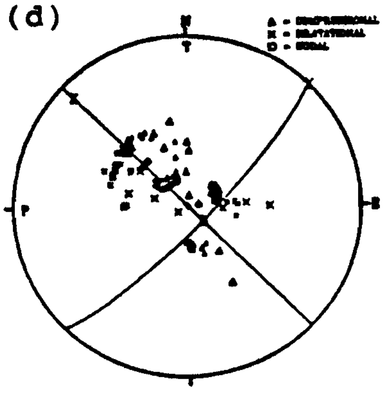

(e)

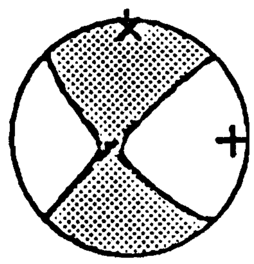

(f)

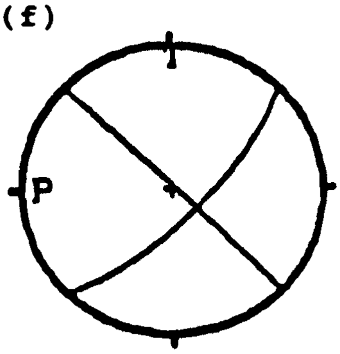

IASPEI
event 34

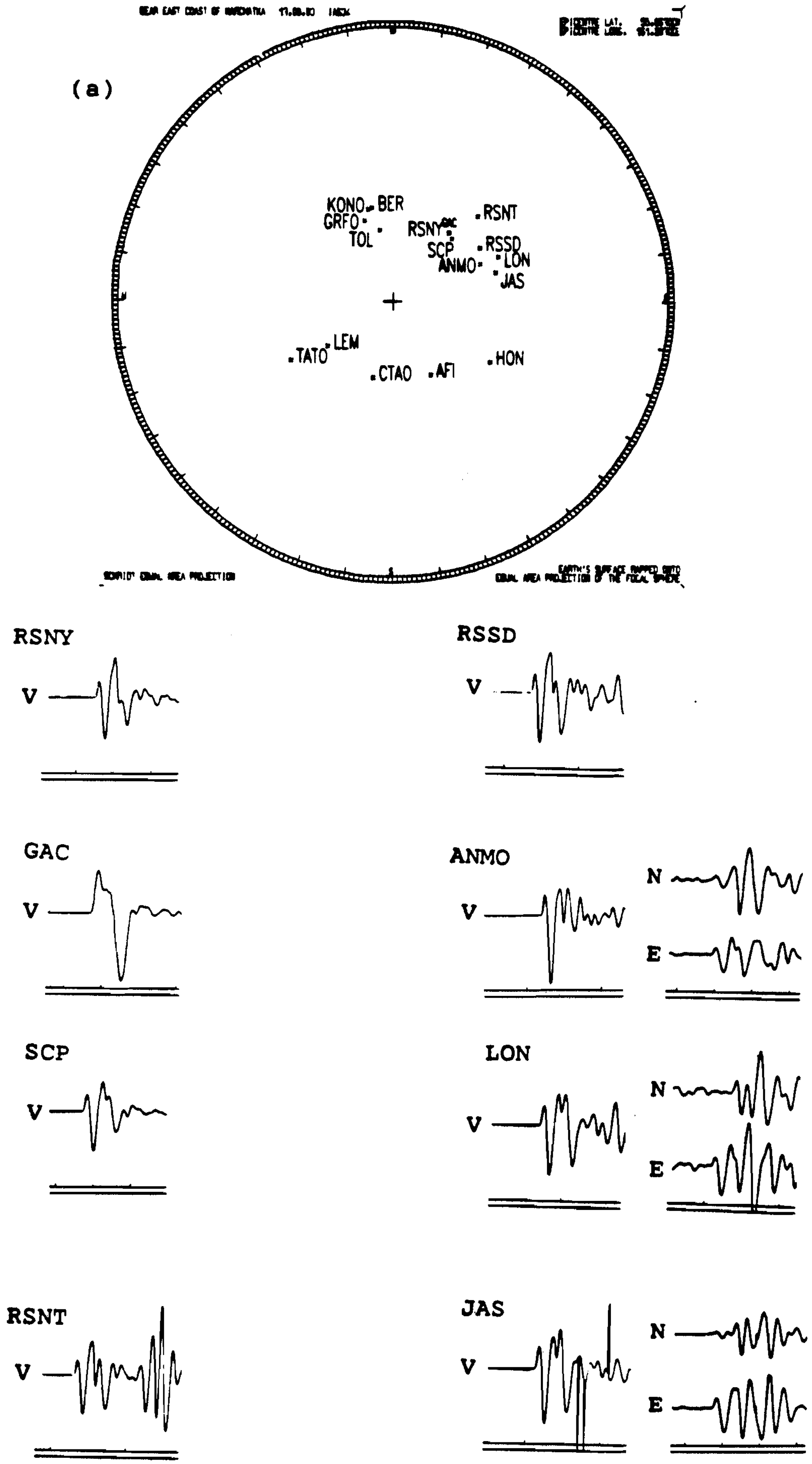

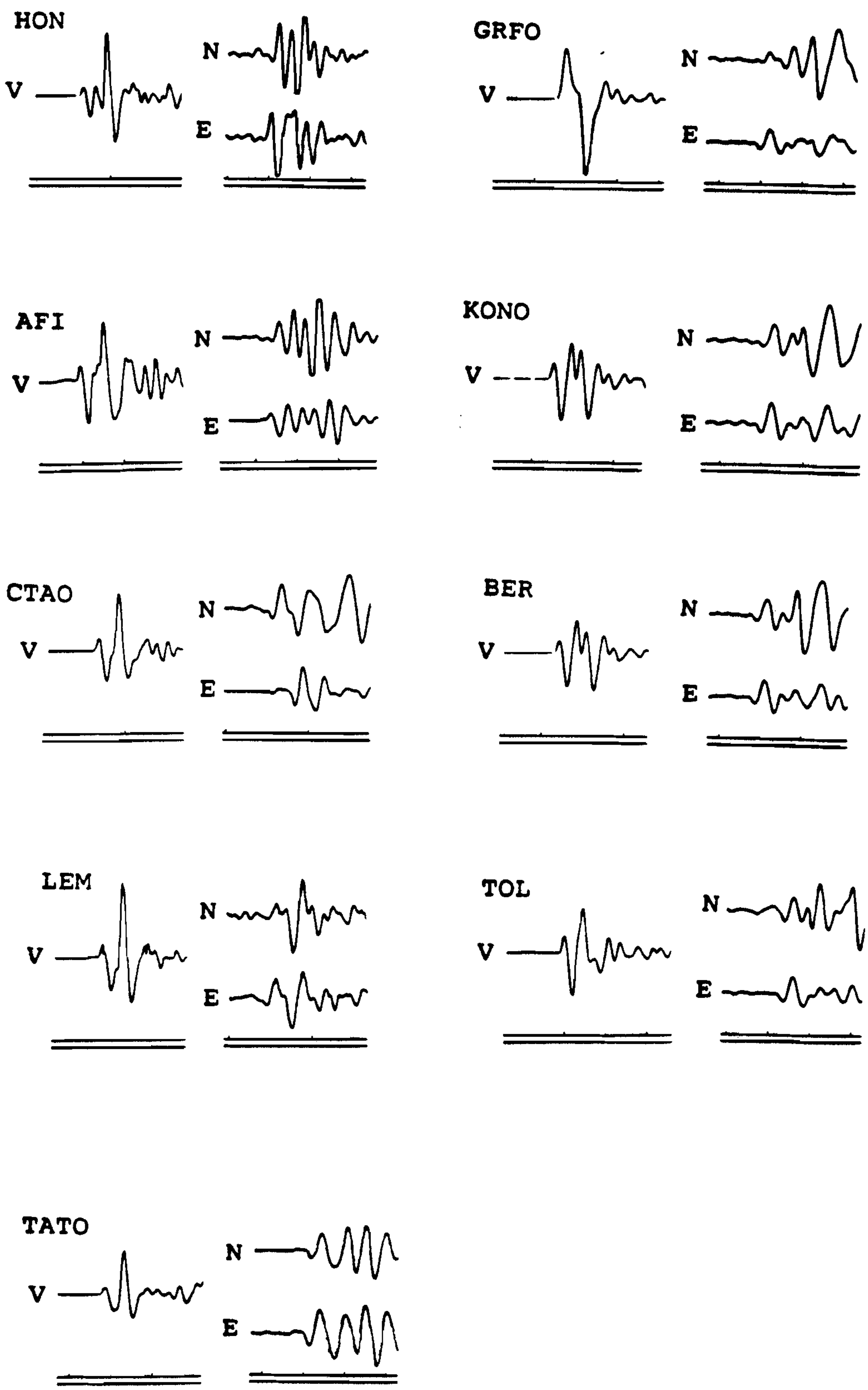
HON
V
N
E
GRFO
V
N
E
AFI
V
N
E
KONO
V
N
E
CTAO
V
N
E
BER
V
N
E
LEM
V
N
E
TOL
V
N
E
TATO
V
N
E

IASPEI
event 34

(b)

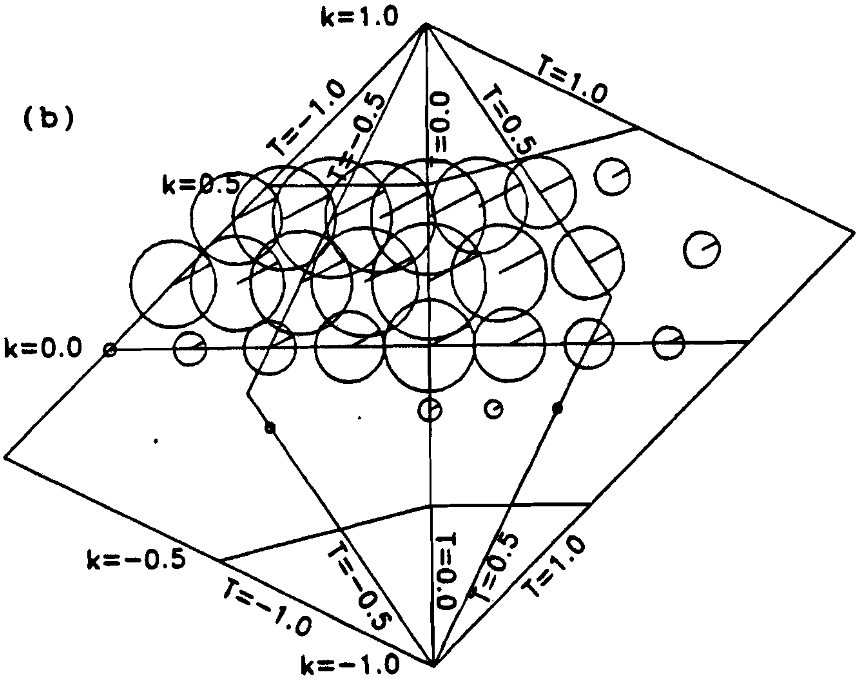

(c)

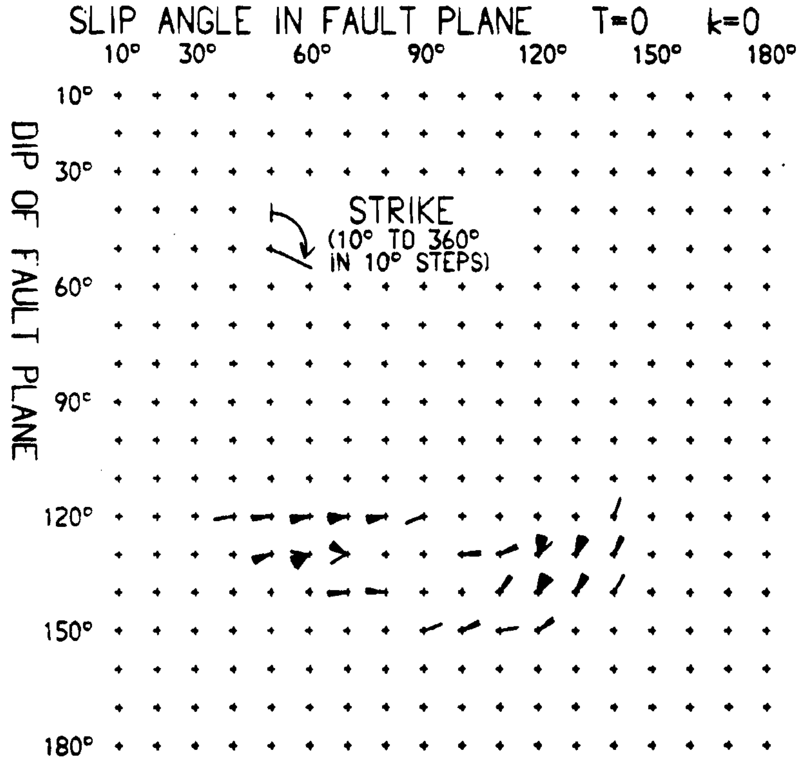

(d)

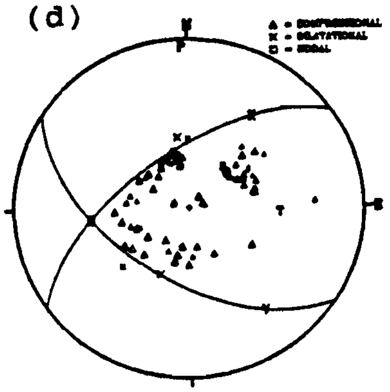

(e)

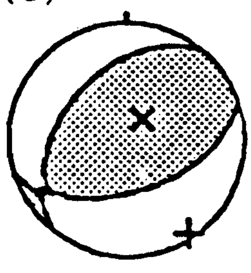

(f)

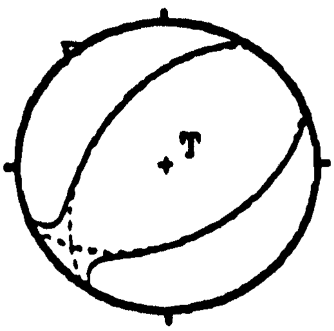

IASPEI
event 35

(b)

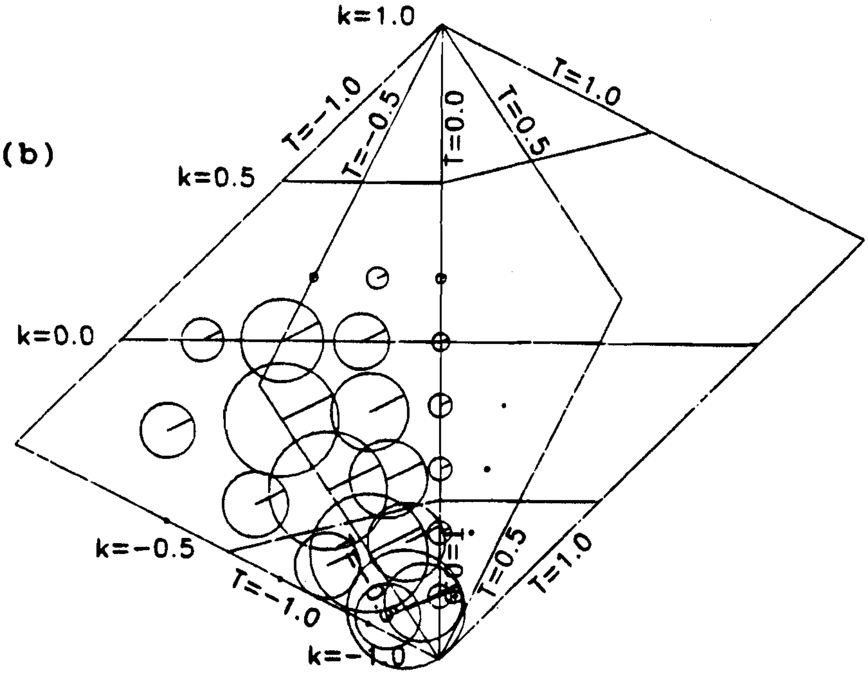

(c)

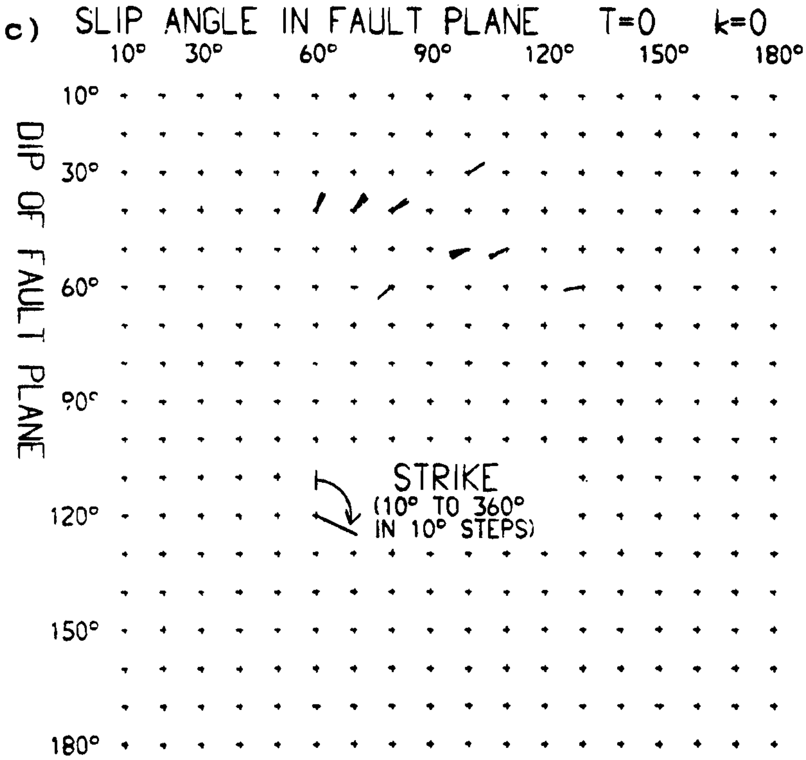

(d)

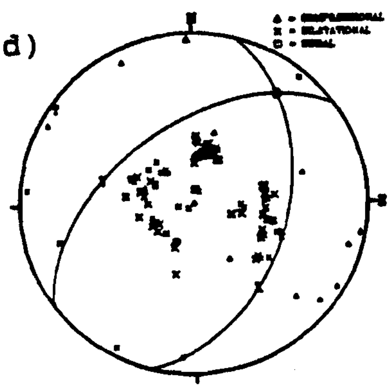

(e)

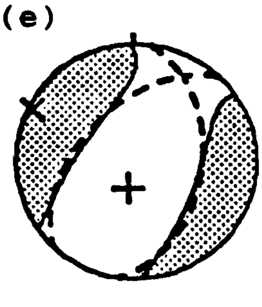

(f)

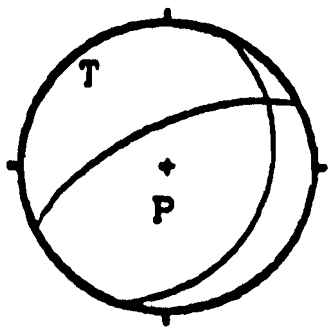

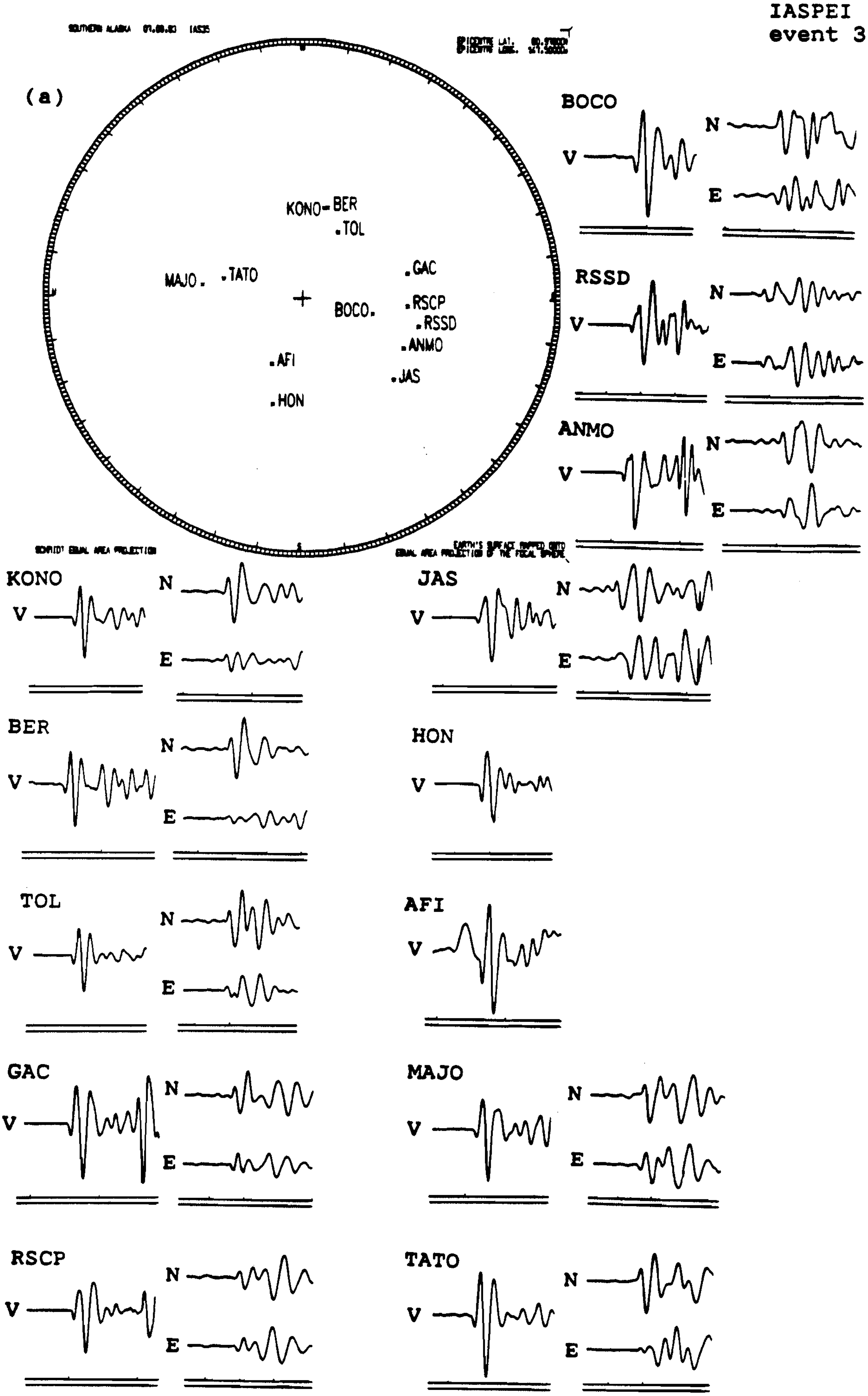
(a)
KONO
BER
TOL
GAC
MAJO
TATO
BOCO
RSCP
RSSD
ANMO
AFI
JAS
HON
BOCO
V
N
E
RSSD
V
N
E
ANMO
V
N
E
KONO
V
N
E
JAS
V
N
E
BER
V
N
E
HON
V
TOL
V
N
E
AFI
V
GAC
V
N
E
MAJO
V
N
E
RSCP
V
N
E
TATO
V
N
E

IASPEI
event 35

(b)

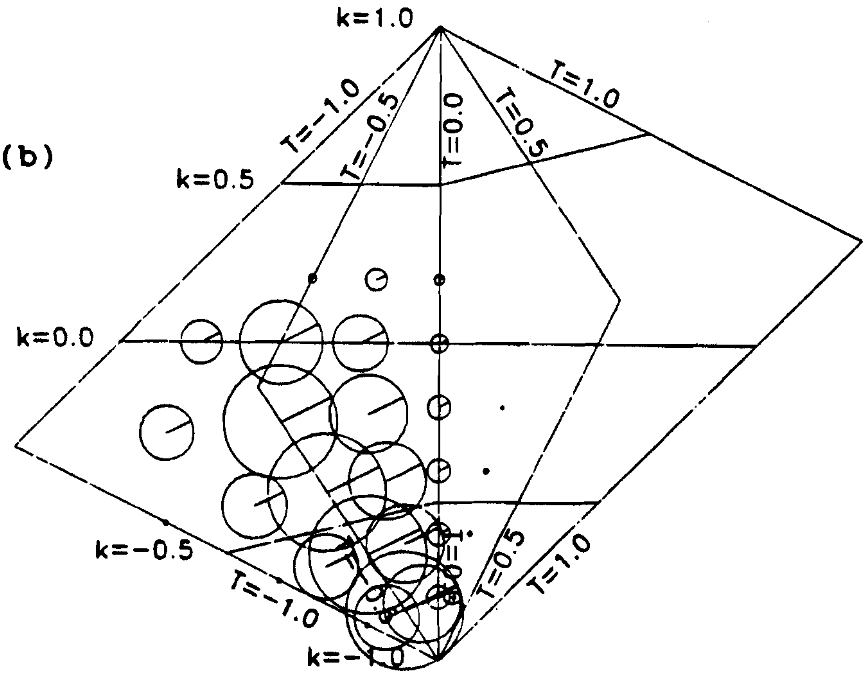

(c)

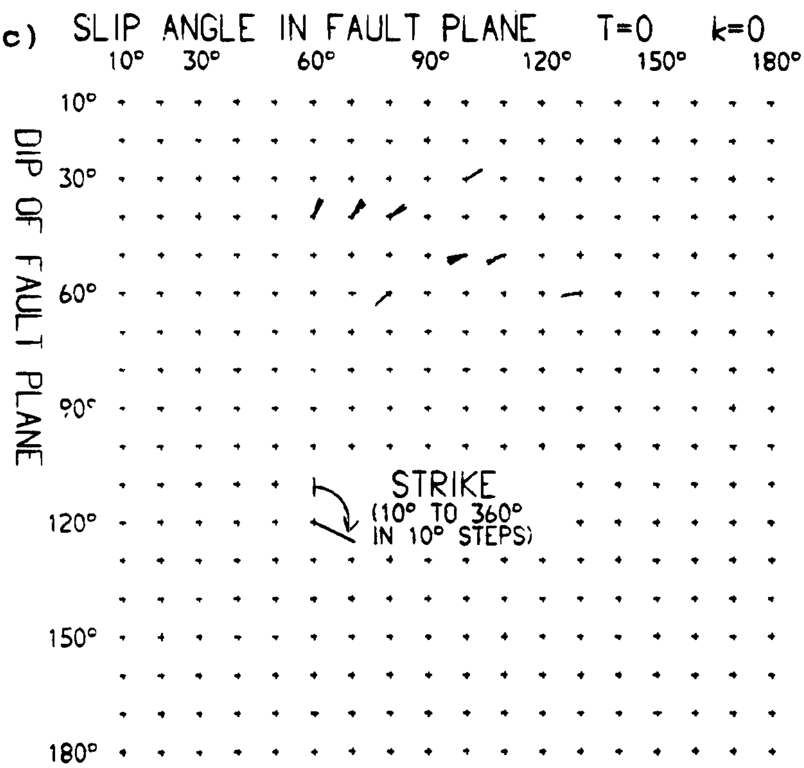

(d)

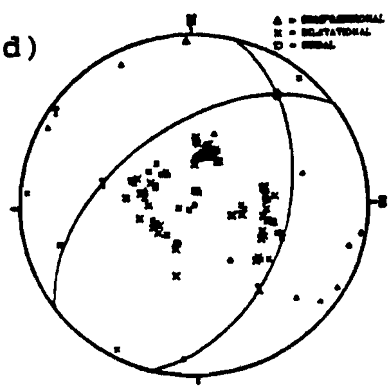

(e)

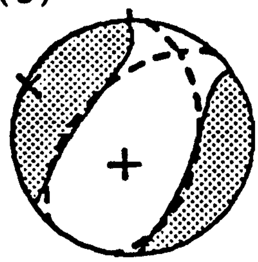

(f)

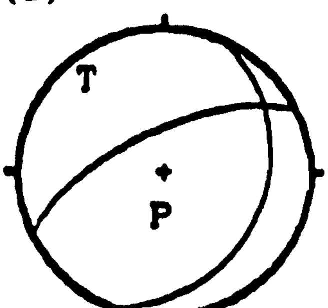

IASPEI
event 36

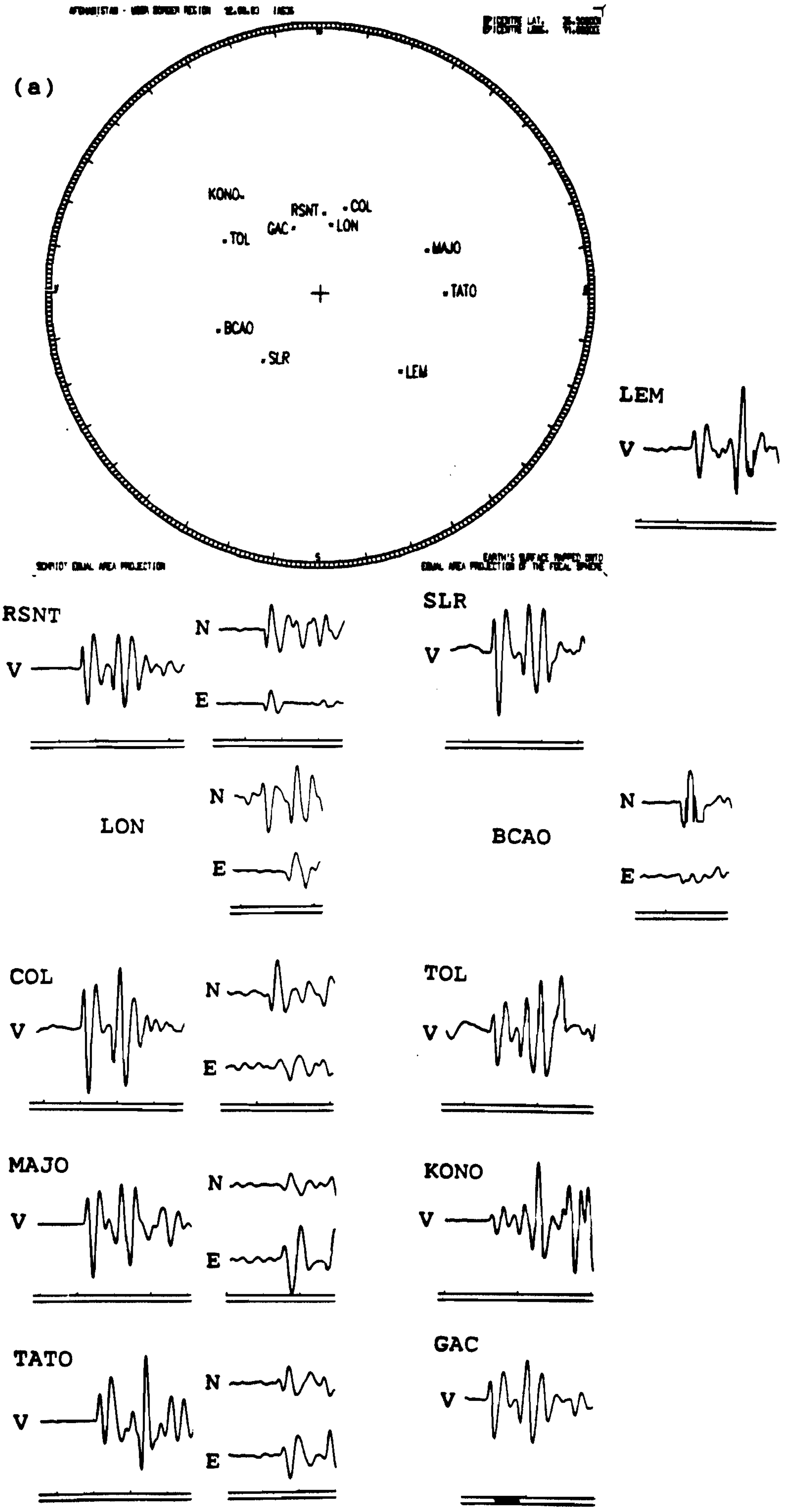

IASPEI
event 36

(b)

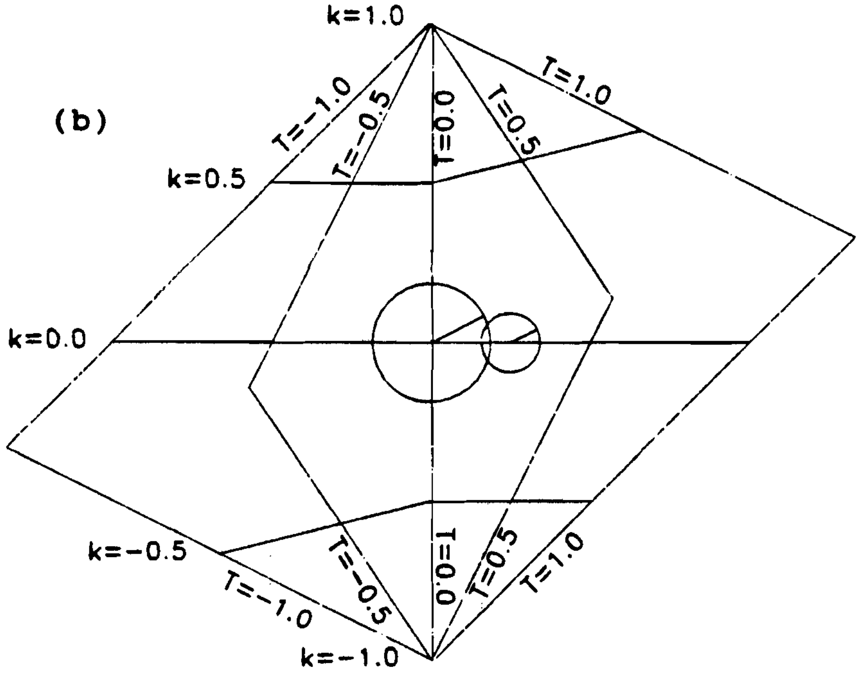

(c)

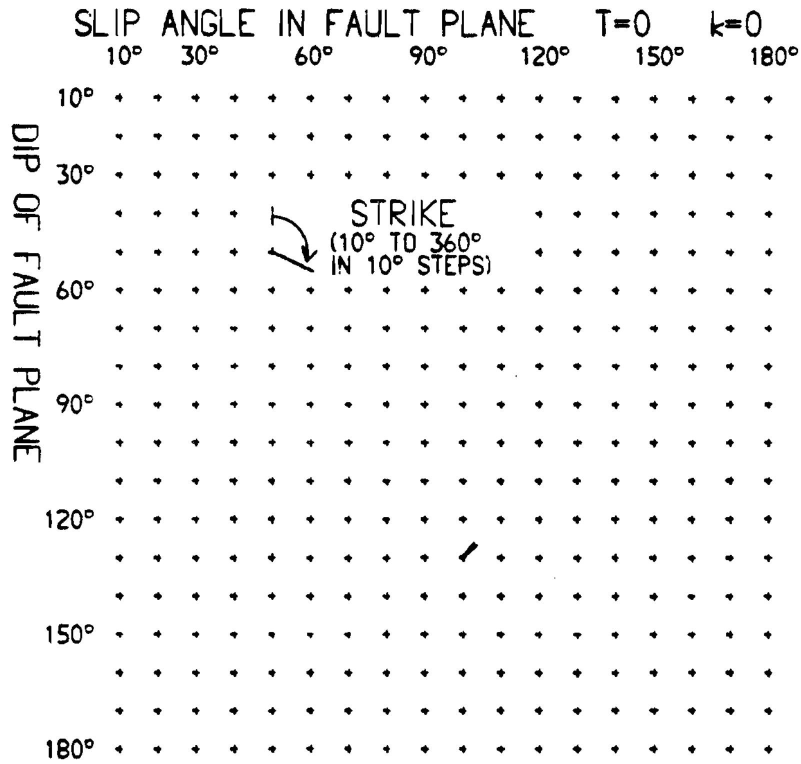

(d)

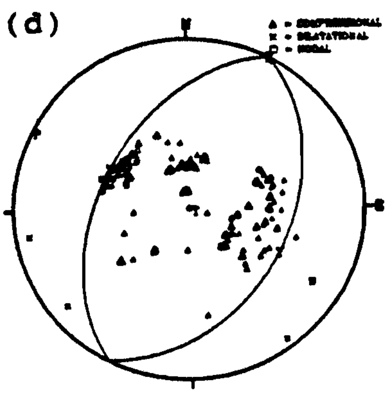

(e)

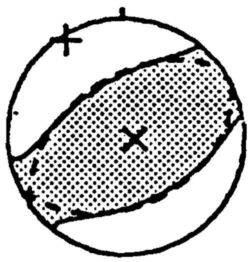

(f)

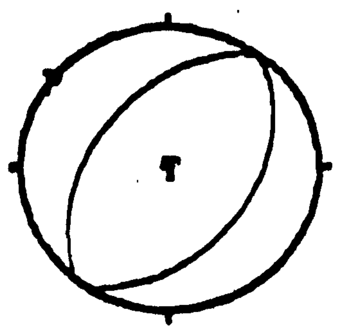

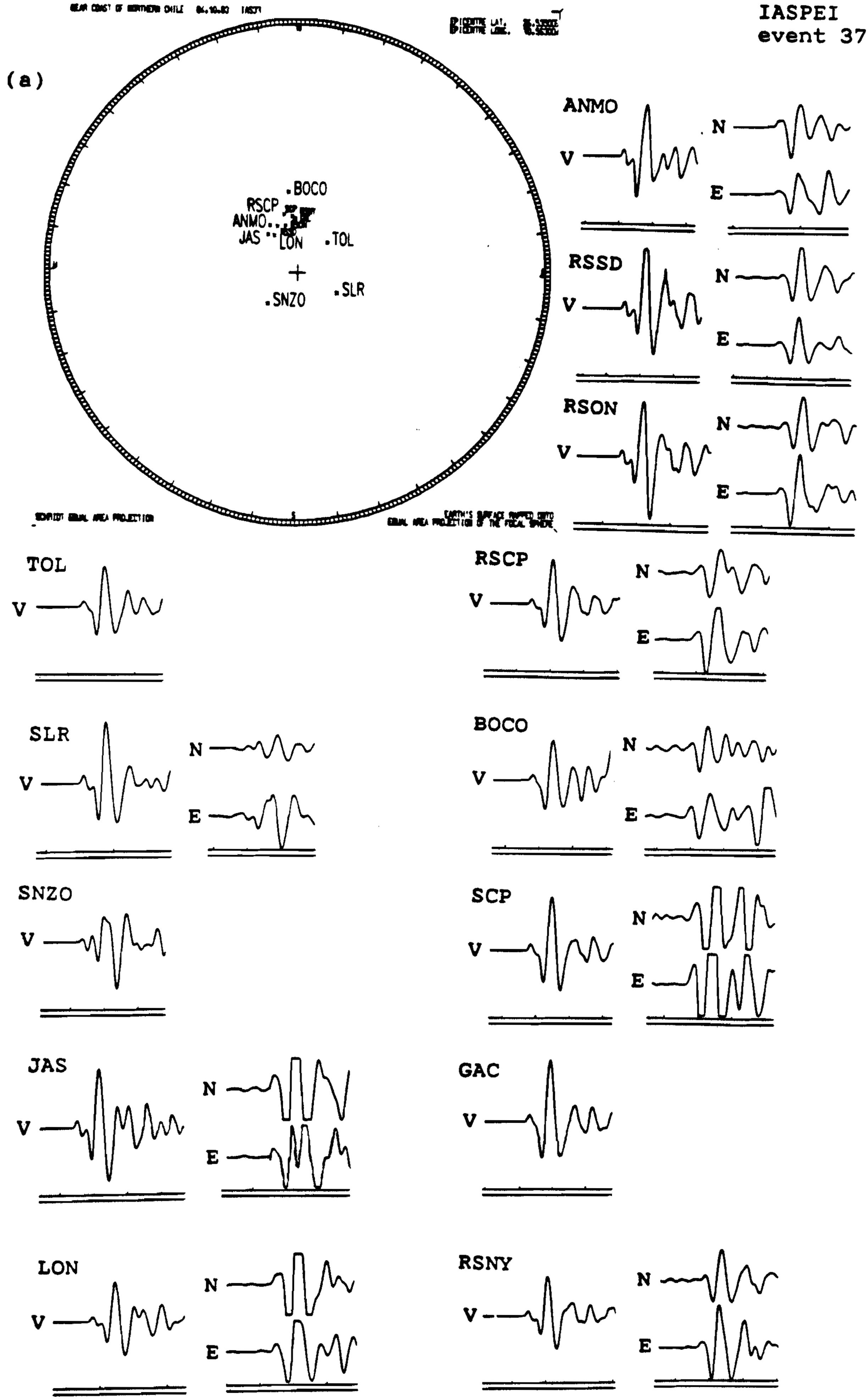
(a)
BOCO
RSCP
ANMO
JAS
LON
TOL
SNZO
SLR
ANMO
RSSD
RSON
TOL
RSCP
SLR
BOCO
SNZO
SCP
JAS
GAC
LON
RSNY
V
N
E

IASPEI
event 37

(b)

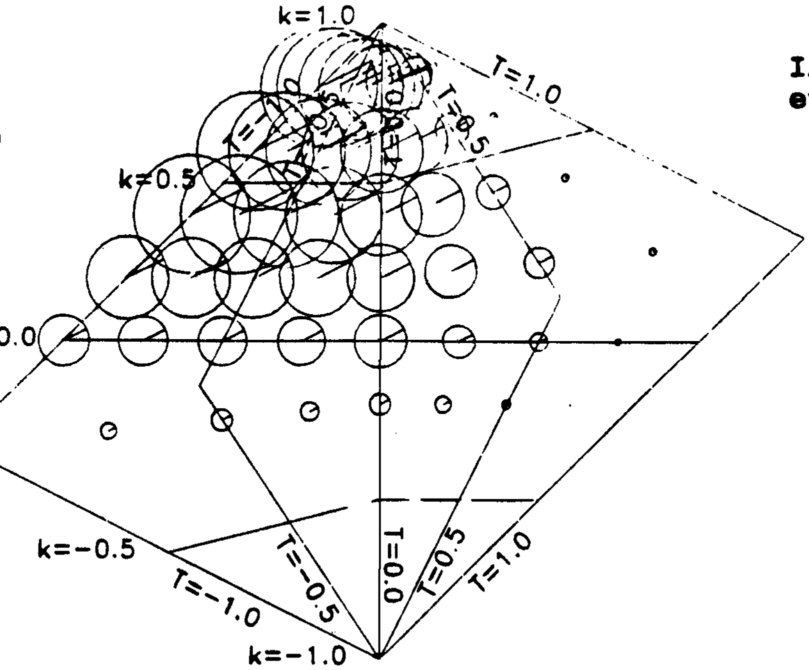

(c)

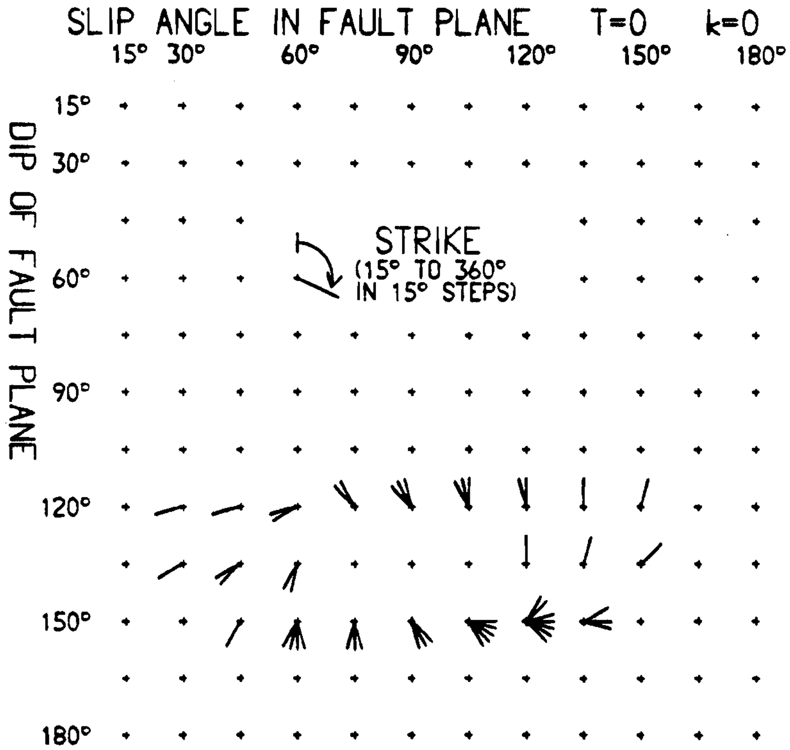

(d)

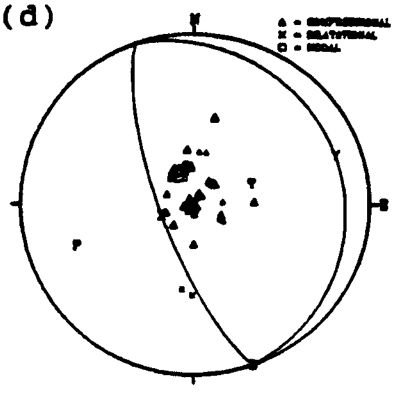

(e)

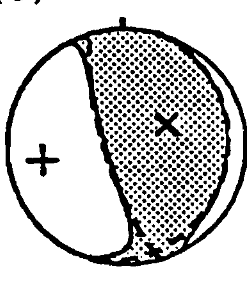

(f)

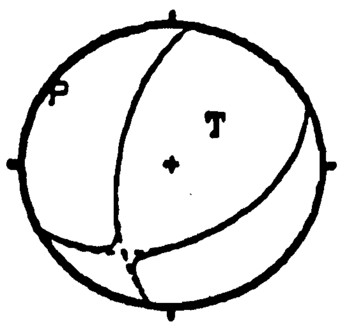

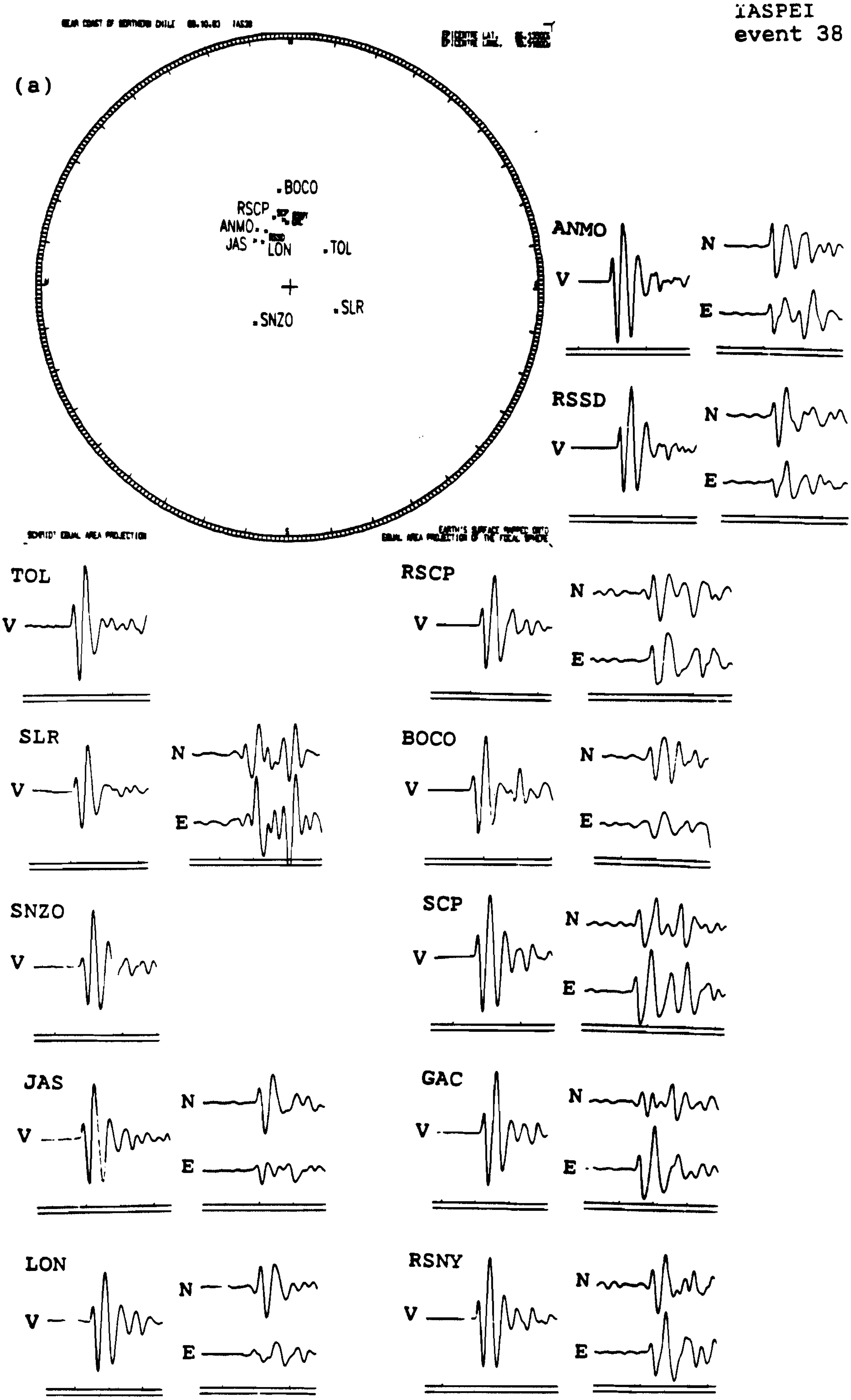
(a)
BOCO
RSCP
ANMO
JAS
LON
TOL
SNZO
SLR
ANMO
V
N
E
RSSD
V
N
E
TOL
V
RSCP
V
N
E
SLR
V
N
E
BOCO
V
N
E
SNZO
V
SCP
V
N
E
JAS
V
N
E
GAC
V
N
E
LON
V
N
E
RSNY
V
N
E

IASPEI
event 38

(b)

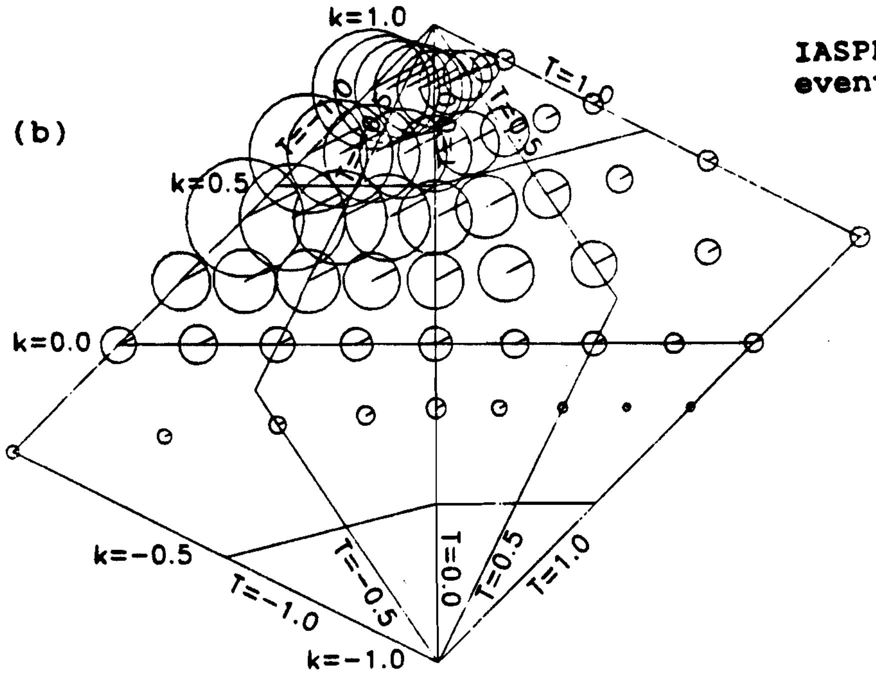

(c)

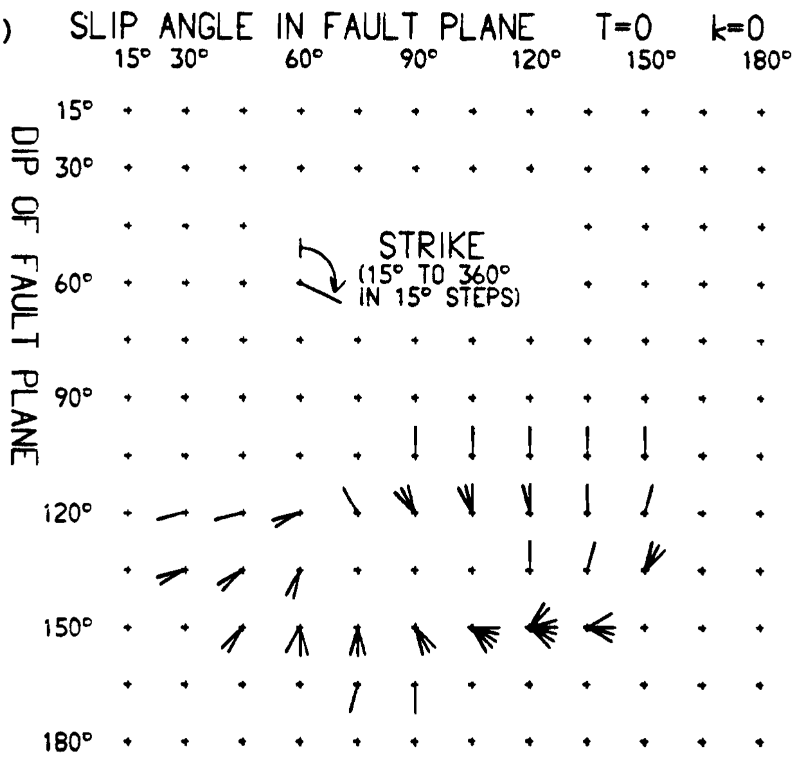

(d)

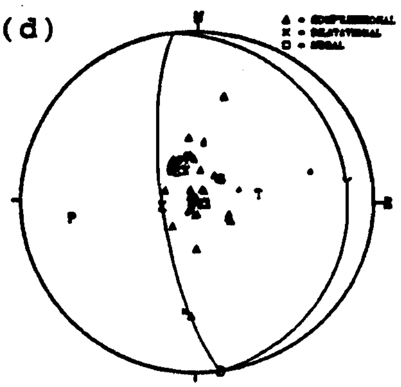

(e)

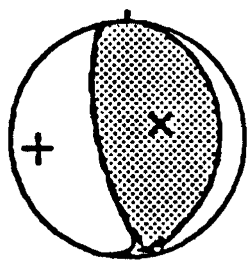

(f)

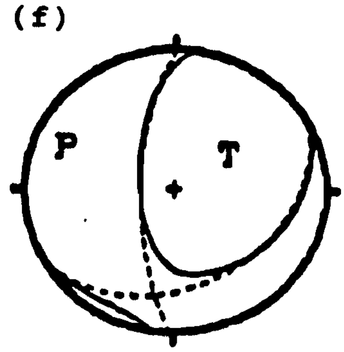

(a)

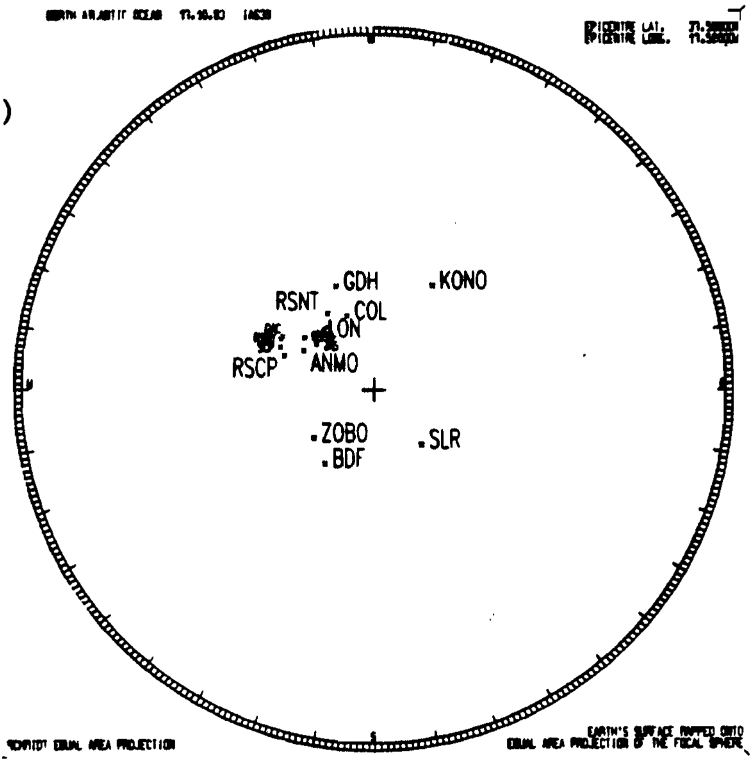
GDH
KONO
RSNT
COL
LON
RSCP
ANMO
ZOBO
BDF
SLR

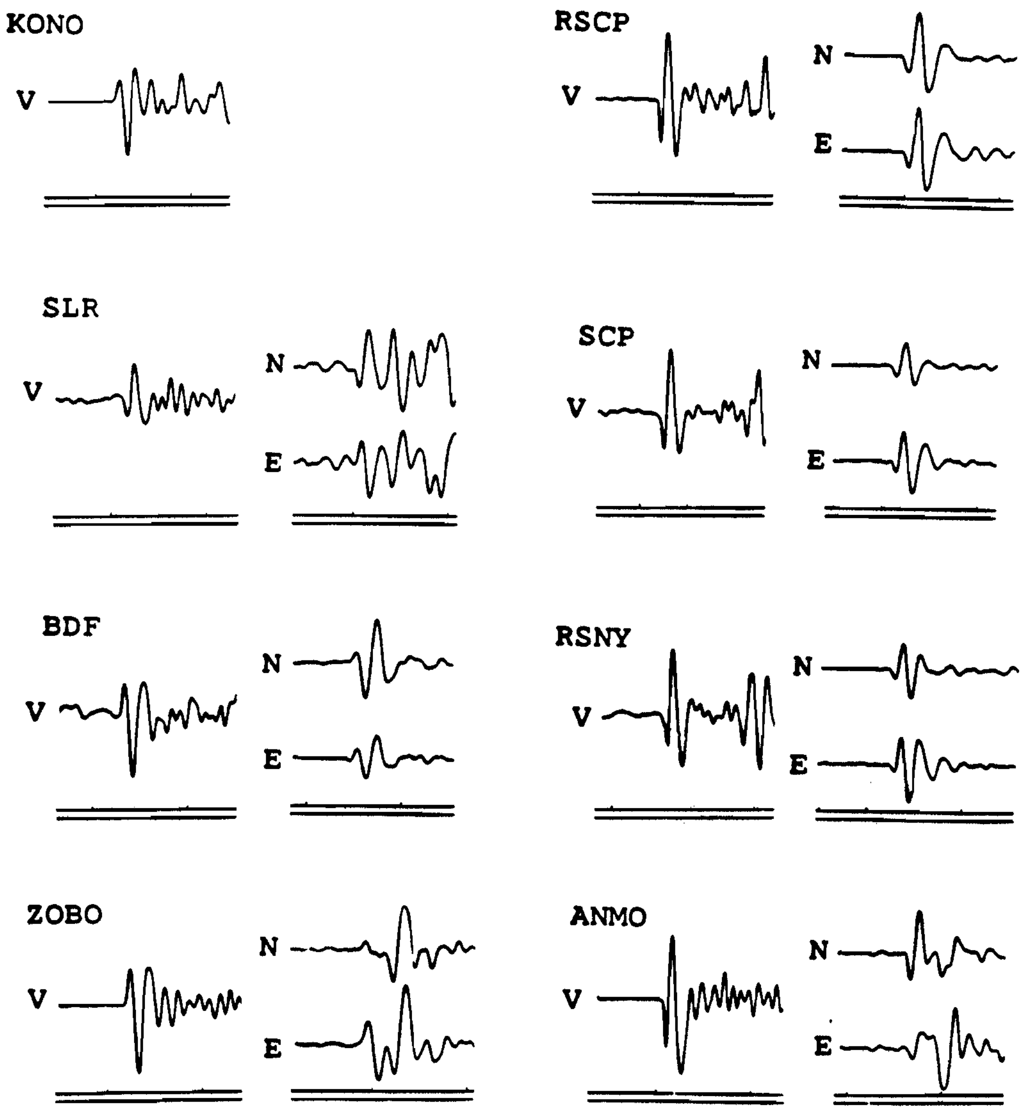
KONO
V
RSCP
V
N
E
SLR
V
N
E
SCP
V
N
E
BDF
V
N
E
RSNY
V
N
E
ZOBO
V
N
E
ANMO
V
N
E

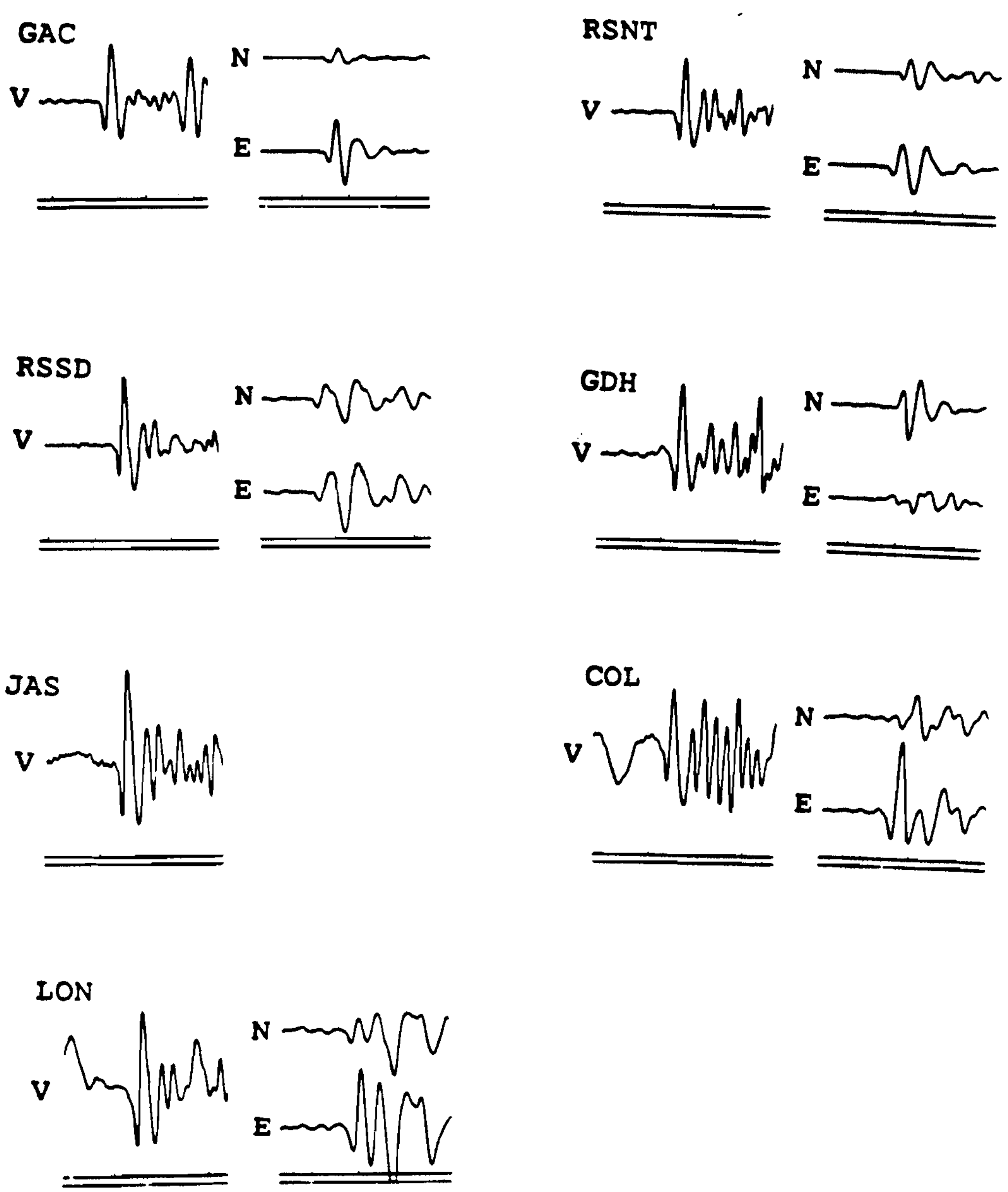
GAC
V
N
E
RSNT
V
N
E
RSSD
V
N
E
GDH
V
N
E
JAS
V
COL
V
N
E
LON
V
N
E

IASPEI event 39

(b)

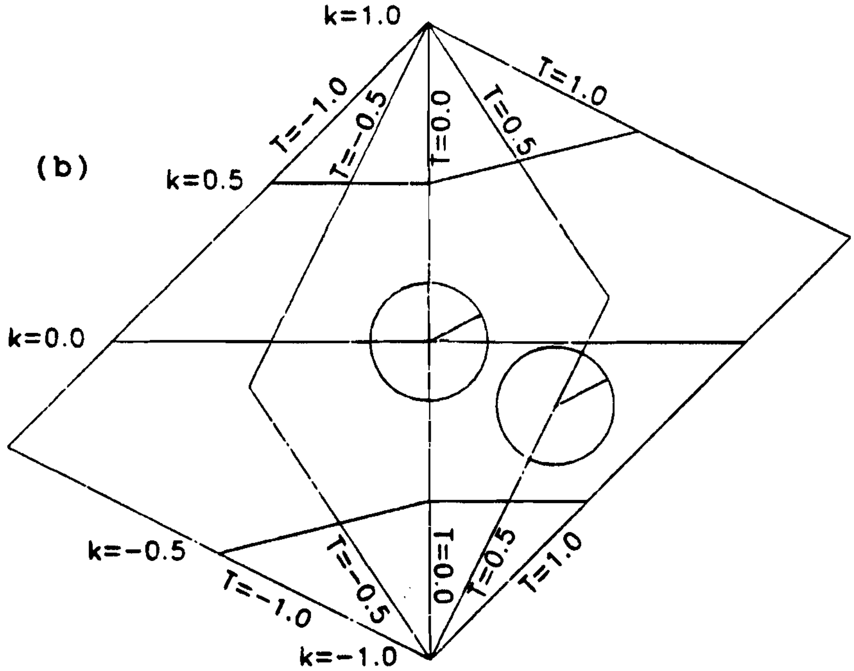

(c)

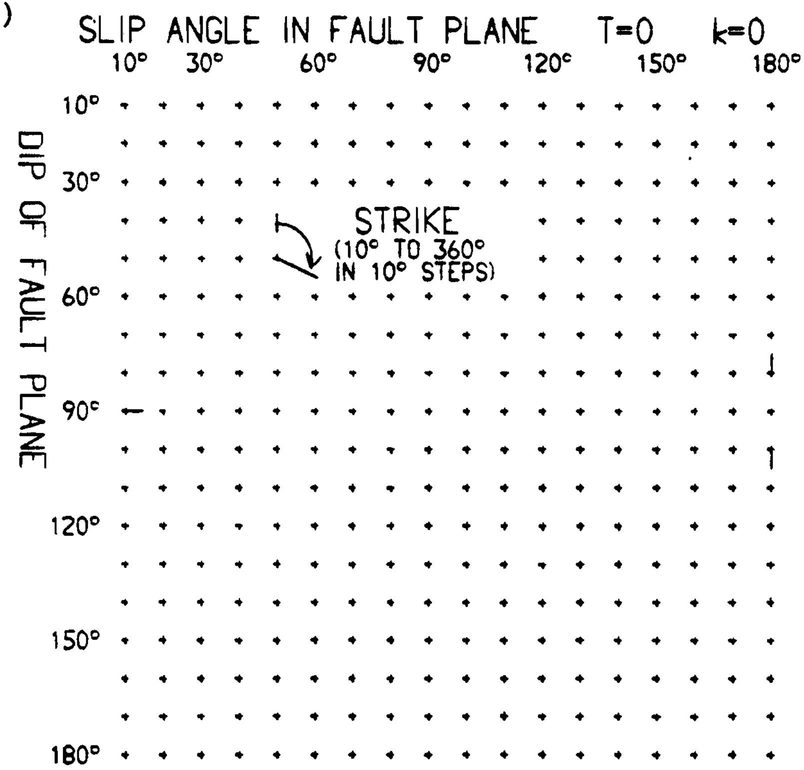

(d)

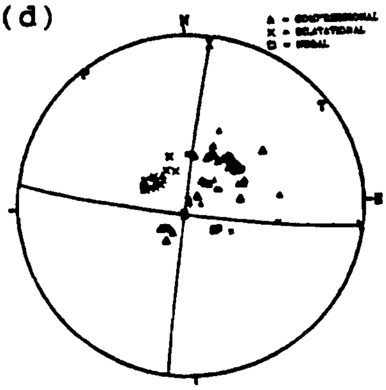

(e)

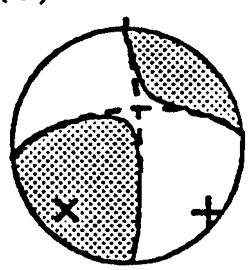

(f)

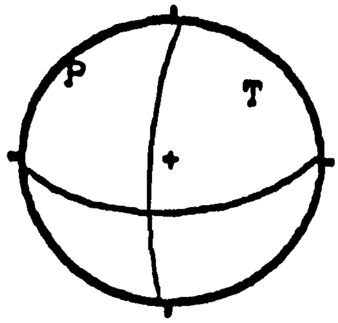

THIS PAGE LEFT BLANK INTENTIONALLY

(a)

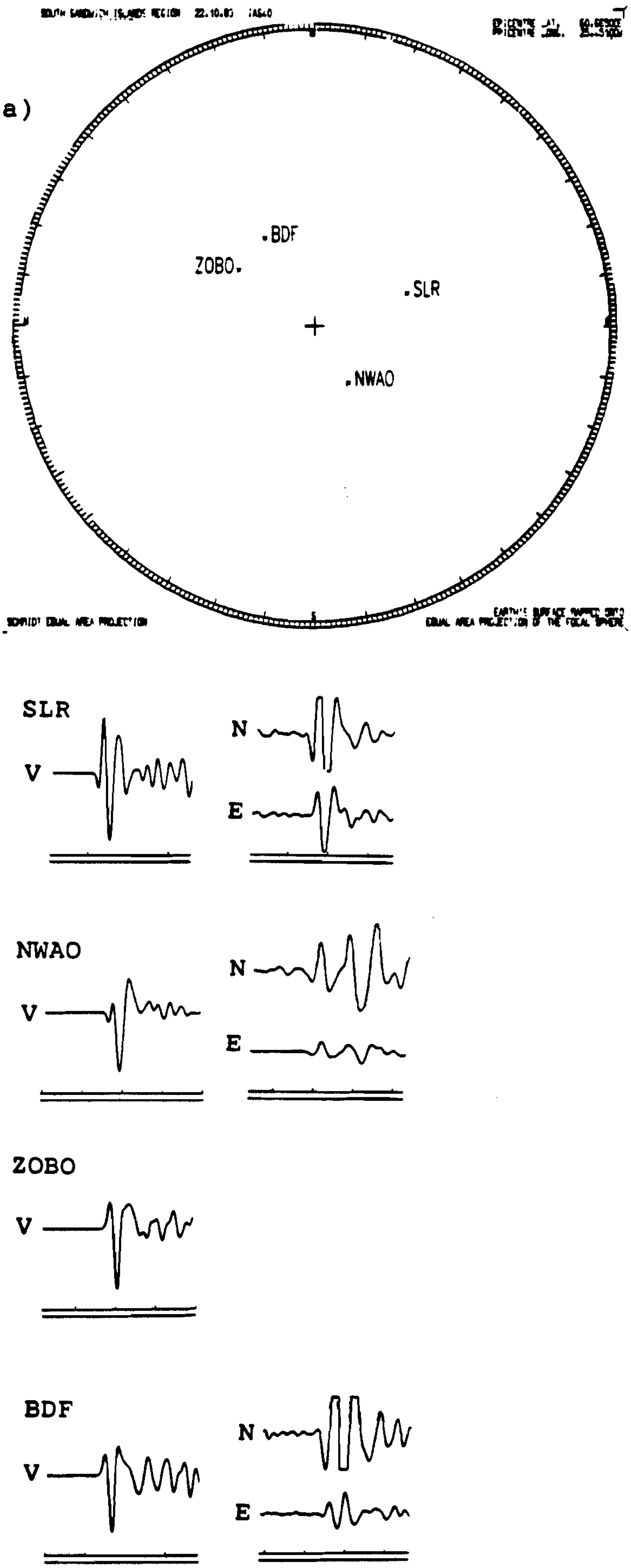

IASPEI event 40

(b)

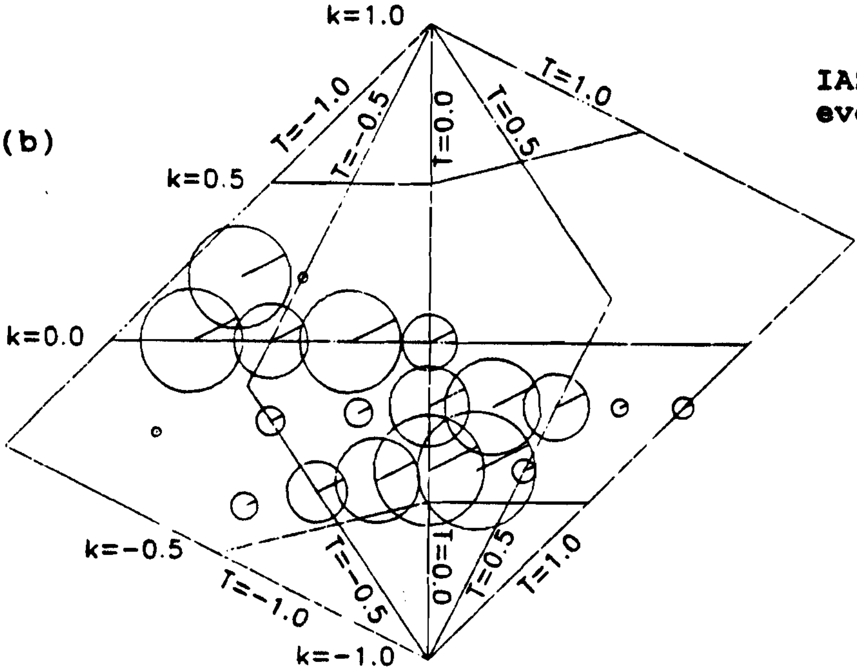

(c)

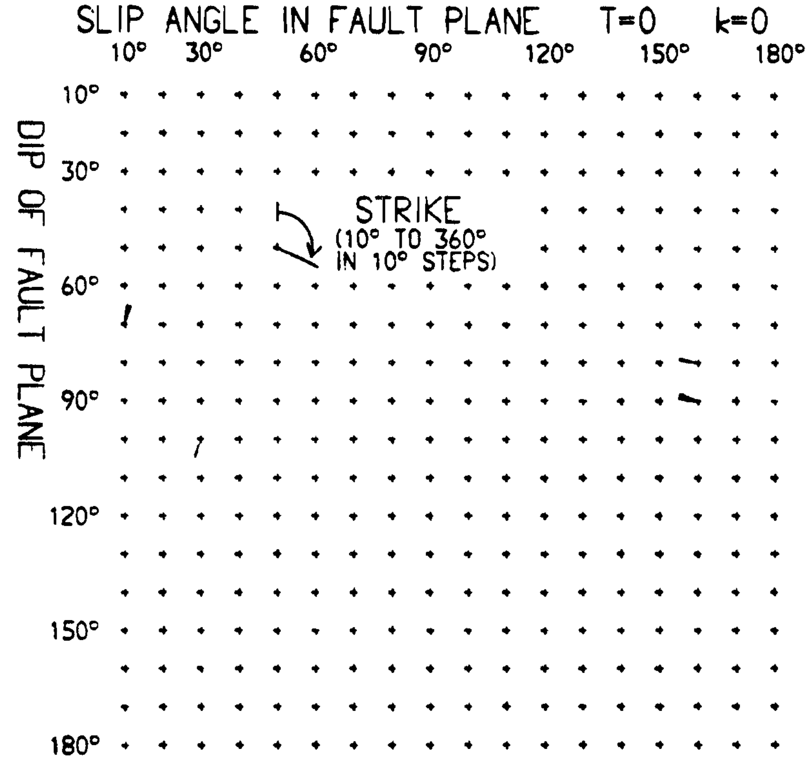

(d)

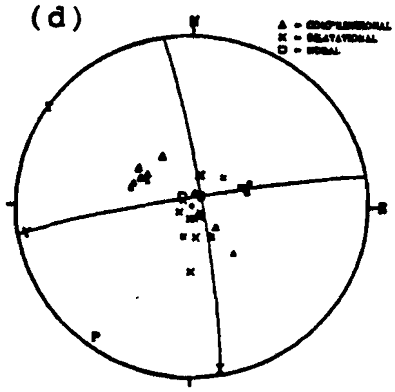

(e)

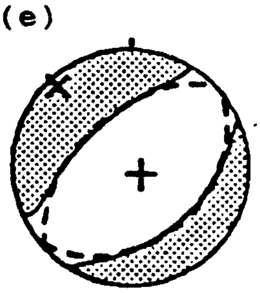

(f)

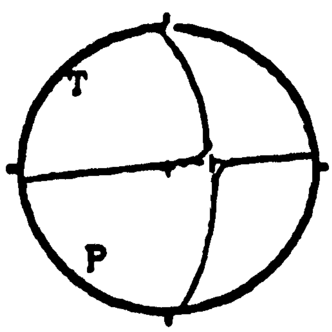

IASPEI
event 41

(a)

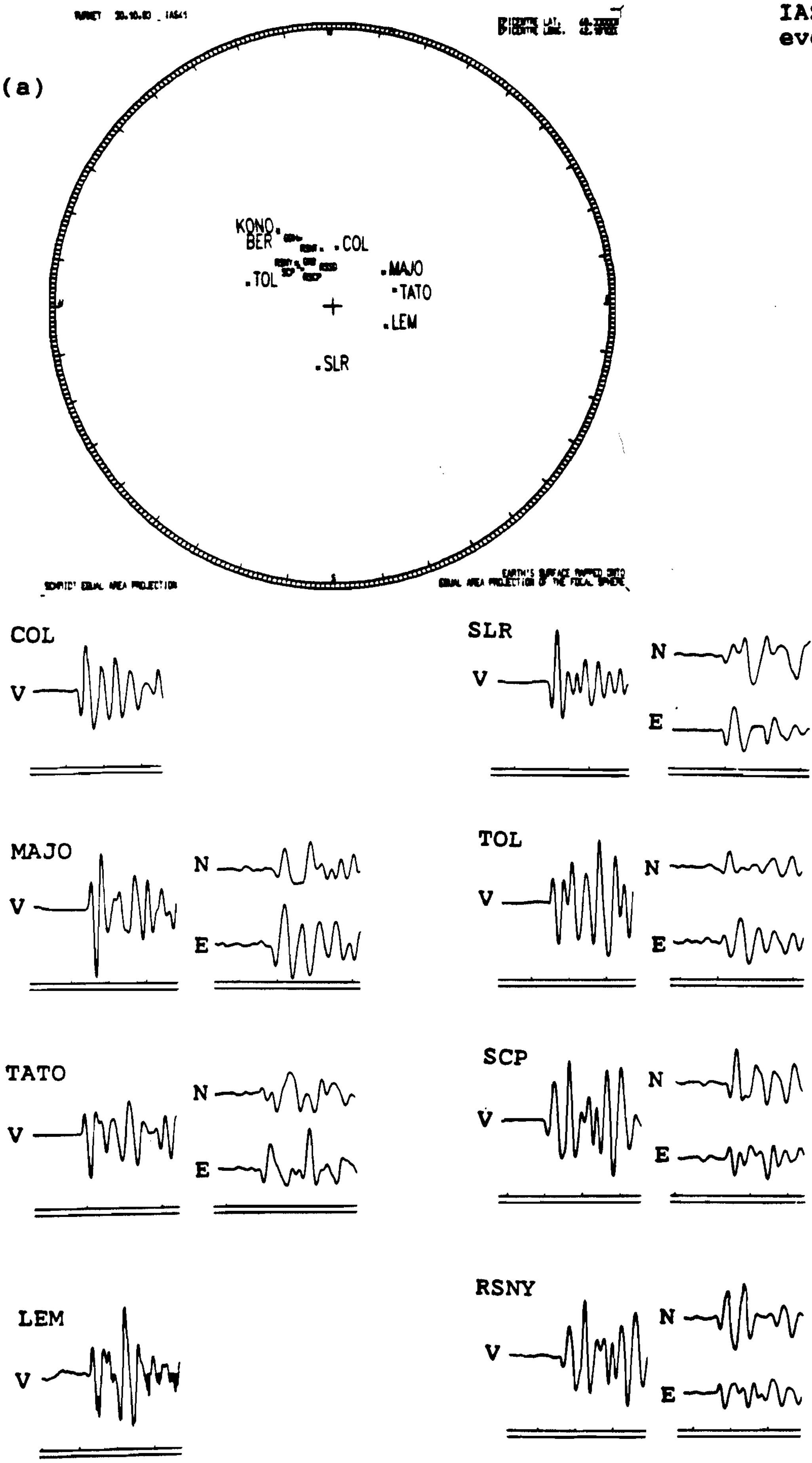

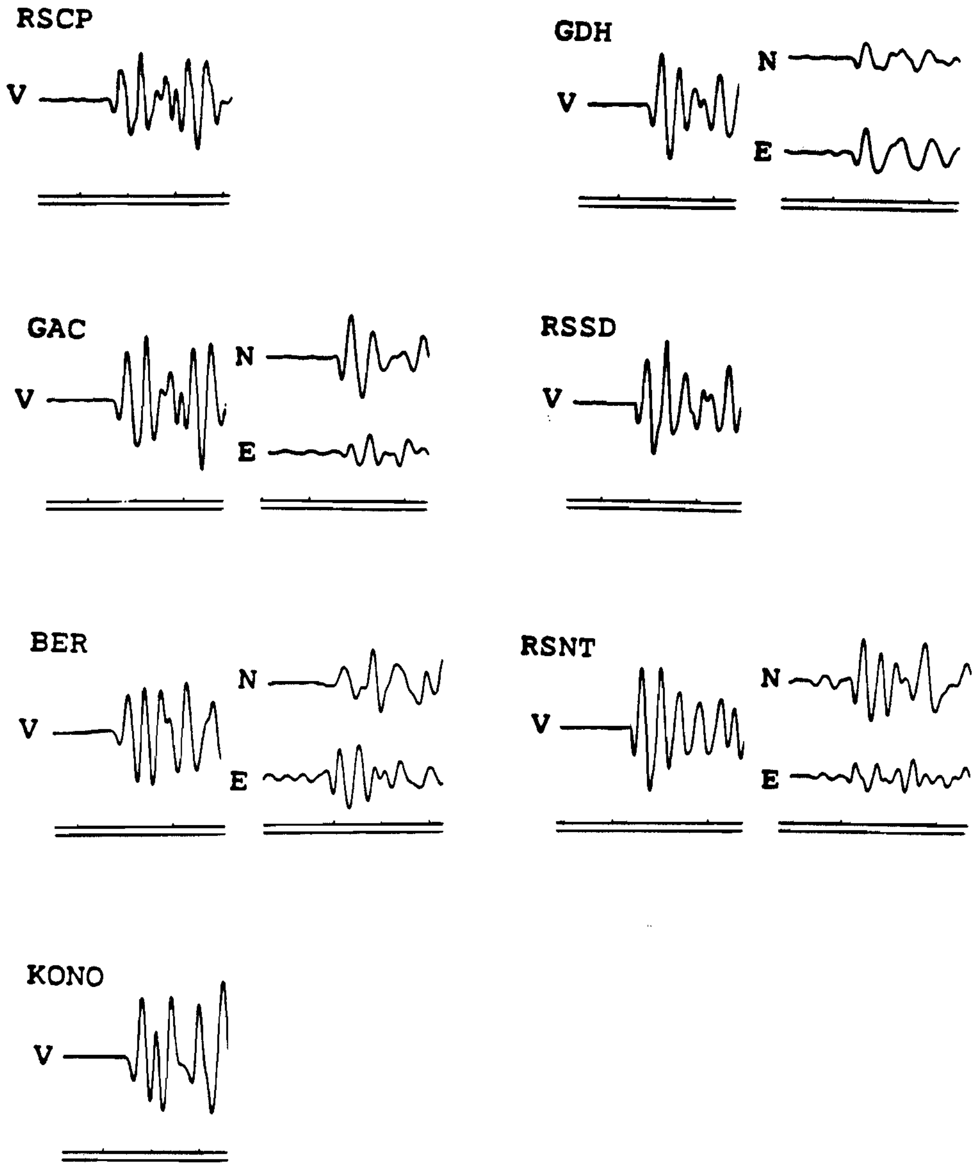
RSCP
V
GDH
N
V
E
GAC
N
V
E
RSSD
V
BER
N
V
E
RSNT
N
V
E
KONO
V

IASPEI event 41

(b)

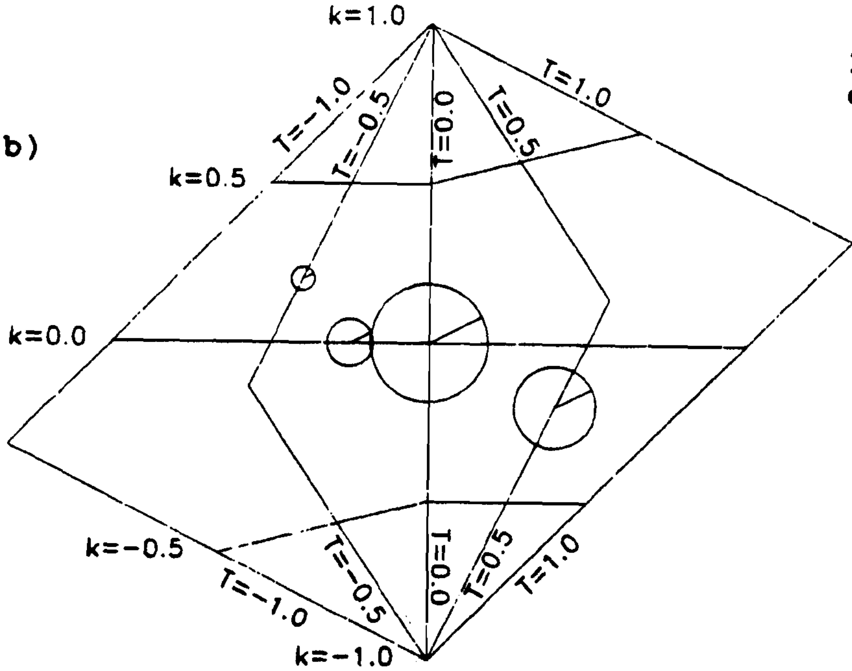

(c)

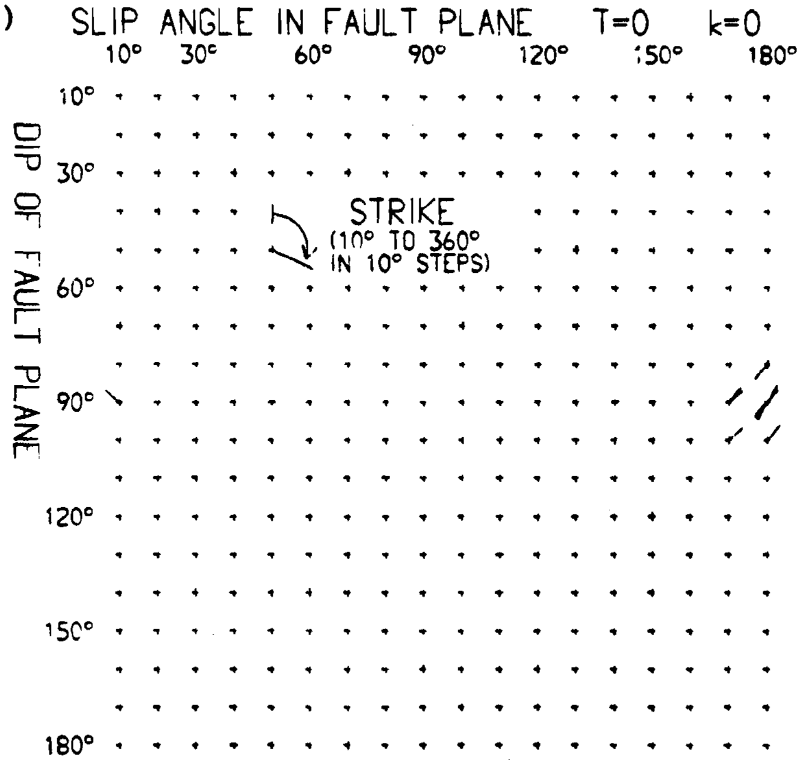

(d)

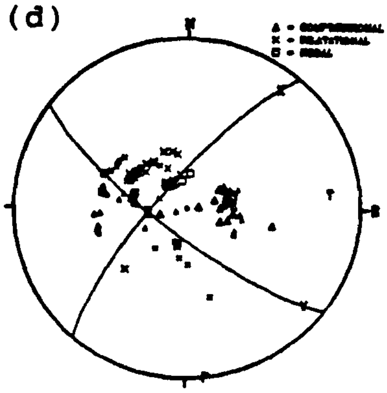

(e)

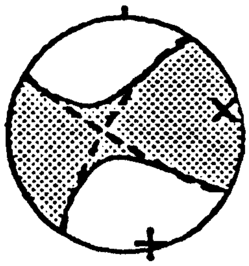

(f)

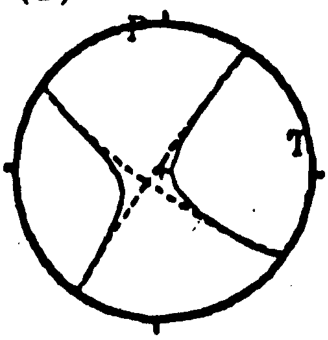

THIS PAGE LEFT BLANK INTENTIONALLY

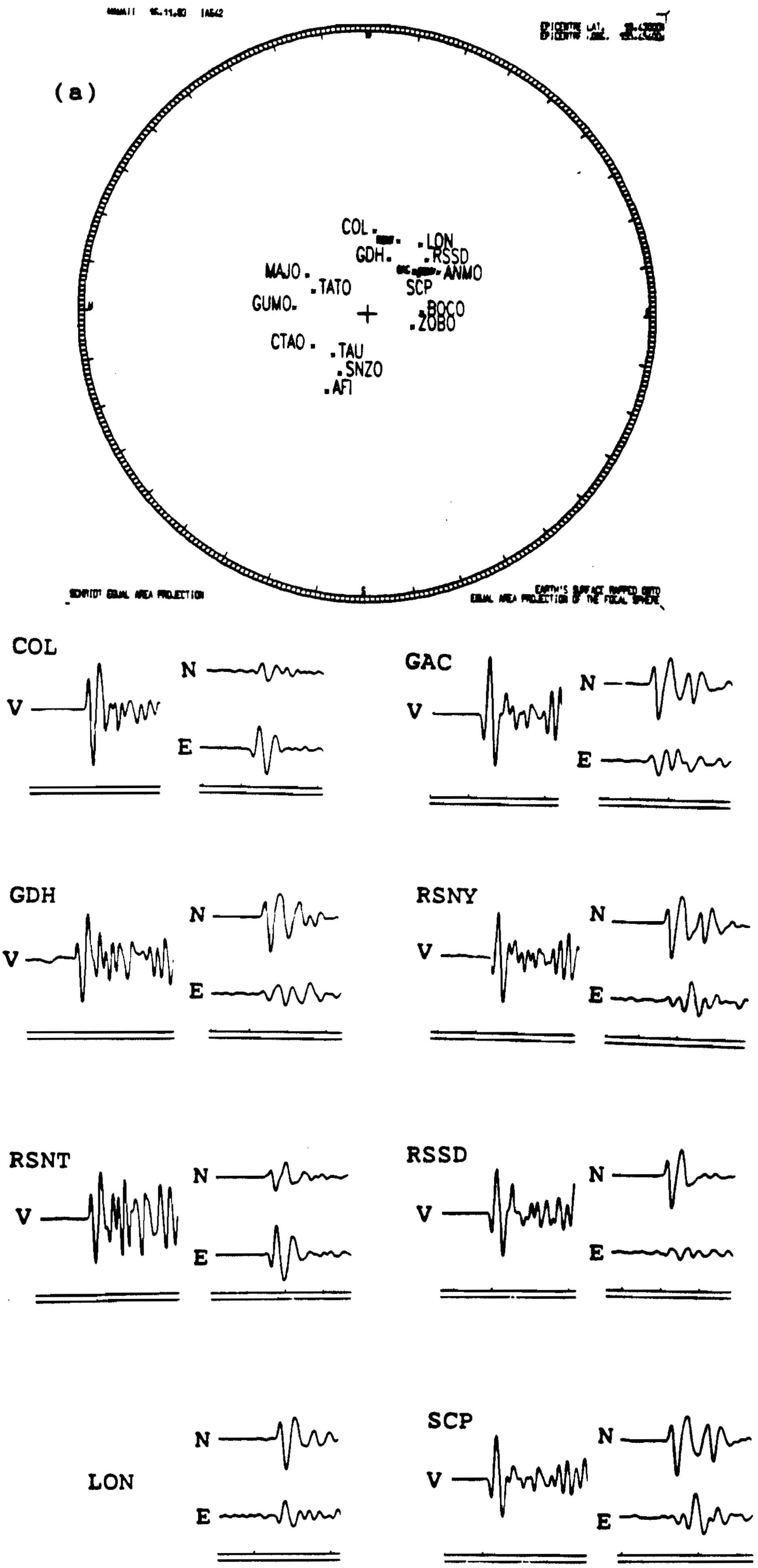
(a)
COL
LON
GDH
RSSD
MAJO
TATO
ANMO
SCP
GUMO
BOCO
ZOBO
CTAO
TAU
SNZO
AFI
COL
V
N
E
GAC
V
N
E
GDH
V
N
E
RSNY
V
N
E
RSNT
V
N
E
RSSD
V
N
E
LON
N
E
SCP
V
N
E

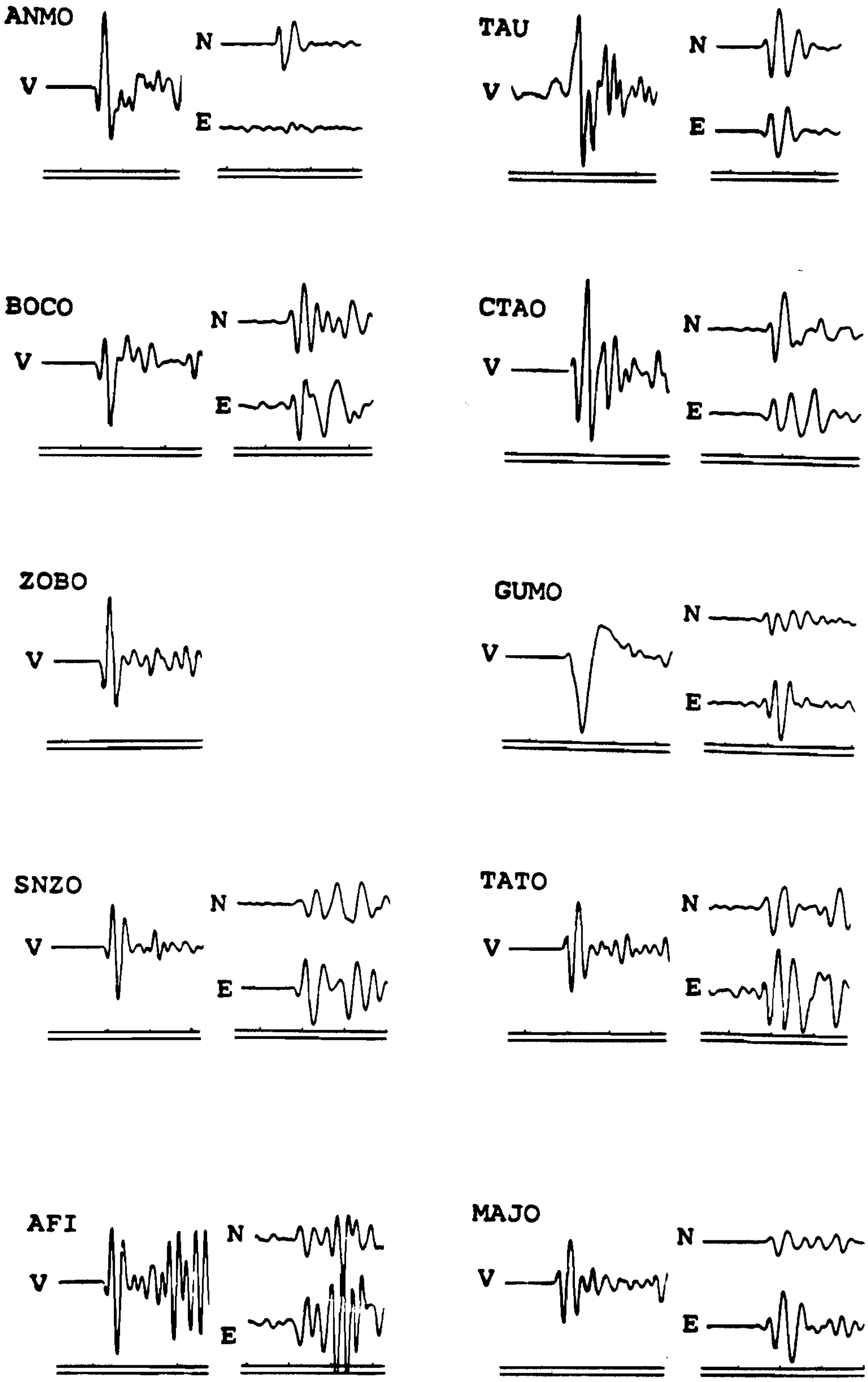
ANMO
V
N
E
TAU
V
N
E
BOCO
V
N
E
CTAO
V
N
E
ZOBO
V
GUMO
V
N
E
SNZO
V
N
E
TATO
V
N
E
AFI
V
N
E
MAJO
V
N
E

IASPEI event 42

(b)

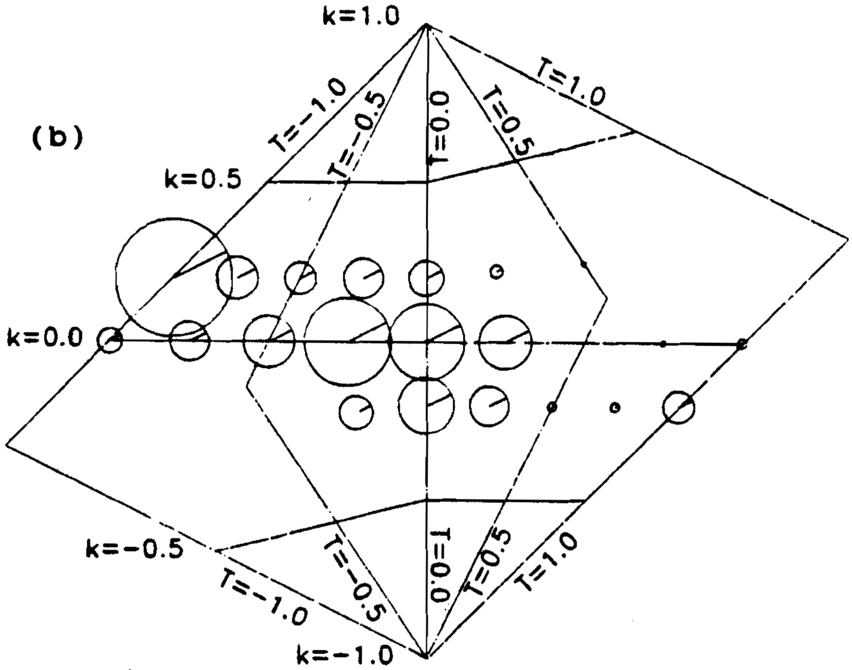

(c)

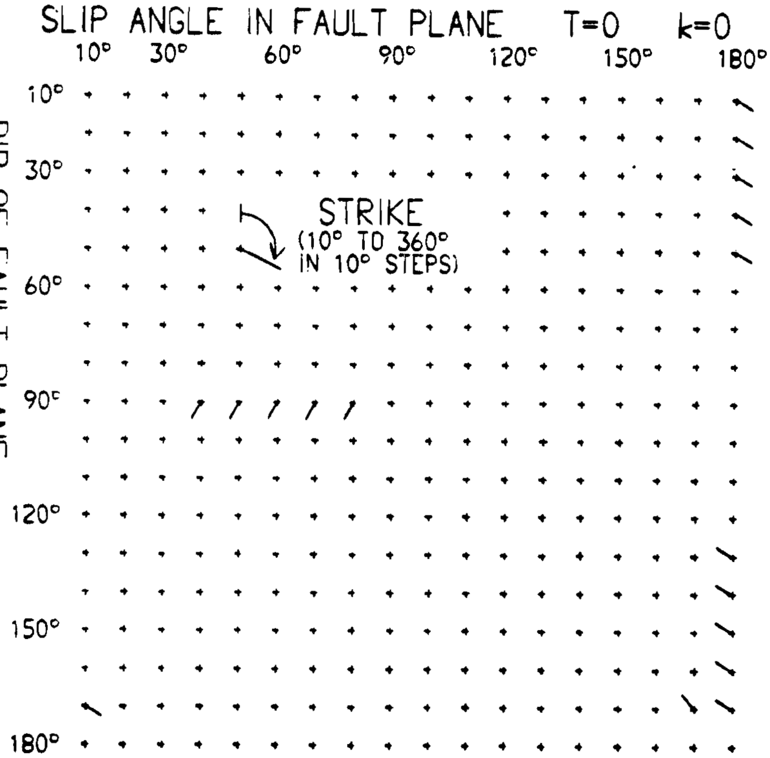

(d)

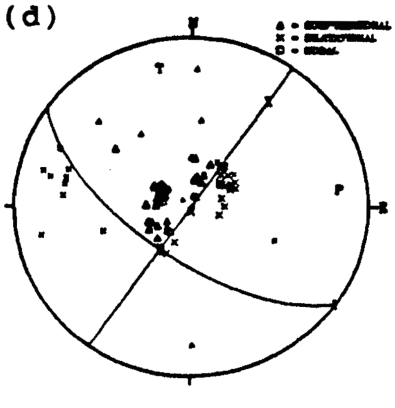

(e)

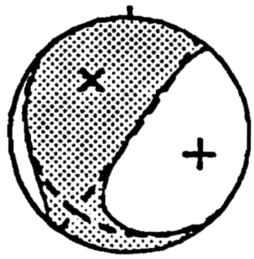

(f)

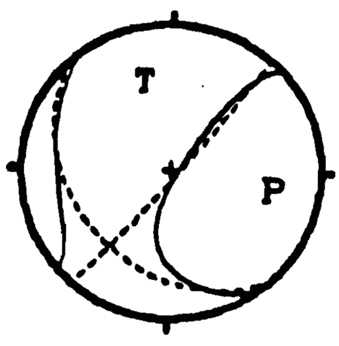

THIS PAGE LEFT BLANK INTENTIONALLY

IASPEI
event 43

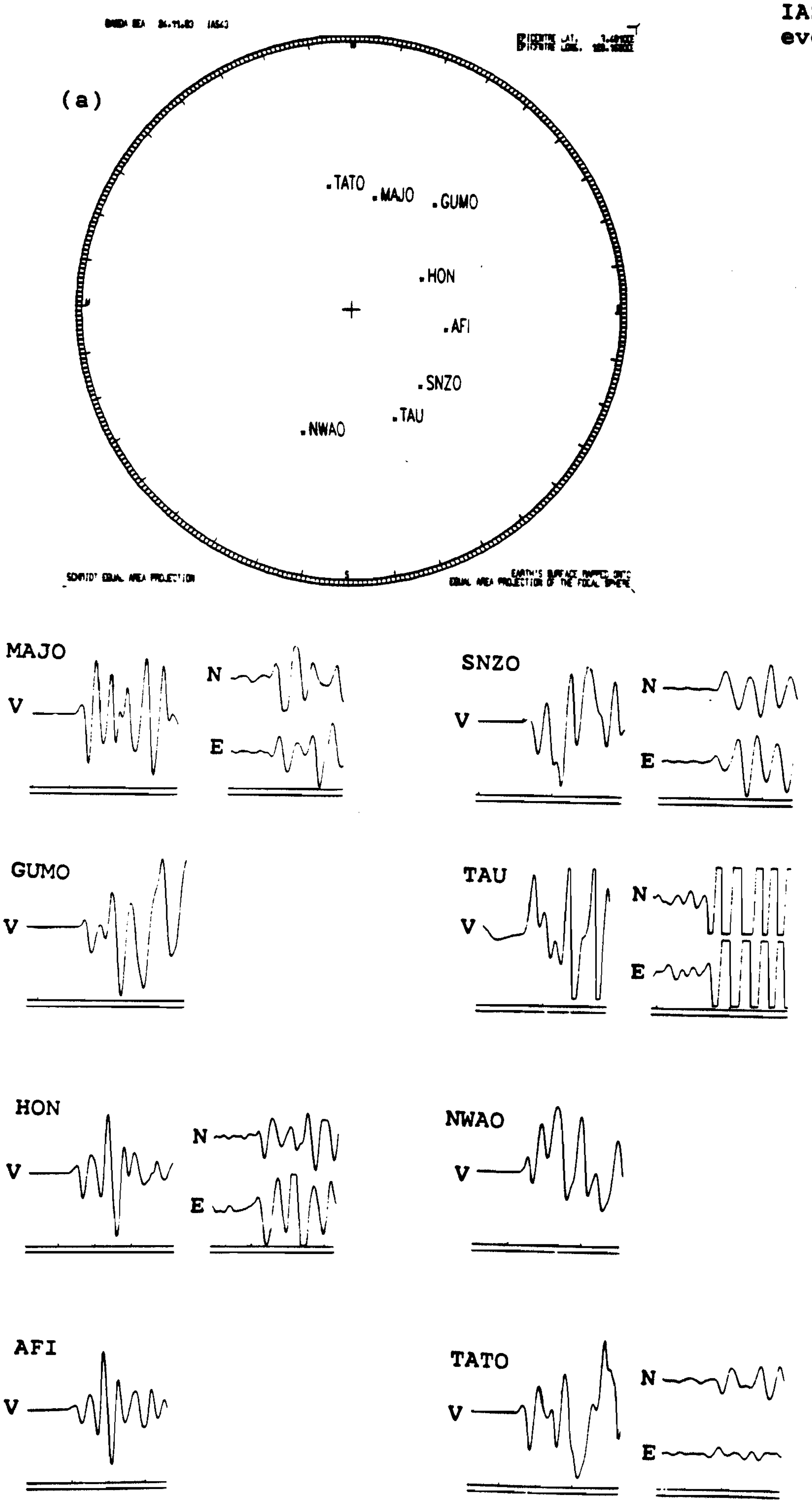

(b)

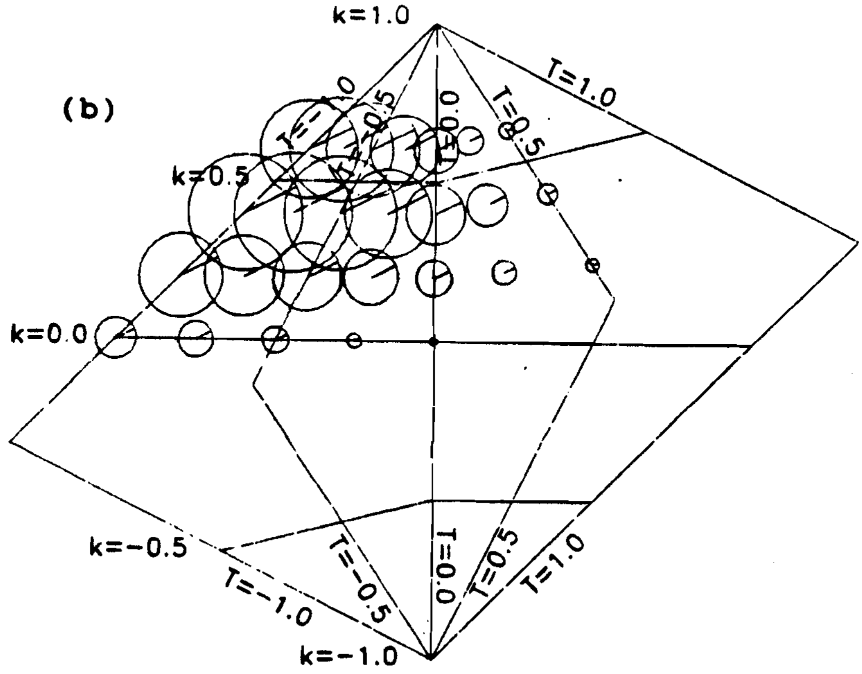
k=1.0
T=1.0
T=0.5
T=0.0
T=-1.0
T=-0.5
k=0.5
k=0.0
k=-0.5
T=-1.0
T=-0.5
T=0.0
T=0.5
T=1.0
k=-1.0

(c)

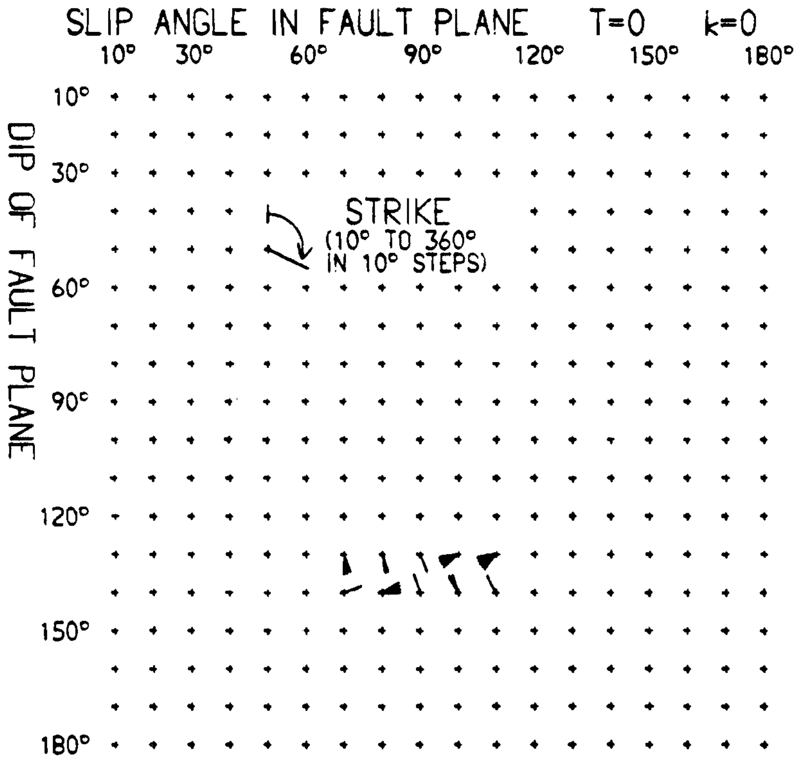
SLIP ANGLE IN FAULT PLANE T=0 k=0
10° 30° 60° 90° 120° 150° 180°
DIP OF FAULT PLANE
10° 30° 60° 90° 120° 150° 180°
STRIKE
(10° TO 360°
IN 10° STEPS)

(d)

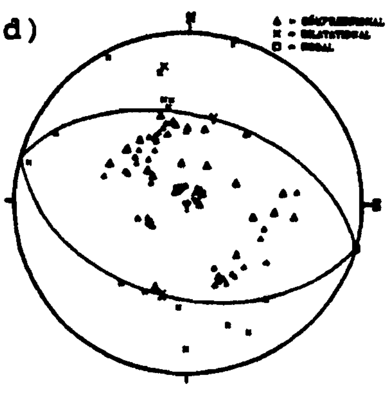

(e)

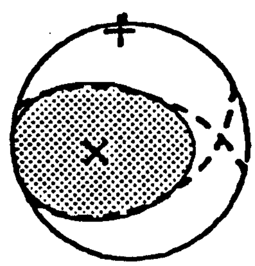

(f)

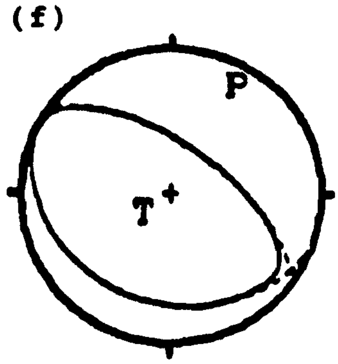
P
T

(a)

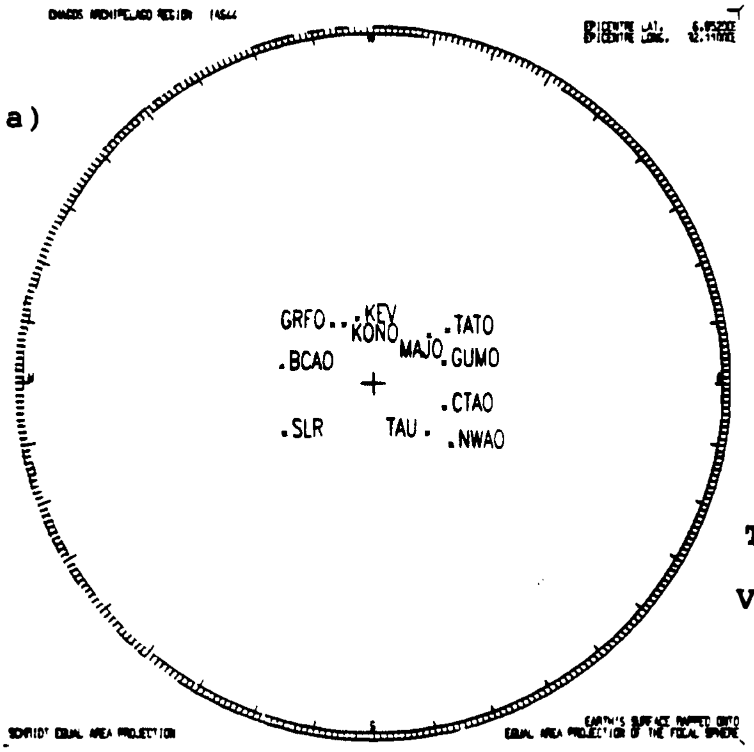
GRFO
KEV
KONO
TATO
MAJO
BCAO
GUMO
CTAO
SLR
TAU
NWAO
SCHMIDT EQUAL AREA PROJECTION
EARTH'S SURFACE MAPPED ONTO EQUAL AREA PROJECTION OF THE FOCAL SPHERE

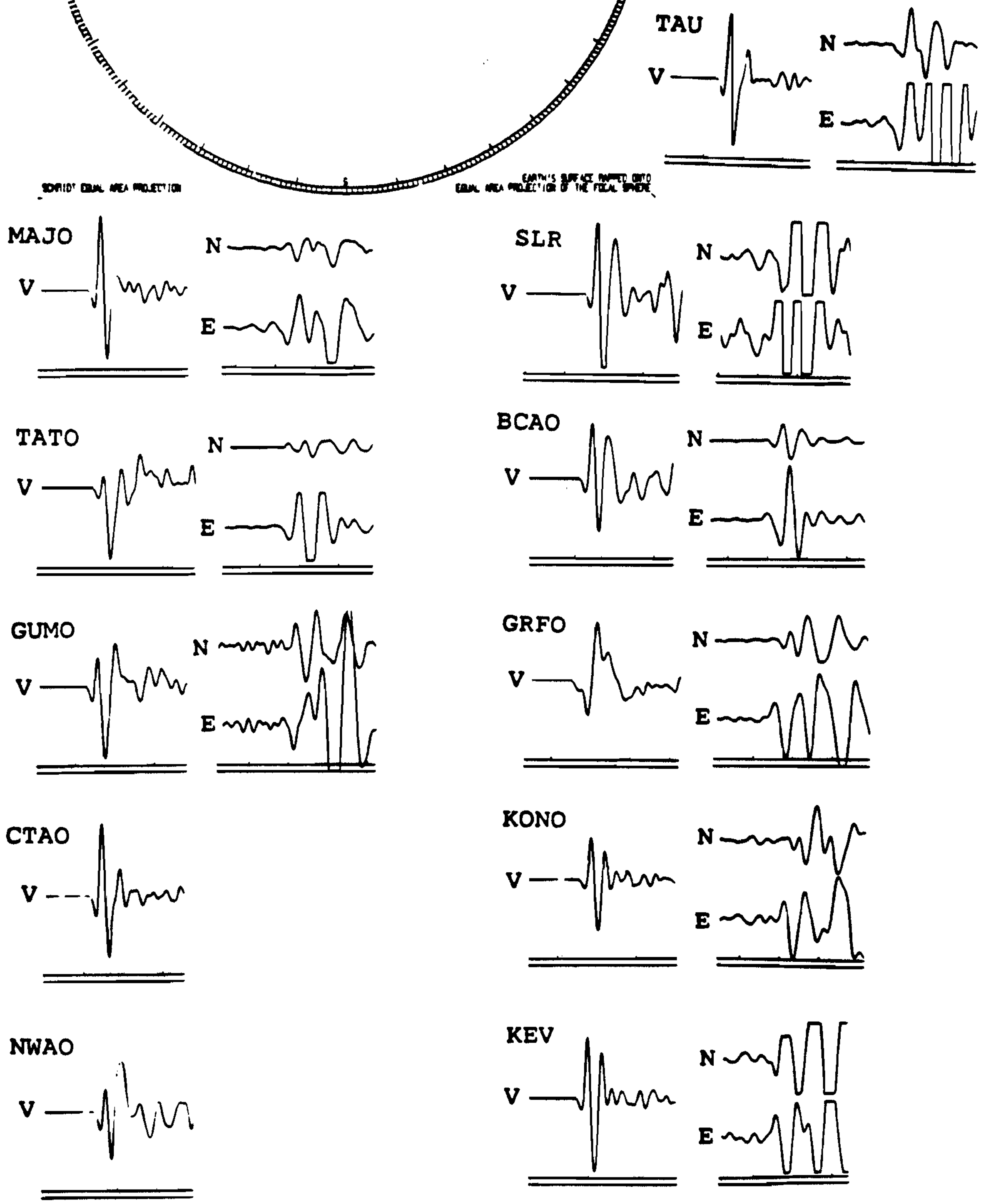
TAU
V
N
E
MAJO
V
N
E
SLR
V
N
E
TATO
V
N
E
BCAO
V
N
E
GUMO
V
N
E
GRFO
V
N
E
CTAO
V
KONO
V
N
E
NWAO
V
KEV
V
N
E

(b)

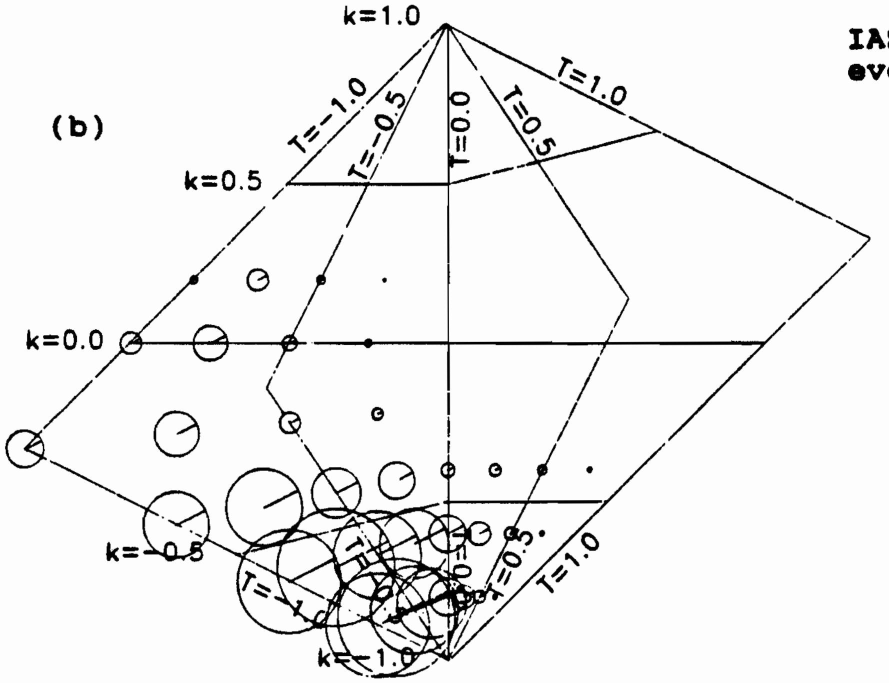

(c) SLIP ANGLE IN FAULT PLANE T=0 k=0

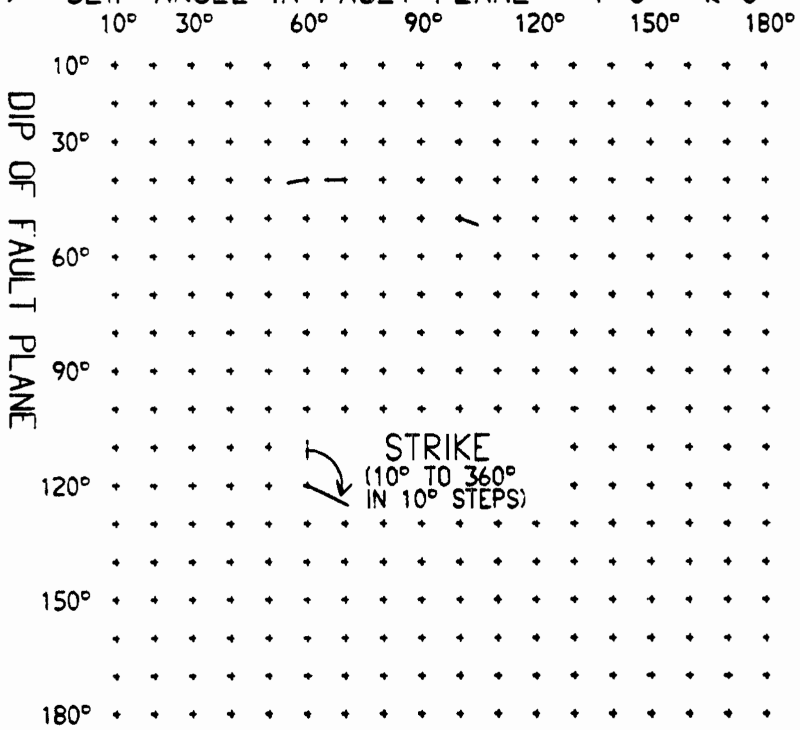

(d)

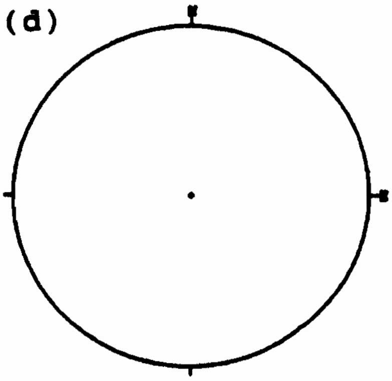

(e)

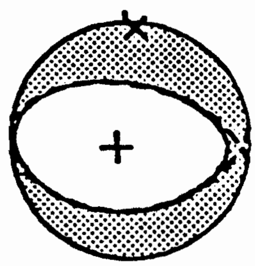

(f)

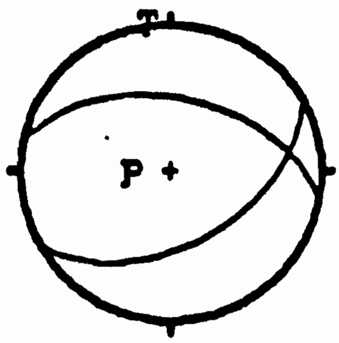

(a)

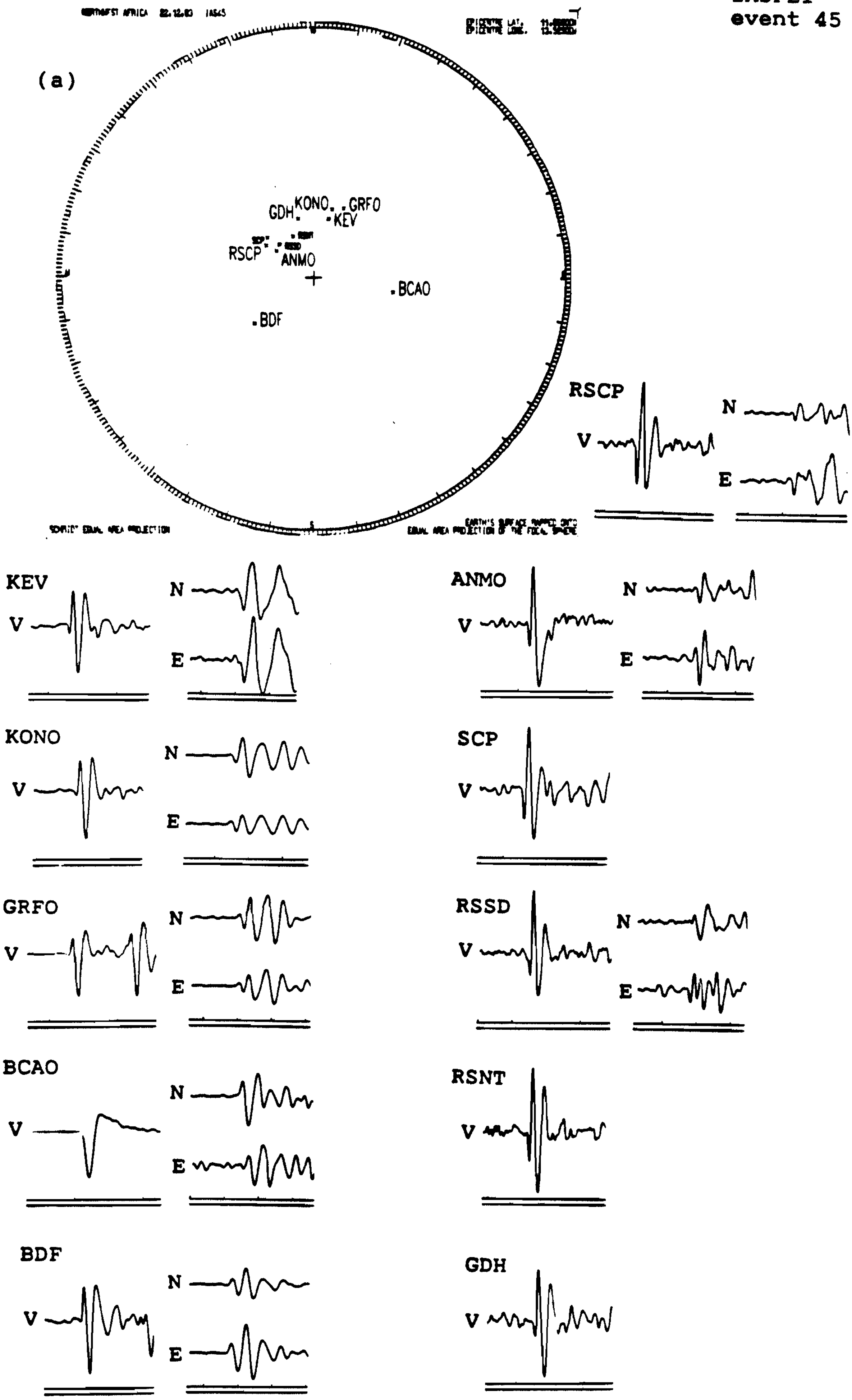
GDH
KONO
GRFO
KEV
RSCP
ANMO
BCAO
BDF
RSCP
V
N
E
KEV
V
N
E
ANMO
V
N
E
KONO
V
N
E
SCP
V
GRFO
V
N
E
RSSD
V
N
E
BCAO
V
N
E
RSNT
V
BDF
V
N
E
GDH
V

IASPEI
event 45

(b)

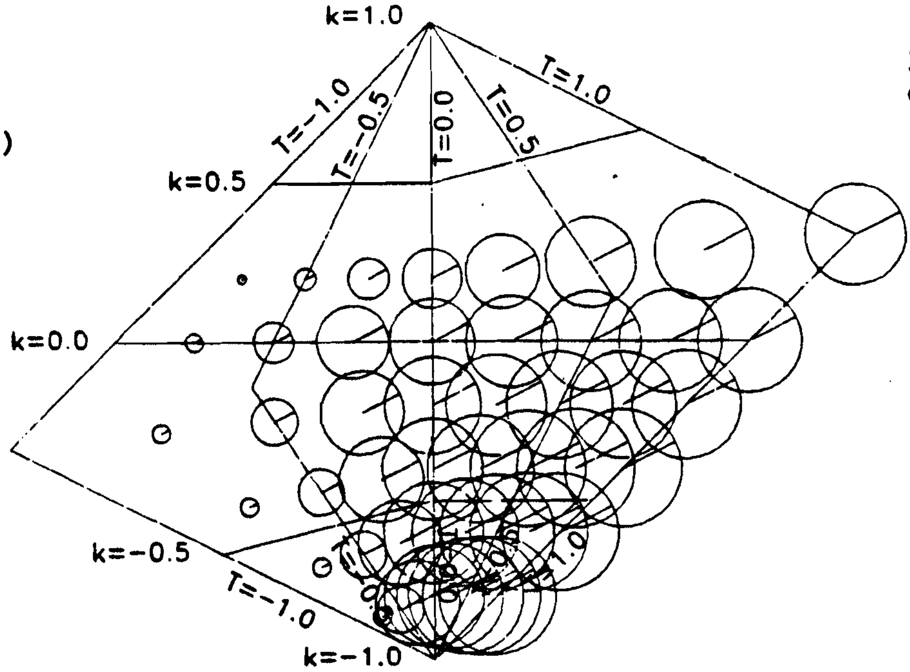

(c)

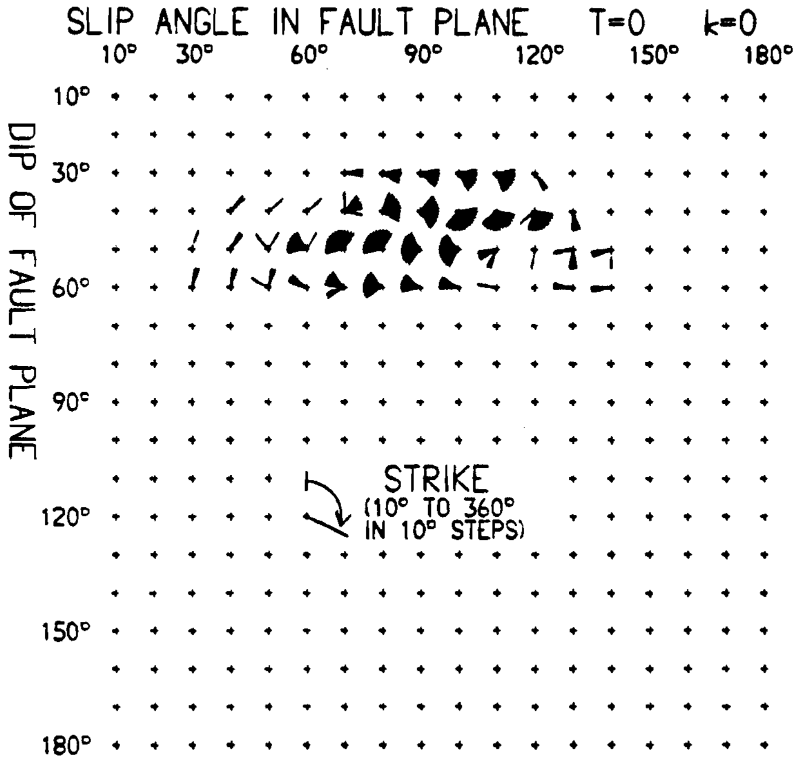

(d)

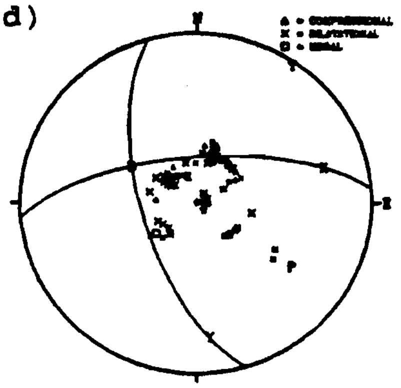

(e)

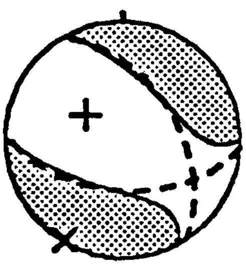

(f)

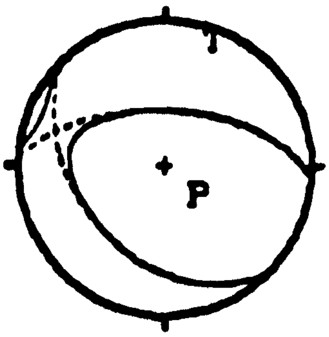

IASPEI
event 46

(a)

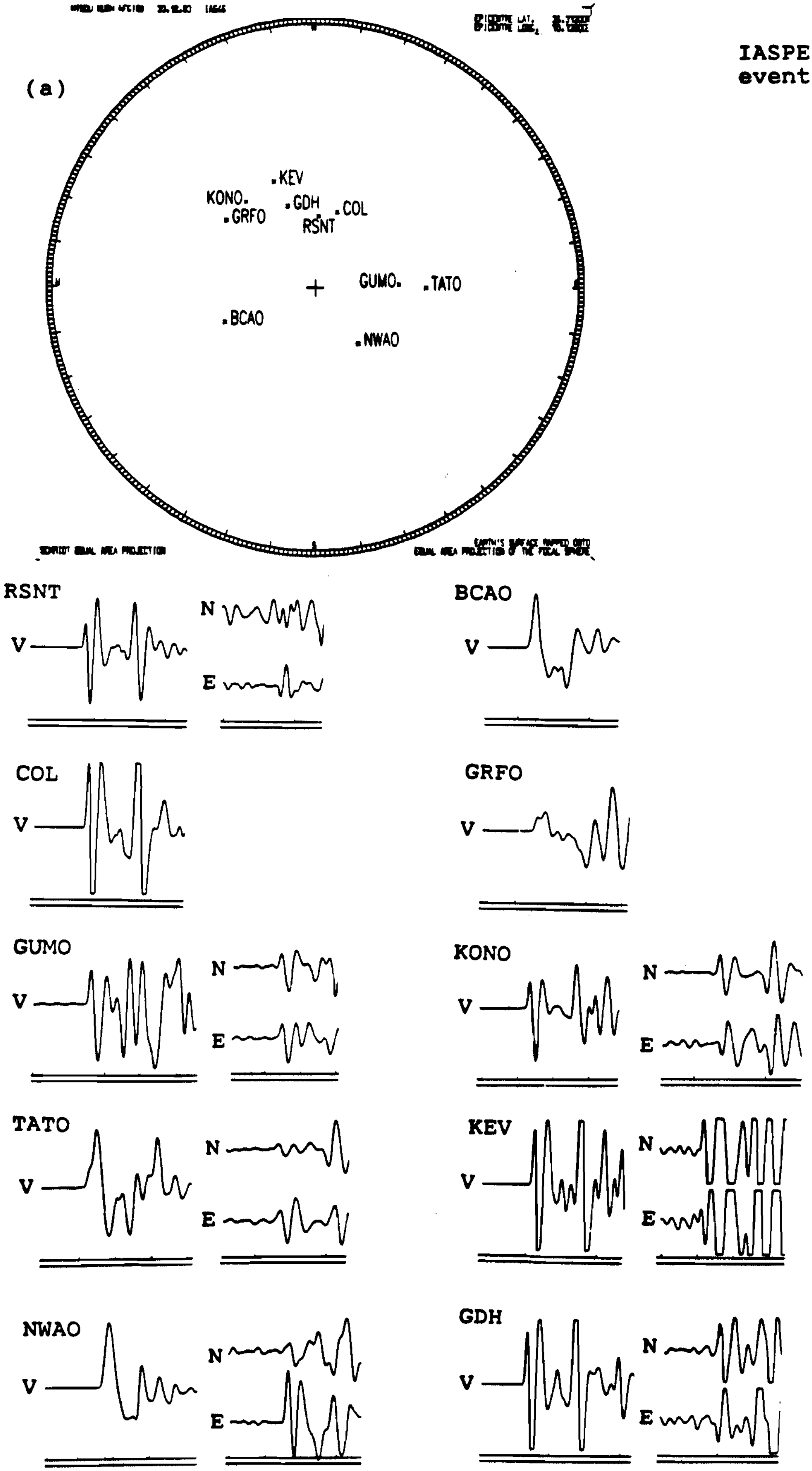

IASPEI
event 46

(b)

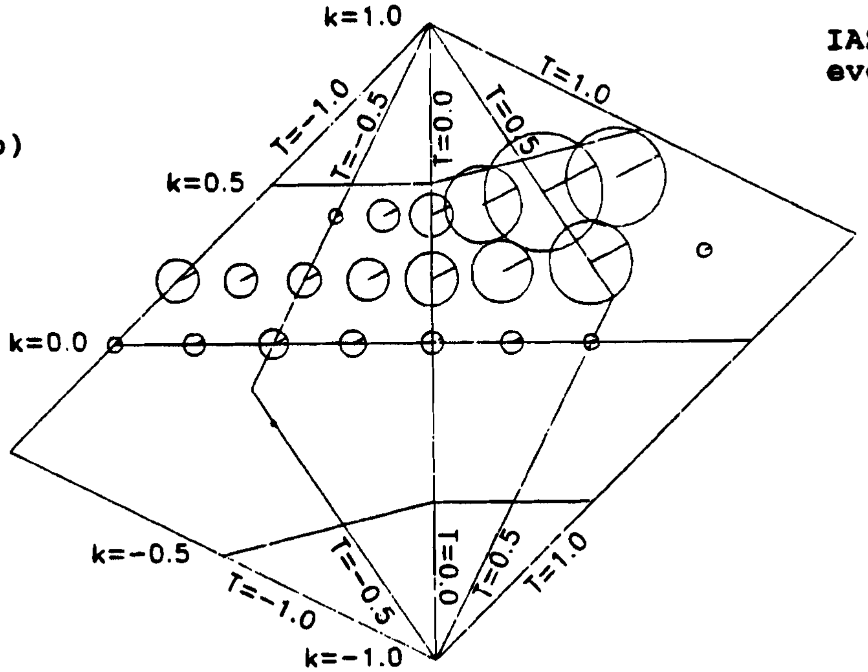

(c)

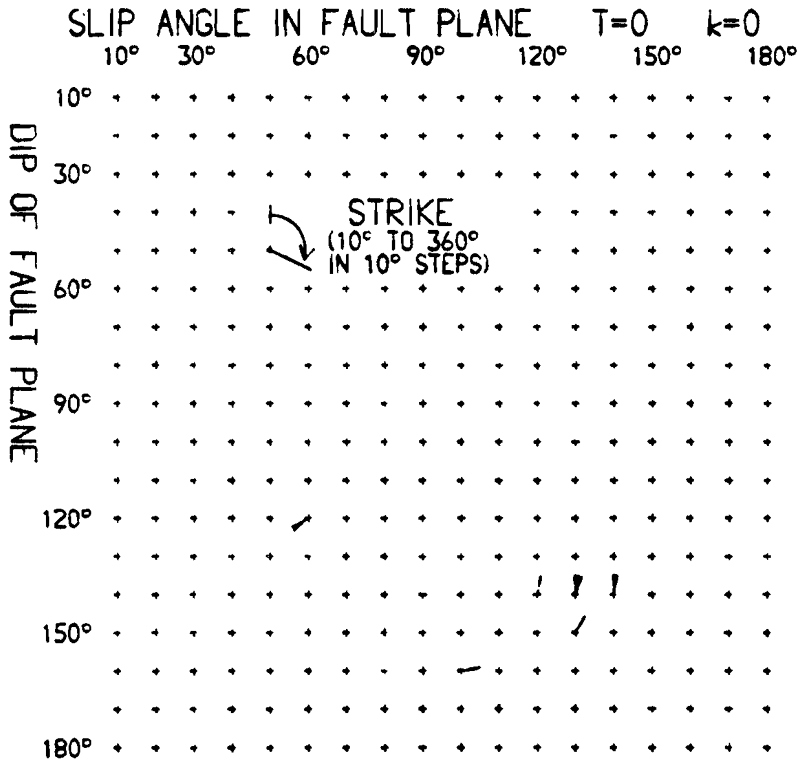

(d)

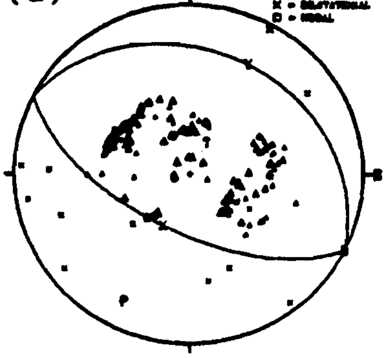

(e)

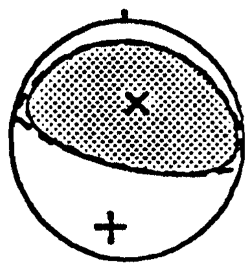

(f)

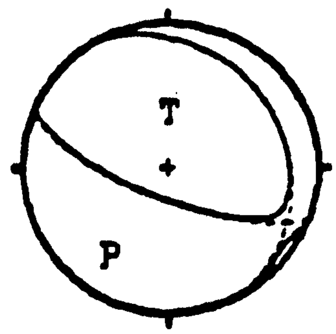

(a)

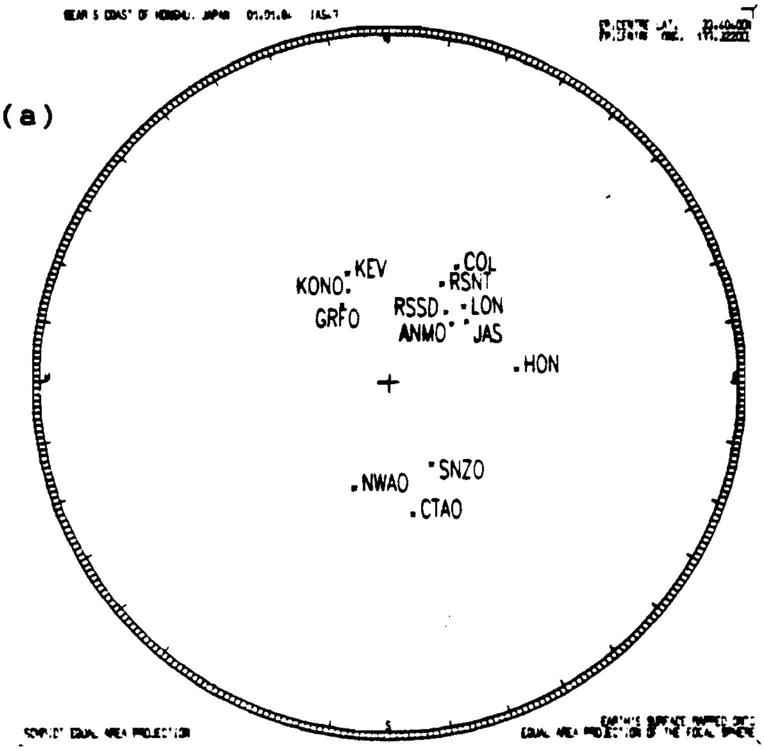
KONO
KEV
COL
RSNT
GRFO
RSSD
LON
ANMO
JAS
HON
SNZO
NWAO
CTAO

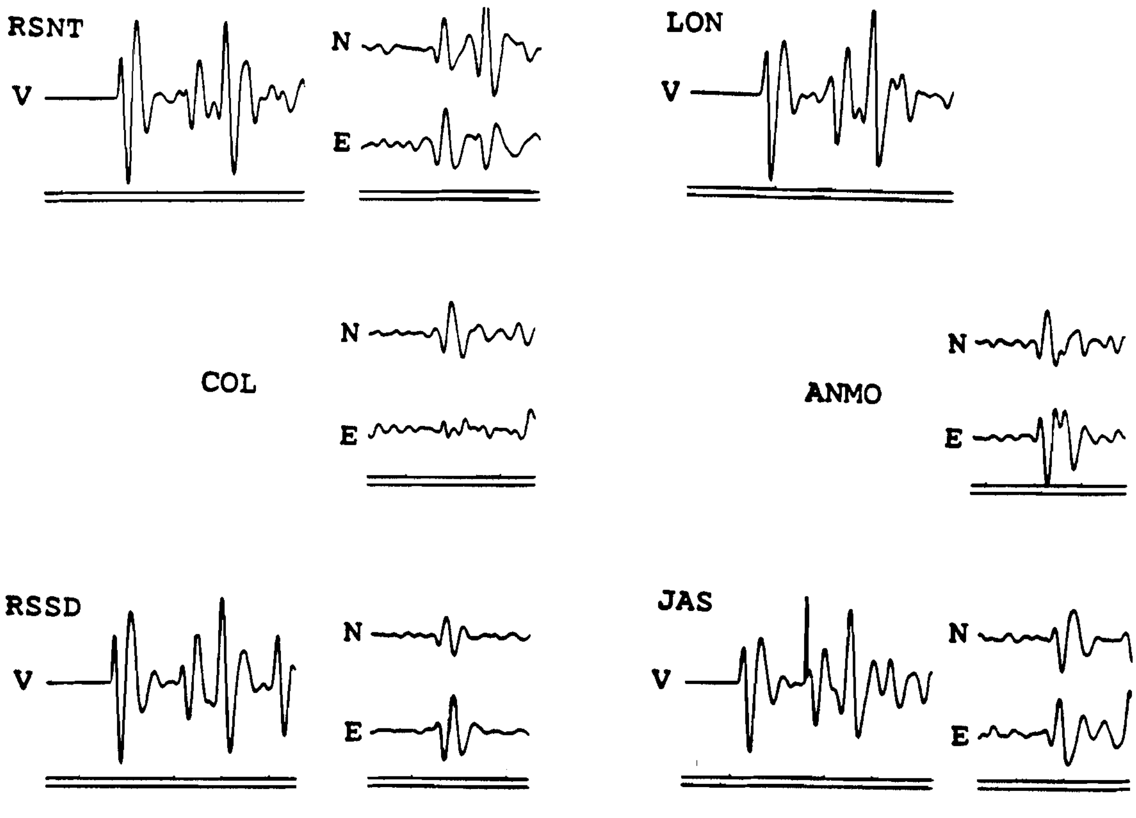
RSNT
V
N
E
LON
V
N
COL
E
N
ANMO
E
RSSD
N
V
E
JAS
N
V
E

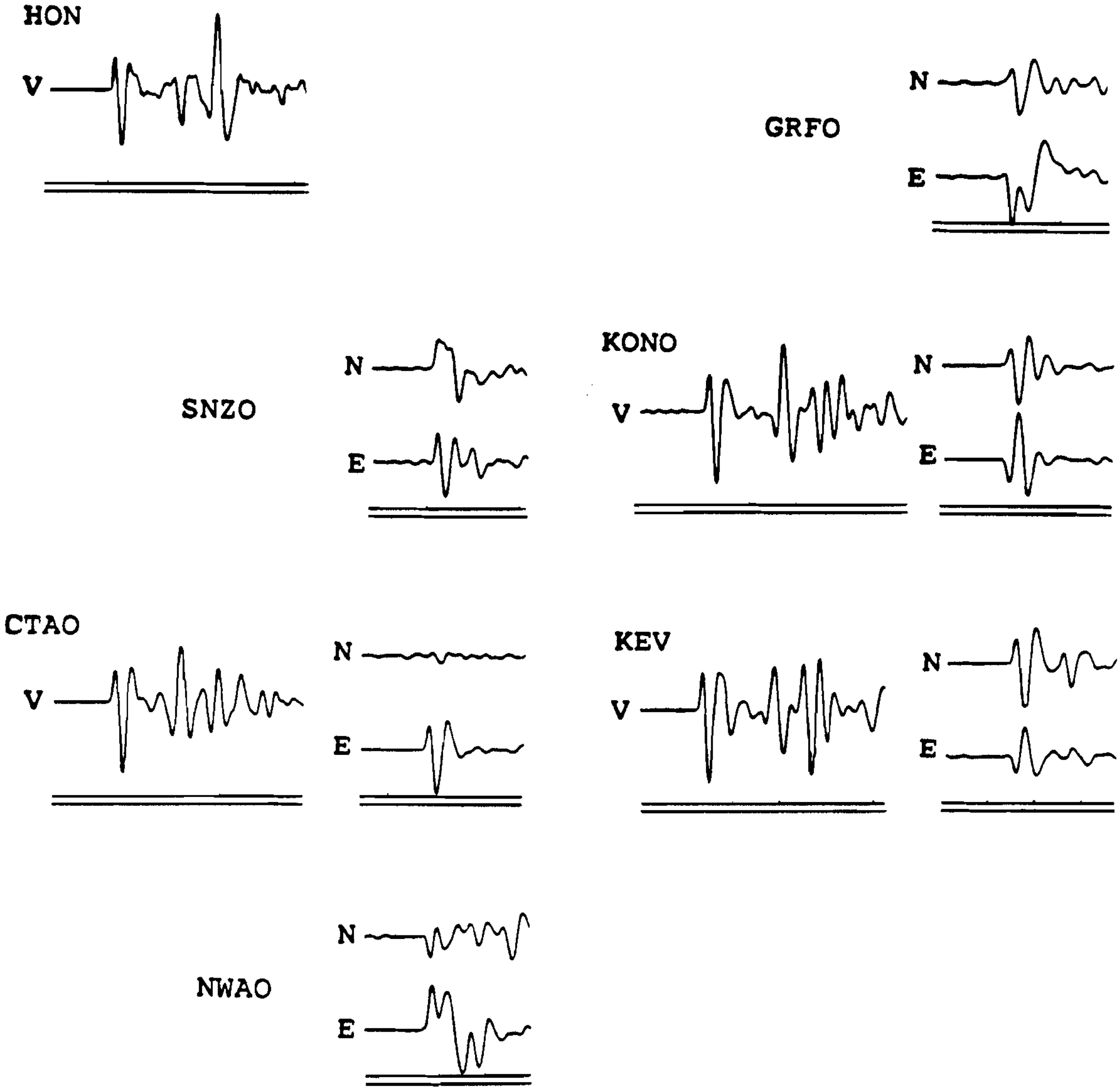
HON
V
GRFO
N
E
SNZO
N
E
KONO
V
N
E
CTAO
V
N
E
KEV
V
N
E
NWAO
N
E

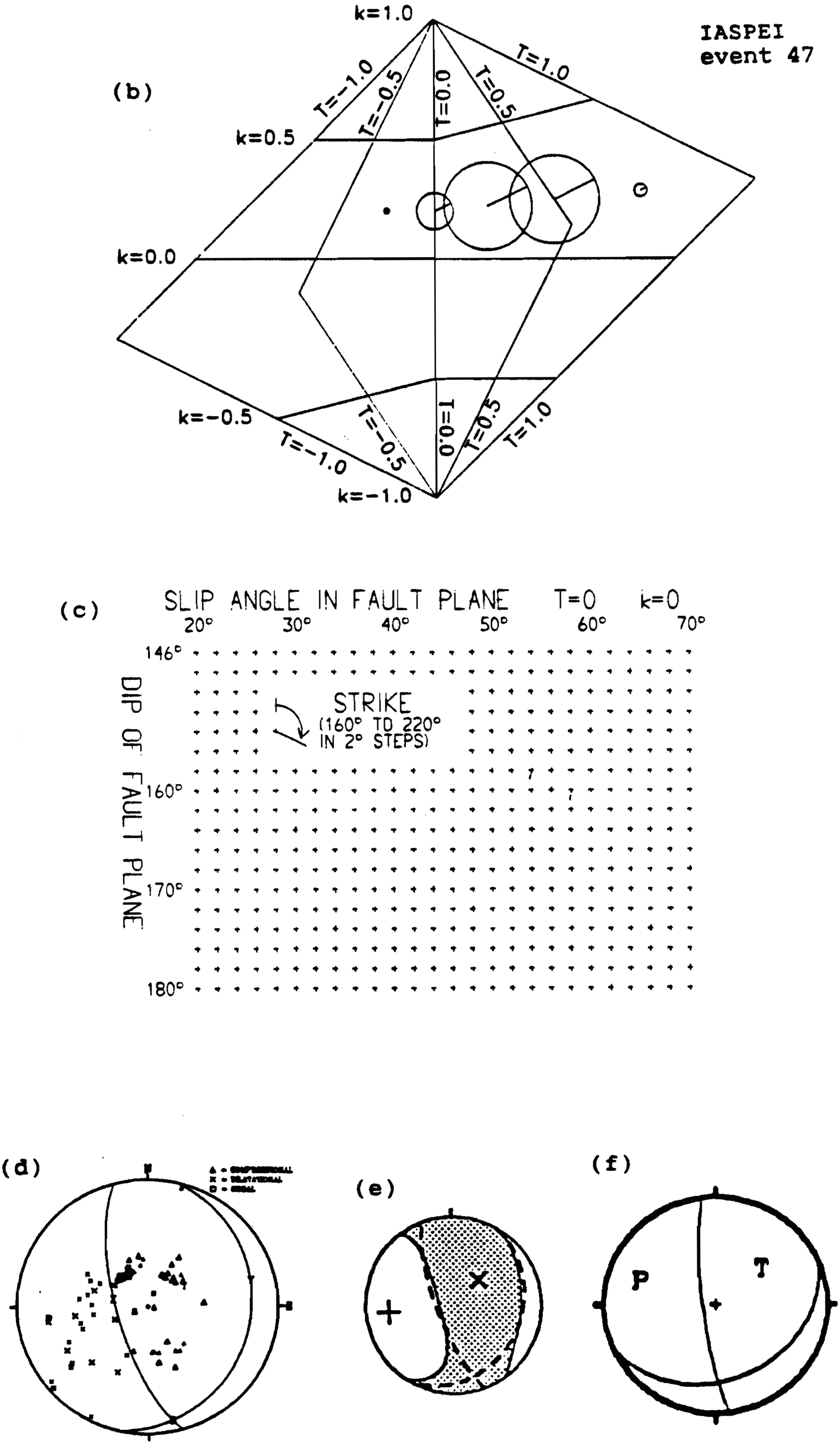
IASPEI
event 47
(b)
k=1.0
k=0.5
k=0.0
k=-0.5
k=-1.0
T=-1.0
T=-0.5
T=0.0
T=0.5
T=1.0
T=-1.0
T=-0.5
T=0.0
T=0.5
T=1.0
(c)
SLIP ANGLE IN FAULT PLANE T=0 k=0
20° 30° 40° 50° 60° 70°
146°
160°
170°
180°
DIP OF FAULT PLANE
STRIKE
(160° TO 220°
IN 2° STEPS)
(d)
(e)
(f)
P
T

THIS PAGE LEFT BLANK INTENTIONALLY

(a)

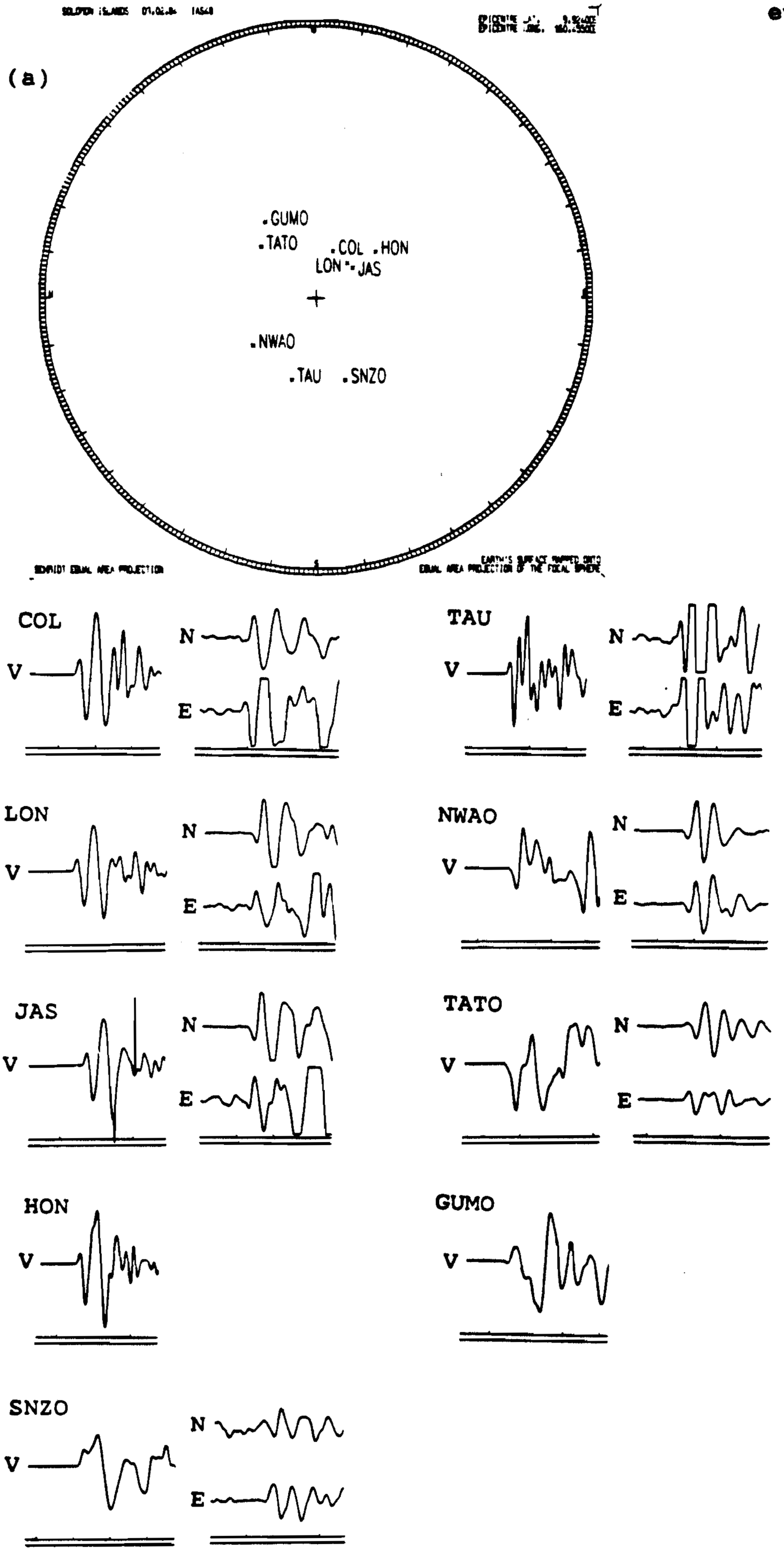
SCHMIDT EQUAL AREA PROJECTION
EARTH'S SURFACE MAPPED ONTO
EQUAL AREA PROJECTION OF THE FOCAL SPHERE
GUMO
TATO
COL
HON
LON
JAS
NWAO
TAU
SNZO
COL
V
N
E
TAU
V
N
E
LON
V
N
E
NWAO
V
N
E
JAS
V
N
E
TATO
V
N
E
HON
V
GUMO
V
SNZO
V
N
E

IASPEI
event 48

(b)

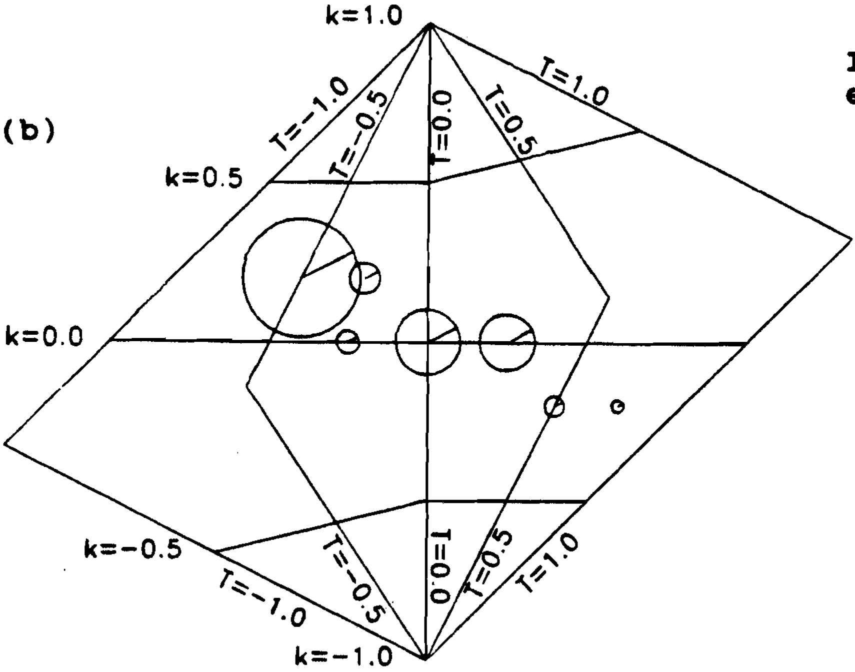

(c)

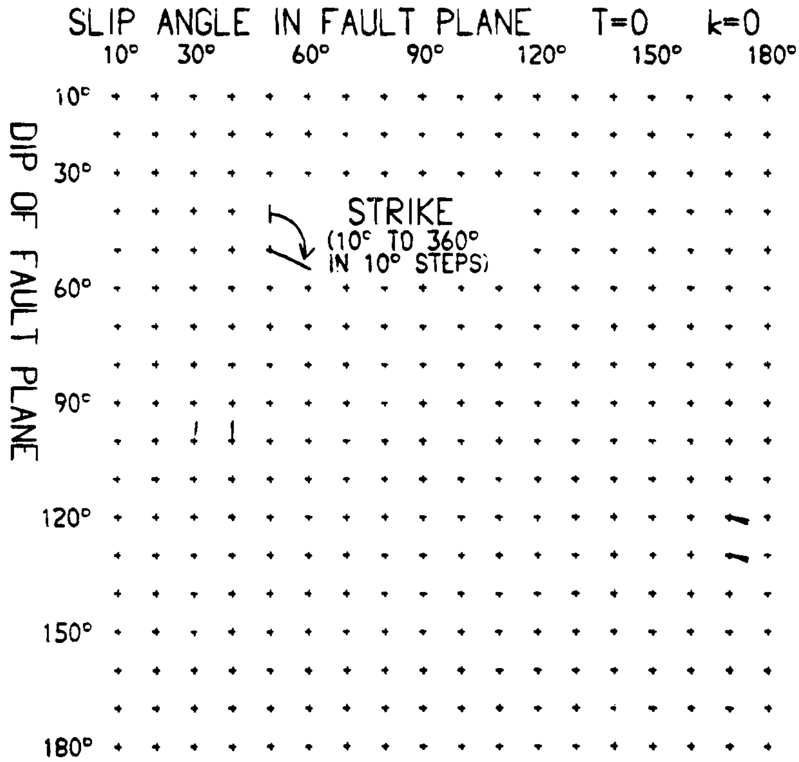

(d)

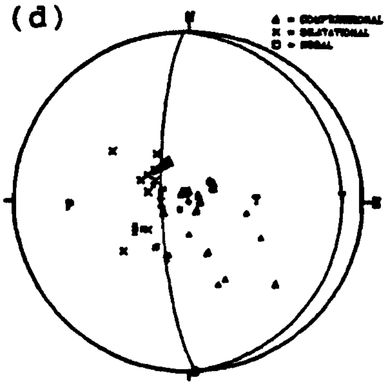

(e)

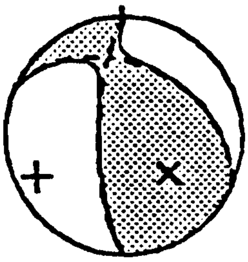

(f)

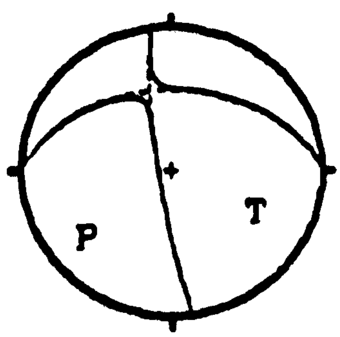

IASPEI
event 49

(a)

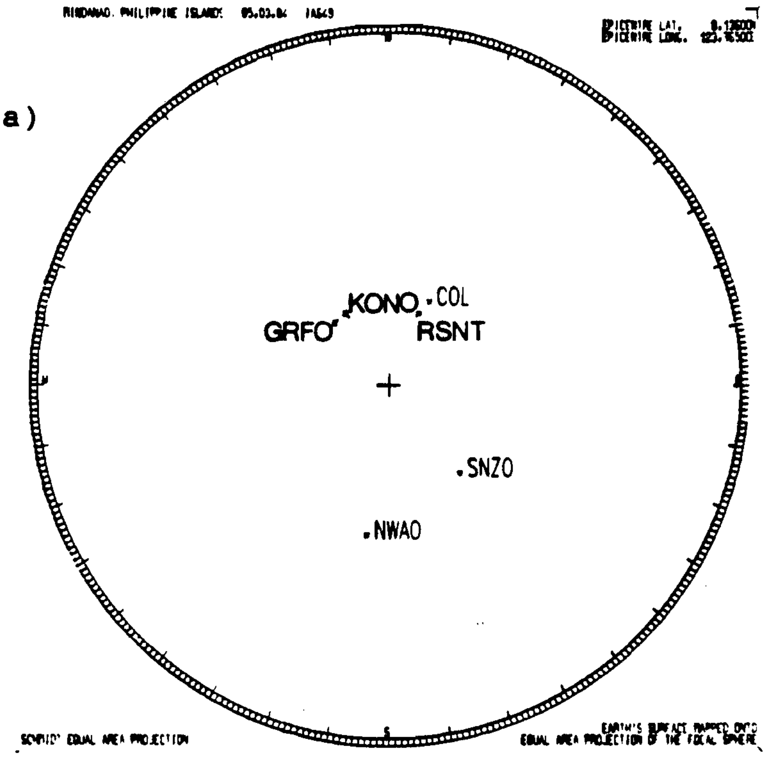

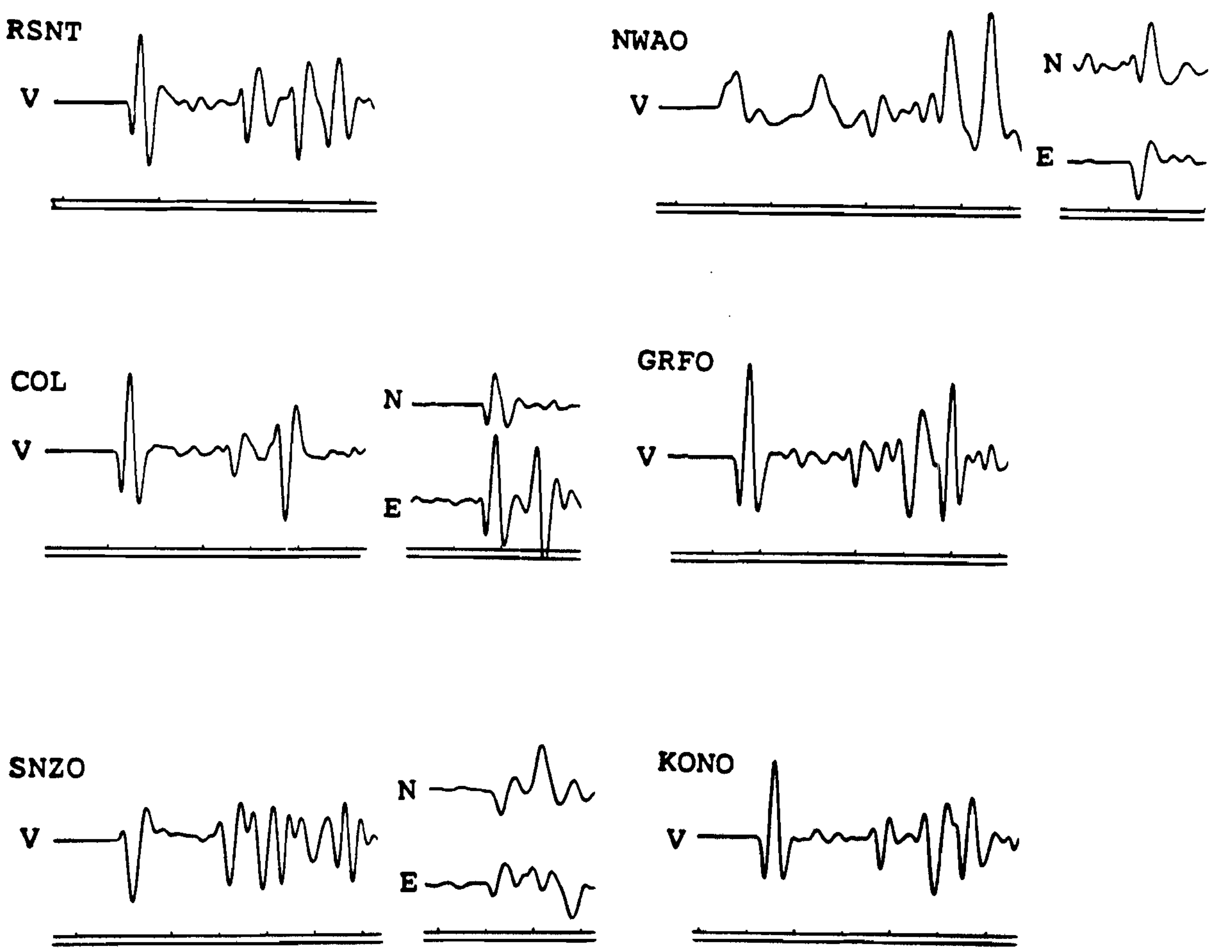

IASPEI
event 49

(b)

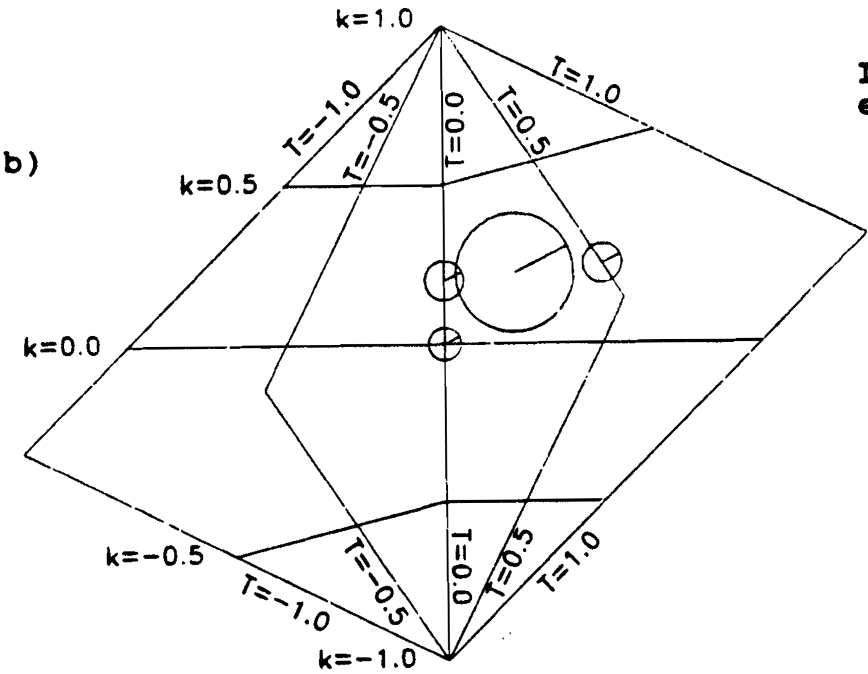

(c)

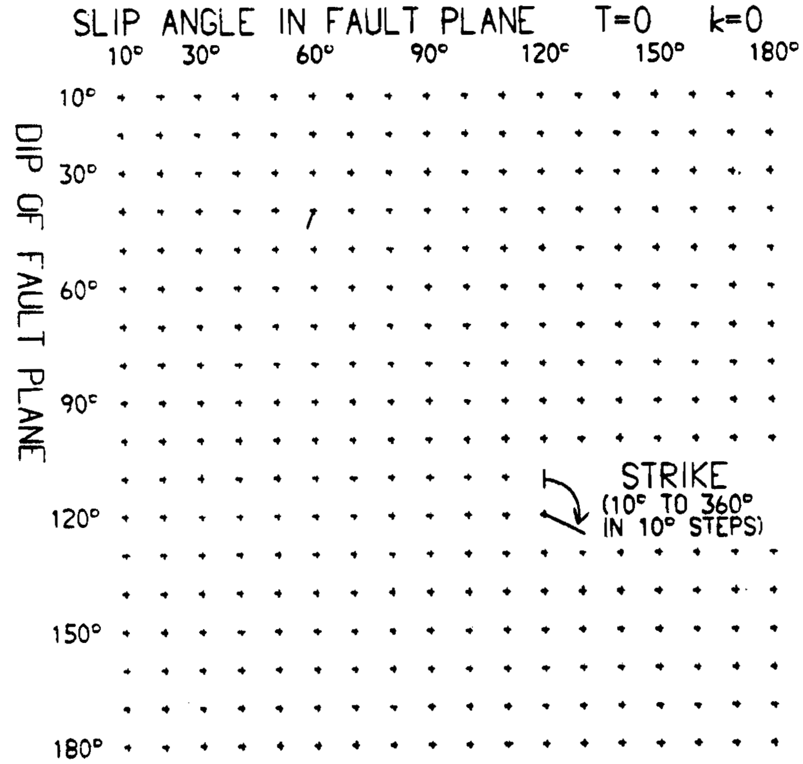

(d)

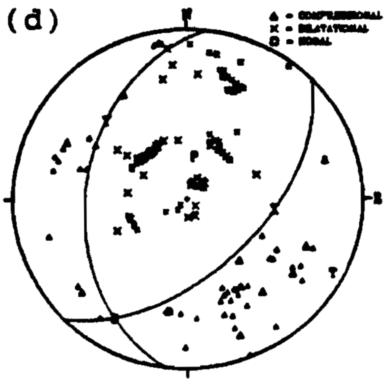

(e)

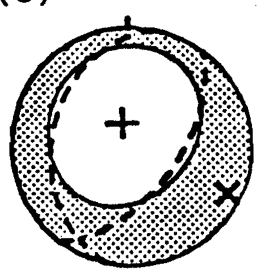

(f)

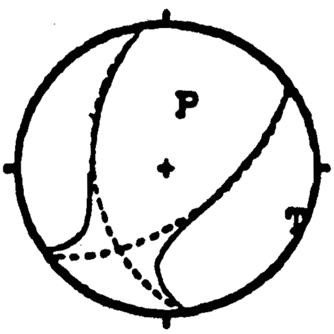

IASPEI
event 50

(a)

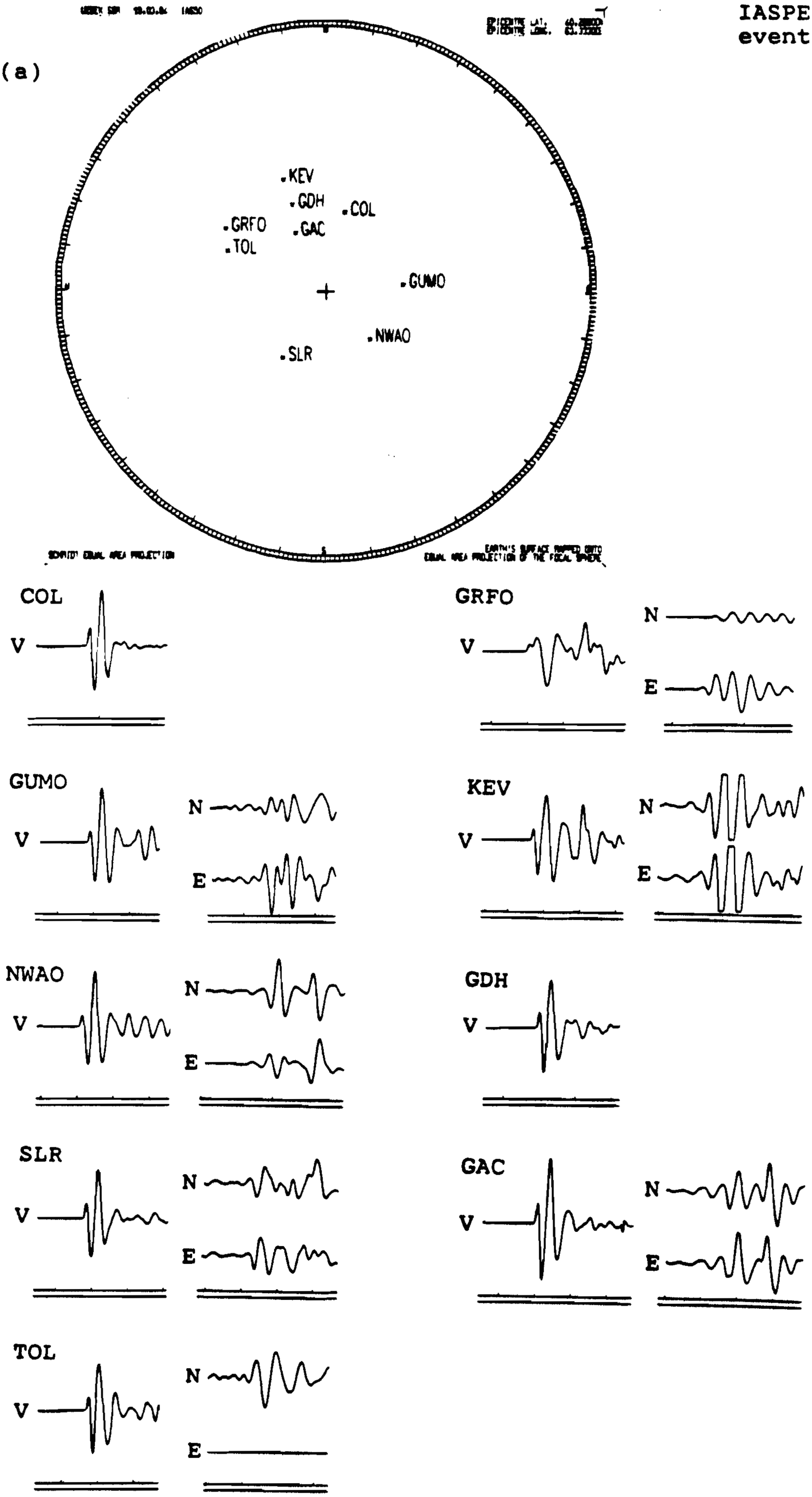

IASPEI
event 50

(b)

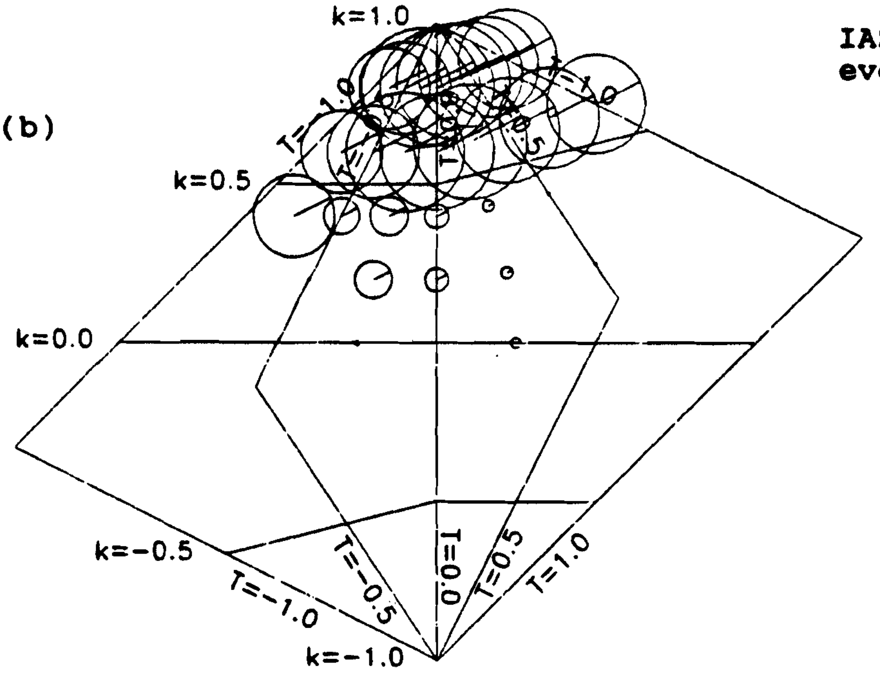

(c)

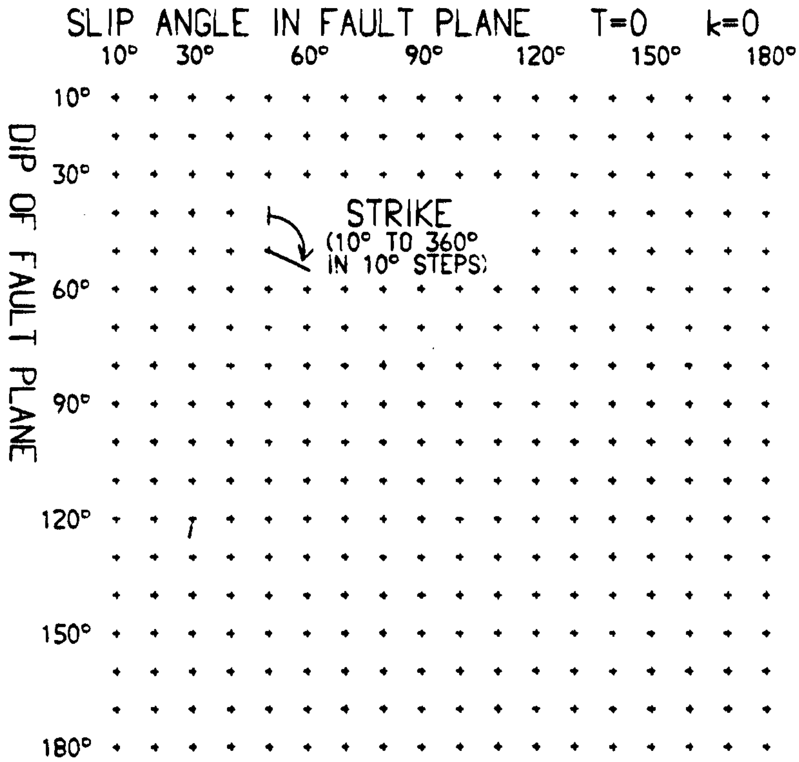

(d)

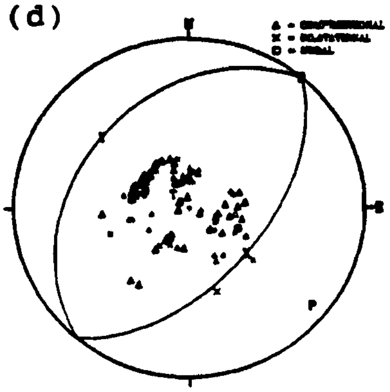

(e)

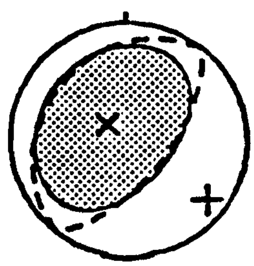

(f)

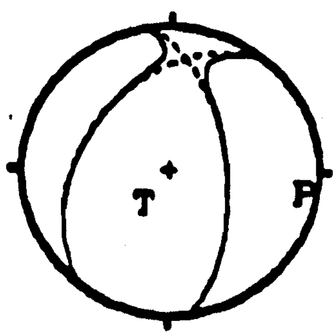

(a)

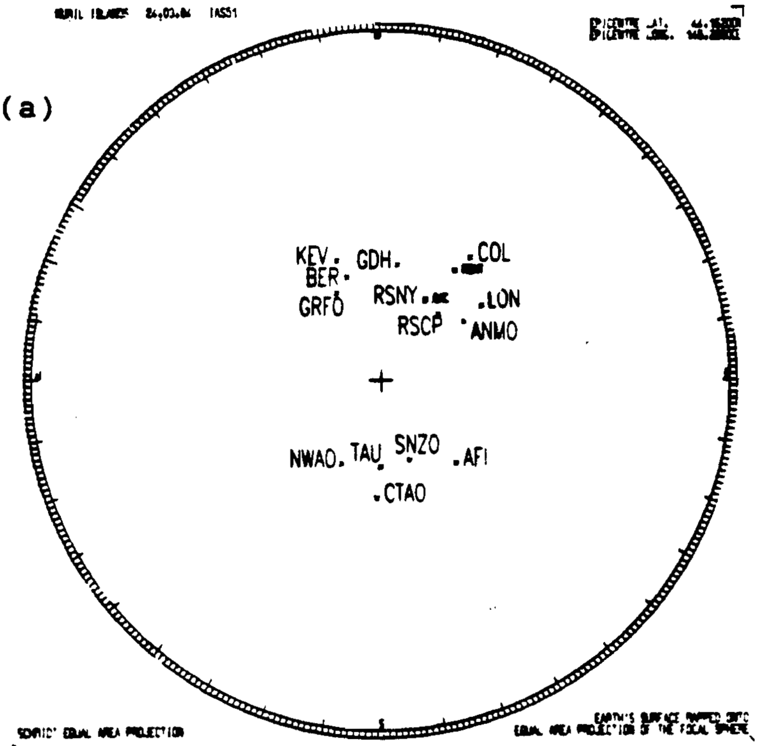
KEV
GDH
COL
BER
GRFO
RSNY
LON
RSCP
ANMO
NWAO
TAU
SNZO
AFI
CTAO

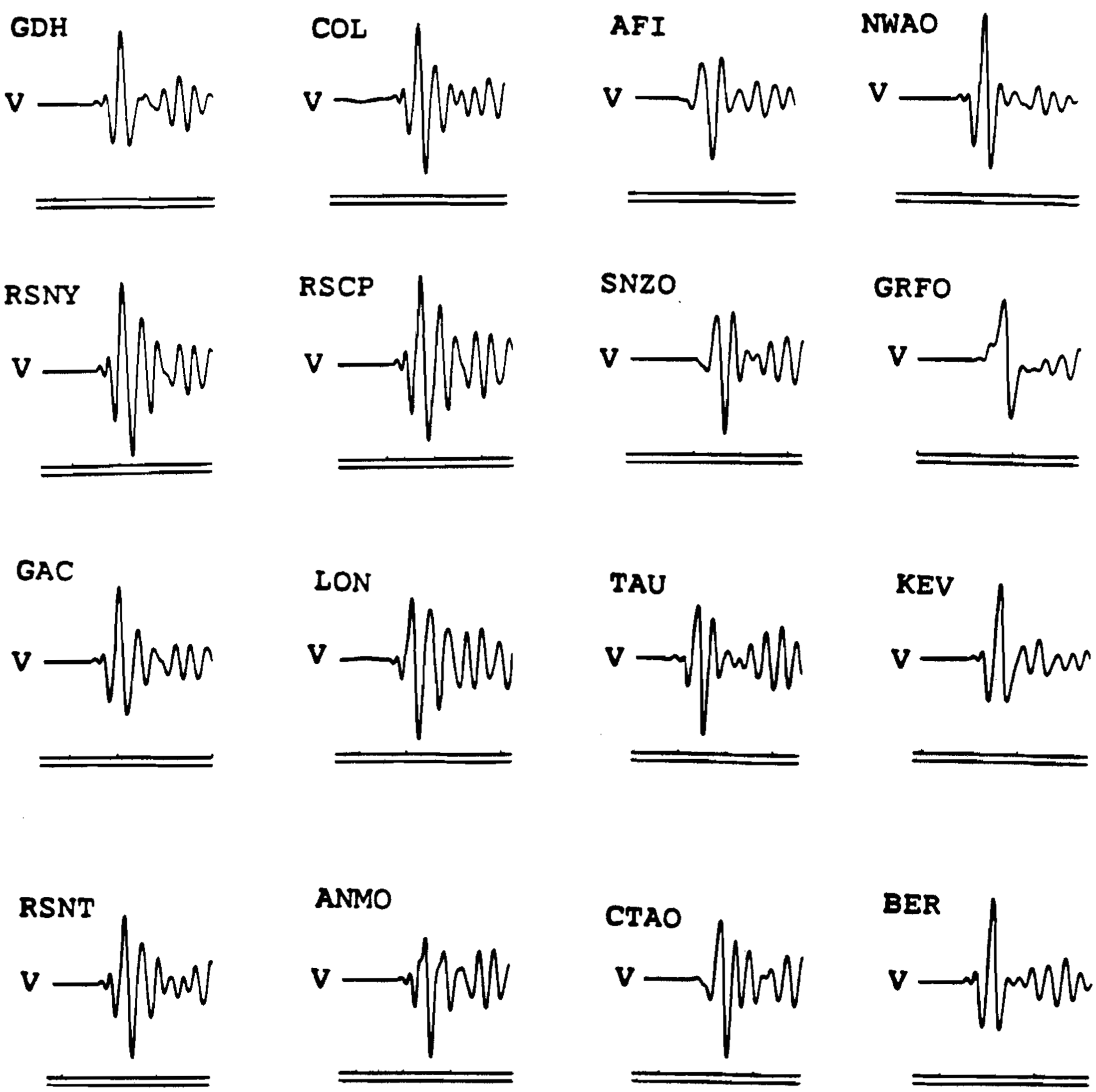
GDH
V
COL
V
AFI
V
NWAO
V
RSNY
V
RSCP
V
SNZO
V
GRFO
V
GAC
V
LON
V
TAU
V
KEV
V
RSNT
V
ANMO
V
CTAO
V
BER
V

IASPEI event 51

(b)

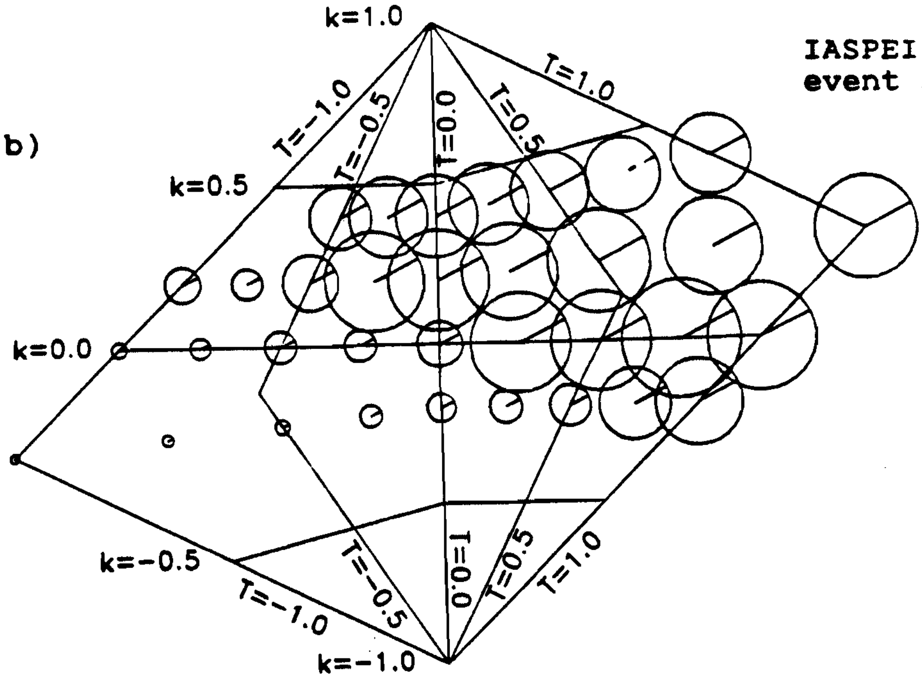

(c)

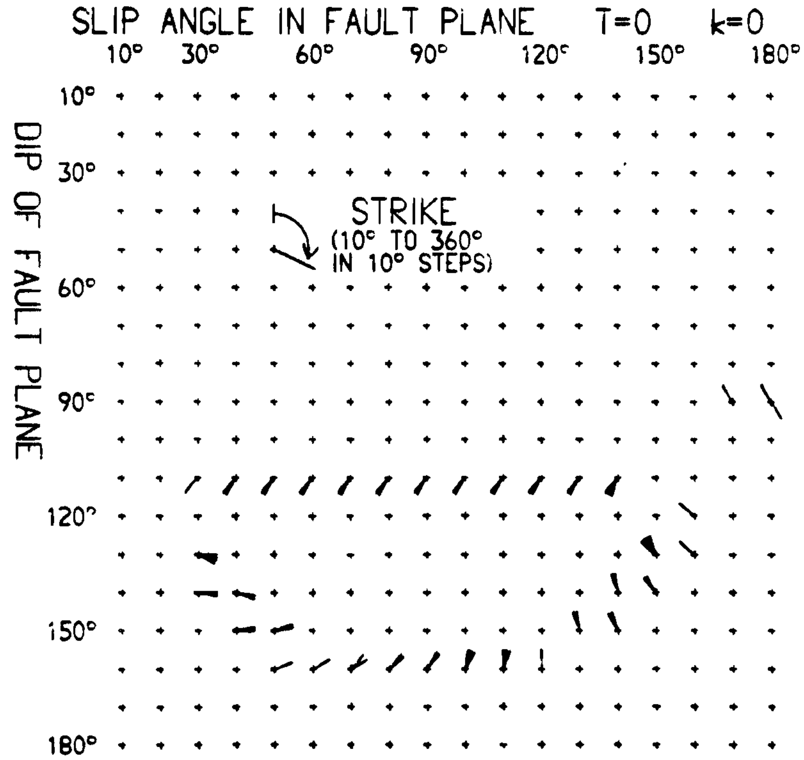

(d)

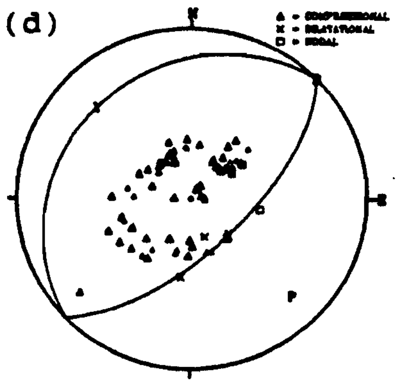

(e)

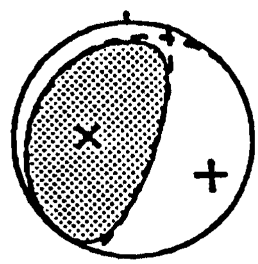

(f)

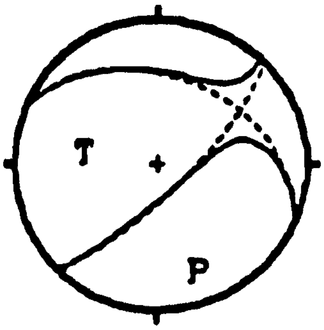

THIS PAGE LEFT BLANK INTENTIONALLY

REFERENCES

1. R G Pearce: "Fault Plane Solutions using Relative Amplitudes of *P* and *pP*". Geophys J R Astr Soc, 50, 381-394 (1977)

2. R G Pearce: "Earthquake Focal Mechanisms from Relative Amplitudes of *P*, *pP* and *sP*: Method and Computer Program". AWRE Report No. O 41/79, HMSO, London (1979)

3. R G Pearce: "Fault Plane Solutions using Relative Amplitudes of *P* and Surface Reflections: Further Studies". Geophys J R Astr Soc, 60, 459-487 (1980)

4. R G Pearce and R M Rogers: "Determination of Earthquake Moment Tensors from Teleseismic Relative Amplitude Observations". J Geophys Res, 94, 775-786 (1989)

5. R M Rogers: "Earthquake Moment Tensors from Telesiesmic Relative Amplitudes". PhD Thesis, University of Wales (1989)

6. C I Pooley, A Douglas and R G Pearce: "The Seismic Disturbance of 1976 March 20, East Kazakhstan: Earthquake or Explosions?" Geophys J R Astr Soc, 74, 621-631 (1983)

7. K L McLaughlin, D W Rivers and M A Brennan: "Pearce Focal Sphere Analysis of Explosion and Earthquake Mechanisms". Teledyne Geotech Report TGAL-TR-83-4 (1983)

8. R E Needham: "First-motion Focal Mechanism Solutions for the IASPEI Earthquakes". Open-file Report 85-458, United States Geological Survey (1985)

9. G Ekström, A M Dziewonski and J H Woodhouse: "Centroid-moment Tensor Solutions for the 51 IASPEI Selected Earthquakes, 1980-1984". Phys Earth Planet Inter, 47, 62-66 (1987)

10. S A Sipkin: "Moment Tensor Solutions Estimated using Optimal Filter Theory for 51 Selected Earthquakes, 1981-1984". Phys Earth Planet Inter, 47, 67-79 (1987)

11. M D Zirbes and B J Moon: "Waveform Catalogue for IASPEI Events". Open-file Report 85-219, United States Geological Survey (1985)

12. R M Rogers and R G Pearce: "Application of the Relative Amplitude Moment-tensor Program to Three Intermediate-depth IASPEI Earthquakes". Phys Earth Planet Inter, 47, 93-106 (1987)

13. J A Hudson, R G Pearce and R M Rogers: "Source Type Plot for Inversion of the Moment Tensor". J Geophys Res, 90, 765-774 (1989)

14. G L Choy and E R Engdahl: "Analysis of Broadband Seismograms from Selected IASPEI Events". Phys Earth Planet Inter, 47, 80-92 (1987)

15. I G Stimpson: "The Relative Amplitude Moment Tensor Method applied to the IASPEI Deep Earthquakes". Phys Earth Planet Inter, 47, 150-158 (1987)

16. S A Sipkin: "Estimation of Earthquake Source Parameters by the Inversion of Waveform Data: Global Seismicity, 1981-1983". Bull Seism Soc Am, 76, 1515-1541 (1986)

17. A M Dziewonski, T A Chou and J H Woodhouse: "Determination of Earthquake Source Parameters from Waveform Data for Studies of Global and Regional Seismicity". J Geophys Res, 86, 2825-2852 (1981)

18. S A Sipkin: "Estimation of Earthquake Source Parameters by the Inversion of Waveform Data: Synthetic Seismograms". Phys Earth Planet Inter, 30, 242-259 (1982)

TABLE 1

Hypocentre Parameters for the IASPEI List Earthquakes

No.	Date	h	min	s	Latitude	Longitude	Dep.	m_b	M_S	Region
1	1/ 1/80	16	42	40.0	38.815 N	27.780 W	10	6.0	6.7	Azores Is.
2	5/25/80	16	33	44.7	37.600 N	118.840 W	5	6.1	6.1	Calif-Nevada border reg.
3	6/29/80	7	20	5.5	34.808 N	139.181 E	15	5.8	6.2	Near S. coast of Honshu, Japan
4	7/29/80	14	58	40.8	29.598 N	81.092 E	18	6.1	6.5	Nepal
5	10/10/80	12	25	23.5	36.195 N	1.354 E	10	6.5	7.3	Algeria
6	10/24/80	14	53	35.1	18.211 N	98.240 W	72	6.4		Cent. Mexico
7	11/ 8/80	10	27	34.0	41.117 N	124.253 W	19	6.2	7.2	Near coast of N. Calif.
8	11/23/80	18	34	53.8	40.914 N	15.366 E	10	6.0	6.9	S. Italy
9	1/18/81	18	17	24.4	38.640 N	142.750 E	33	6.1	6.9	Near coast of Honshu, Japan
10	1/23/81	21	13	51.7	30.927 N	101.098 E	33	5.7	6.8	Sichuan Province, China
11	7/ 6/81	3	8	24.2	22.293 S	171.742 E	33	6.9	7.0	Loyalty Is. reg.
12	10/28/81	4	34	17.8	31.272 S	110.649 W	10	6.2	6.2	Easter Island reg.
13	11/22/81	15	5	20.6	18.752 N	120.839 E	24	6.2	6.5	Luzon, Philippine Is.
14	11/27/81	17	21	45.8	42.913 N	131.076 E	543	5.8		E. USSR-N.E. China border reg.
15	1/ 3/82	14	9	50.5	0.972 S	21.870 W	10	5.8	6.5	Cent. Mid-Atlantic Ridge
16	1/ 9/82	12	53	51.9	46.984 N	66.656 W	10	5.7	5.2	New Brunswick
17	8/ 5/82	20	32	53.0	12.597 S	165.931 E	31	6.2	7.1	Santa Cruz Is.
18	9/ 6/82	1	47	2.7	29.325 N	140.360 E	176	6.5		S. of Honshu, Japan
19	12/13/82	9	12	48.1	14.701 N	44.379 E	5	6.0	6.0	W. Arabian Peninsula
20	2/13/83	1	40	11.0	39.945 N	75.135 E	16	5.6	6.2	S. Xinjiang, China
21	4/ 3/83	2	50	1.2	8.717 N	83.123 W	37	6.5	7.3	Costa Rica
22	4/ 4/83	2	51	34.4	5.723 N	94.722 E	79	6.6		N. Sumatra
23	4/11/83	8	18	10.1	10.419 N	62.764 W	40	6.0	5.9	Near coast of Venezuela
24	4/18/83	10	58	51.3	27.793 N	62.054 E	64	6.5		S. Iran
25	5/ 2/83	23	42	37.8	36.219 N	120.317 W	10	6.2	6.5	Cent. Calif.
26	5/26/83	2	59	59.6	40.462 N	139.102 E	24	6.8	7.7	Near W. Coast of Honshu, Japan
27	6/ 1/83	1	59	54.7	17.038 S	174.605 W	179	6.2		Tonga Is.
28	6/ 2/83	20	12	50.7	9.512 S	71.249 W	598	5.9		Peru-Brazil border reg.
29	6/ 9/83	18	46	0.9	51.414 N	174.111 W	21	6.2	5.8	Andreanof Is., Aleutian Is.
30	6/21/83	6	25	27.4	41.346 N	139.099 E	10	6.7	6.9	Hokkaido, Japan reg
31	6/24/83	9	6	45.8	24.176 N	122.402 E	44	6.1	6.7	Taiwan reg.
32	7/12/83	15	10	3.4	61.031 N	147.286 W	37	6.1	6.4	S. Alaska
33	8/ 6/83	15	43	51.2	40.142 N	24.766 E	2	6.2	7.0	Aegean Sea
34	8/17/83	10	55	54.1	55.867 N	161.287 E	63	6.6		Near E. coast of Kamchatka
35	9/ 7/83	19	22	5.2	60.976 N	147.500 W	45	6.2	6.2	S. Alaska
36	9/12/83	15	42	8.6	36.502 N	71.082 E	209	6.1		Afghanistan-USSR border
37	10/ 4/83	18	52	13.3	26.535 S	70.563 W	15	6.4	7.3	Near coast of N. Chile
38	10/ 9/83	11	25	40.6	26.135 S	70.518 W	16	5.9	6.2	Near coast of N. Chile
39	10/17/83	19	36	21.5	37.588 N	17.520 W	10	6.0	6.3	N. Atlantic Ocean
40	10/22/83	4	21	35.0	60.665 S	25.451 W	24	6.5	6.8	S. Sandwich Is. reg.
41	10/30/83	4	12	27.1	40.330 N	42.187 E	12	6.1	6.9	Turkey
42	11/16/83	16	13	0.1	19.430 N	155.454 W	12	6.4	6.7	Hawaii
43	11/24/83	5	30	34.2	7.481 S	128.168 E	179	6.4		Banda Sea
44	11/30/83	17	46	0.7	6.852 S	72.110 E	10	6.6	7.6	Chagos Archipelago reg.
45	12/22/83	4	11	29.2	11.866 N	13.529 W	11	6.4	6.2	N.W. Africa
46	12/30/83	23	52	39.9	36.372 N	70.738 E	214	6.6		Hindu Kush reg.
47	1/ 1/84	9	3	37.6	33.404 N	137.322 E	374	6.5		Near coast of Honshu, Japan
48	2/ 7/84	21	33	20.5	9.924 S	160.455 E	14	6.5	7.5	Solomon Is.
49	3/ 5/84	3	33	51.2	8.136 N	123.765 E	651	6.7		Mindanao, Philippine Is.
50	3/19/84	20	28	39.8	40.288 N	63.333 E	26	6.5	7.0	Uzbek SSR
51	3/24/84	9	44	2.6	44.162 N	148.289 E	43	6.1	7.1	Kuril Is.

From the Monthly Listings of the National Earthquake Information Center.

TABLE 2

Classification of the IASPEI List Earthquakes

Numbers of the events falling into each category, with constraint on source type and orientation for each

Shallow, Group A Constraint on			Shallow, Group B Constraint on		
Event No.	Source Type*	Orientation*	Event No.	Source Type*	Orientation*
2	A	W	1	S	S
4	W	W	3	S	S
5	W	W	7	S	S
6	W	W	9	W	W
8	W	W	10	S	A
11	A	W	12	S	S
13	W	W	15	S	S
16	W	W	17	A	A
21	W	A	19	A	S
22	W	W	20	S	S
23	W	W	24	S	S
26	S	S	25	A	A
30	W	A	29	A	A
32	A	A	31	W	A
34	A	A	33	S	A
35	A	A	39	S	S
37	W	W	40	A	S
38	W	W	41	S	S
44	W	W	42	A	S
45	W	W	48	S	S
50	A	A	51	W	W

Intermediate-depth Constraint on			Deep Constraint on		
Event No.	Source Type*	Orientation*	Event No.	Source Type*	Orientation*
18	A	S	14	S	S
27	A	A	28	A	S
36	S	S	47	S	S
43	W	W	49	S	S
46	A	A			

*W = Weak
A = Average
S = Strong (see text)

TABLE 3

Solutions Obtained by Other Authors for the IASPEI Earthquakes
All angles are in degrees

Event	Ekström et al (CMT)				Sipkin (MSE)				Needham (FM)		
	σ	δ	ψ	T	σ	δ	ψ	T	σ	δ	ψ
1	147	82	164	0.12	234	99	15	0.00	60	95	15
2	175	60	111	-0.69	109	72	30	-0.59	5	82	173
3	173	105	162	0.44	199	89	175	0.11	No solution		
4	288	111	91	0.05	282	115	83	0.03	70	132	120
5	235	131	91	0.20	44	117	65	0.07	60	120	90
6	105	64	78	0.18	117	68	64	0.00	No solution		
7	143	85	26	0.20	120	90	1	0.02	50	90	177
8	305	58	83	0.07	158	58	136	0.05	140	20	90
9	203	99	87	-0.06	209	103	112	0.00	190	98	90
10	143	82	170	-0.41	139	92	175	0.03	222	92	0
11	247	91	130	-0.26	288	105	84	-0.01	78	162	90
12	233	93	170	-0.10	62	90	172	0.04	142	101	0
13	130	54	83	0.07	336	52	119	-0.35	140	45	90
14	344	93	112	0.09	339	97	117	0.11	343	95	90
15	170	81	170	0.05	274	89	10	-0.12	0	100	174
16	14	128	63	0.03	335	115	120	-0.61	252	112	50
17	346	113	89	0.13	358	112	125	0.06	341	120	90
18	356	72	144	0.49	354	70	154	-0.01	58	70	35
19	307	48	66	0.31	324	62	71	-0.15	340	75	90
20	320	87	14	-0.30	324	89	7	0.21	245	107	90
21	297	120	92	-0.05	319	117	113	0.24	305	107	90
22	27	125	126	-0.01	32	128	124	-0.09	180	125	140
23	140	58	64	-0.01	312	62	76	-0.11	239	50	130
24	237	55	82	-0.10	156	92	4	-0.36	200	100	22
25	327	130	87	-0.03	123	108	83	0.28	127	110	90
26	204	121	77	-0.24	10	125	109	-0.13	348	112	90
27	36	66	92	0.07	47	63	96	0.24	48	68	90
28	185	53	102	0.27	145	49	85	0.16	150	45	80
29	242	107	89	0.07	234	103	81	-0.02	238	102	90
30	30	131	73	0.32	186	130	96	0.29	196	150	90

TABLE 3 (Continued)

Event	Ekström et al (CMT)				Sipkin (MSE)				Needham (FM)		
	σ	δ	ψ	T	σ	δ	ψ	T	σ	δ	ψ
31	268	111	110	-0.16	281	98	76	0.00	260	113	58
32	235	66	117	0.25	249	73	117	0.04	233	65	110
33	228	86	15	0.03	315	89	163	0.00	315	90	170
34	252	127	69	-0.02	34	132	112	0.09	55	117	140
35	225	52	114	-0.49	244	66	111	0.00	15	45	60
36	55	130	96	0.26	38	132	88	0.01	28	132	90
37	345	104	99	0.15	8	119	125	0.02	340	106	90
38	348	111	97	0.04	1	108	117	-0.24	352	106	90
39	179	99	155	-0.11	3	101	149	0.00	9	92	175
40	226	53	88	-0.19	265	89	155	-0.02	350	85	4
41	301	97	15	0.24	34	93	171	-0.13	40	103	167
42	215	93	68	0.24	220	94	55	0.43	215	90	25
43	107	124	61	-0.32	126	117	83	-0.04	285	136	90
44	282	51	100	0.08	281	49	120	0.00	No solution		
45	94	54	50	-0.42	272	59	64	0.10	265	68	28
46	283	109	88	-0.07	292	107	104	-0.04	297	118	90
47	341	106	108	0.50	353	100	119	0.00	345	110	100
48	2	108	55	-0.07	352	97	47	0.02	358	103	90
49	38	58	104	0.70	54	60	132	-0.26	45	55	114
50	218	117	90	-0.38	172	121	116	0.06	220	125	90
51	200	106	99	-0.10	225	106	126	0.14	225	115	90

TABLE 4

Number of Incompatible RAMP Phase Pairs for other Authors' Solutions to the IASPEI Earthquakes

Event	Class*	Ekström et al (CMT)		Sipkin (MSE)		Needham (FM)	
		P	*S*	*P*	*S*	*P*	*S*
1	SB	2	0	6	2	2	1
2	SA	0	0	0	2	1	2
3	SB	2	2	0	1	No solution	
4	SA	0	0	0	0	0	6
5	SA	0	0	0	2	0	1
6	SA	0	1	0	2	No solution	
7	SB	0	3	3	2	0	1
8	SA	0	0	1	4	4	1
9	SB	0	0	0	0	1	1
10	SB	3	0	0	0	0	0
11	SA	0	1	3	2	1	1
12	SB	1	0	0	1	1	0
13	SA	0	0	0	2	0	1
14	D	4	0	4	0	1	2
15	SB	3	0	0	3	0	3
16	SA	0	1	0	3	0	5
17	SB	1	2	2	2	0	2
18	I	9	1	9	1	3	2
19	SB	1	2	1	2	0	2
20	SB	4	0	1	2	0	6
21	SA	0	2	0	7	1	11
22	SA	0	0	0	0	0	7
23	SA	0	1	1	2	0	2
24	SB	6	1	3	5	0	4
25	SB	3	4	1	1	1	1
26	SA	0	4	0	4	0	9
27	I	3	0	0	0	2	0
28	D	13	1	2	0	1	0
29	SB	0	1	0	0	0	0
30	SA	0	4	0	3	0	7

TABLE 4 (Continued)

Event	Class*	Ekström et al (CMT)		Sipkin (MSE)		Needham (FM)	
		P	*S*	*P*	*S*	*P*	*S*
31	SB	0	2	0	3	0	3
32	SA	1	2	4	4	1	1
33	SB	6	3	2	1	1	1
34	SA	1	0	0	1	1	3
35	SA	0	1	1	2	0	0
36	I	1	0	1	1	0	2
37	SA	1	1	0	0	1	0
38	SA	0	0	0	0	0	0
39	SB	9	4	4	4	0	2
40	SB	2	2	0	2	1	2
41	SB	7	3	0	2	0	2
42	SB	1	0	2	0	1	3
43	I	4	1	4	1	1	1
44	SA	0	4	0	5	No solution	
45	SA	0	4	0	1	0	1
46	I	2	0	2	1	1	1
47	D	5	0	4	1	6	3
48	SB	2	1	2	2	0	3
49	D	2	0	4	2	3	0
50	SA	0	2	0	4	0	1
51	SB	1	N/A	1	N/A	0	N/A

*Class: SA = Shallow, Class A; SB = Shallow, Class B;
I = Intermediate Depth; D = Deep

TABLE 5

Number of Incompatible Phase Pairs for Shallow Earthquakes

	Group A		Group B	
	P	*S*	*P*	*S*
MSE	10	50	26	35
FM	10	59	8	37
CMT	3	28	54	30

TABLE 6

Concordant Solutions

For each method, the solutions for those events marked with a star fall within the region of fully compatible solutions found using RAMP

Event	Class*	Ekström et al (CMT)	Sipkin (MSE)	Needham (FM)
2	SA	*		
4	SA	*	*	
5	SA	*		
8	SA	*		
9	SB	*	*	
10	SB		*	*
13	SA	*		
22	SA	*	*	
27	I		*	
29	SB		*	*
35	SA			*
37	SA		*	
38	SA	*	*	*
51	SB			*

*Class: SA = Shallow, group A SB = Shallow, group B
I = Intermediate depth

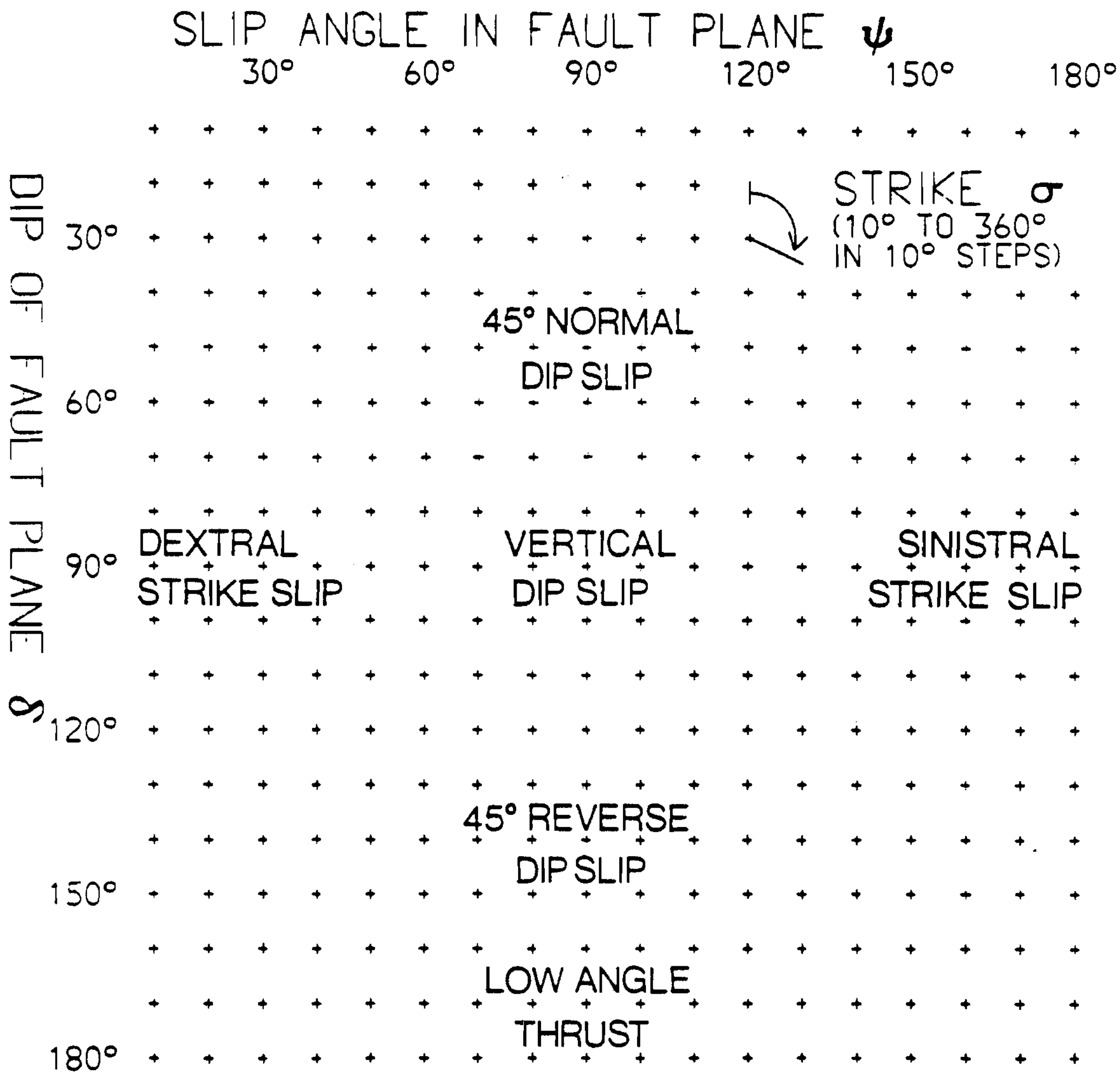

FIGURE 1. THE VECTORPLOT, ANNOTATED TO SHOW THE POSITIONS OF MAJOR FAULT TYPES. EACH VECTOR DRAWN ON SUCH A PLOT REPRESENTS A COMPATIBLE ORIENTATION OF A SPECIFIED SOURCE TYPE (AFTER ROGERS AND PEARCE (12))

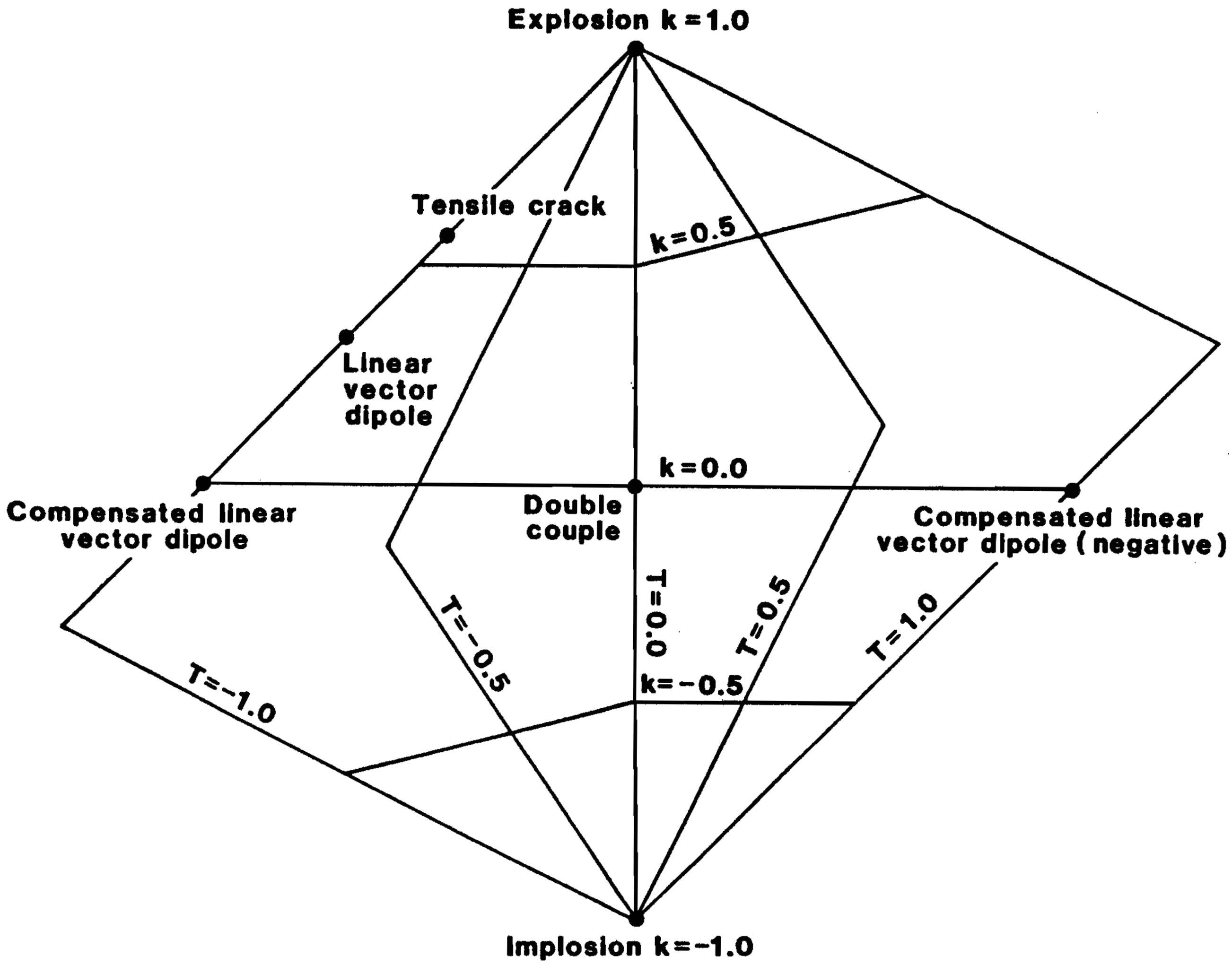

FIGURE 2. THE SOURCE TYPE PLOT, ANNOTATED TO SHOW THE POSITIONS OF SEVERAL WIDELY PROPOSED SOURCE TYPES (AFTER ROGERS AND PEARCE (12))

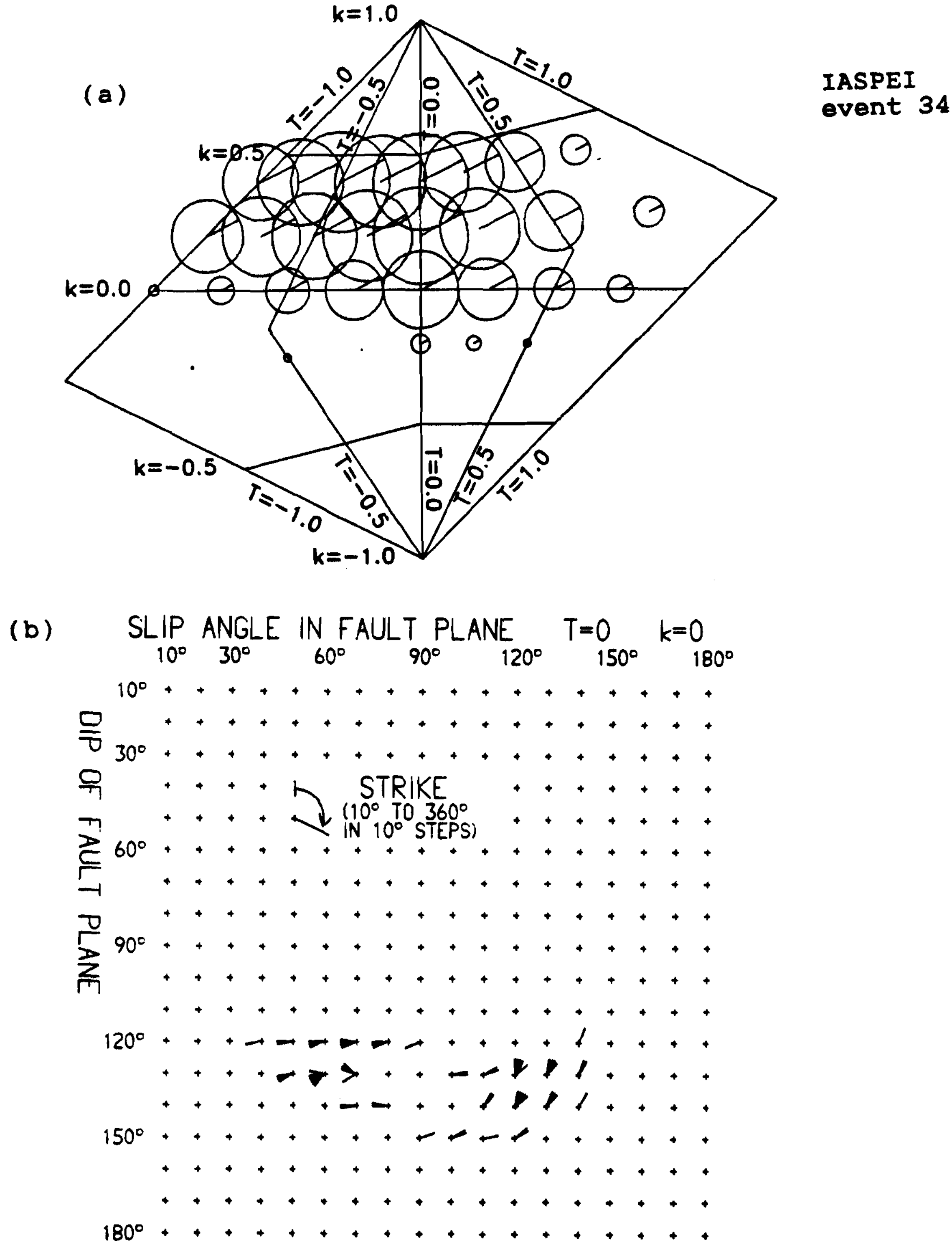

FIGURE 3. RESULTS FOR TWO TYPICAL GROUP A EARTHQUAKES

For earthquake 34, (a) shows a source type plot indicating the number of compatible orientations of each source type, and (b) shows a vectorplot representation of the compatible orientations of the double couple.
For this earthquake, constraints on both source type and orientation are classed as "average".

(c)

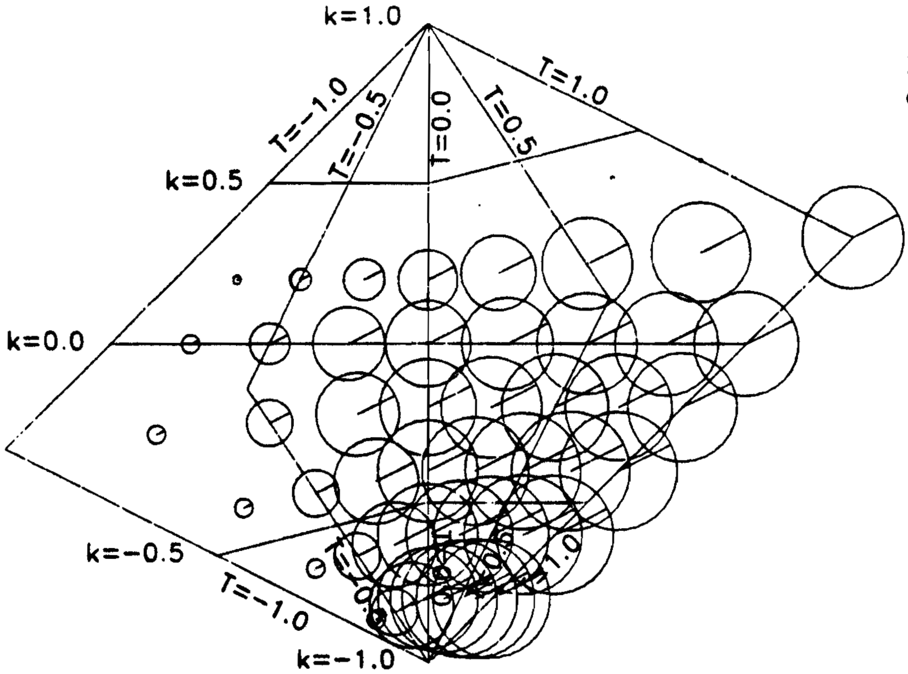

(d)

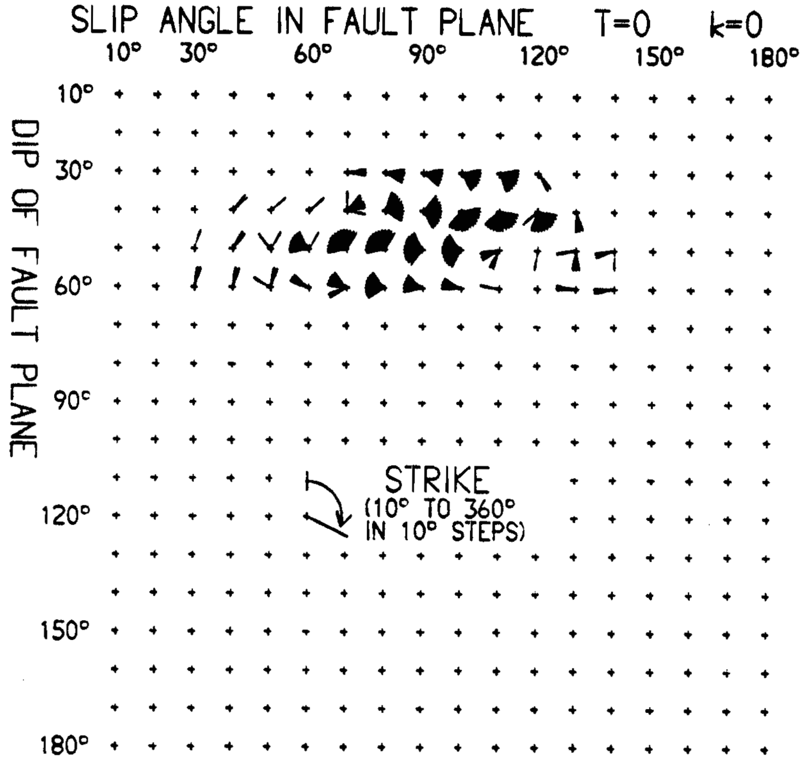

For earthquake 45, (c) shows a source type plot indicating the number of compatible orientations of each source type, and (d) shows a vectorplot representation of the compatible orientations of the double couple.
For this earthquake, constraints on both source type and orientation are classed as "weak".

IASPEI
●vent 26

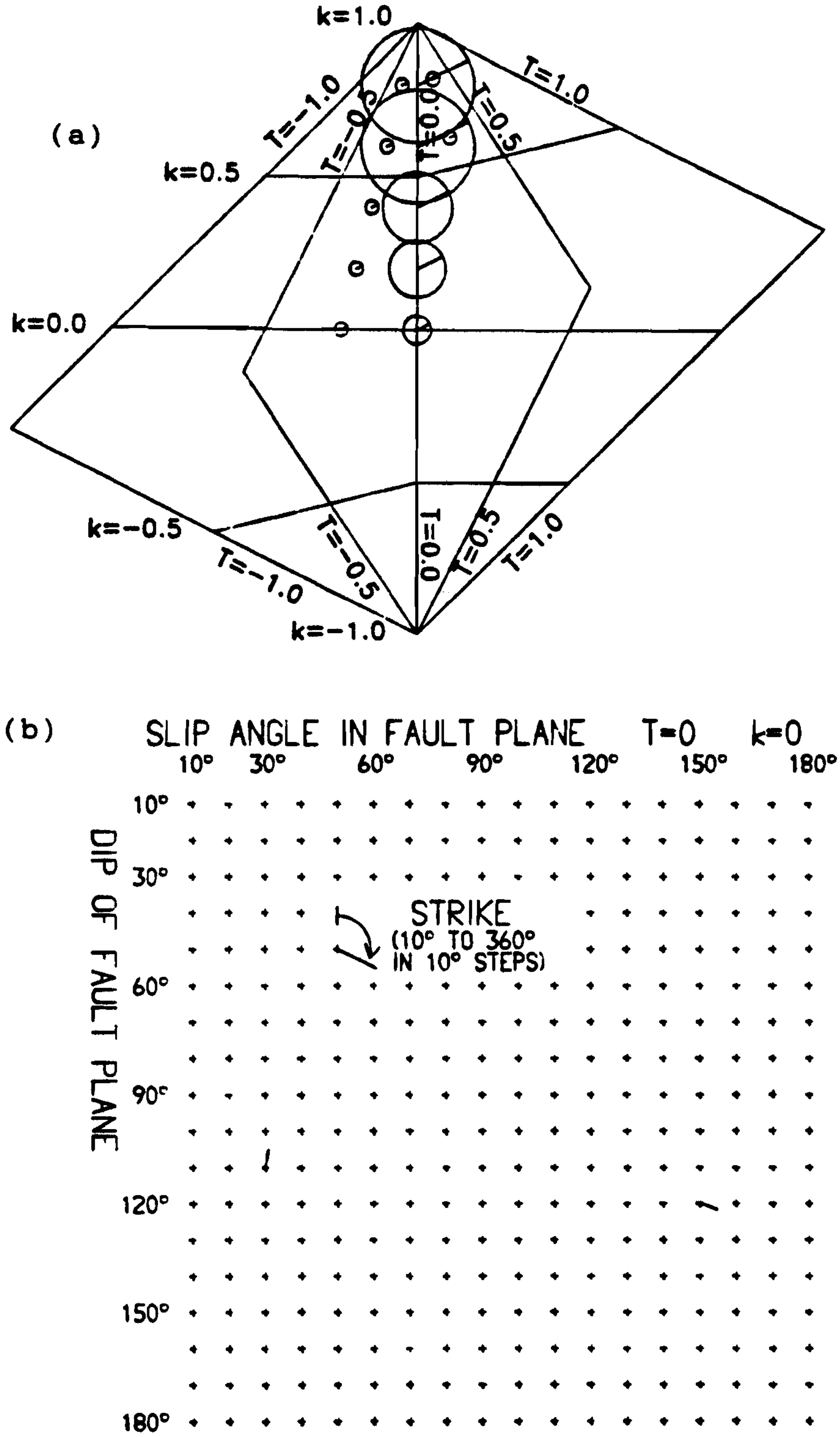

FIGURE 4. RESULTS FOR EARTHQUAKE 26

(a) Shows a source type plot indicating the number of compatible orientations of each source type, and (b) shows a vectorplot representation of the compatible orientations of the double couple.

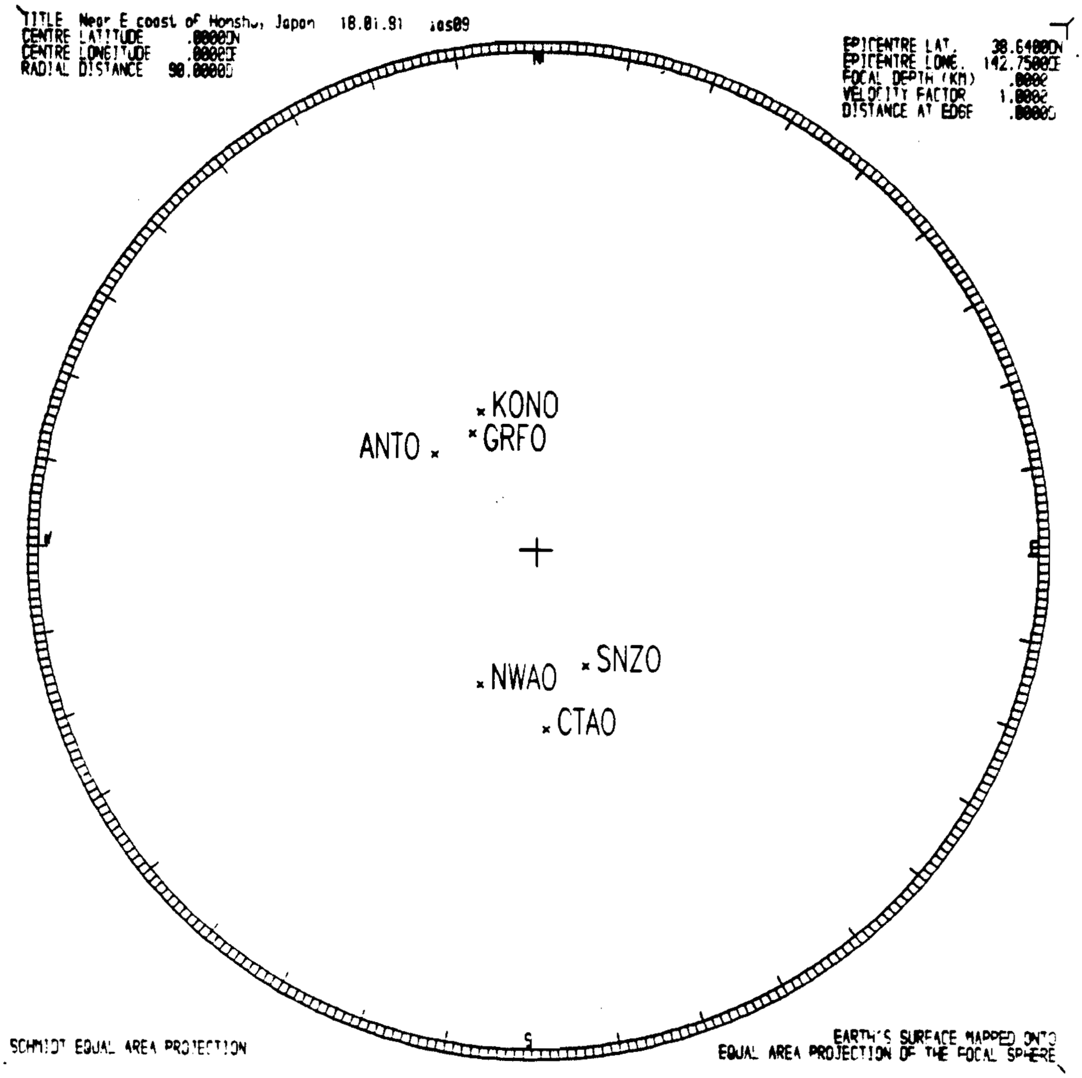

FIGURE 5. LOWER HEMISPHERE PLOT SHOWING THE DISTRIBUTION OF STATIONS FROM WHICH OBSERVATIONS WERE MADE FOR EARTHQUAKE 9

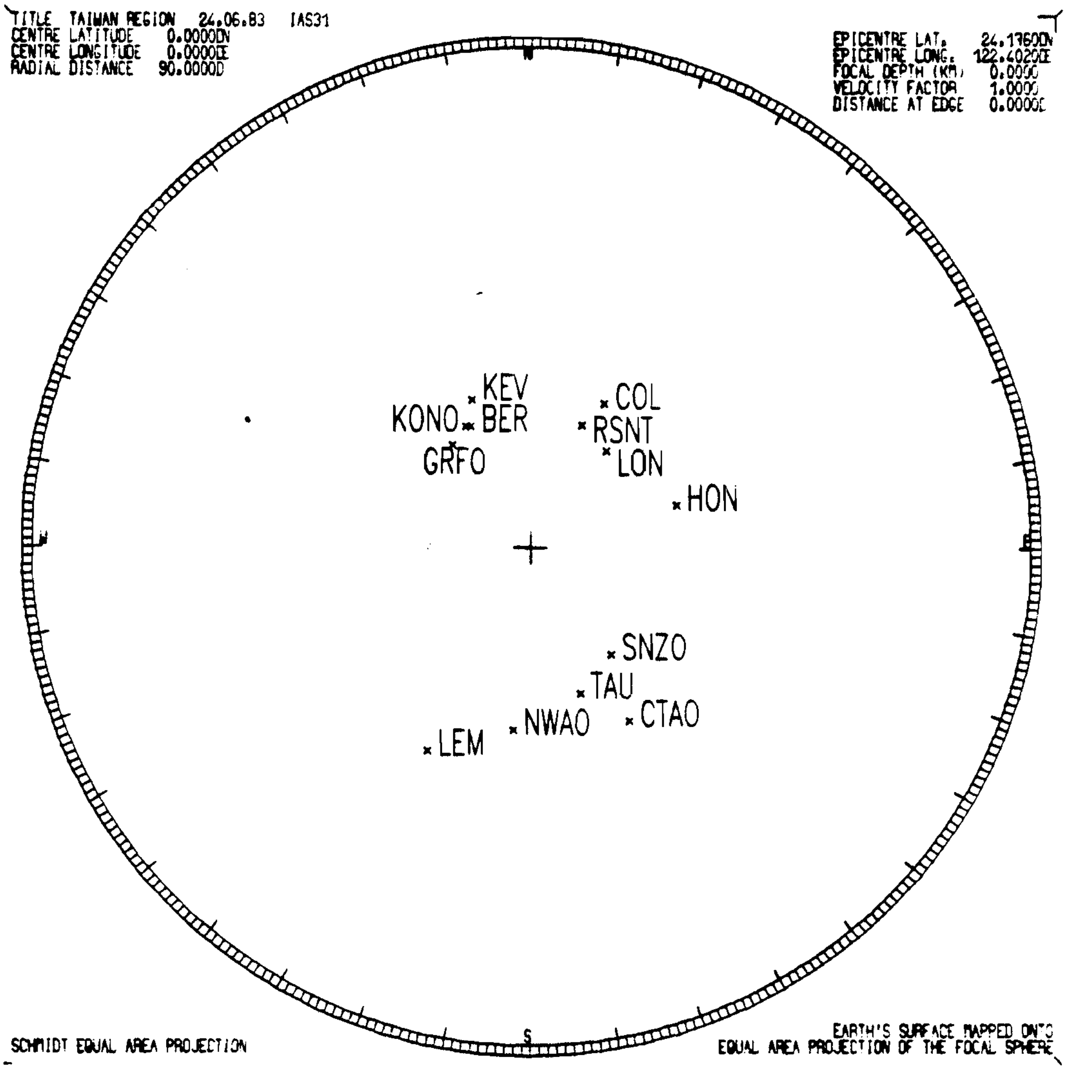

<u>**FIGURE 6. LOWER HEMISPHERE PLOT SHOWING THE DISTRIBUTION OF STATIONS FROM WHICH OBSERVATIONS WERE MADE FOR EARTHQUAKE 31**</u>

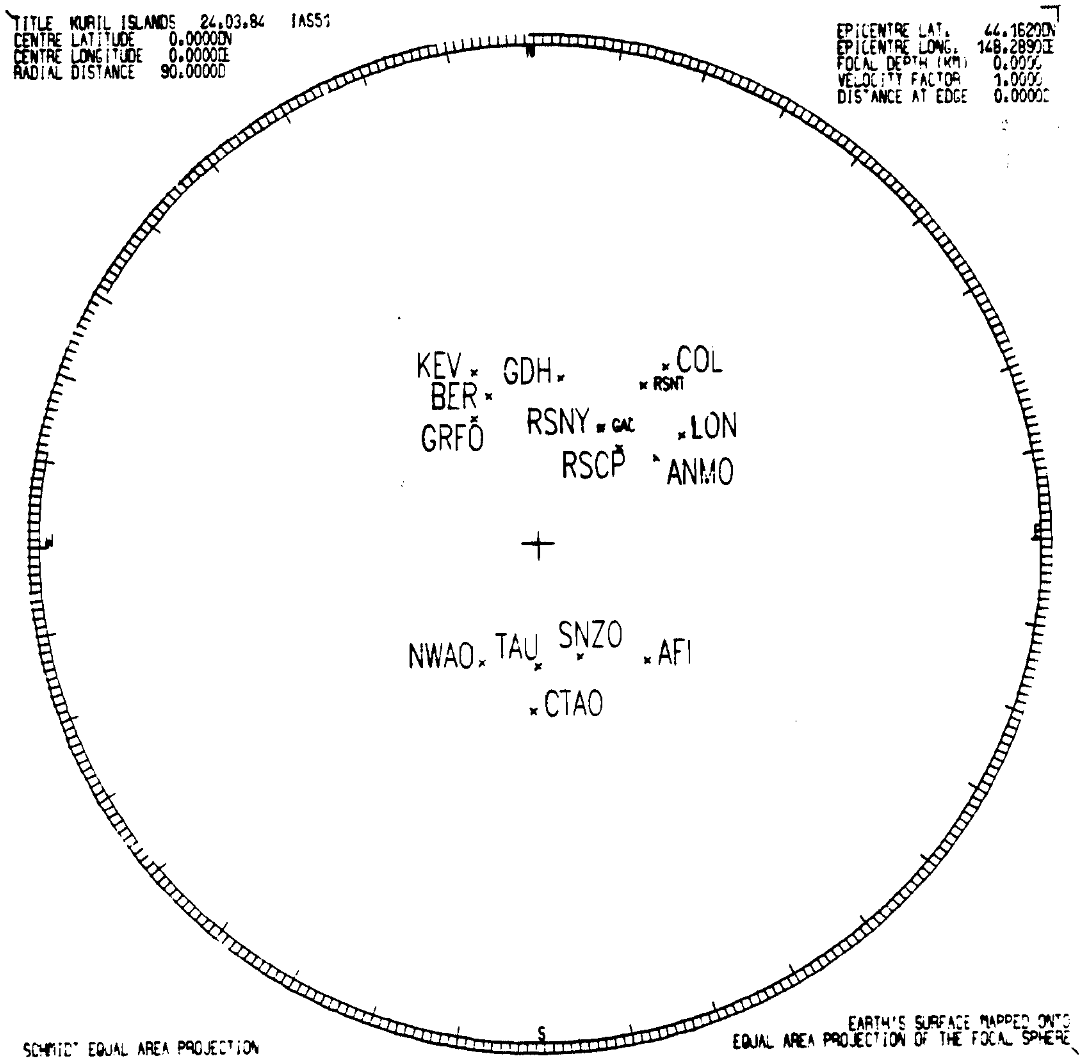

<u>**FIGURE 7. LOWER HEMISPHERE PLOT SHOWING THE DISTRIBUTION OF STATIONS FROM WHICH OBSERVATIONS WERE MADE FOR EARTHQUAKE 51**</u>

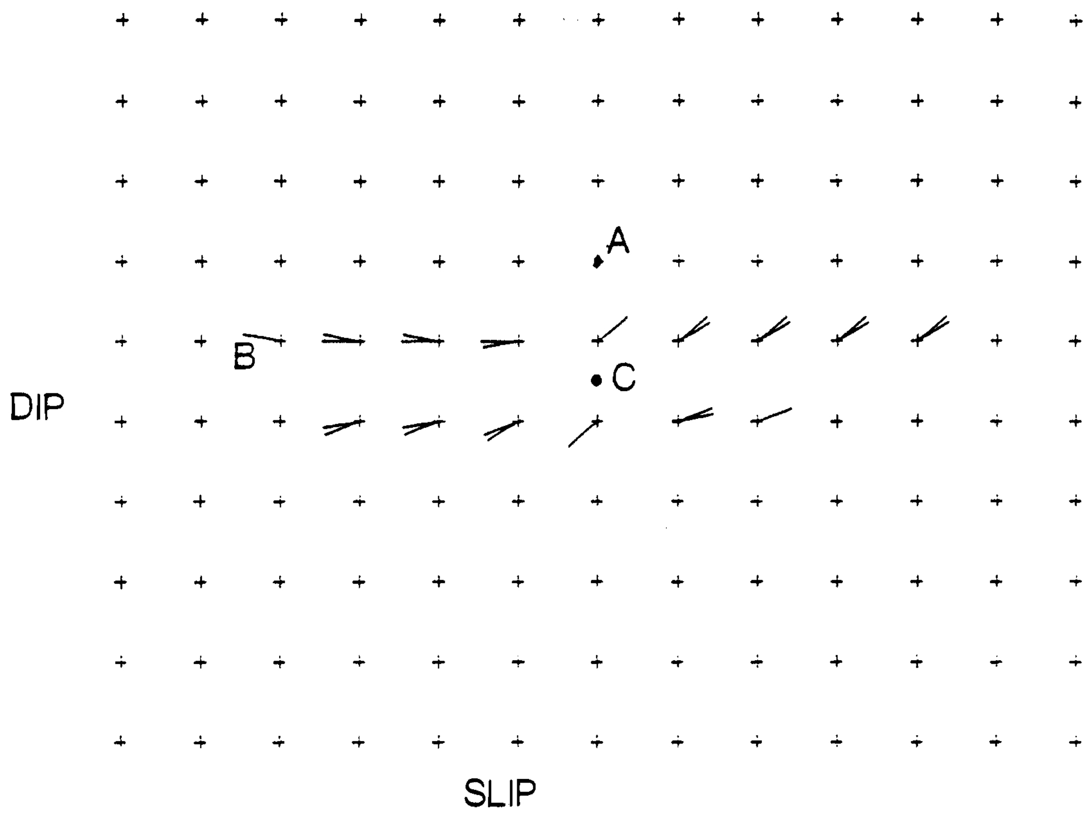

FIGURE 8. A MECHANISMS AT "A" ON THE VECTORPLOT IS LESS COMPATIBLE THAN THE MECHANISM INDICATED BY THE VECTOR "B", EVEN THOUGH "A" IS CLOSER TO THE CENTROID OF THE DISTRIBUTION OF COMPATIBLE MECHANISMS, AT "C"

UK UNLIMITED

Available from
HER MAJESTY'S STATIONERY OFFICE
49 High Holborn, London W.C.1
71 Lothian Road, Edinburgh EH3 9AZ
9-12 Princess Street, Manchester M60 8AS
Southey House, Wine Street, Bristol BS1 2BQ
258 Broad Street, Birmingham B1 2HE
80 Chichester Street, Belfast BT1 4JY
or through any bookseller.

Printed in England

ISBN 0 85518191 5

UK UNLIMITED